

STRUCTURAL EVOLUTION OF THE JOYITA HILLS,
SOCORRO COUNTY, NEW MEXICO

William C. Beck

Submitted in Partial fulfillment of the
Requirements for the Degree of
Doctor of Philosophy in Geology

New Mexico Institute of Mining and Technology

Socorro, New Mexico

May, 1993

TABLE OF CONTENTS

Table of Contents	i
List of Figures	iv
List of Tables	vi
List of Appendices	vii
List of Plates	viii
Acknowledgments	ix
Abstract	xi
Introduction	1
Part 1: STRUCTURAL DATA FROM THE JOYITA UPLIFT: IMPLI- CATIONS FOR ANCESTRAL ROCKY MOUNTAIN DEFORMATION WITHIN CENTRAL AND SOUTHERN NEW MEXICO	4
INTRODUCTION	5
STRUCTURAL ANALYSIS	8
Mid-Tertiary normal fault systems	9
Laramide strike-slip fault systems	11
Ancestral Rocky Mountain fault systems	11
North-striking normal faults	11
Northwest-striking normal faults	18
Proterozoic mylonites and foliations	18
Depositional basin trends	22
DISCUSSION AND INTERPRETATION	24
CONCLUSIONS	28
Part 2: POLYDEFORMATION IN THE JOYITA HILLS, CENTRAL NEW MEXICO, U.S.A.: STRUCTURAL ANALYSIS THROUGH CONSIDERATION OF INITIAL FRACTURING	29
INTRODUCTION	30
Study area	33
REASONING, TERMINOLOGY AND METHODS	35
STRUCTURAL ANALYSIS	44
Normal fault systems	46
Strike-slip fault systems	50

Thrust fault systems	54
Ancestral Rocky Mountain normal faults	59
Proterozoic basement structures and reactivation	62
Unknown faults	64
Joint orientations	64
INTERPRETATION	69
DISCUSSION	74
Part 3: NEW FUSULINID DATA AND MULTIPLE EPISODES OF ANCESTRAL ROCKY MOUNTAIN DEFORMATION IN THE JOYITA HILLS, SOCORRO COUNTY, NEW MEXICO	77
INTRODUCTION	78
GENERAL STRATIGRAPHIC RELATIONSHIPS	80
Pennsylvanian strata	80
Permian strata	83
ATOKAN DEFORMATION	92
WOLFCAMPIAN FUSULINIDS	93
SUMMARY	99
Part 4: STRUCTURAL AND TECTONIC EVOLUTION OF THE JOYITA HILLS, CENTRAL NEW MEXICO: IMPLICATIONS OF BASEMENT CONTROL ON RIO GRANDE RIFT	101
INTRODUCTION	102
METHOD OF ANALYSIS	107
PROTEROZOIC BASEMENT STRUCTURES	109
ANCESTRAL ROCKY MOUNTAIN DEFORMATION	110
General stratigraphic relationships	110
Ancestral Rocky Mountain structures	115
Interpretation of Ancestral Rocky Mountain deformation	119
LARAMIDE DEFORMATION	123
General stratigraphic relationships	123
Laramide structures	125
Interpretation of Laramide deformation	129
RIO GRANDE RIFT DEFORMATION	135
General stratigraphic relationships	135

Rio Grande rift structures	136
Interpretation of Rio Grande rift deformation	139
SUMMARY	142
SUMMARY	145
REFERENCES	147
APPENDIX A	156
APPENDIX B	in pocket
PLATES	in pocket

LIST OF FIGURES

Part 1: STRUCTURAL DATA FROM THE JOYITA UPLIFT: IMPLI- CATIONS FOR ANCESTRAL ROCKY MOUNTAIN DEFORMATION WITHIN CENTRAL AND SOUTHERN NEW MEXICO	
Figure 1.1. Pennsylvanian paleogeographic map showing the location of major uplifts and depositional basins and the location of the modern-day Joyita Hills	6
Figure 1.2. Generalized Paleozoic stratigraphic section	7
Figure 1.3. Mid-Tertiary normal fault systems	10
Figure 1.4. Laramide strike-slip fault systems	12
Figure 1.5. Generalized geologic map of the Joyita Hills	13-14
Figure 1.6. Generalized cross section	16-17
Figure 1.7. North-striking ancestral Rocky Mountain normal faults	19
Figure 1.8. Northwest-striking ancestral Rocky Mountain normal faults	20
Figure 1.9. Preferred orientations of Proterozoic foliations	21
Figure 1.10. Modified Pennsylvanian isopach map superimposed with early Wolfcampian paleocurrent directions	23
Figure 1.11. Hypothetical late Paleozoic, north-trending, left-lateral wrench zone within central and southern New Mexico	27
Part 2: POLYDEFORMATION IN THE JOYITA HILLS, CENTRAL NEW MEXICO, U.S.A.: STRUCTURAL ANALYSIS THROUGH CONSIDERATION OF INITIAL FRACTURING	
Figure 2.1. Generalized geologic map of northeast Socorro County	31-32
Figure 2.2. Generalized stratigraphy exposed within the Joyita Hills and El Valle de La Joya	34
Figure 2.3. Hypothetical fracture patterns for shallow crustal deformation	36
Figure 2.4. Examples of relationships between fractures and bedding	38-41
Figure 2.5. Primary data set of all planar structural elements	45
Figure 2.6. Fracture systems associated with Rio Grande rift	47-48
Figure 2.7. Laramide strike-slip fault systems	51-52
Figure 2.8. Laramide thrust fault systems	55-56
Figure 2.9. Supplemental data	60-61
Figure 2.10. Joint orientations	65-66
Figure 2.11. Generalized elastic plate theory	71-72

Part 3: NEW FUSULINID DATA AND MULTIPLE EPISODES OF
ANCESTRAL ROCKY MOUNTAIN DEFORMATION IN THE
JOYITA HILLS, SOCORRO COUNTY, NEW MEXICO

Figure 3.1. Pennsylvanian paleogeographic index map showing the location of major uplifts and depositional basins	79
Figure 3.2. Generalized Paleozoic stratigraphic section in the Joyita Hills	81
Figure 3.3. Selected photographs of lithologies and features in the Bursum and Abo formations	85–88
Figure 3.4. Generalized geologic map of the Central Canyon area	89
Figure 3.5. Generalized cross section along the early Wolfcampian normal fault	90–91
Figure 3.6. Cross-sectional exposure of the Atokan fault	94
Figure 3.7. Fusulinids recovered from limestones within the Bursum	97–98

Part 4: STRUCTURAL AND TECTONIC EVOLUTION OF THE JOYITA
HILLS, CENTRAL NEW MEXICO: IMPLICATIONS OF BASEMENT
CONTROL ON RIO GRANDE RIFT

Figure 4.1. Generalized geologic map of northeast Socorro County	103–104
Figure 4.2. Generalized stratigraphy exposed to the west (Joyita Hills) and east (El Valle de La Joya) of the East Joyita fault	105–106
Figure 4.3. Lower-hemisphere, equal-area projections of regional bedding, Proterozoic and late Paleozoic structural orientations	111–112
Figure 4.4. Modified Pennsylvanian isopach map superimposed with early Wolfcampian paleocurrent data	114
Figure 4.5. Generalized cross section normal to one of the north-striking, ancestral Rocky Mountain normal faults	116–117
Figure 4.6. Inferred divergent, sinistral wrench fault system superimposed on Pennsylvanian paleogeographic map	122
Figure 4.7. Lower-hemisphere, equal-area projections of Laramide strike-slip fault, thrust fault and fold axis orientations	126–127
Figure 4.8. Generalized structural profile of Laramide uplift west of the East Joyita fault	132
Figure 4.9. Plan view of structural relationships west of the East Joyita fault after Laramide uplift and prior to deposition of the Spears Formation	133–134
Figure 4.10. Lower-hemisphere, equal-area projections of Rio Grande rift normal fault, dike and detachment fault orientations	137–138

LIST OF TABLES

Part 3: NEW FUSULINID DATA AND MULTIPLE EPISODES OF
ANCESTRAL ROCKY MOUNTAIN DEFORMATION IN THE
JOYITA HILLS, SOCORRO COUNTY, NEW MEXICO

Table 3.1. Fusulinid identifications 95

LIST OF APPENDICES

APPENDIX A: COMPUTER PROGRAMS	156
Program ROTATE	157
Program CONVRT	173
Program SCHMDT	178
 APPENDIX B: FIELD DATA	 in pocket

LIST OF PLATES

Plate 1: Geologic map of the Joyita Hills area, Socorro County,
New Mexico..... in pocket

Plate 2: Cross sections in pocket

ACKNOWLEDGMENTS

The author thanks R.M. Chamberlin, C.E. Chapin, W.X. Chavez, D.B. Johnson and J.W. Schlue for serving as committee members, for their comments and critical reviews of the dissertation, and for their help in the field on various aspects of this project. A special thanks to my primary advisor, C.E. Chapin, for his thoughts, ideas and encouragement throughout this project. The project was funded primarily through the New Mexico Bureau of Mines and Mineral Resources (F.E. Kottlowski, Director; succeeded by C.E. Chapin, Director), and without this funding the dissertation would not have been possible. A research grant supplied by the New Mexico Geological Society also helped defray the costs of this project. Additional thanks are due to the Sevilleta National Wildlife Refuge (T.M. Stans, Manager), for granting access to the study area.

Several others provided critical reviews of one or more of the following manuscripts, and their individual efforts were much appreciated. P.W. Bauer, S.M. Cather, R.W. Harrison and F.E. Kottlowski edited Part 1; P.W. Bauer, A.E. Burford, C.E. Chapin, J.M. Connor, L.B. Goodwin, W.C. Haneberg, and A.R. Sanford edited Part 2; A.K. Armstrong, C.E. Chapin and F.E. Kottlowski edited Part 3; and S.M. Cather, W.C. Haneberg and S. Ralser edited Part 4. Additional thanks are due to D.A. Myers, who provided fusulinid identifications, and to O.J. Anderson, S.N. Hayden and S.G. Lucas for their help with the stratigraphy.

I would also like to thank the many friends that I have encountered during this project: Brian and Julie Brister, Bob and Dorothy Colpitts, Bruce, Caroline and Abigail Hallett, Ron and Linda Linden, Kurt, Ann and Sage Panter, David and Monica Silvils, Bill McIntosh and Nelia Dunbar, Robert Lee and Naishing Chi, Mark Boryta, Jenny Boryta, Ed Hagan, Mike Knoper, Chris McKee, and Maureen Wilks. Each in

their own way has made this place somewhat more tolerable. I also thank my family for their never-ending support, both moral and financial.

Finally, I owe a special thanks and debt of gratitude to A.E. Burford, an early mentor who emphasized the benefit of evaluating small-scale structures in an attempt to develop structural interpretations, and to C.E. Chapin, who emphasized the benefit of incorporating stratigraphic observation with structural data in order to formulate a tectonic synthesis.

ABSTRACT

Phanerozoic sedimentary and volcanic sequences exposed in the Joyita Hills area (northeast Socorro County, New Mexico) record the faults, folds and other structures that developed in response to three orogenic events: Ancestral Rocky Mountain, Laramide and Rio Grande rift. Additional exposures of Proterozoic augen gneiss in the core of the Joyita Hills reveal three preferred orientations of high-angle to vertical, gneissic to mylonitic foliations. These strike to the north, northwest and east-northeast. Proterozoic amphibolite dikes parallel the east-northeast foliations. Comparison of Phanerozoic fault and dike orientations with attitudes of Proterozoic foliations and amphibolite dikes indicates that reactivation of basement anisotropies was a common factor during each Phanerozoic deformational event.

Reactivation of Proterozoic foliations during ancestral Rocky Mountain (late Paleozoic) tectonism resulted in basins and uplifts of north and northwest trend. Bounding faults separating these basins and uplifts were high-angle to subvertical normal faults. Fault striae define displacements as normal, left-oblique slip on north-striking faults and as dip slip on northwest-striking faults. Fault orientations and displacements, when combined with isopach, paleocurrent and biostratigraphic (fusulinid) data, indicate that late Paleozoic deformation in the Joyita Hills area was the result of north trending, divergent, sinistral wrench faulting.

Laramide tectonism reactivated Proterozoic structures in a strike-slip sense. North-striking (synthetic) and east-northeast-striking (antithetic) faults are interpreted as conjugate shears that developed within a north-trending, dextral wrench fault system. Additional dextral wrench faults strike northeast, and parallel the Montosa and Del Curto fault zones. Laramide deformation also resulted in thrust faulting and folding of strata. However, these structures were a lesser component of Laramide deformation, and were apparently related to Laramide wrench fault systems.

Mid-Tertiary (Oligocene-Miocene) extension associated with the Rio Grande rift developed along both high-angle and low-angle normal faults. High-angle normal fault and dike systems strike to the north-northeast, northwest and east-northeast. The latter two fault and dike systems strike parallel to northwest- and east-northeast-striking Proterozoic foliations and amphibolite dikes. In addition, north-striking foliations and ancestral Rocky Mountain faults observed along the East Joyita fault influenced the orientation and location of this major, down-to-the-east normal fault. Low-angle (0° - 30°) normal faults strike north and north-northeast, and postdate the high-angle normal fault and dike systems. The low-angle normal faults are interpreted as extensional detachment faults. Orientation data from west-tilted Oligocene volcanic strata, when combined with the orientations of detachment faults and associated striae, indicate that the hanging wall displacement direction was to the east and east-southeast.

INTRODUCTION

The Joyita Hills area, as used herein, refers to the Joyita Hills proper (also known as Los Canoncitos) and El Valle de La Joya, which lies to the east (Plate 1). Rocks exposed within these areas include Proterozoic augen gneiss and amphibolite dikes, and Phanerozoic sedimentary and volcanic sequences and igneous intrusives. This succession of rocks provides a fairly complete representation of the Phanerozoic stratigraphy in central New Mexico, and affords the opportunity to evaluate structural styles associated with three recognized deformational events. Specifically, these include the ancestral Rocky Mountain, Laramide and Rio Grande rift orogenies. Although Proterozoic rocks are exposed in the core of the Joyita Hills, the dissertation focuses on analysis of structures that developed during the Phanerozoic. Proterozoic structures (preferred orientations of foliations and amphibolite dikes) have been determined in order to evaluate the influence of reactivation during Phanerozoic deformation. Structures observed within the Phanerozoic section include normal faults (including low-angle detachment faults), thrust faults and strike-slip faults, joints, mafic and felsic dikes, and a limited number of folds. The dissertation combines detailed mapping at a scale of 1:12,000, structural analysis, and observation of stratigraphic relationships in order to formulate structural and tectonic syntheses for Phanerozoic deformation in the Joyita Hills area.

Structural analyses use a relatively simple concept earlier documented by Beck (1984) and Beck and Burford (1985). Specifically, field observation indicates that tectonically induced fractures (e.g., joints and faults, the latter typically of small displacement) most commonly maintain consistent orientations with respect to bedding. These relationships are demonstrated by comparing fractures plotted with respect to bedding to fractures plotted with respect to their field-recorded orientations. Fracture orientations, when plotted with respect to bedding, form concentrations that are

increased in maxima percent value and define fracture patterns (composed of both shear and tensile orientations) compatible with Anderson's (1951) models for shallow crustal, brittle deformation. These relationships are interpreted to indicate that fractures had been superimposed on the stratified sequences while bedding was horizontal; fracture orientations plotted with respect to bedding are then used to infer the orientations of applied stress for Laramide and Rio Grande rift tectonisms.

The dissertation that follows is composed of four separate, but related parts, each forming an integral part of the whole. Each part was written for publication and was designed to stand alone as a journal article, and each builds on information provided in the previous part(s). Part 1 presents an interpretation of ancestral Rocky Mountain deformation, and integrates structural and stratigraphic data from the Joyita Hills with isopach and paleocurrent data. Late Paleozoic structures in the Joyita Hills are compatible with previously documented ancestral Rocky Mountain structures in the Sacramento Mountains (Pray, 1961) and in the Sierra Nacimiento area (Baars, 1982). Consequently, a tectonic interpretation of late Paleozoic deformation has been formulated that is considered relevant to the broader area of central and southern New Mexico.

Part 2 provides a detailed discussion of the analytical method used in the dissertation, and focuses on Laramide and Rio Grande rift deformation. Specific structures, including joints, faults, dikes and fold axes, are used to infer applied stress orientations, and both structural orientations and applied stress orientations are correlated with a specific tectonic event (Laramide or Rio Grande rift). Part 2 also presents data from ancestral Rocky Mountain deformation and discusses why the analytical technique cannot be applied to late Paleozoic structures. Proterozoic data are also presented in order to demonstrate the influence of basement anisotropies on Phanerozoic deformation. Lastly, Part 2 compares the analytical technique with a recognized alternative (elastic plate theory).

Part 3 returns to ancestral Rocky Mountain deformation, and provides new information (largely stratigraphic and biostratigraphic) relevant to the timing of late Paleozoic tectonism.

Part 4 is a summary paper, and presents an interpretation of each Phanerozoic deformational event in a temporal sequence. In other words, Part 4 is intended to provide a geologic history of the Joyita Hills area, and incorporates structural and stratigraphic data in order to formulate a complete structural and tectonic synthesis. One of the primary arguments developed in Part 4, and to a lesser extent throughout the dissertation, is that reactivation of basement anisotropies was a common occurrence during Phanerozoic deformation. The extent to which reactivation occurred in the Joyita Hills area should not be considered as an isolated occurrence, but rather as another example of a natural phenomenon that has been recognized on almost every continent. Additional studies, which include both theoretical considerations and specific examples of reactivation in a variety of tectonic settings, have been provided by Watson *et al.* (1986), Sykes (1978) and Watterson (1975).

In addition to these four parts, the computer programs used in the dissertation and a tabulation of all field data have been provided in Appendices A and B. Lastly, the geologic map and cross sections (Plates 1 and 2) have been provided in the end pocket.

Part 1

**STRUCTURAL DATA FROM THE JOYITA UPLIFT: IMPLICATIONS
FOR ANCESTRAL ROCKY MOUNTAIN DEFORMATION WITHIN
CENTRAL AND SOUTHERN NEW MEXICO**

Submitted to the New Mexico Geological Society 1991 Guidebook

April 1, 1991

INTRODUCTION

Regional relationships of ancestral Rocky Mountain deformation, including the location, trend, relative timing and magnitude of individual uplifts and depositional basins, were summarized by Kluth (1986) and Kluth and Coney (1981). Within New Mexico, late Paleozoic tectonism resulted in a series of north- and northwest-trending uplifts and basins. Although the general trends and locations of these structures have been well-defined on the basis of stratigraphic studies (Kottowski, 1960), specific folds and faults have seldom been recognized, and little is known about the structural style associated with basin and uplift development.

On the basis of stratigraphic relationships, several investigators (Read and Wood, 1947; Kottowski, 1960; Kottowski and Stewart, 1970; Baars, 1982; Siemers, 1983) have interpreted the modern-day Joyita Hills area (Fig. 1.1) as the location of a late Paleozoic, north-trending positive feature (the Joyita uplift). In addition, geologic mapping and biostratigraphic (fusulinid) analysis (Kottowski and Stewart, 1970) documented an angular unconformity between Pennsylvanian and Permian strata and defined the Joyita uplift as an early Wolfcampian tectonic element (Fig. 1.2).

The purpose of this paper is to present new structural data from the Joyita Hills and interpret its relationship to the adjacent Lucero and San Mateo basins. Observations indicate that ancestral Rocky Mountain faults within the Joyita Hills are the result of reactivation of Proterozoic mylonite zones, and are comparable, in both orientation and sense of offset, to those identified as late Paleozoic faults in the Albuquerque Basin to the north (Baars, 1982) and the Sacramento Mountains to the southeast (Otte, 1959; Pray, 1961). These similarities indicate that each area was subjected to the same style of deformation during ancestral Rocky Mountain tectonism. Fault orientations and kinematic indicators, when combined with existing isopach maps (Kottowski, 1960; Baars, 1982) and available paleocurrent data (Altares, 1990), define a north-trending, divergent, left-lateral wrench fault system extending from the Sierra Nacimiento area

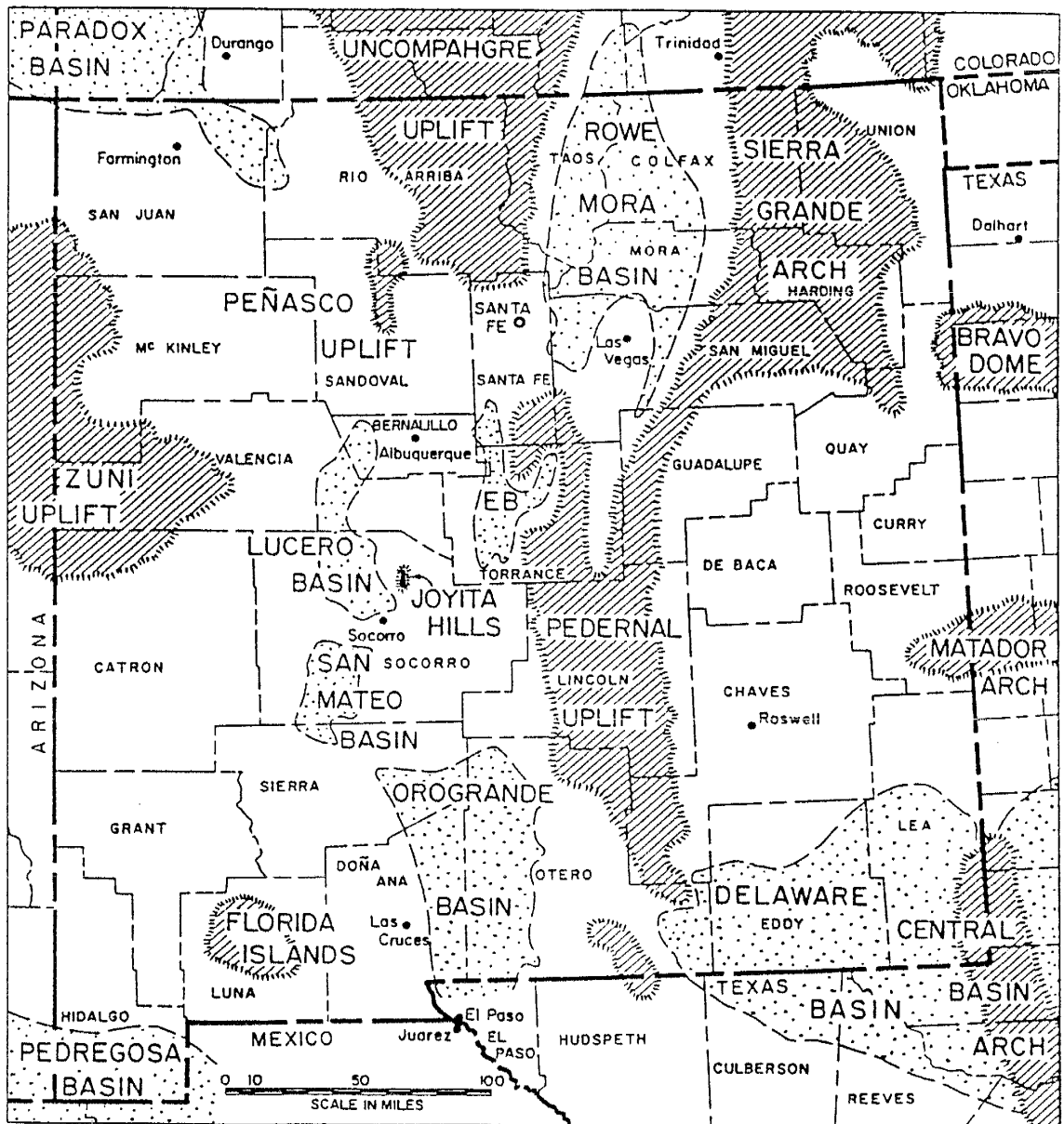


Figure 1.1. Pennsylvanian paleogeographic index map showing the location of major uplifts and depositional basins, and the location of the modern-day Joyita Hills (late Paleozoic Joyita uplift) in north-central Socorro County. From Kottlowski and Stewart (1970).

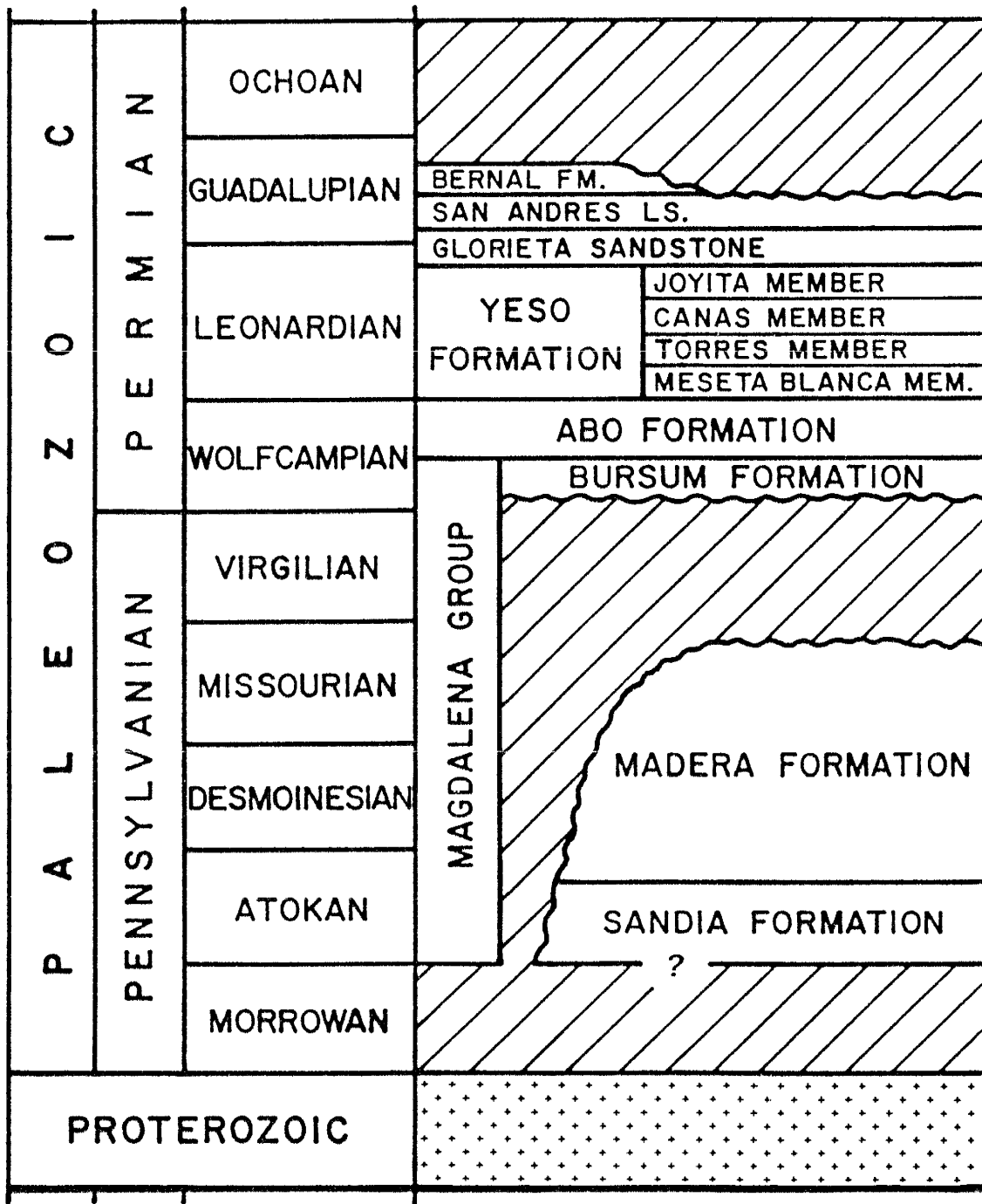


Figure 1.2. Generalized Paleozoic stratigraphic section within the Joyita Hills.

Mesozoic and Cenozoic stratigraphic units (not shown) are also exposed within the Joyita Hills and within adjacent areas (El Valle de La Joya) to the east and south.

Modified from Osburn and Lochman-Balk (1983).

southward through the Joyita Hills as a result of late Paleozoic tectonism. Similar structural features in the Sacramento Mountains are believed to be related to the same stress system.

STRUCTURAL ANALYSIS

In addition to ancestral Rocky Mountain deformation, the Joyita Hills area has also been subjected to tectonism during the Laramide orogeny and Rio Grande rift extension. A fundamental aspect of these events appears to be reactivation of existing structures. As a result, faults associated with the younger Phanerozoic tectonic events (dominantly normal and strike-slip faults) have been superimposed on structures of early Wolfcampian (Bursum Formation) and Pennsylvanian age, which makes recognition of ancestral Rocky Mountain structures difficult.

Fortunately, stratigraphic sequences that represent most of the known section within central New Mexico are well exposed within the Joyita Hills and adjacent areas to the east and south (El Valle de La Joya). Middle Permian (Leonardian and Guadalupian) and Mesozoic sedimentary strata, plus Cenozoic volcanic sequences, all postdate ancestral Rocky Mountain deformation, yet predate tectonism associated with Laramide and Rio Grande rift tectonic events. These exposures provide an opportunity to define and document Laramide and Rio Grande rift fault orientations and structural styles, which in turn provide the means by which ancestral Rocky Mountain structures may be properly reoriented and evaluated. In addition, exposures of Proterozoic rocks within the core of the Joyita Hills provide the opportunity to evaluate the influence of existing basement structures on each of the younger tectonic events.

A brief note concerning the method of analysis is required before proceeding. Field observation of brittle structures, including joint, fault, fault striae and dike orientations, indicates that each respective structural feature maintains consistent angular relationships with respect to bedding. The brittle structures (which are preferentially aligned with respect to the applied stress field), therefore, were superimposed on bedding prior

to any appreciable reorientation of strata that were horizontal at the beginning of a given deformational event. As such, in areas where rotation has occurred, proper analysis of brittle structures (and ultimately the orientation of the applied stress field) requires the restoration of strata to horizontal and a corresponding rotation of fracture patterns. In repeatedly deformed rocks, sequential rotations are required. Brittle structures are therefore treated as early-formed features within a given deformational event. This process resolves data that are initially a meaningless array of dispersed data and produces joint, striation, dike and fault patterns that define realistic orientations for principal stress axes according to Anderson's (1951) theories on near-surface brittle failure. In this paper, fault orientations associated with Laramide and Rio Grande rift deformation are presented in this manner. The combined effects of mid-Tertiary and Laramide rotation are removed in order to restore late Paleozoic and Proterozoic structures to their post-ancestral Rocky Mountain orientations.

Mid-Tertiary normal fault systems

Faults associated with the development of the Rio Grande rift define three distinct sets of conjugate normal faults (Fig. 1.3) in Proterozoic metamorphic rocks through Tertiary volcanic sequences. The two dominant sets strike to the north-northeast and northwest, respectively. Associated slickenside striations define fault displacements as dip slip. A third conjugate fault pattern, numerically less significant than the other two, strikes east-northeast. Each conjugate set defines a distinct orientation of principal stress axes, in which σ_1 ($\sigma_1 > \sigma_2 \sim \sigma_3$) was vertical (Anderson, 1951), and σ_2 was parallel to fault strike. Tertiary volcanic units within the Joyita Hills strike to the north-northeast and dip 25° – 30° to the west-northwest, indicating that the down-to-the-west rotation developed while the north-northeast-striking fault system was active. In that all three conjugate sets of normal faults are restored to realistic orientations by removing the effects of down-to-the-west rotation, each fault system must have been superimposed on bedding prior to rotation. Therefore, the northwest-striking

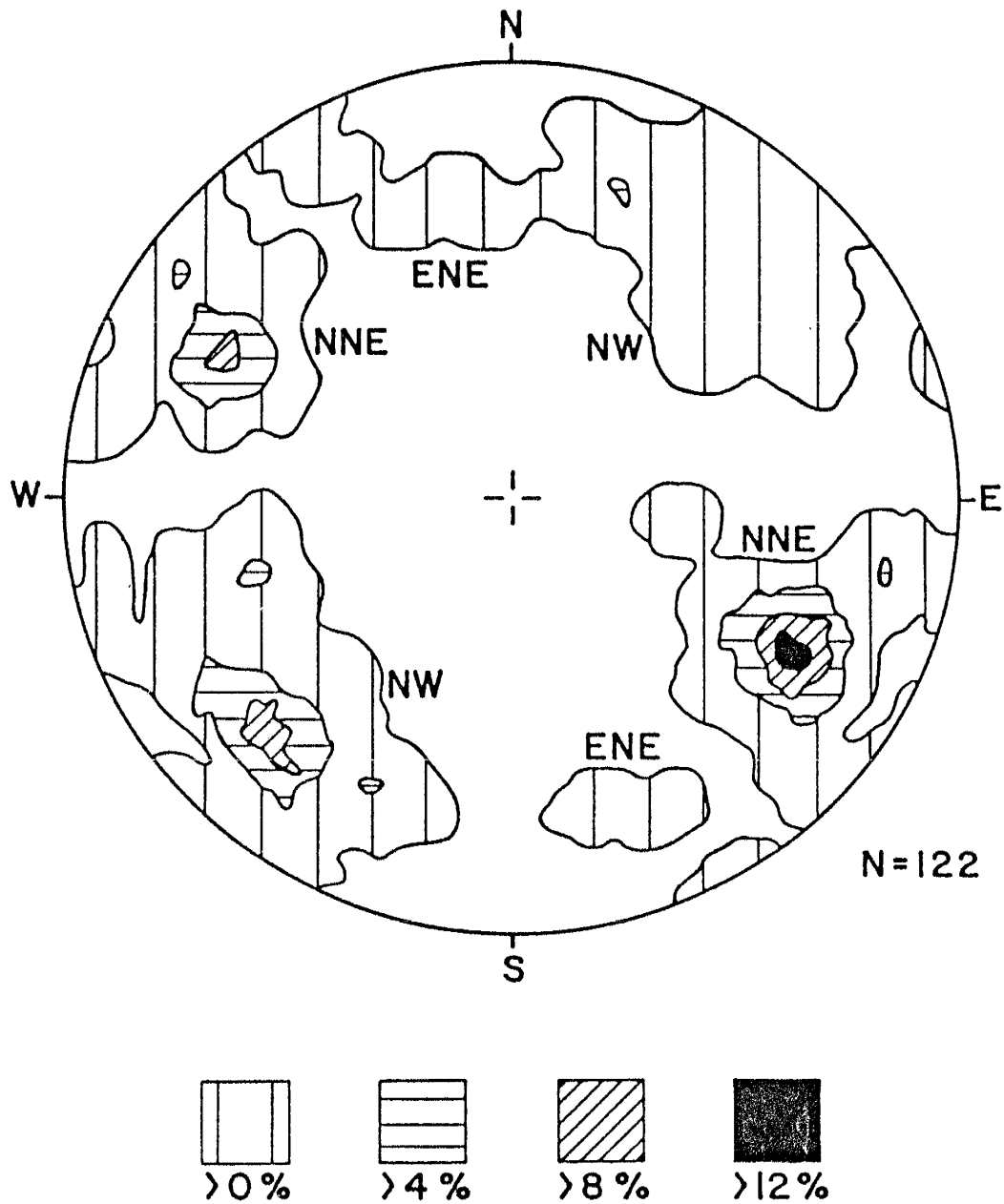


Figure 1.3. Mid-Tertiary normal fault systems. Fault orientations define conjugate pairs striking to the north-northeast (NNE), northwest (NW) and east-northeast (ENE). Lower-hemisphere, equal-area projection of poles to fault planes. Contoured at 0, 4, 8 and 12 percent intervals per one percent area.

and east–northeast–striking normal fault systems must predate the north–north–east–striking normal fault system.

Laramide strike–slip fault systems

Near vertical strike–slip faults cut Proterozoic through Cretaceous rocks (Fig. 1.4) and are marked by nearly horizontal fault striae. These faults define two separate conjugate sets of strike–slip faults (σ_2 vertical). North–striking synthetic shears (interpreted as both synthetic (NNE) and secondary synthetic (NNW) shears) and east–northeast–striking antithetic shears developed in a north–trending, right–lateral wrench zone (Christie–Blick and Biddle, 1985, fig. 5a; Chapin, 1983). Brown (1987) documented right–lateral, strike–slip displacement along the northeast–striking Montosa fault zone, which lies 13 mi (21 km) to the east of the Joyita Hills. A conjugate set of right–lateral, northeast–striking (synthetic) shears and less well–defined northwest–striking (antithetic) shears within the Joyita Hills are thought to be related to movement along the Montosa fault zone.

Ancestral Rocky Mountain fault systems

Two sets of normal faults which offset early Wolfcampian (Bursum Formation) strata, Pennsylvanian strata and Proterozoic rocks (Fig. 1.5) are interpreted to be ancestral Rocky Mountain faults because: 1) they cannot be traced into, nor found within, middle to late Wolfcampian (Abo Formation) or younger strata; or 2) they display differences in fault character between Bursum and older rocks versus Abo and younger strata. Respectively, the two fault sets consist of north–striking, west–dipping normal faults and northwest–striking, southwest–dipping normal faults. Both sets were reactivated during Tertiary rifting.

North–striking normal faults

A series of near vertical, north–striking faults have only been observed within Proterozoic, Pennsylvanian and early Wolfcampian rocks. These faults are all marked with

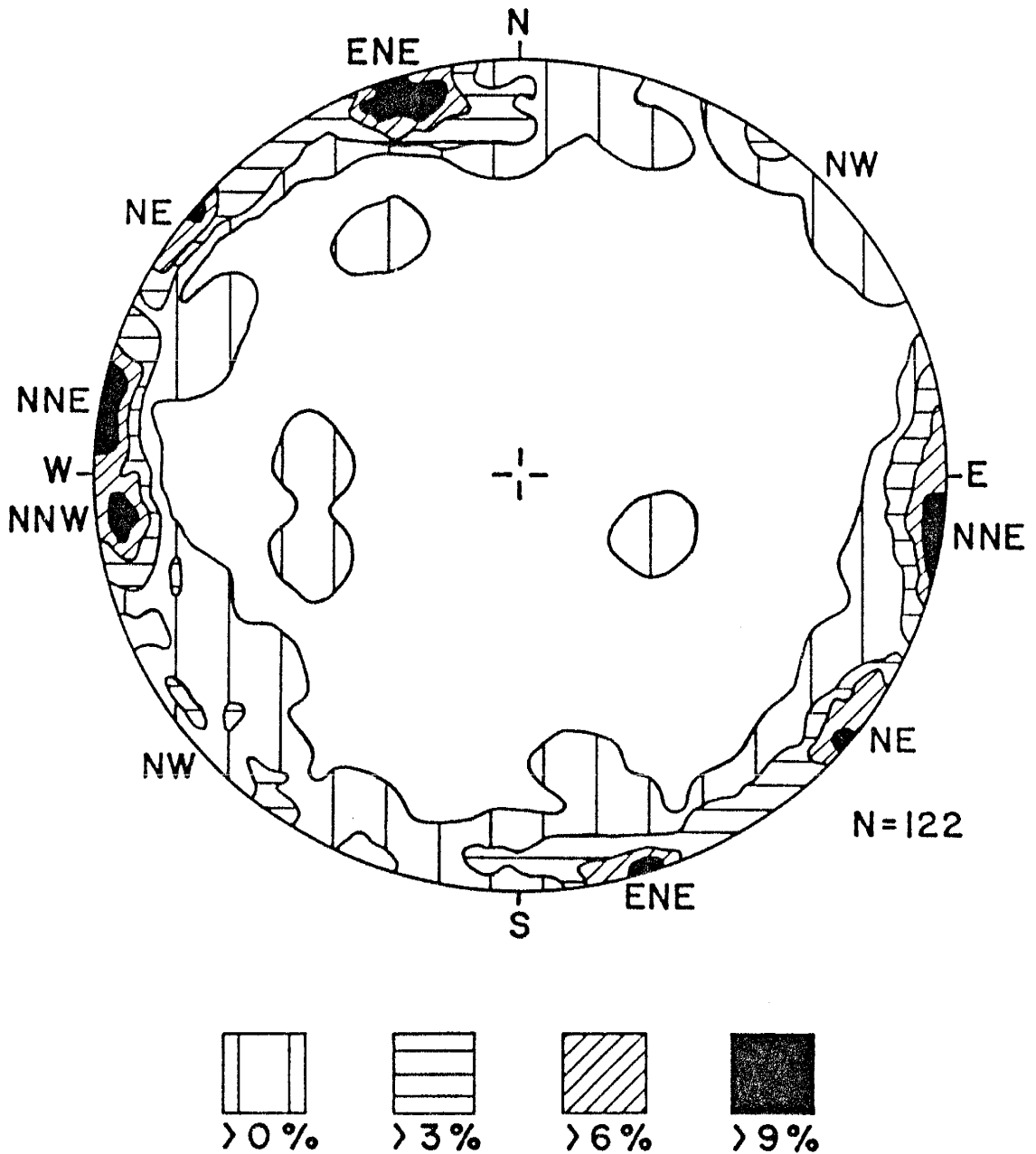
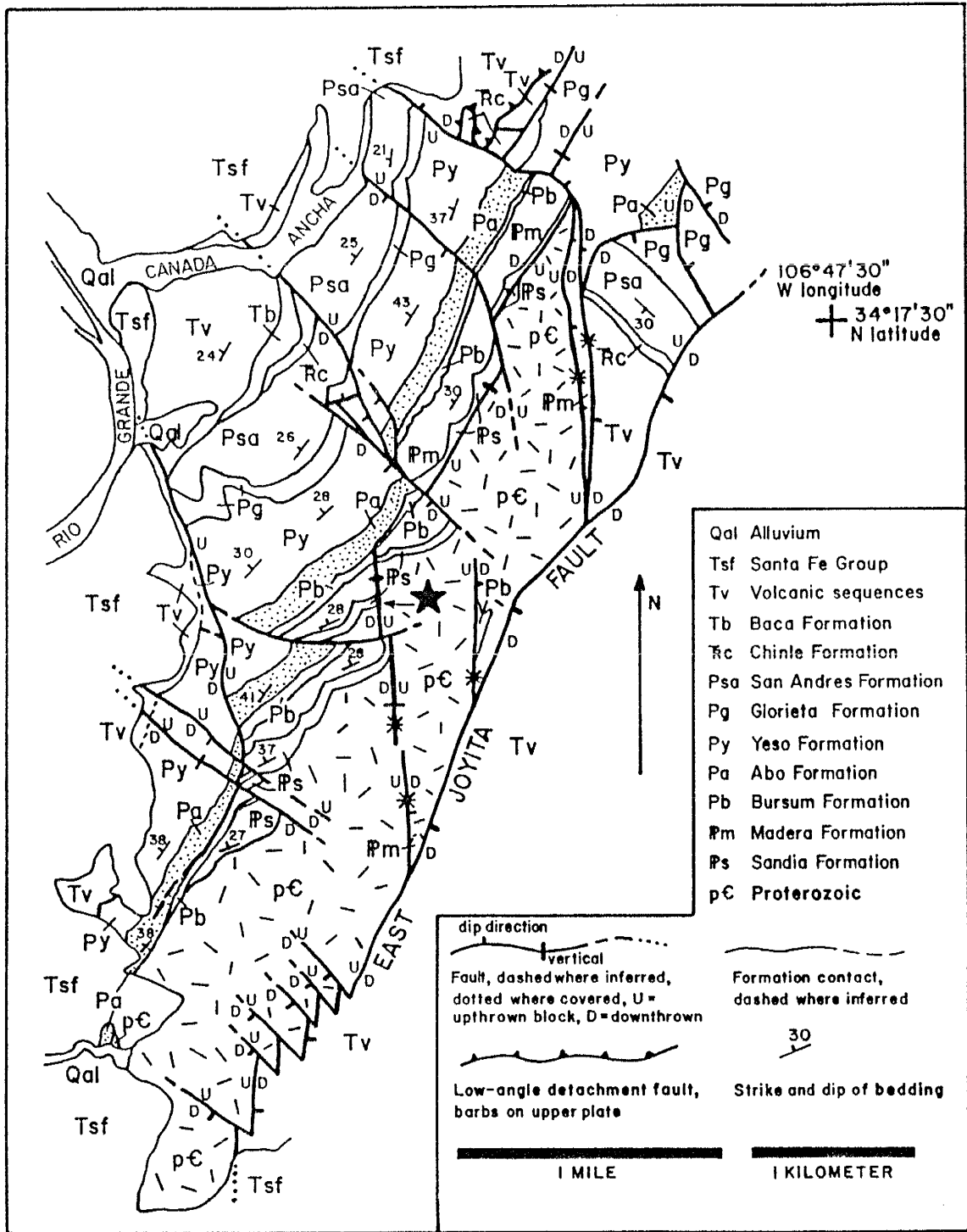


Figure 1.4. Laramide strike-slip fault systems. Near-vertical strike-slip faults striking to the north-northeast (NNE), north-northwest (NNW) and east-northeast (ENE) define a north-trending, right-lateral wrench fault system. Additional strike-slip faults strike northeast (NE) and northwest (NW). Lower-hemisphere, equal-area projection of poles to fault planes. Contoured at 0, 3, 6 and 9 percent intervals per one percent area.

Figure 1.5. Generalized geologic map of the Joyita Hills. Star denotes westernmost north–striking fault described in text and illustrated in Figure 1.6. Other north–striking faults are designated with asterisk pattern along fault trace. Sandia and Madera Formations are successively truncated southward by the Bursum Formation. The Abo Formation (stipple pattern) truncates the Bursum Formation and is in depositional contact with Proterozoic rocks in the southern Joyita Hills. Modified from Kottlowski and Stewart (1970).

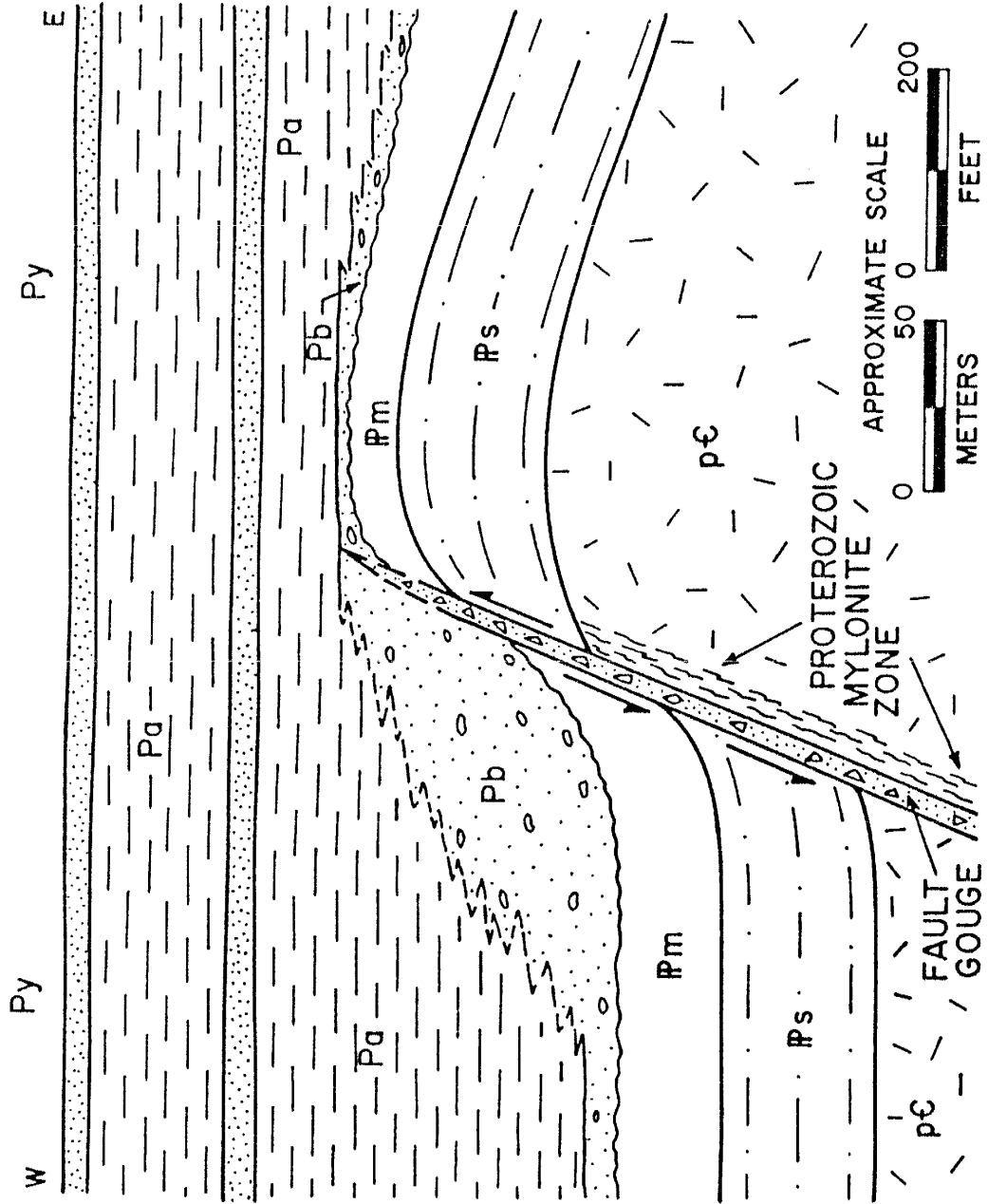


fault striae that plunge 50° – 60° south and display both down–to–the–west and down–to–the–east displacements. The westernmost fault of this series can be traced from Proterozoic rocks into the overlying Sandia, Madera and Bursum Formations, but is overlain by unfaulted strata of the Abo Formation, and is therefore interpreted as an ancestral Rocky Mountain fault (Fig. 1.6). Down–to–the–west fault displacement juxtaposes middle Madera Formation limestones in the hanging wall against the Sandia Formation/Proterozoic contact in the footwall. Stratigraphic separation is approximately 300 ft (100 m). Associated folding deformed the Sandia, Madera and Bursum units into an anticlinal (footwall, east block) and synclinal (hanging wall, west block) fold pair. Erosionally thinned strata of the Madera Formation in the footwall are overlain by depositionally thinned Bursum/Abo Formation sequences, which thicken to both east and west. This westernmost fault, although complicated by younger, cross–cutting faults and poor exposure along the Bursum/Abo Formation contact, is interpreted to be a buried ancestral Rocky Mountain fault that has not been reactivated.

Fault and striation orientations observed along the more eastward of the north–striking faults are the same as those observed along the westernmost fault. Therefore, each of the north–striking faults is thought to have been active as a down–to–the–west fault during late Paleozoic tectonism. Yet the observed displacement on the more eastward of these faults is down–to–the–east. In one outcrop, south–plunging striations have been overprinted by dip slip (near vertical) striations, indicating that these eastward faults have been reactivated by younger tectonism. The easternmost faults are found in proximity to the East Joyita fault, and the down–to–the–east displacement is considered to be the result of reactivation of this ancestral Rocky Mountain fault trend during Tertiary, down–to–the–east, dip–slip displacement along the East Joyita fault.

Rotation of regional bedding within Abo and younger strata to horizontal restores these near–vertical, north–striking faults to their post–ancestral Rocky Mountain

Figure 1.6. Generalized cross section along westernmost north-striking normal fault. Cross section has been restored to its post-ancestral Rocky Mountain orientation by removing 30° of down-to-the-west rotation about a N35°E, horizontal axis. Py = Yeso; Pa = Abo; Pb = Bursum; Pm = Madera; Ps = Sandia; p-C = Proterozoic basement. Fault and contacts dashed where obscured.



orientation which was north–striking and west–dipping at 65° – 70° , with a normal sense of displacement (Fig. 1.7; Baars, 1982, figs. 3 and 4). The fold hinge then plunges 10° – 15° north. South–plunging striations and mullion observed along these faults, when similarly rotated, rake 63° southward, and define fault displacement as normal, left–oblique slip.

Northwest–striking normal faults

Field relationships indicate that northwest–striking normal faults were active during both Tertiary rifting and ancestral Rocky Mountain deformation. Where they cut Abo Formation and younger strata, northwest–striking normal faults occur along discrete fault planes with limited brecciation, and display conjugate dip directions to the southwest and northeast (Fig. 1.3). In contrast, northwest–striking normal faults cutting only Bursum and older rock sequences occur as 10 to 20 ft (3 to 7 m) wide zones of highly brecciated rock, and dip consistently to the southwest.

Restored orientations of northwest–striking normal faults cutting only Bursum Formation and older rock sequences strike northwestward and dip steeply (75° – 80°) to the southwest (Fig. 1.8). Striations on these faults, when comparably restored, indicate nearly pure dip–slip displacement.

Proterozoic Mylonites and Foliations

Proterozoic rocks within the core of the Joyita Hills are gneissic to mylonitic. Foliations (Fig. 1.9) define three distinct trends: East–northeast, north, and northwest. Comparison of north– and northwest–striking foliations with ancestral Rocky Mountain brittle fault orientations (Figs. 1.7 and 1.8) indicates that orientations are similar. Through direct field observation, the westernmost north–striking brittle fault that offsets only Proterozoic rocks, and Sandia, Madera and Bursum Formations is known to have overprinted and reactivated a north–striking mylonite zone. Northwest–striking

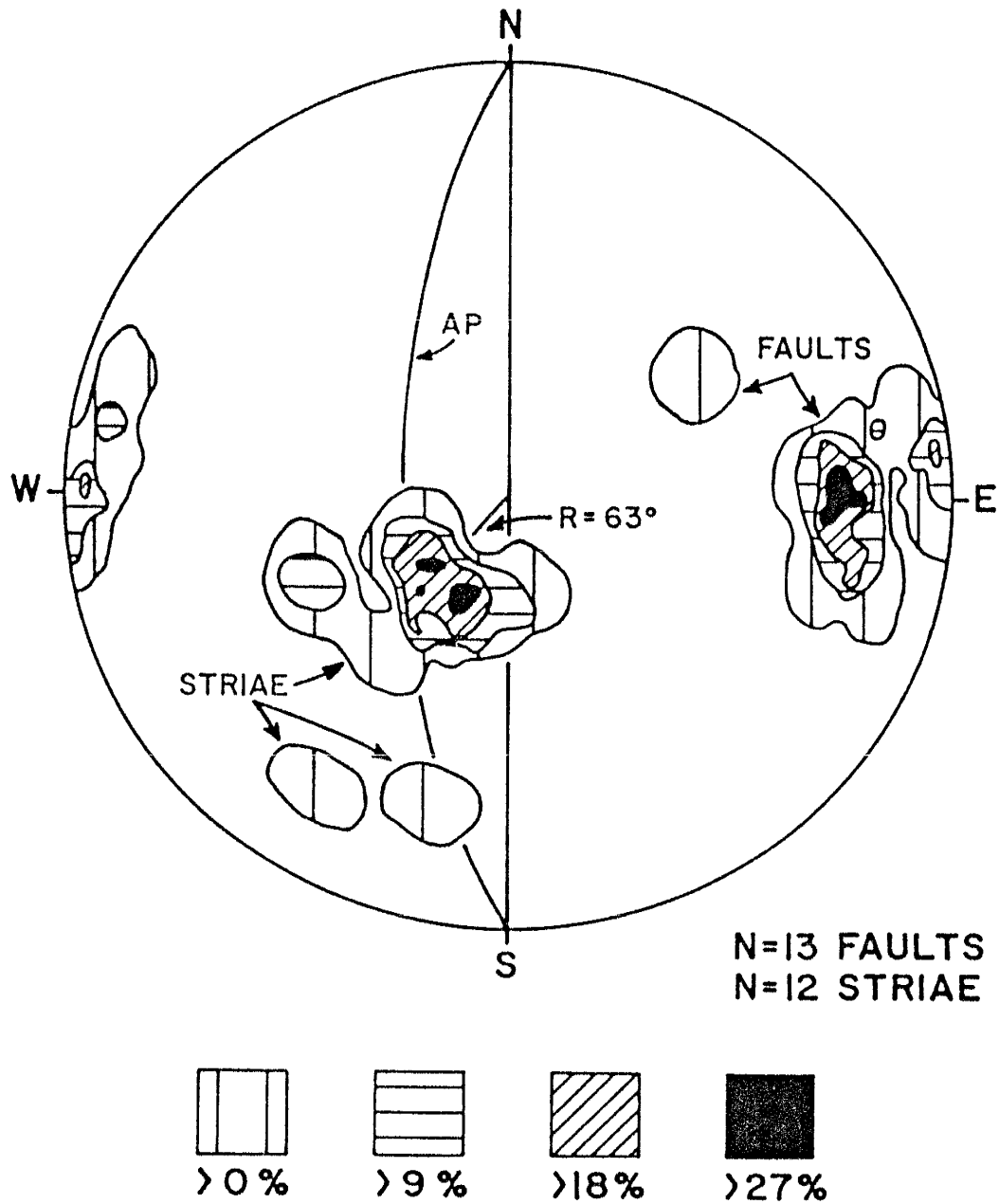


Figure 1.7. North-striking ancestral Rocky Mountain normal faults. Composite, lower-hemisphere, equal-area projection of poles to fault planes and fault striae. Contoured at 0, 9, 18 and 27 percent intervals per one percent area. AP defines average fault plane orientation; R defines approximate angle of rake of fault striae.

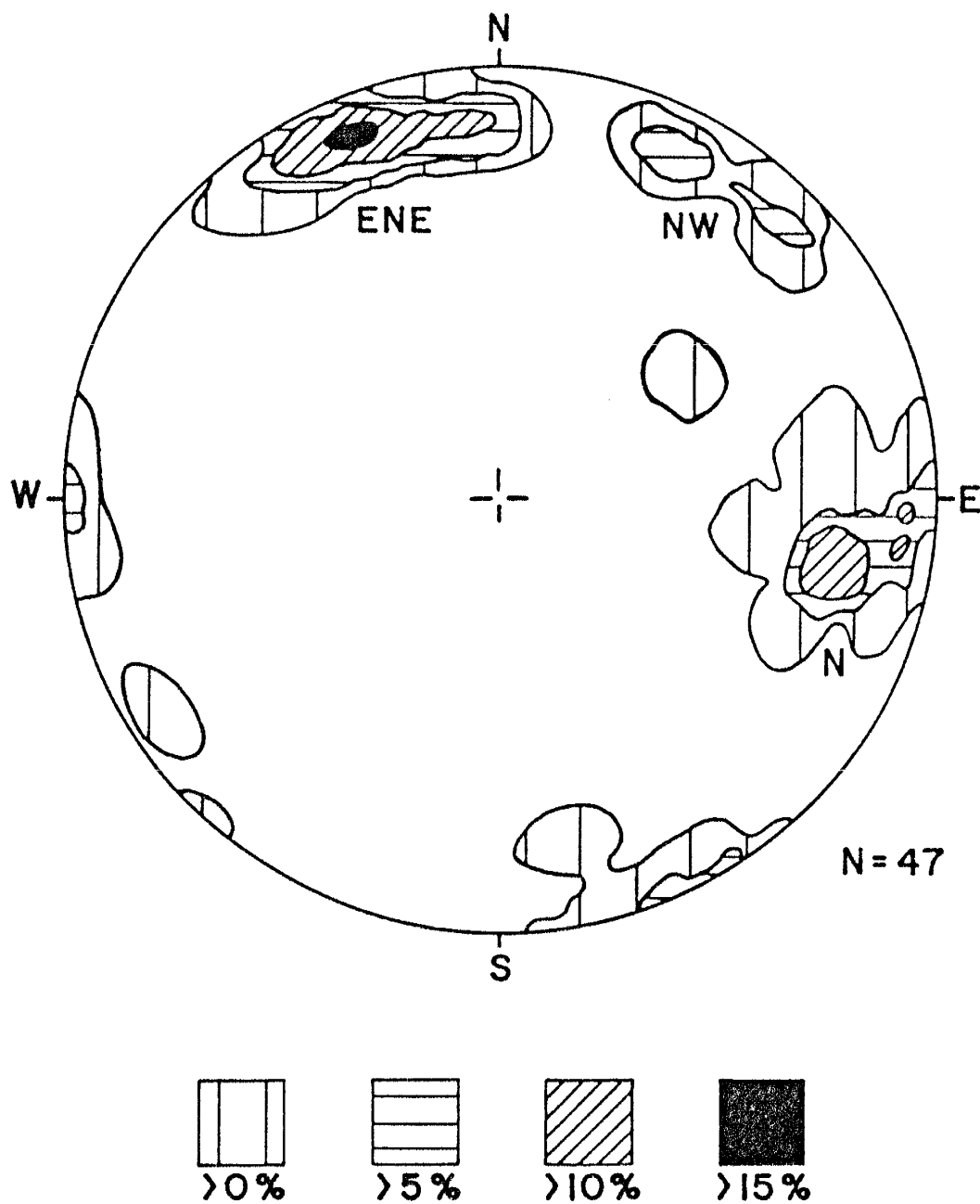


Figure 1.9. Preferred orientations of Proterozoic gneissic to mylonitic foliations define three common trends: North (N), northwest (NW) and east-northeast (ENE) Lower-hemisphere, equal-area projection of poles to foliations, contoured at 0, 5, 10 and 15 percent intervals per one percent area.

brittle faults display comparable orientations to northwest–striking foliations; however, direct observation of reactivation has not yet been demonstrated in the field.

Comparison of gneissic and mylonitic foliations with Laramide (Fig. 1.4) and Rio Grande rift (Fig. 1.3) structures further illustrates the influence of Proterozoic foliations on the development of younger Phanerozoic structures. In short, the Phanerozoic structural evolution of the modern–day Joyita Hills was strongly influenced by basement control and the repeated reactivation of existing Proterozoic foliations and mylonite zones during each major Phanerozoic tectonic event.

Depositional Basin Trends

A mineral exploration hole on the west flank of the Magdalena Mountains, south of Kelly, cored 2009 ft (612 m) of Pennsylvanian strata (Krewedl, 1974; Chapin, unpublished core log). This indicates that the San Mateo and Lucero basins are one continuous, north–trending basin (Fig. 1.10) which bounds the Joyita uplift to the west. [The Lucero portion of this basin is mislabeled as the Acoma sag on figure 2 of Baars, 1982. Note also that the thickness of the Pennsylvanian System in the Ladron Mountains used by Baars for the isopachs of figure 2 is much less than that reported by either Kottowski, 1960, or Siemers, 1983.] A prong extending southeastward from the San Mateo/Lucero basin bounds the Joyita uplift to the south and southwest. Isopach trends (Fig. 1.10; Kottowski, 1960) between the modified San Mateo/Lucero basin and the Joyita uplift parallel the fault trends defined as ancestral Rocky Mountain normal faults and delineate the uplift margins.

When paleocurrent data from early Wolfcampian Bursum strata (Altares, 1990) are superimposed on the Pennsylvanian isopach map (Fig. 1.10), it appears that the southeast–trending prong of the San Mateo/Lucero basin may have been more extensive than originally defined by Kottowski (1960). Altares' (1990) field area spans the north–south dimension of the prong. Paleocurrent data north of the prong indicate paleoflow directions to the west, southwest and south, that is, basinward with respect

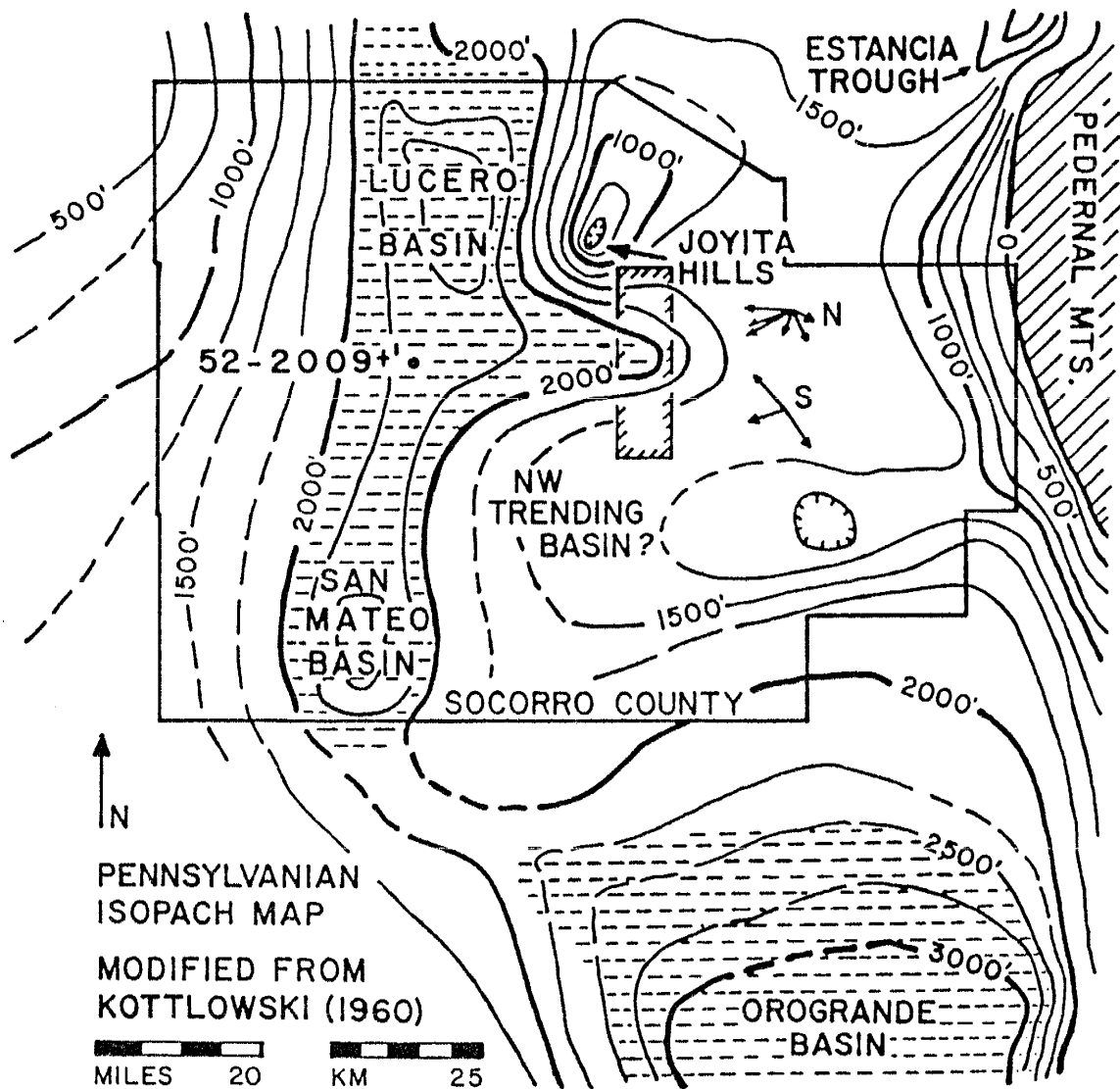


Figure 1.10. Modified Pennsylvanian isopach map superimposed with early Wolfcampian paleocurrent directions from Altares (1990). Hatchured box outlines location of Altares (1990) field area. Paleocurrent directions (vector means) labeled N and S are from the north and south of Altares' field area; length of each vector is proportional to vector strength. Drill-core data (C.E. Chapin, unpublished core log; control point number 52, Kottowski, 1960) documents stratigraphic thickness of Pennsylvanian rocks to be in excess of 2000 ft (610 m), and redefines the Lucero and San Mateo basins as one continuous, north-trending basin.

to the prong. Paleocurrent data south of the prong, however, do not show north- and northeast-directed paleoflow directions as would be expected from isopach trends along the southern margin of the prong. Thus, the axis of the prong lay farther to the southwest. Isopachs between the San Mateo/Lucero basin and the Orogrande basin to the southeast are poorly defined, due to a paucity of control points. However, the combination of the southeast-trending prong of the San Mateo/Lucero basin, paleoflow directions to the west, southwest and south, and a southeast-trending trough between the southern end of the San Mateo/Lucero basin and the northern end of the Orogrande basin suggests that the two basins were connected by a (perhaps complex) southeast-trending channel during the late Paleozoic. Alternatively, the San Mateo/Lucero basin may be a fragment of another basin displaced northward by Laramide, right-lateral wrench faults (Chapin and Cather, 1981; Chapin, 1983).

DISCUSSION AND INTERPRETATION

Two normal fault systems have been identified as ancestral Rocky Mountain in age. Although each fault trend has been reactivated to some extent during subsequent tectonism, existing isopach maps confirm both fault trend and sense of displacement. Brittle kinematic indicators (striations and mullion structures) define fault displacements as dominantly dip slip, with north-striking faults showing a component of left slip. Furthermore, fault orientations are either known to represent (north-striking faults) or can be reasonably concluded to represent (northwest-striking faults) reactivation of Proterozoic shear zones. The fault orientations associated with the Joyita uplift, and basin trends within Socorro County, are comparable to structures identified as ancestral Rocky Mountain structures to both the north and south.

To the north, as originally proposed by Read and Wood (1947) and confirmed by Baars (1982), anomalously thin Pennsylvanian sequences define a north-trending, structurally positive element extending from the Nacimiento-San Pedro area (Penasco uplift of Kottowski and Stewart, 1970; Fig. 1.1) southward to the Joyita Hills. Fault

orientations (Figs. 1.6 and 1.7) are comparable to those of Baars (1982, figs. 3 and 4) for the western margin of the uplift. The redefined San Mateo/Lucero basin (Fig. 1.10) borders the uplift on the west.

In the Sacramento Mountains to the south, faults with similar styles have been interpreted as late Paleozoic structures (Roswell Geological Society, 1956; Otte, 1959; Pray, 1961). Dip-slip displacement occurred along a series of north-striking, high-angle and vertical, normal faults (e.g., Fresno, Arcente, Alamo and Bug Scuffle faults), some of which (Alamo and Bug Scuffle) show a scissors-like sense of displacement. The area between the eastern shelf sediments exposed in the Sacramento Mountains and the Orogrande basin has been interpreted by Pray (1961) to be a narrow, north-south transition zone. This transition zone was probably a west-dipping normal fault zone (Roswell Geological Society, 1956) comparable to west-dipping faults exposed within the Sacramento Mountains, and similar to basin boundaries in the San Mateo/Lucero basin to the north.

The anticlinal/synclinal folds exposed within the Sacramento Mountains (Pray, 1961) are commonly associated with the dominantly down-to-the-west normal faults, and are comparable in both style and orientation to the fold exposed within the Joyita Hills along the westernmost, north-striking normal fault (Fig. 1.6). If analogy can be made with structures in the Joyita Hills, then the north-striking normal faults within the Sacramento Mountains may represent reactivation of basement structures. The north-trending folds commonly associated with north-striking normal faults probably represent a flexure of sedimentary strata above older basement flaws as these faults propagated upsection and cut into overlying strata.

Baars (1982) documented several episodes of displacement along the Nacimiento fault during ancestral Rocky Mountain deformation, the youngest in post-Madera, pre-Abo time. Within the Joyita Hills, Kottlowski and Stewart (1970) defined the timing of major uplift as early Wolfcampian, and Pray (1961) concluded that ancestral

Rocky Mountain deformation within the Sacramento Mountains was late Pennsylvanian to early Wolfcampian. Therefore, the timing of the latest, and perhaps the major, phase of uplift within the three areas was approximately synchronous.

It cannot be stated with certainty that the southern end of the modified San Mateo/Lucero basin and the northern end of the Orogrande basin were connected by a southeast-trending trough. However, northwest-trending isopachs, as originally drawn by Kottowski (1960), and early Wolfcampian paleocurrent data (Altares, 1990), support this interpretation. As defined, basin locations and trends suggest that a continuous, and perhaps quite complex, depositional channel extended from the San Mateo/Lucero basin to the Orogrande basin during the late Paleozoic (Figs. 1.10 and 1.11).

In central New Mexico, ancestral Rocky Mountain tectonism resulted in basins and uplifts of dominantly north and subordinate northwest trend. The San Mateo/Lucero and Orogrande basins are aligned in a north-trending, left-stepping en-echelon pattern. The two basins were probably connected by a southeast-trending channel. Bounding structures are high-angle to vertical normal faults, with north-striking faults showing a component of left slip. Restored fault geometries and kinematic indicators, when combined with spatial relationships of basin location and trend, define an overall system compatible with subsidiary left-lateral displacement along a north-striking, dominantly normal fault zone extending through central and southern New Mexico (Fig. 1.11). The inferred wrench fault system must have been largely divergent in order to accommodate fault displacements that were dominantly dip slip. The inferred southeast-trending basin between the San Mateo/Lucero and Orogrande basins is envisaged as either a releasing bend or a rhomb-graben between two left-stepping, north-striking wrench faults (Ramsay and Huber, 1987, figs. 23.37 and 23.38; Sylvester, 1988, fig. 20). The latter alternative is presented in Figure 1.11. Although fault geometries and associated kinematics are compatible with this interpretation, the

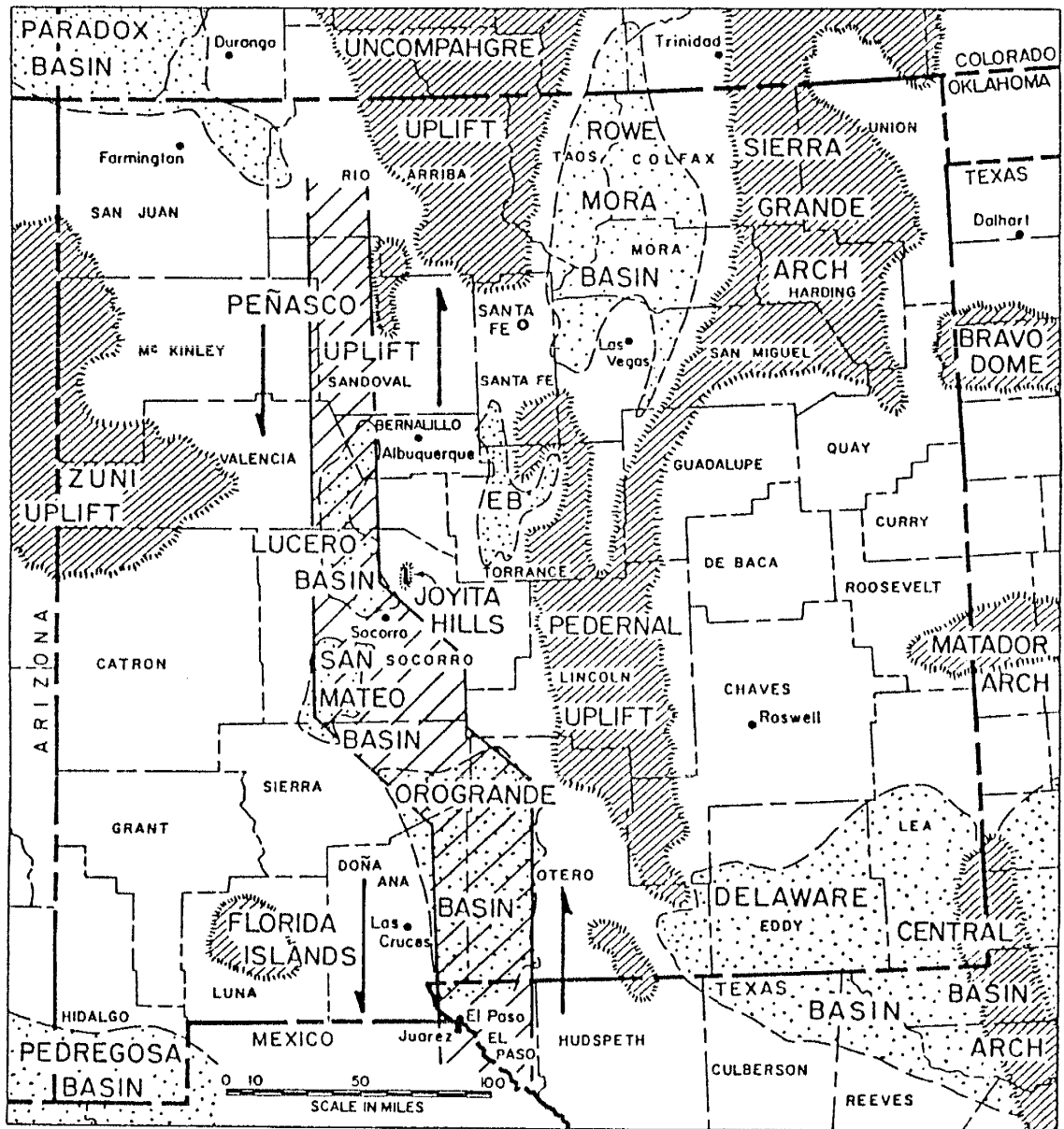


Figure 1.11. Hypothetical late Paleozoic, north-trending, left-lateral wrench zone within central and southern New Mexico. North-trending basins (San Mateo/Lucero basin and Orogrande basin) developed within principal zones of left-lateral shear. The inferred northwest-trending basin connecting the southern end of the San Mateo/Lucero basin and the northern end of the Orogrande basin is shown as a rhomb-graben between two left-stepping, left-lateral shear zones.

principal hindrance to demonstrating such a wrench zone is due to younger deformation. Laramide, right-lateral, north-trending wrench systems have been interpreted within New Mexico by Chapin and Cather (1981) and Chapin (1983), along the Nacimiento fault by Baltz (1967), and within the Joyita Hills (Fig. 1.4). Overprinting of strike-slip systems of comparable trend but opposite sense of displacement makes reconstruction difficult. However, it is important to note that restoration of approximately 60 mi (100 km) of Laramide right-slip (Chapin and Cather, 1981; Chapin, 1983) would significantly diminish the northeast-southwest dimension of the rhomb-graben depicted in Figure 1.11. Restoration would roughly align the southeast-trending prong at the southern end of the Lucero basin with the northwest-trending trough at the northwestern end of the Orogrande Basin (Fig. 1.10).

CONCLUSIONS

This paper has presented new structural data from the Joyita uplift and drill-core data from the adjacent Lucero and San Mateo basins. The structural data define the Joyita uplift as a north-trending positive element, bound to the west and southwest by depositional basins. Drill-core data indicate that the San Mateo and Lucero basins are one continuous, north-trending basin. The basin probably extends southeastward into the Orogrande basin.

Although the area from which these data are obtained is relatively small with respect to the area to which they are applied, fault orientations and modified basin trends are compatible with interpretations of previous investigators in adjacent areas. The similar basin and uplift trends, fault orientations and sense of offset, and timing of deformation indicates that, during the ancestral Rocky Mountain orogeny, a large area of the crust in New Mexico experienced a comparable deformational history. The combination of basin and uplift geometries, brittle kinematic indicators and available paleocurrent data suggest a north-trending, divergent, left-lateral wrench system extended through central and southern New Mexico during the late Paleozoic.

Part 2

**POLYDEFORMATION IN THE JOYITA HILLS, CENTRAL NEW MEXICO,
U.S.A.: STRUCTURAL ANALYSIS THROUGH CONSIDERATION OF
INITIAL FRACTURING**

Submitted to the Journal of Structural Geology

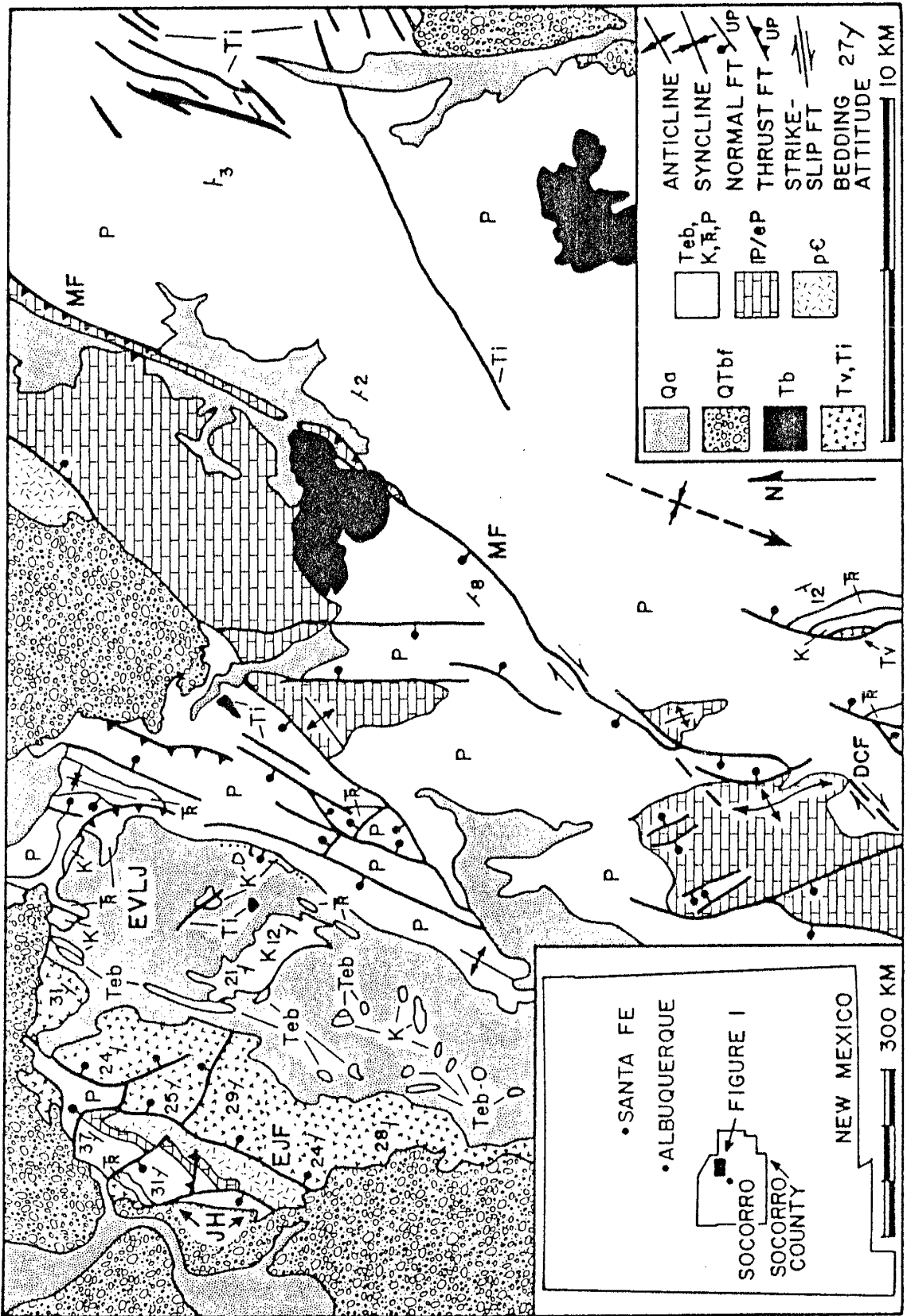
April 30, 1992

INTRODUCTION

Detailed field observation of more than 1700 joint, fault, fault striation and dike orientations within sedimentary and volcanic rocks of the Joyita Hills, central New Mexico, indicates that tectonically induced brittle fractures do not demonstrate preferred orientations with respect to three-dimensional space, *per se*, as is simply assumed in classical orientation analyses. More specifically, observation indicates that each of the forementioned structural elements form consistent angular relationships with respect to bedding. These relationships can be readily demonstrated by plotting fracture orientations with respect to bedding, which is accomplished by computerized rotation of inclined strata to horizontal combined with a corresponding rotation of observed fracture patterns. This analytical method, therefore, treats joints and faults as structures superimposed upon bedding prior to any appreciable rotation within a given deformational event. Plotting tectonically induced fracture patterns with respect to bedding, rather than with respect to three-dimensional space, readily defines realistic orientations of applied stress fields in which the fracture patterns accord with Anderson's (1951) theories of near-surface faulting. Resultant interpretations indicate that both joints and small-displacement faults are mainly early formed structural elements within a specific tectonic episode.

This analytical technique has been applied to fracture orientations observed within the Phanerozoic stratigraphy of the Joyita Hills area of central New Mexico, USA (Fig. 2.1) and has been used to evaluate stress orientations associated with Rio Grande rift and Laramide tectonism. Comparative analysis of fault orientations, plotted with respect to three-dimensional space (field-recorded orientations), versus those plotted with respect to bedding (computerized rotation, or "restored" orientations) form the basis of the following analyses. Fault orientations are supplemented with fault striation, joint, fold axis and dike orientations, most of which, in the interest of minimizing figures, are presented as "restored" orientations. The arguments that follow discuss

Figure 2.1. Generalized geologic map of northeast Socorro County, New Mexico. Data presented herein were collected from Proterozoic and Phanerozoic exposures within the Joyita Hills (JH) and El Valle de La Joya (EVLJ). Regional faults include the East Joyita fault (EJF), Del Curto fault (DCF) and Montosa fault (MF). pЄ = Proterozoic; P/eP = Pennsylvanian and earliest Permian strata; P = Permian strata; T₃ = Triassic strata; K = Cretaceous strata; Teb = Eocene basin deposits; Tv = Oligocene volcanics; Ti = Oligocene intrusives (dikes and plugs); Tb = Pliocene basalt flows; QTbf = Quaternary and Tertiary basin fill; Qa = Quaternary alluvium. Modified from Osburn (1984) and Myers *et al.* (1986).



resultant interpretations and implications of initial fracturing as a fundamental aspect of shallow crustal, brittle deformation.

It is emphasized from the outset that the consistency between fracture orientation and bedding may be alternatively attributed to elastic plate theory combined with bedding-parallel frictionless slip. Practical applications of this kind have been provided by Reches (1978) and Jackson and Pollard (1990). Their respective analyses are cited because both provide a thorough and reasonable account for their observations and interpretations, and both provide a means of comparing a recognized analytical technique with the analytical technique utilized herein. It is also emphasized that the concept of joint and fault generation during the early stages of deformation is not new (e.g., Melton, 1929; Parker, 1942; Reches, 1976, 1978; Beck, 1984; Beck and Burford, 1985). The results of this study indicate that the concept of initial fracturing provides a viable alternative to elastic plate theory and frictionless boundary conditions to account for the consistency between fracture orientation and bedding. Moreover, the results indicate that workers cannot assume, without evidence, that faults and joints in any area have maintained the orientations in which they formed. Careful consideration of later reorientation of these brittle structures allows analysis in areas where rotation subsequent to jointing and faulting can be demonstrated.

Study area

The Joyita Hills area is a complexly faulted, west-tilted, normal-fault block within northeast Socorro County, New Mexico (Fig. 2.1). Exposures of Proterozoic augen gneiss within the core of the Joyita Hills are overlain by approximately 4 km of inclined Phanerozoic sedimentary and volcanic strata within the Joyita Hills and adjacent areas to the east (El Valle de La Joya; Figs. 2.1, 2.2). These exposures reveal a wealth of structures associated with crustal extension, wrench tectonics and to a lesser extent, compressional thrusting. Phanerozoic structures are the result of at least three recognizable orogenic episodes: Ancestral Rocky Mountain, Laramide and Rio Grande rift.

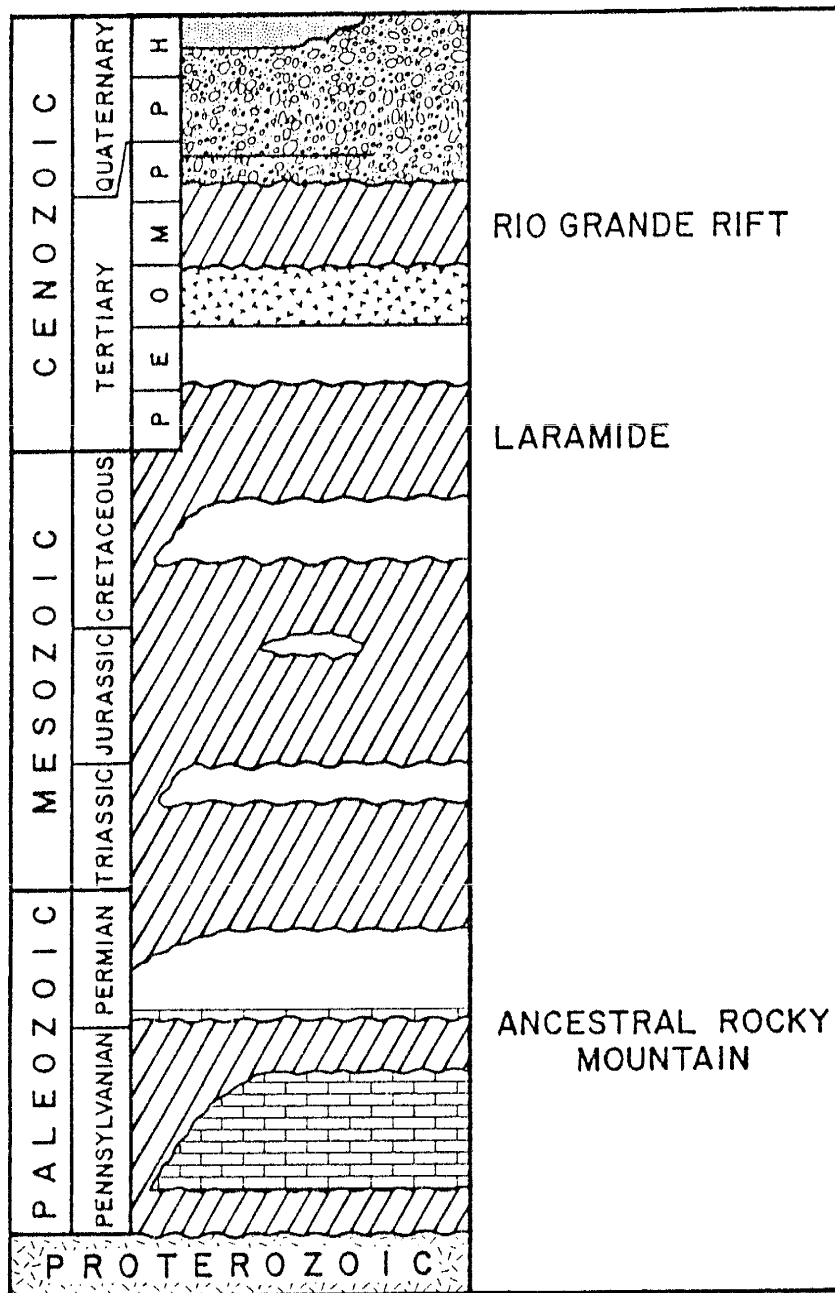


Figure 2.2. Generalized stratigraphy exposed within the Joyita Hills and El Valle de La Joya. Initially horizontal sedimentary and/or volcanic sequences were deposited prior to and after each recognized tectonic episode, allowing a direct correlation between observed fracture patterns and specific orogenic events. Patterns correlate with those of Fig. 2.1; diagonal rule indicates absence (either non-deposition or erosion) of stratigraphic record. Modified from Osburn and Lochman-Balk (1983).

A fundamental aspect of this deformation appears to be reactivation of existing structures. Fortunately, each known Phanerozoic tectonic event was separated by a period of tectonic quiescence and deposition of initially horizontal sedimentary and/or volcanic sequences, which record fracture patterns and structural styles that developed during each succeeding orogeny. The stratigraphic sequences that specific fracture patterns and associated structural styles overprint, and just as importantly, those which they do not, are used to correlate specific stress–field orientations with individual tectonic events.

Although both ductile (Proterozoic) and brittle (Phanerozoic) structures are well exposed, emphasis has been placed on brittle structures superimposed on the Phanerozoic stratigraphy. Foliations within Proterozoic basement rocks are gneissic to mylonitic, and are cross–cut by amphibolite, pegmatite and aplite dikes. Preferred orientations of foliations have been determined in order to evaluate the influence of basement control and the extent to which reactivation of existing structures has occurred.

REASONING, TERMINOLOGY AND METHODS

It should be emphasized that the reasoning behind the method of analysis does not stem from either mathematical or mechanical considerations, but rather is the result of direct field observation. Fracture patterns, formed by either joints, faults or occasionally both, formed angular relationships similar to those proposed by Anderson (1951) for near–surface brittle failure. Anderson theorized that in near–surface, brittle deformation, the applied stress field should be oriented such that one of the principal stress axes should be vertical, and two principal stress axes horizontal (Fig. 2.3). Conjugate faults (Hobbs *et al.* 1976; Davis, 1984; Price, 1966; Price and Cosgrove, 1990; complementary faults of Anderson, 1951) would be symmetrically disposed about these axes, such that each fault orientation would make an equal angle with respect to horizontal. Observation in the field, however, indicated that what appeared to be conjugate

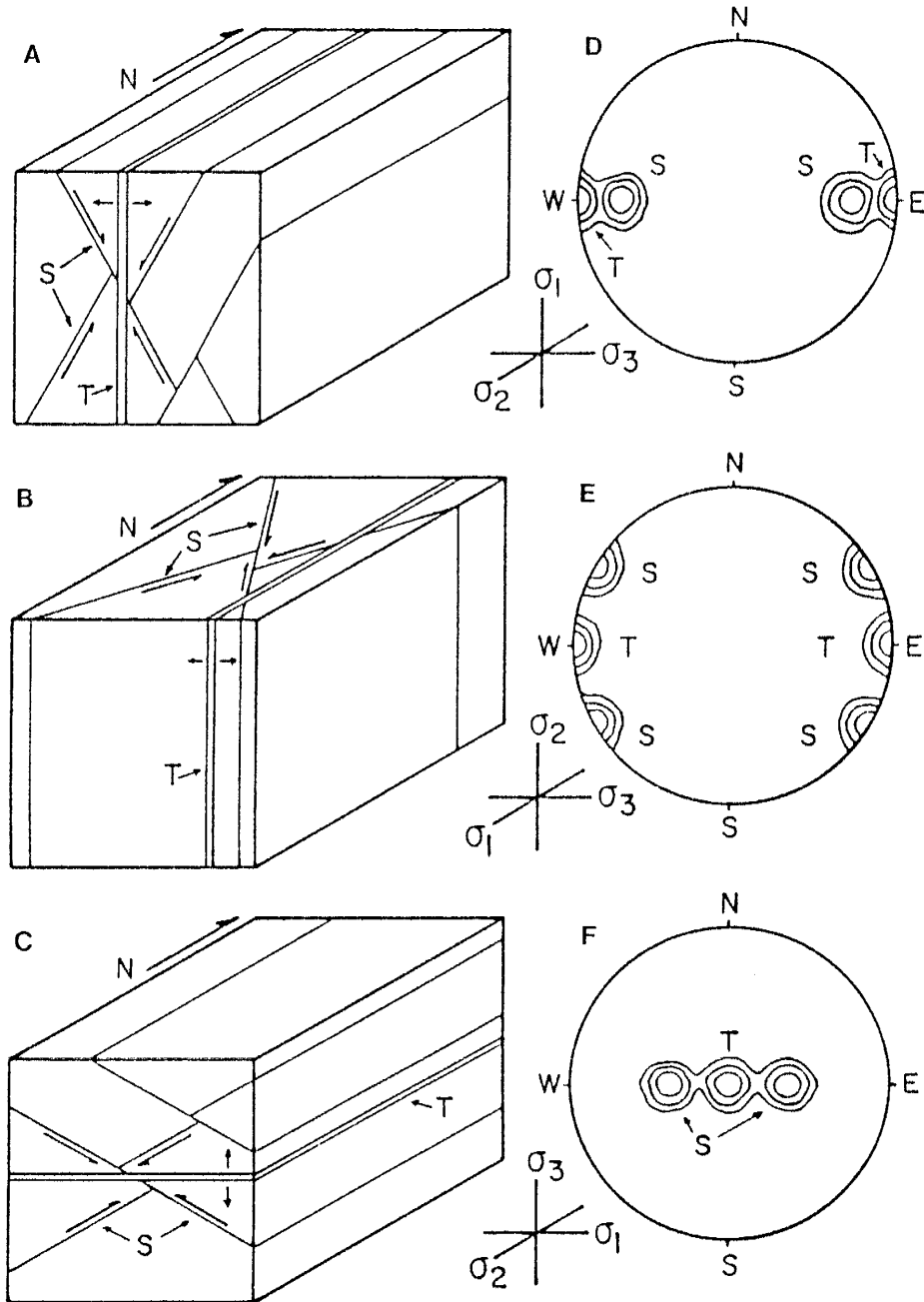


Figure 2.3. Hypothetical fracture patterns for shallow crustal, brittle deformation as proposed by Anderson (1951). Block diagrams represent: A) Normal faulting, σ_1 vertical; B) strike-slip faulting, σ_2 vertical; C) thrust faulting, σ_3 vertical. Diagrams D, E and F illustrate stereographic representation of poles to fracture planes for each system, respectively, assuming numerous fractures are plotted. All diagrams referenced to north; T and S denote tensile and shear fractures.

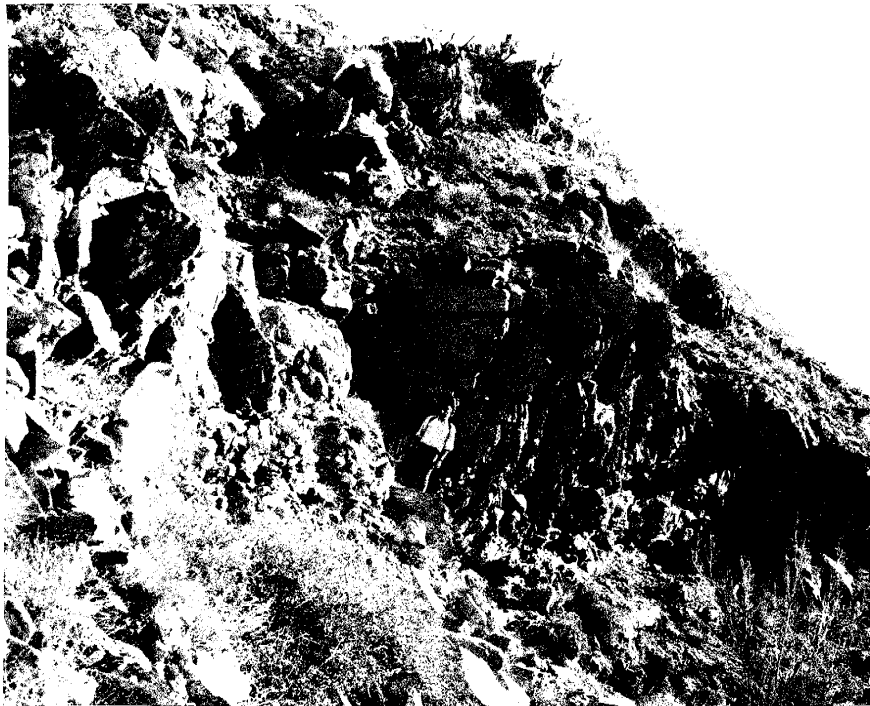
shear patterns (formed by either joints, faults, or both) were not equally disposed with respect to horizontal, but rather were equally inclined with respect to bedding (a pervasive planar fabric that was originally horizontal; Fig. 2.4). More specifically, small- to medium-scale faults that exhibited little or no drag, and occurred as either single fault orientations or as conjugate pairs, very consistently cut bedding at roughly 30° (thrust faults), 60° (normal faults), or 90° (strike-slip faults). The most straightforward interpretation is that these structures (which were preferentially aligned with respect to the applied stress field) were superimposed on bedding while bedding was consistently oriented, and therefore, while bedding was still horizontal. The concept of joint and fault generation during the early stages of deformation is not entirely new (e.g., Melton, 1929; Parker, 1942; Reches, 1976, 1978; Beck, 1984; Beck and Burford, 1985). Most of these studies dealt primarily with joints, and to a lesser extent small faults, and concluded that these brittle structures predated observed folds. The shear joints of Reches (1976, p. 1654) would be classified as small faults within the context of this study, and although Reches (1978, fig. 15) discussed whether small faults within steeply inclined strata may have formed while bedding was horizontal, he did not favor this conclusion. In the following analyses, joints and small faults are treated as early formed structures within a given deformational event and initial fracturing is interpreted as a fundamental aspect of shallow crustal, brittle deformation.

Data collection has been coordinated with detailed geologic mapping at a minimum scale of 1:12,000 (1:6,000 where structurally complex). Attitudes of structural elements, including bedding, systematic joints (Davis, 1984; Price, 1966; Price and Cosgrove, 1990), fault, fault striation (either aligned crystal fibres or linear abrasion grooves; Durney and Ramsay, 1973; Ramsay and Huber, 1983; Davis, 1984; Price and Cosgrove, 1990), fold axis and dike orientations are described and recorded in the field at specific stations. Joints are classified as either mineralized or "featureless" (Davis, 1984), and are thoroughly scanned for evidence of slip. If evidence of slip has been

Figure 2.4. Examples of relationships between fractures and bedding. A) Conjugate normal faults and shear joints cut across bedding at roughly 60°; B) simulation of computerized restoration of bedding to horizontal. Conjugate shears are now equally inclined to both bedding and horizontal; C) steeply dipping inferred strike-slip fault. Fault plane is normal to bedding; striae within the fault plane are parallel to the line of intersection formed by the fault plane and bedding plane. Computerized restoration of bedding to horizontal would reorient the fault plane to vertical, striae to horizontal; D) conjugate microfaults indicative of thrust faulting. Restoration of bedding to horizontal would reorient microfaults such that they would be equally inclined with respect to horizontal (σ_3 vertical).



(a)



(b)

Figure 2.4, continued. Examples of relationships between fractures and bedding. A) Conjugate normal faults and shear joints cut across bedding at roughly 60°; B) simulation of computerized restoration of bedding to horizontal. Conjugate shears are now equally inclined to both bedding and horizontal; C) steeply dipping inferred strike-slip fault. Fault plane is normal to bedding; striae within the fault plane are parallel to the line of intersection formed by the fault plane and bedding plane. Computerized restoration of bedding to horizontal would reorient the fault plane to vertical, striae to horizontal; D) conjugate microfaults indicative of thrust faulting. Restoration of bedding to horizontal would reorient microfaults such that they would be equally inclined with respect to horizontal (σ_3 vertical).



(c)



(d)

detected, either through minute offset of bedding, abrasion grooves, or aligned crystal fibres, the fracture is classified as a fault. Observed displacements (net slip) on individual faults range from less than 1 cm to several km (as along the East Joyita fault, which displays approximately 3 km of Tertiary, down to the east, normal displacement, Fig. 2.1). Most of the faults observed and used in the analyses record relatively small displacements, and typically exhibit net slips on the order of a few meters to a hundred meters. Small- to medium-scale faults are far more numerous than large-scale (regional) faults. Faults are classified in the field as normal, thrust (reverse) or strike-slip faults (Anderson, 1951). Strike-slip faults are further classified as right- or left-lateral (dextral or sinistral, respectively; Anderson, 1951) through the use of 'fault steps' (Durney and Ramsay, 1973; Hobbs *et al.* 1976; chattermarks of Davis, 1984) on the fault surface. As might be expected, not all faults are readily categorized into these three fault categories. In outcrops where the style of faulting has not been determined, due to outcrop over a small area lacking specific marker horizons, or where a small-scale fault could not be traced to marker horizons, the fault is classified as "unknown".

Computerized analysis of field data makes use of two FORTRAN programs. Rotation is accomplished through the use of program FABSTAT (Perry, 1981), and plotting utilizes program SCHMDT (Beasley, 1981). Both programs have been somewhat modified. Modifications to FABSTAT include expanding input and output formats to accommodate quadrant as well as azimuth notation, linear data as well as planar data, and output formats compatible with the input formats of SCHMDT. Modifications to program SCHMDT include adapting the program to print at 8 (rather than 6) lines per inch, and to print at every printing site (as opposed to alternate printing sites) to enhance definition of preferred orientations (maxima or concentrations).

In the analyses that follow, orientations of field data are referred to as "field-recorded" data. Once these data have been run through the rotation program, they are referred to as "restored" data. Data sets are plotted on lower-hemisphere,

equal-area (Schmidt) projections (Philips, 1971; Priest, 1985) and analyzed according to their field-recorded orientations. The same data sets are then run through the rotation program, which treats all data from a specific field station individually. In other words, the planar and linear orientations observed at a specific outcrop are restored using the bedding orientation at that locale, rather than using regional dip. Bedding is rotated to horizontal about an axis parallel to strike, by an amount equal to the field-recorded dip. Observed linear and planar structural elements are rotated in the same sense and by the same amount, about the same axis, and restored orientations are mathematically calculated. The restored data set is then plotted and compared to the projection of field-recorded data.

Regional bedding, in some cases, must be used to restore data. Evidence of fault drag indicates that the original angular relationship between bedding and the fault has been destroyed within the drag-folded strata. If evidence of drag is present in only one fault block, the bedding orientation to be used for rotation is recorded in the opposing fault block. If both blocks show evidence of drag, regional bedding is used to restore the fault to its inferred original orientation. Similarly, regional bedding is used to restore structural orientations where bedding is absent, as in the Proterozoic core of the Joyita Hills.

Interpretations of principal stress directions are made in accordance with theoretical aspects of fracture orientation with respect to the applied stress field (Fig. 3) as indicated by Anderson (1951), Davis (1984) and Price and Cosgrove (1990). The applied stress field consists of three mutually perpendicular (orthogonal) stress axes, designated as σ_1 , σ_2 and σ_3 (principal axes of maximum, intermediate and minimum compressive stress, respectively). Structural elements are oriented with respect to the applied stress field such that σ_1 bisects the acute angle between the conjugate faults. The line of intersection formed by the conjugate faults is parallel to σ_2 . The obtuse angle between conjugate faults is bisected by σ_3 . Fault striae are parallel to the line of

intersection formed by the σ_1/σ_3 plane and the respective conjugate fault planes. Tensile fractures (mineralized joints, veins and dikes) open normal to the fracture plane and are parallel to the σ_1/σ_2 plane.

STRUCTURAL ANALYSIS

The principal data set is illustrated in a composite plot (Fig. 2.5) of all brittle, planar structures (joints, dikes and faults), plotted with respect to three-dimensional space as well as with respect to bedding. Additional data, including fault striae, fold axis, Proterozoic basement foliations, and ancestral Rocky Mountain fault orientations (Beck and Chapin, 1991) are treated separately. Inspection of both field-recorded (Fig. 2.5a) and restored (Fig. 2.5b) orientations reveals that planar orientations are distributed over much of each stereonet and maxima are of relatively low percentage value. This is attributed to the effects of overprinting and mutual interference of multiple fracture orientations associated with multiple deformational events. The fundamental difference between the two diagrams is in the spatial distribution of maxima orientations. With reference to Fig. 2.3, preferred orientations observed in the plot of field-recorded data show little to no compatibility with theoretical fracture patterns that would be expected in Andersonian, shallow crustal deformation. In contrast, restored orientations demonstrate two distinct fracture patterns that could be indicative of conjugate faults and bisecting tensile fractures associated with stress fields in which σ_1 was vertical. However, the planar orientations plotted in Fig. 2.5 include the joints, faults and dikes that formed in response to a minimum of three deformational events. For this reason, the initial data has been subdivided on the basis of like structural elements and plotted separately in the following categories: Normal faults, strike-slip faults, thrust faults, unknown faults, dikes and joints. Fault striae observed on each of the four fault categories are plotted separately and presented with the corresponding fault plot. The following analyses compare field-recorded fault orientations with restored fault orientations, because it is felt that of the foregoing categories, faults are most definitive.

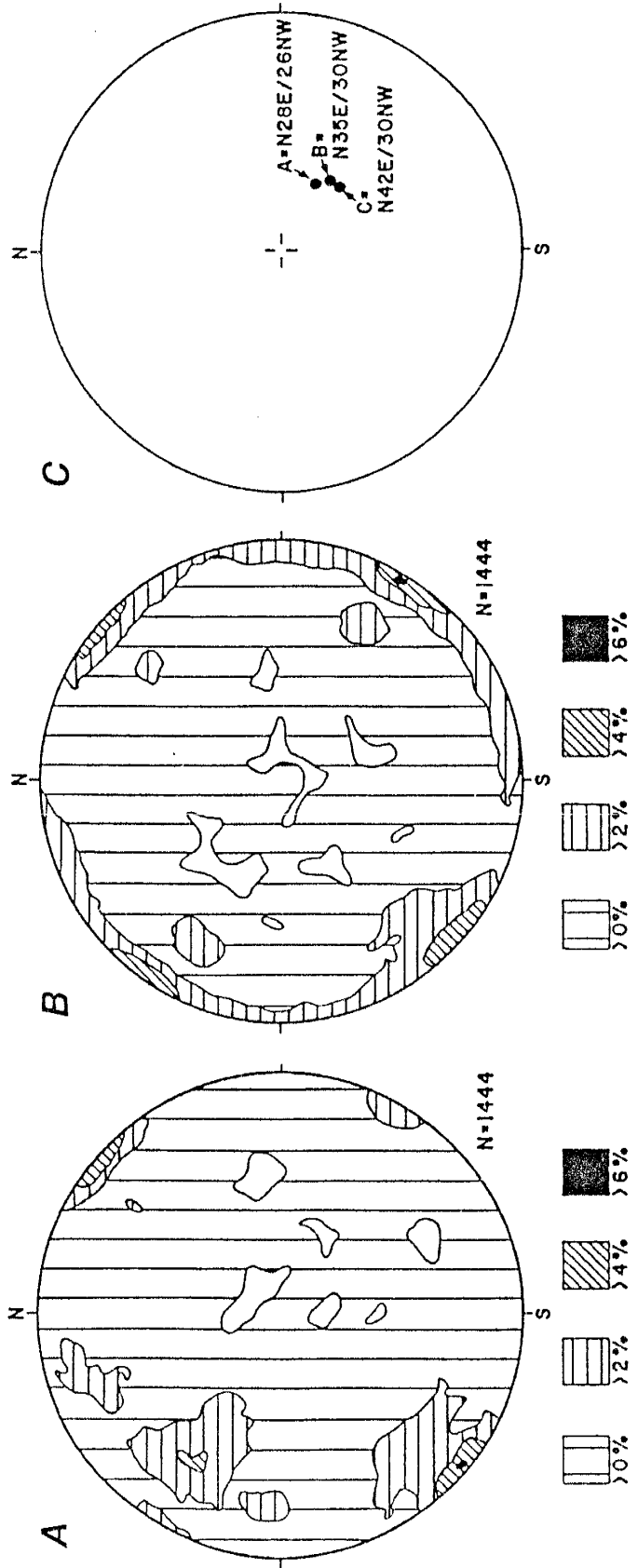


Figure 2.5. Primary data set of all planar structural elements (joints, dikes and faults). A) Field-recorded orientations; B) restored orientations; C) average bedding orientations, where A represents Tertiary volcanics (post-Laramide, pre- and syn-Rio Grande rift sequences; refer to Fig. 2.2); B represents mid-early Permian through Eocene sedimentary rocks (post-ancestral Rocky Mountain, pre- and syn-Laramide sequences); and C represents Pennsylvanian and earliest Permian strata (pre- and syn-ancestral Rocky Mountain sequences). All diagrams represent poles to planes, A and B contoured at specified intervals per 1% area in lower-hemisphere, equal-area projections.

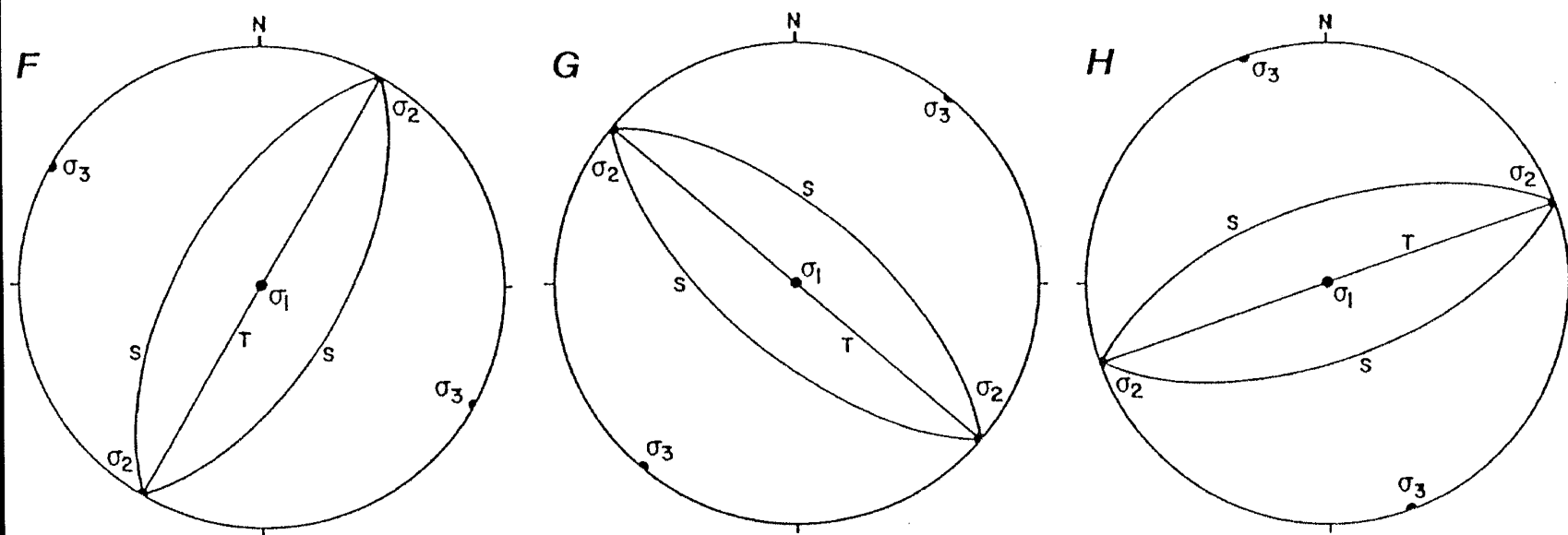
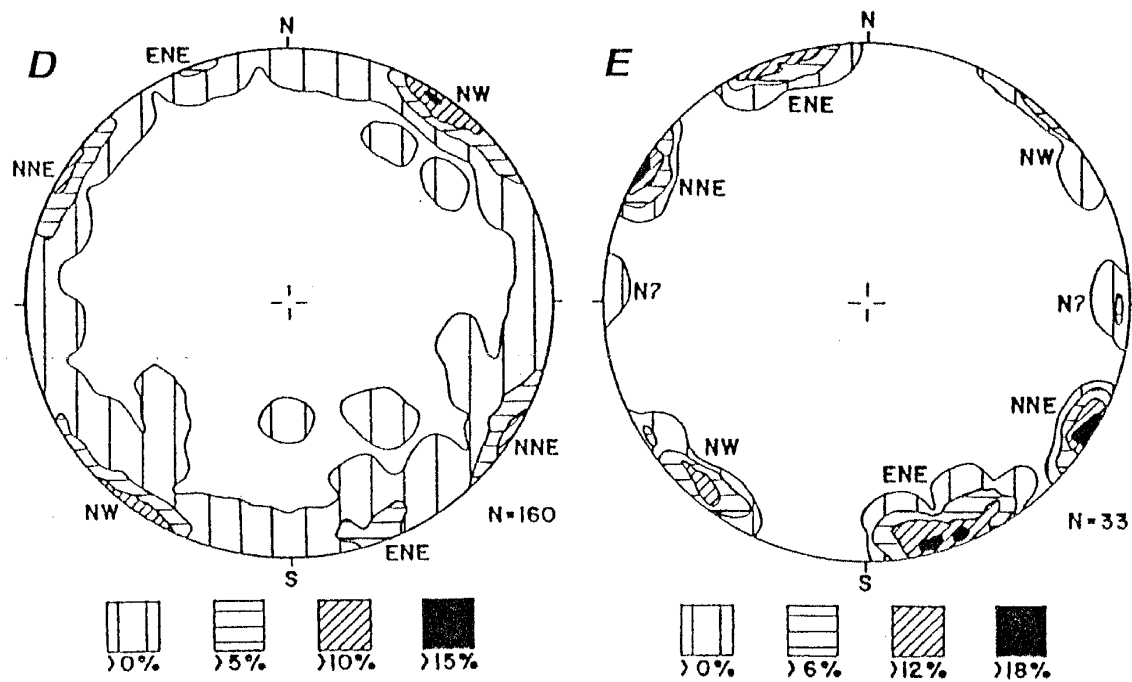
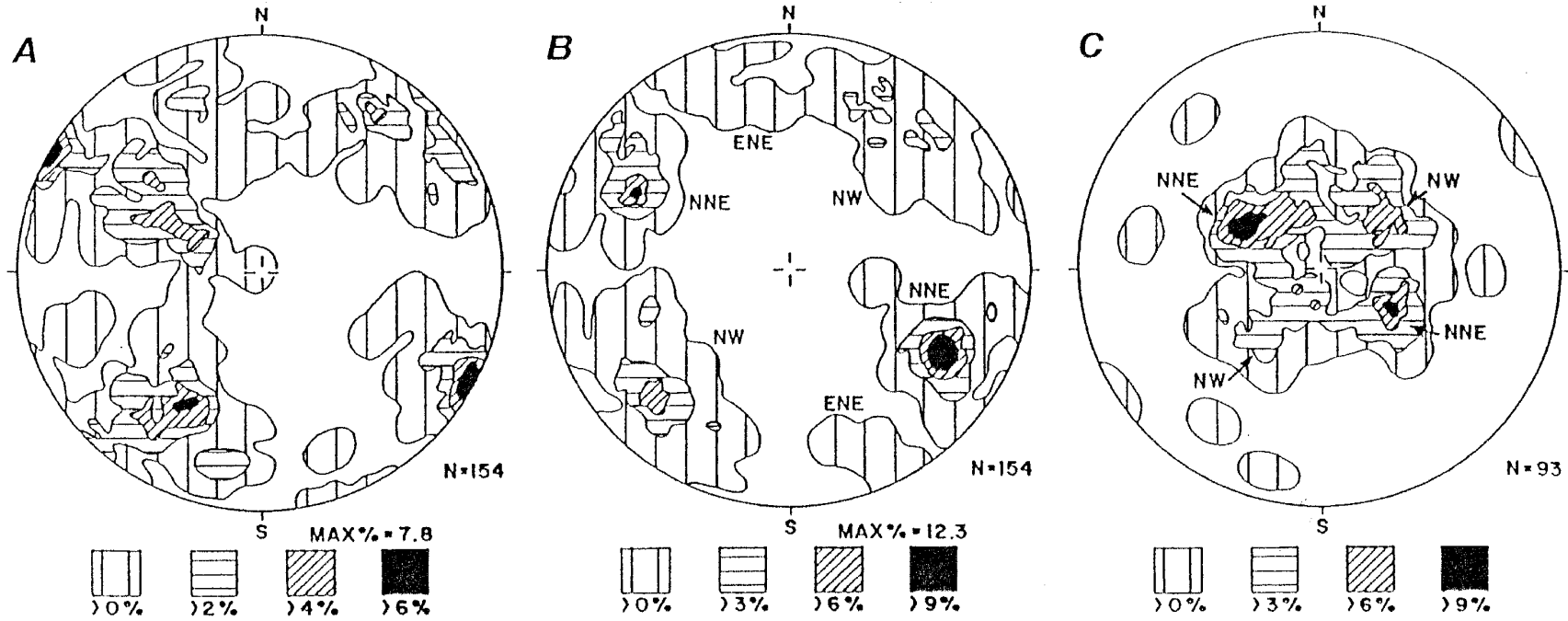
Fault orientations are supplemented with fault striae, joint and dike orientations, where appropriate, and compatible orientations grouped into fracture (joint and/or fault) systems. The stratigraphic sequences that a recognizable fracture pattern overprints is used to correlate structural styles with specific tectonic events.

Normal fault systems

A series of normal faults offset Tertiary volcanics and older rocks, and are associated with the development of the Rio Grande rift. Field-recorded normal faults demonstrate a variety of orientations, and are marked by dip-slip or oblique-slip striations. Comparison of field-recorded and restored normal fault orientations (Fig. 2.6a,b) clearly demonstrates that normal faults typically cut bedding at 60° – 65° . When restored, normal fault orientations form maxima that are either enhanced as discrete concentrations and/or increased in maxima percent value. Normal faults plot as diametrically opposed concentrations that define three separate and distinct pairs of conjugate normal faults. The two dominant conjugate pairs strike to the north-northeast and northwest, respectively. A third pair of conjugate faults, numerically less significant than the other two, strikes to the east-northeast. Each conjugate pair is compatible with Andersonian theories on near-surface normal fault orientations, and defines a dihedral angle of approximately 55° – 60° .

Fault striae (Fig. 2.6c), when comparably restored, define dip-slip fault displacements. Striae associated with the north-northeast-striking and northwest-striking fault systems are fairly well defined: Striae associated with the east-northeast-striking normal faults are not numerically sufficient to form distinct concentrations. Preferred orientations of mineralized joints and veins (Fig. 2.6d) and mafic dikes (Fig. 2.6e), when comparably restored, define three distinct maxima. Each of these maxima define sub-vertical tensile fractures that strike north-northeast, northwest, and east-northeast, and respectively bisect the acute angle formed by each pair of conjugate normal faults.

Figure 2.6. Fracture systems associated with Rio Grande rift (Oligocene – Miocene) tectonism. A) Field – recorded normal fault orientations; B) restored normal faults, conjugate pairs strike to the north – northeast (NNE), northwest (NW) and east – north-east (ENE); C) restored normal fault striae (labelled with respect to fracture system, rather than trend of striae); D) restored mineralized joints and veins; E) restored mid – Tertiary mafic dikes. North – striking (N) dikes are also present, but no compatible preferred orientations of faults (B) or mineralized joints (D) have been observed. F, G and H) Inferred stress field orientations. Poles to planes (A, B, D and E) and lineations (C) contoured at specified intervals per 1% area in lower – hemisphere, equal – area projections.



The combination of conjugate normal faults marked by dip-slip fault striae and bisecting tensile fractures define three separate and distinct fracture systems that are compatible with theoretical considerations of Anderson (1951). Normal faults associated with each of the six inferred shear orientations, and mafic dikes from each of the three inferred tensile orientations have been observed within Tertiary volcanic sequences. Therefore, each of the three normal fault systems was active during deformation associated with the development of the Rio Grande rift.

Tertiary volcanic rocks within the Joyita Hills strike north-northeast and dip 25° – 30° to the west-northwest (Figs. 2.1 and 2.5c). That both bedding and normal faults strike to the north-northeast, and that the faults are marked by dip-slip striae, geometrically necessitates that rotation occurred about an axis that was horizontal and parallel to strike of bedding and faults (and therefore parallel to σ_2) of the north-northeast-striking fracture system. Therefore, rotation occurred while the north-northeast stress field was active. Fractures associated with all three fracture systems plot as enhanced maxima and form compatible systems when bedding is restored to horizontal, which indicates that fractures associated with each fracture system must have been superimposed upon bedding prior to rotation about the north-northeast-trending axis. If the fractures associated with any system post-dated the rotation of bedding, restoration (which effectively simulates a rotation of strata) would cause the fractures to be redistributed and plot as scatter rather than as enhanced maxima (behavior of this kind is discussed in the section on thrust faults). Therefore, the generation of fractures associated with each fracture system must predate rotation about the north-northeast-trending, horizontal axis.

Inferred stress field orientations for each of the respective normal fault systems are provided in Fig. 2.6(f,g and h). Inferred stress fields were oriented such that σ_1 was vertical; σ_2 and σ_3 , respectively were parallel and perpendicular to fault strike within each system. Each stress field orientation (and resultant fracture pattern) can be

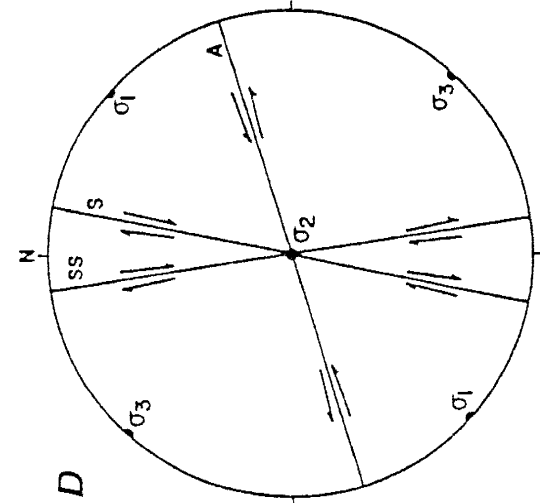
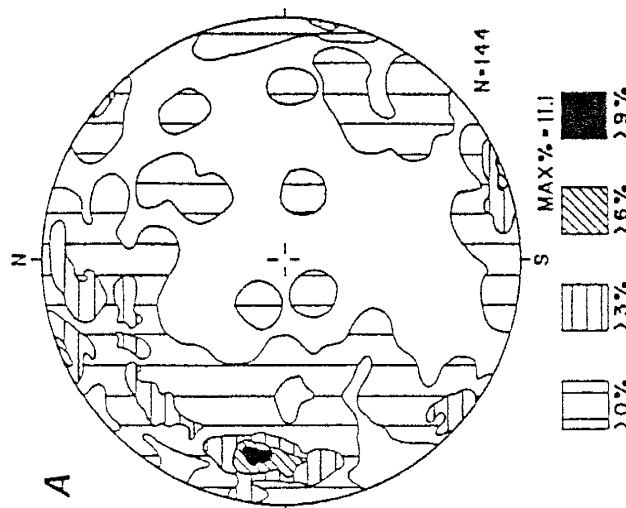
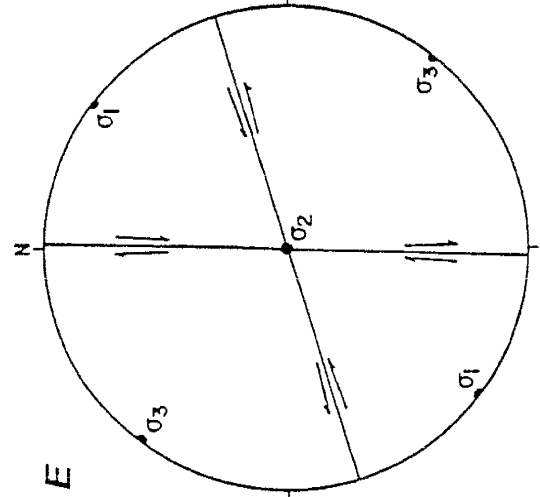
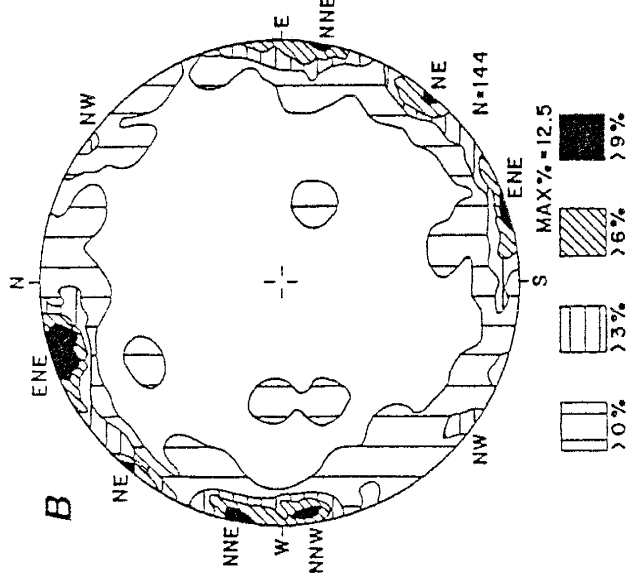
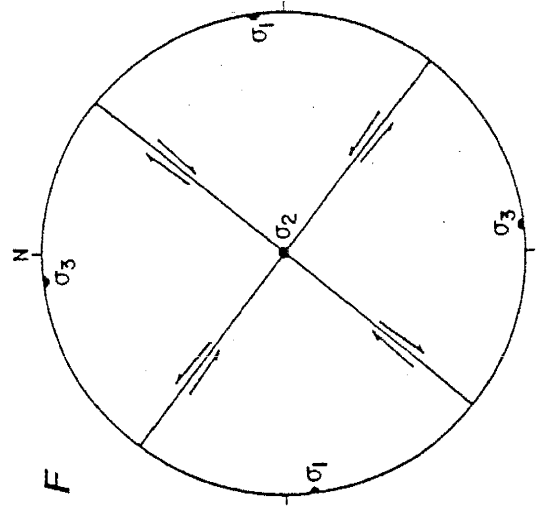
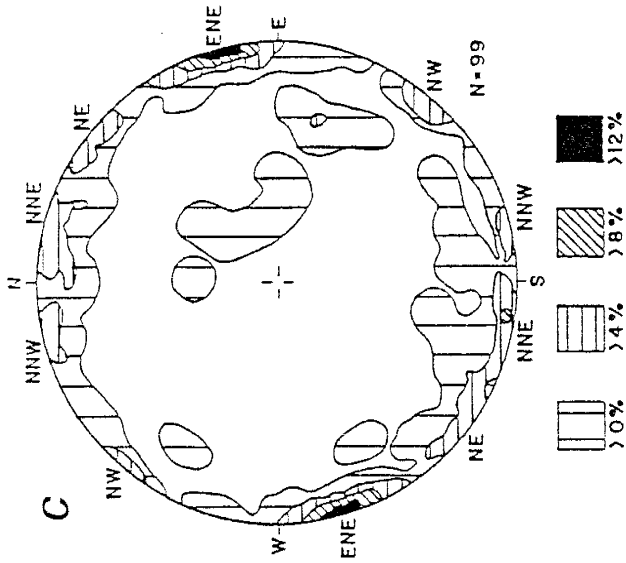
related to reactivation of existing structures (discussed below in the section on reactivation). Therefore, an alternative interpretation is considered equally viable, in which the three (apparently distinct) fracture systems are indicative of one overall stress field where σ_1 (vertical) $>$ $\sigma_2 \sim \sigma_3$. In this interpretation, small changes in the relative magnitudes of σ_2 and σ_3 would allow significant changes in the direction of extension, with fracture patterns preferentially aligned parallel to existing structural grains.

Strike-slip fault systems

Strike-slip faults observed in the field most commonly offset Proterozoic through Cretaceous rocks, and are marked by oblique- to sub-horizontal striations. A limited number of strike-slip faults (<2%) have been observed within Tertiary volcanic rocks. Comparison of field-recorded versus restored strike-slip faults (Fig. 2.7a,b) indicates that strike-slip faults also demonstrate preferred angular relationships with respect to bedding, and are typically oriented at right angles to the bedding plane. When restored, strike-slip faults plot as near-vertical planes, and observed maxima orientations are both enhanced as discrete concentrations and/or increased in maxima percent value. Restored fault striae (Fig. 2.7c) plot as sub-horizontal to horizontal lineations that correspond with each observed fault maxima. Strike-slip faults form at least four concentrations that respectively strike north-northwest, north-northeast, northeast and east-northeast; northwest-striking faults are less common. Northeast- and east-northeast-striking fault orientations form discrete maxima. North-northwest- and north-northeast-striking faults may be alternatively interpreted as either a single or dual maxima. These faults are considered as two distinct fault populations for two reasons: 1) northerly striking strike-slip faults have plotted as two populations throughout the data collection process; and 2) northerly trending fault striae (Fig. 2.7c) also plot as two populations of lineations.

Fault steps on strike-slip faults have been used to determine the sense of offset. Fault steps are interpreted as "pull-apart" structures, the steep face of which, relative

Figure 2.7. Laramide strike-slip fault systems. A) Field-recorded strike-slip fault orientations; B) restored strike-slip faults, preferred orientations strike to the north-northwest (NNW), north-northeast (NNE), northeast (NE), east-northeast (ENE) and less commonly to the northwest (NW); C) restored fault striae; preferred orientations correspond to each observed concentration of restored strike-slip faults in B. D, E and F) Inferred stress field orientations, where S = synthetic, SS = secondary synthetic, and A = antithetic shears. Poles to planes (A and B) and lineations (C) contoured at specified intervals per 1% area in lower-hemisphere, equal-area projections.



to the fault block in which they are found, faces the direction of displacement of the opposing fault block (Durney and Ramsay, 1973). When interpreted in this manner, faults that strike north–northwest, north–northeast and northeast are defined as dextral faults, and east–northeast striking faults are sinistral. The sense of displacement is not always consistent, and fault steps occasionally indicate dextral and sinistral displacement along different fault planes of the same orientation. However, the sense of displacement previously stated for the foregoing fault trends is compatible with a minimum of 75% of the observations.

The foregoing strike–slip faults and their respective sense of offset are interpreted to be related to two separate wrench fault systems. Dextral faults that strike north–northeast and north–northwest, when combined with sinistral faults that strike east–northeast, are interpreted as respective parts of a north–trending, right–lateral wrench fault system, and are respectively interpreted as synthetic, secondary synthetic and antithetic strike–slip faults (or using Riedel shear terminology, R, P and R' shears; Christie–Blick and Biddle, 1985, fig. 5). The dihedral angle between synthetic and antithetic faults approximates 60° . When interpreted in this manner, inferred stress axes associated with the inferred dextral wrench system are oriented such that σ_1 was horizontal, trending northeast; σ_2 was vertical; and σ_3 was horizontal, trending northwest (Fig. 2.7d). As defined, the north–trending, dextral wrench fault system is compatible with interpretations of Chapin and Cather (1981) and Chapin (1983) for Laramide deformation within New Mexico. An alternative interpretation, in which the north–striking faults are considered as a single fault population, yields a stress field orientation as depicted in Fig. 2.7(e).

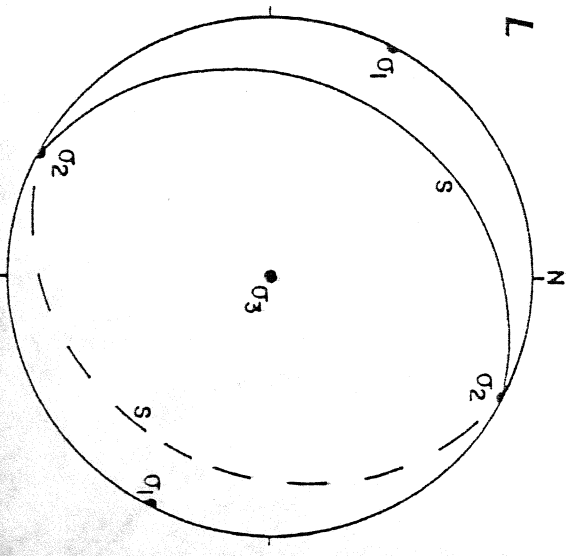
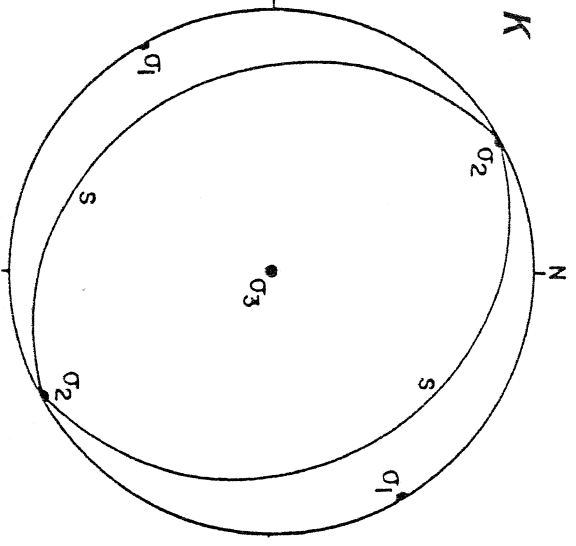
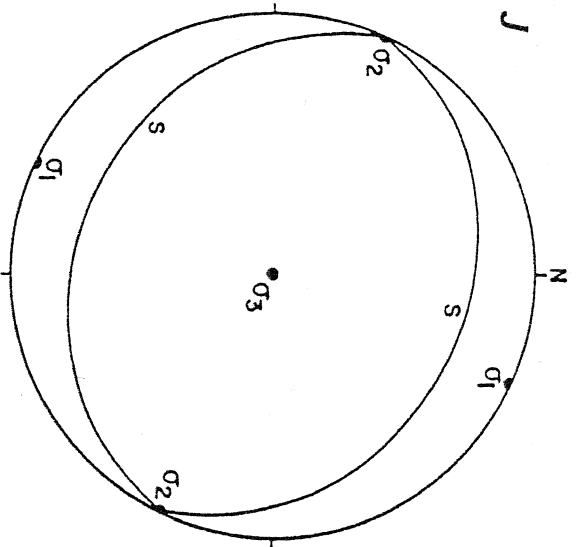
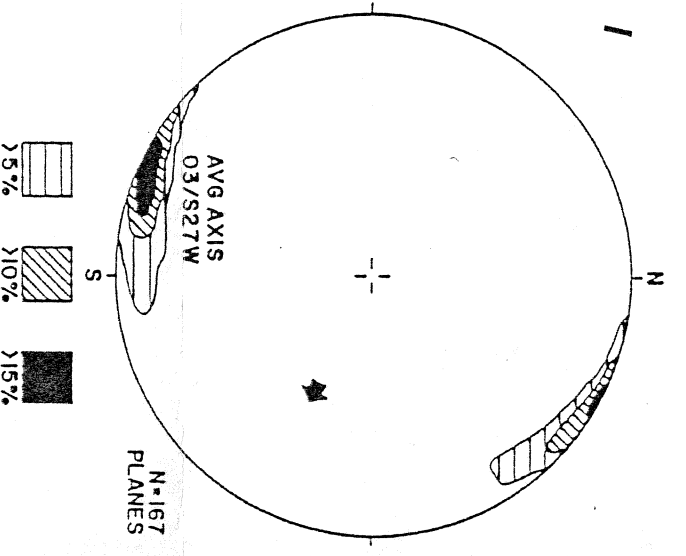
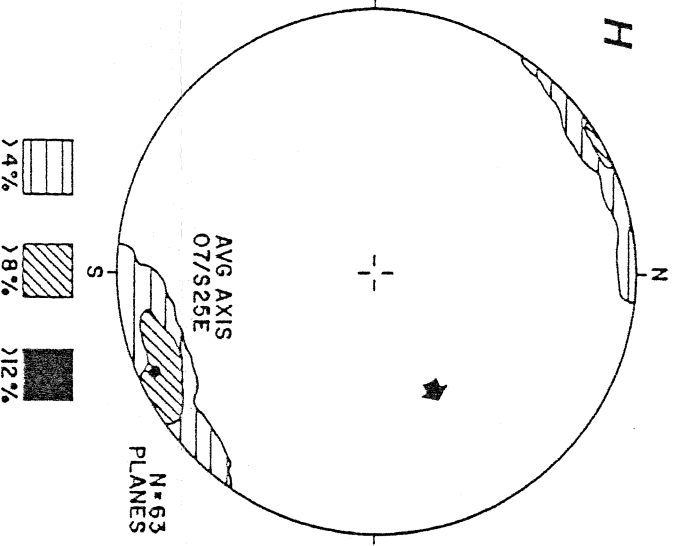
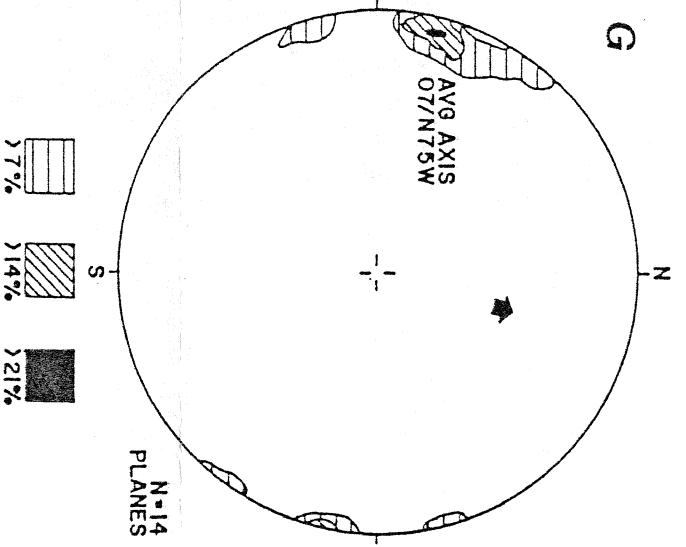
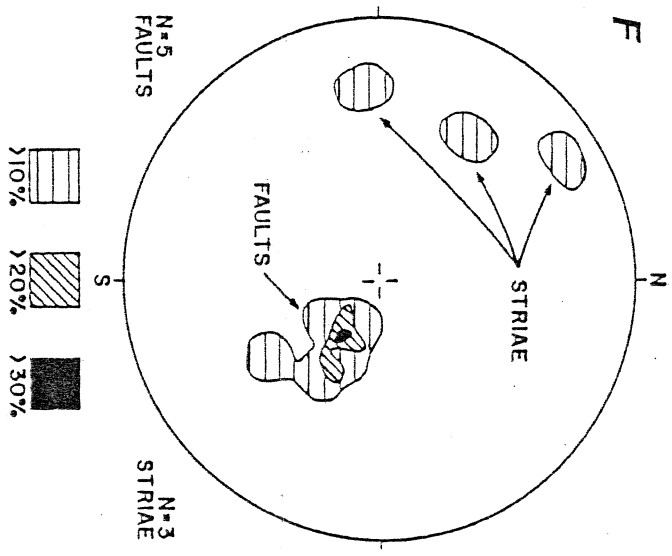
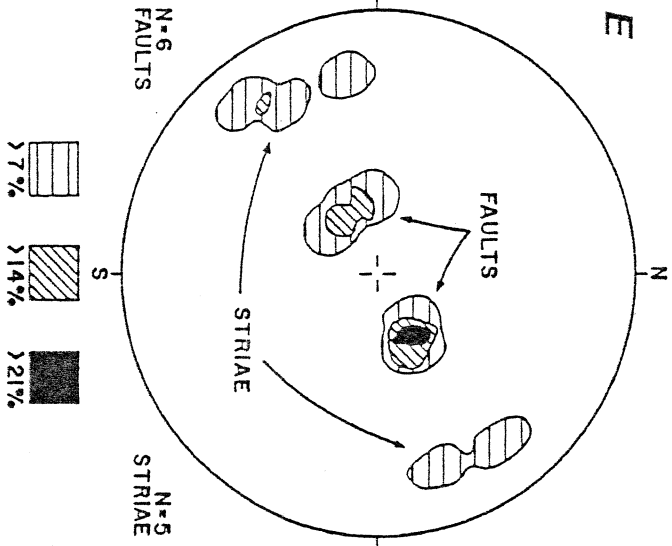
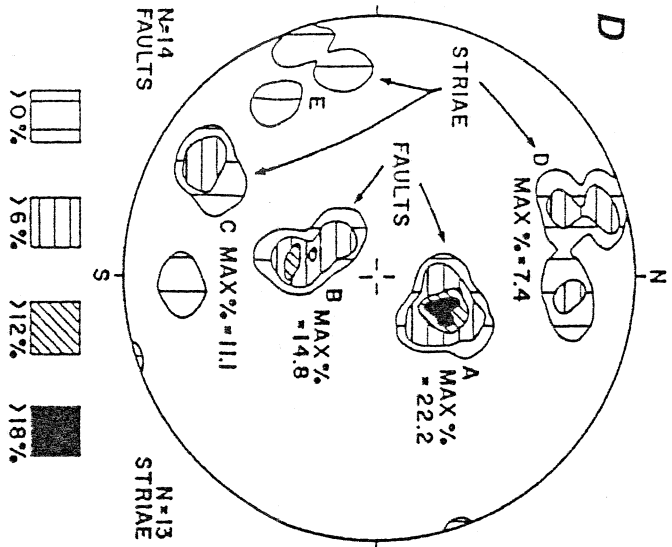
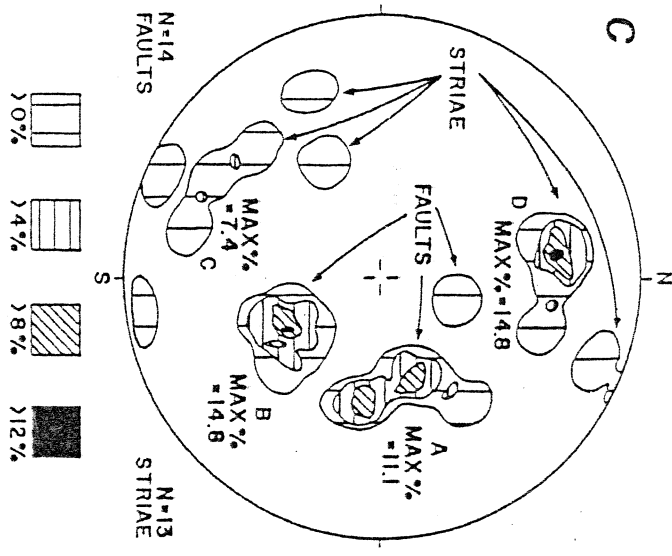
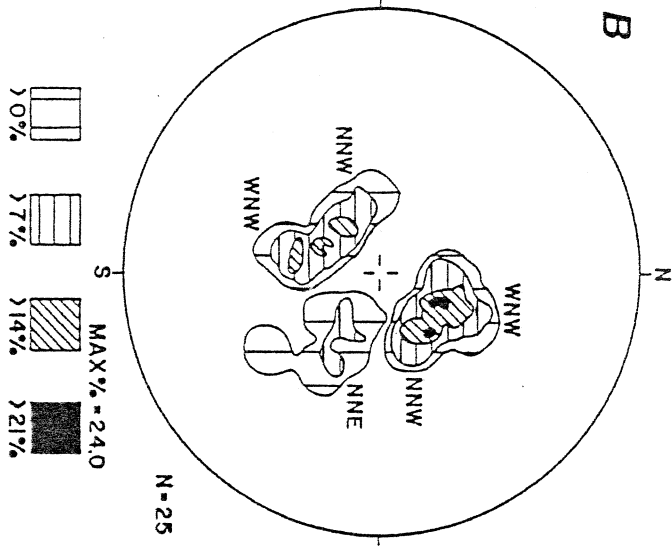
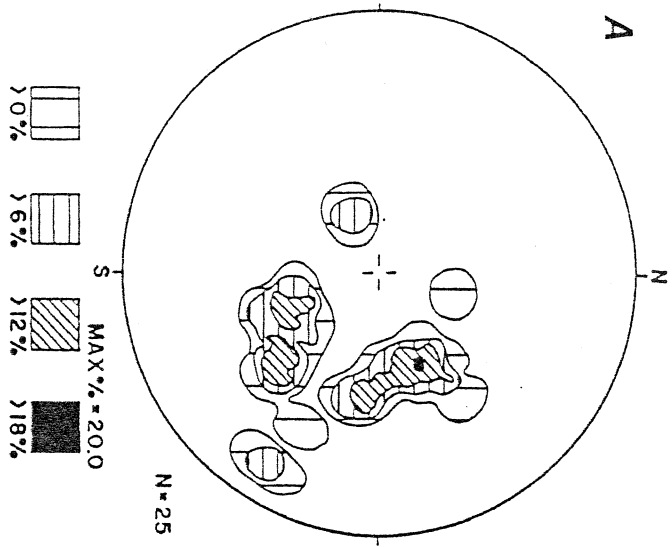
Other strike–slip faults strike northeast and to a lesser extent, northwest. Fault steps define displacement as dextral along the northeast–striking faults. Definitive fault steps have been observed along the northwest–striking faults in only one location. Although the sense of displacement was defined as sinistral, one reading is inadequate

for definitive interpretation. Dextral displacement has been documented along the northeast–striking Montosa fault zone (Fig. 2.1; Brown, 1987). The dextral strike–slip faults observed within the Joyita Hills and El Valle de La Joya are thought to be related to dextral displacement along the Montosa and Del Curto fault systems. The northwest–striking faults may represent the antithetic fault orientation with respect to the northeast–striking faults. Spatial relationships between the dextral strike–slip faults and a north–northwest–trending anticlinal flexure (Fig. 2.1) may be interpreted as a convergent overstep structure associated with dextral wrenching along the left–stepping, northeast–striking faults. This interpretation would also be compatible with the dextral wrench faulting interpretations of Chapin and Cather (1981) and Chapin (1983) within New Mexico. When considered as a conjugate pair of strike–slip faults, the dihedral angle approximates 90° , which is anomalous in comparison to other stress fields defined herein. One explanation could be that the orientation of the antithetic shears within this inferred wrench fault system were controlled by northwest–striking basement structures (presented below in the discussion of Proterozoic foliations). When treated as a conjugate pair, inferred stress axes were oriented such that σ_1 was horizontal, trending east–west; σ_2 was vertical; and σ_3 was horizontal, trending north–south (Fig. 2.7f). This may or may not be a valid correlation.

Thrust fault systems

Reverse faults (Fig. 2.8) observed within the study area are much less common than either normal faults or strike–slip faults. Reverse faults are commonly moderate to high angle and marked by dip–slip and oblique–slip fault striae. Comparison of field–recorded reverse fault orientations (Fig. 2.8a) with those of restored reverse faults (Fig. 2.8b) indicates that when restored, observed maxima are enhanced as distinct maxima, increased in maxima percent value, and plot as low–angle structures, or true thrust faults, in accordance with Andersonian theory. Observed maxima are apparently the result of three distinct fault systems. One system strikes west–northwest,

Figure 2.8. Laramide thrust fault systems. A) Field-recorded reverse fault orientations; B) restored reverse faults, preferred orientations strike to the west-northwest (WNNW), north-northwest (NNW) and north-northeast (NNE; singular maxima); C) composite plot of field-recorded, WNW-striking thrust faults and contained striae; D) composite plot of restored, WNW-striking thrust faults and contained striae; E) Composite plot of restored NNW-striking thrust faults and contained striae; F) composite plot of NNE-striking thrust faults and contained striae; G, H and I) restored fold axes trend to the WNW, SSE (NNW) and SSW (NNE), respectively. Black arrows denote observed vergence direction. J, K and L) Inferred stress field orientations, shear plane dashed where inferred. Poles to planes (A and B), composite poles to planes and lineations (C, D, E and F) and contoured beta diagrams (G, H and I) contoured at specified intervals per 1% area in lower-hemisphere, equal-area projections.



and is composed of a conjugate pair of thrust faults. A second system, also defined by conjugate thrust fault orientations, strikes north–northwest. A third system, represented by a single fault maximum rather than by a conjugate pair, strikes north–northeast. When restored, all thrust faults plot at roughly 25° – 30° to horizontal and conjugate pairs form dihedral angles of approximately 50° – 55° . Thrust faults and associated folds have been observed within Pennsylvanian through Cretaceous strata and are therefore attributed to Laramide deformation. Restoration for thrust fault systems involves a two–stage process: Thrust faults and associated striae, combined with the specific bedding orientation in which they are recorded, are restored (26° about a horizontal axis trending to $N28^{\circ}E$; Fig. 2.5c) to compensate for rotation associated with Rio Grande rift deformation. Residual bedding inclination is then restored to horizontal and thrust faults and associated striae rotated by a comparable amount.

Fault striae are somewhat problematic because: 1) the number of observations associated with the thrust fault systems is limited; and 2) thrust faults were reactivated during subsequent deformation. Some striae are thought to represent reactivation for the following reasons. Comparison of west–northwest–striking thrust faults and contained striae in field–recorded orientations versus restored orientations (Fig. 2.8c,d) indicates that some individual concentrations (labelled A and C) are enhanced as distinct maxima and/or increased in maxima percent value, others (labelled B and E) remain relatively unchanged, and concentration D is actually diminished as a discrete maximum and decreased in maximum percent value when restored. When restored, fault orientations (maxima A and B) plot as a conjugate pair. The combination of faults with compatible striae (concentration C) are interpreted as respective elements of the west–northwest–striking thrust fault system. Additional striae orientations (labelled D and E) are incompatible with the inferred thrust fault system. Each can be argued to be the result of subsequent reactivation of the west–northwest–striking faults. Striae labelled D are parallel to the line of intersection formed by the fault planes

(concentration B) and the σ_1/σ_3 plane of the east–northeast–striking normal fault system (Fig. 2.6h). In other words, it is interpreted that these incompatible striae are indicative of renewed slip on existing Laramide thrust planes while the east–northeast–striking normal fault system was active during mid–Tertiary tectonism. Similarly, incompatible striae (labelled E) in Fig. 2.8(d) are interpreted to be the result of reactivation of the west–northwest–striking thrust faults while the north–northwest–striking thrust fault system was active (Fig. 2.8e; both are Laramide fault systems). Thrust faults and striae of the north–northwest– and north–northeast–striking thrust fault systems are less problematic (Fig. 2.8e,f).

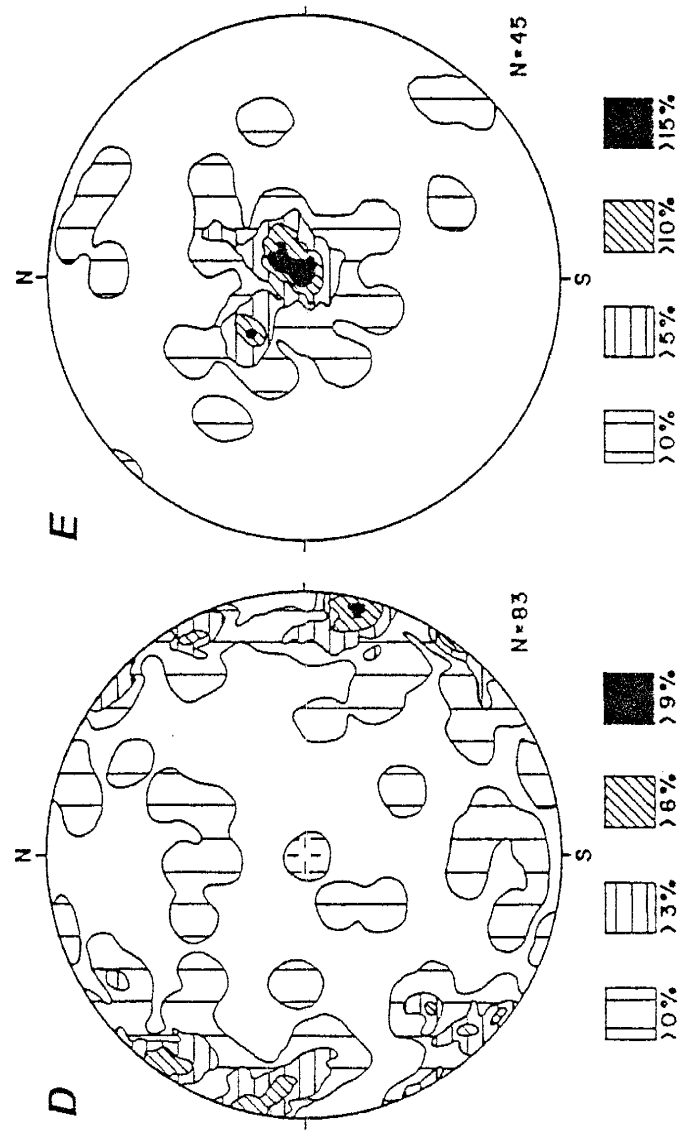
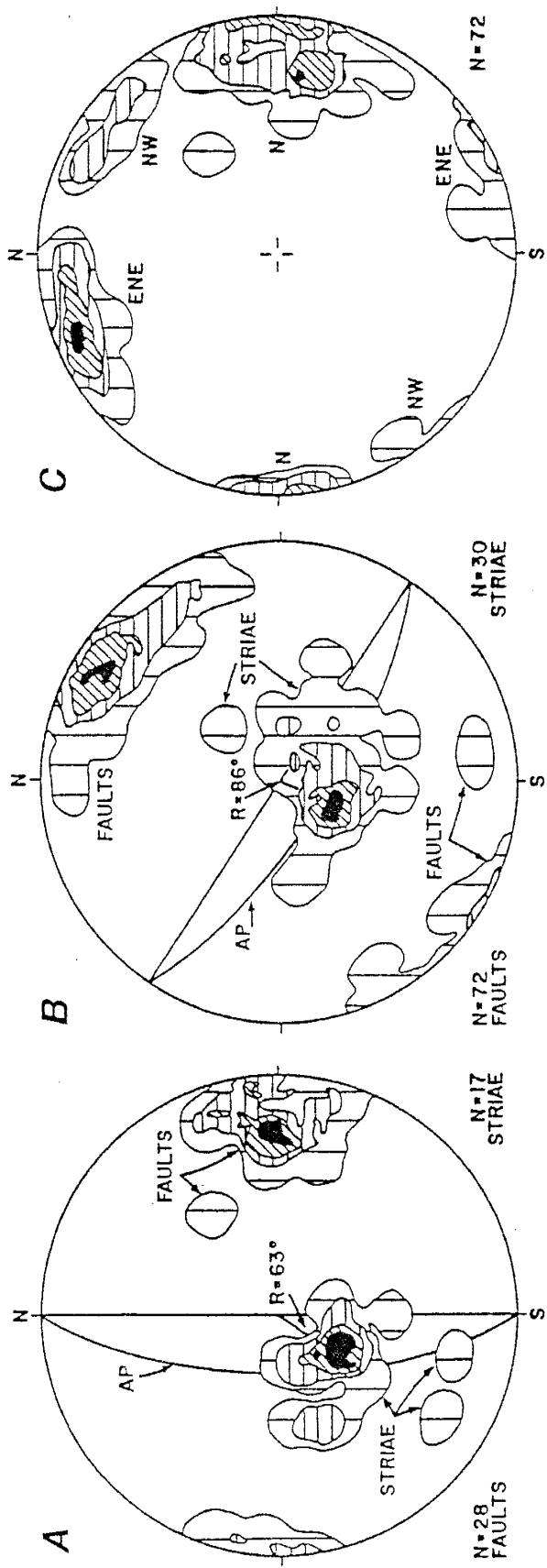
A limited number of folds have also been observed in the Joyita Hills area, and are typically small–scale, localized folds or broad, open folds that occupy a small areal percentage of the field area. North–northeast–trending folds are most common, and become more pronounced to the east and northeast of the study area (Fig. 2.1). Folds have been observed within Cretaceous and older strata, and no folds (other than fault drag) have been observed within Tertiary volcanic rocks. Therefore, compressional thrusting and the generation of these folds is attributed to Laramide deformation. Restored fold axes (Figs. 2.8g,h and i; restored by removing 26° of down–to–the–west rotation about a horizontal, N28°E axis, Fig. 2.5c) define three distinct fold orientations that trend west–northwest, north–northwest and north–northeast. Each fold axis is sub–horizontal to horizontal, and is sub–parallel to the inferred orientation of σ_2 associated with each inferred thrust fault system. Therefore, folds are combined with respective thrust fault systems on the basis of the compatibility of fault strike and fold axis trend. For each respective thrust–fault and fold system, the inferred stress field (Fig. 2.8j,k and l) is interpreted to have been oriented such that σ_1 was horizontal, and perpendicular to thrust fault strike and fold axis trend; σ_2 was horizontal, and parallel to fault strike and fold axis trend; and σ_3 was vertical.

Ancestral Rocky Mountain normal faults

Structural and tectonic aspects of ancestral Rocky Mountain (late Paleozoic) deformation within the Joyita Hills have been discussed previously by Beck and Chapin (1991). Two distinct normal fault trends are interpreted to have been active during early Wolfcampian (earliest Permian) tectonism. Restoration has been accomplished by removing the combined effects of Laramide and Rio Grande rift, down-to-the-west rotations (approximately 29° about a $N32^\circ E$ axis; Fig. 2.5c). Restoration defines the faults as north-striking and northwest-striking normal faults (Fig. 2.9a,b). Restored fault striae define fault displacements as dominantly dip slip, with north-striking, west-dipping normal faults showing a component of left slip (striae rake approximately 63° southward). Fault orientations and kinematic indicators, when combined with the spatial distribution and trend of basins and paleocurrent data, suggest a north-trending, left-lateral wrench fault system through central and southern New Mexico during the late Paleozoic (Beck and Chapin, 1991).

The foregoing fault trends have been treated separately from the primary data set (Fig. 2.5) for several reasons. Most of the faults interpreted to be ancestral Rocky Mountain faults occur as wide gouge zones and exhibit fault drag where earliest Permian and older sedimentary sequences have been juxtaposed against Proterozoic basement rocks. Therefore, the original angular relationship between the fault plane and bedding, which is the fundamental basis upon which the analytical process described herein is formulated, has been masked. In addition, all but one of these faults have been reactivated during younger tectonism. The amount of fault drag and associated axis of rotation attributable to younger tectonism versus that attributable to ancestral Rocky Mountain deformation is not known. Further, the overprinting of ancestral Rocky Mountain structures makes application of the analytical technique described herein difficult. Distinguishing small-scale, north-striking strike-slip faults that originated during Laramide dextral wrenching from those that may have originated

Figure 2.9. Supplemental data (data displayed in Fig. 2.9A,B and C are not part of the primary data set, Fig. 2.5a,b; see text). A,B) Composite plots of north–striking and northwest–striking ancestral Rocky Mountain normal faults and contained striae, respectively. AP denotes average fault plane; R denotes approximate rake of striae; C) preferred orientations of Proterozoic foliations strike to the north (N), east–northeast (ENE) and less commonly to the northwest (NW); D,E) restored ‘unknown’ faults (D) and contained striae (E). Composite poles to planes and lineations (A, B), poles to planes (C, D) and lineations (E) contoured at specified intervals per 1% area in lower–hemisphere, equal–area projections.



during inferred ancestral Rocky Mountain sinistral wrenching (Beck and Chapin, 1991) is not readily accomplished. For example, fault steps observed on north–striking wrench faults attributed to Laramide deformation (those found within post–ancestral Rocky Mountain strata) in some cases indicate sinistral, rather than dextral displacement. Similarly, small–scale normal faults of northwest strike superimposed on earliest Permian and older rocks may have originated during either mid–Tertiary or ancestral Rocky Mountain tectonism. Therefore, the apparent reactivation of ancestral Rocky Mountain structures in a similar sense of offset (normal offset along northwest–striking, southwest–dipping faults) or similar structural style (dextral versus sinistral strike–slip along north–striking vertical faults) renders application of the analytical technique to ancestral Rocky Mountain structures less definitive in the determination of applied stress field orientations than it was for either Laramide or Rio Grande rift tectonism.

Proterozoic basement structures and reactivation

Exposures of Proterozoic augen gneiss within the core of the Joyita Hills display a multitude of planar features, including gneissic to mylonitic foliations, and amphibolite, aplite and pegmatite dikes. Restored foliations (Fig. 2.9c) define three common orientations. All are high angle to vertical, and respectively strike north, northwest and east–northeast. North– and east–northeast–striking foliations are most common.

Reactivation of basement fabrics occurred during each Phanerozoic orogenic event. Proterozoic foliations apparently served as planes of weakness that were repeatedly reactivated in a brittle manner during the Phanerozoic. North–striking, west–dipping normal faults and northwest–striking, southwest–dipping normal faults of ancestral Rocky Mountain age (Figs. 2.9a,b) are both comparably oriented to north– and northwest–striking foliations in Proterozoic rocks. North–striking faults of ancestral Rocky Mountain age have been observed to be directly superimposed upon and reactivate a

Proterozoic mylonite zone (Beck and Chapin, 1991). Northwest-striking faults are also thought to represent reactivation of parallel northwest-striking foliations.

Reactivation of basement fabrics can also be logically concluded to have occurred in younger orogenic events. Fault and dike orientations associated with both Laramide and Rio Grande rift tectonisms are of comparable orientations to Proterozoic foliations, and both dip-slip and strike-slip fault striations have been observed on foliation planes.

Both strike-slip and thrust faults have been attributed to Laramide deformation. Strike-slip faults are most common, with thrust faults and associated folds comparatively less numerous. Laramide strike-slip fault orientations are comparable to those of Proterozoic foliations. Notably, north- and east-northeast-striking-wrench faults (Fig. 2.7b) are subparallel to north- and east-northeast-striking foliations (Fig. 2.9c). Other strike-slip faults strike northwest (Fig. 2.7b), and are subparallel to northwest-striking foliations.

Fault and dike orientations that developed during mid-Tertiary extension define three distinct stress field orientations, each of which resulted in normal faulting. Planar (dike and fault) orientations within each fracture system respectively strike to the north-northeast, northwest and east-northeast (Fig. 2.6f,g and h). The northwest and east-northeast striking fault and dike systems were apparently controlled by the northwest- and east-northeast-striking basement fabrics. At present, no basement fabric of north-northeast strike has been recognized that can give a similar correlation for the north-northeast-striking normal fault and dike system. Rather, this latter fault and dike system is thought to be the result of reactivation of north-northeast-striking thrust faults of Laramide origin. Similarly, exposed Proterozoic rocks in the footwall of the East Joyita fault indicate that north-striking foliations influenced both the location and orientation of the modern-day East Joyita fault, a major down-to-the-east

normal fault during mid-Tertiary extension (approximately 3 km stratigraphic throw; Fig. 2.1).

Unknown faults

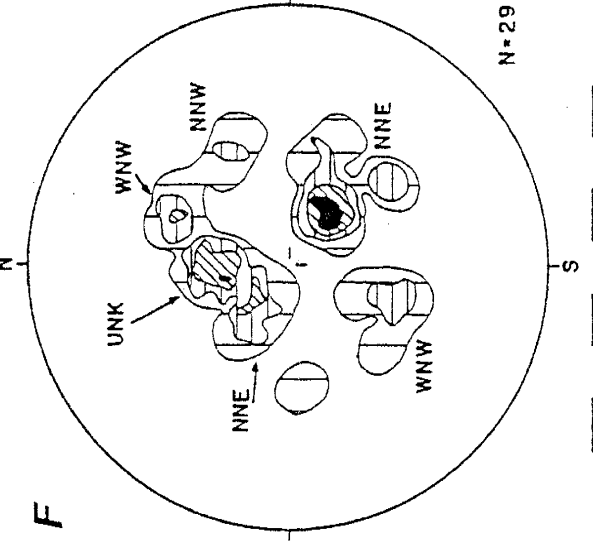
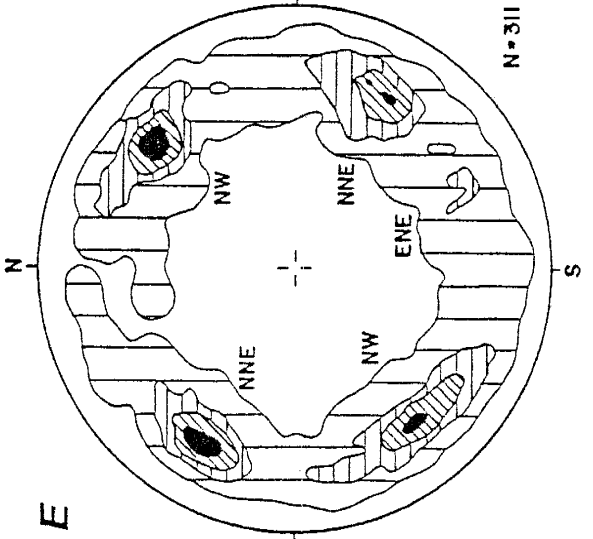
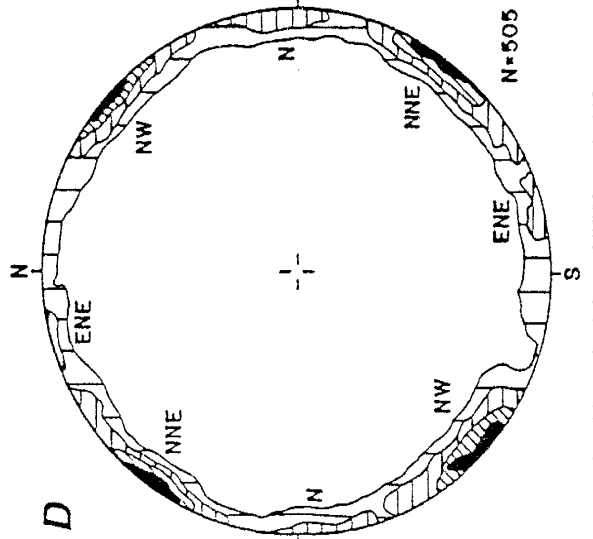
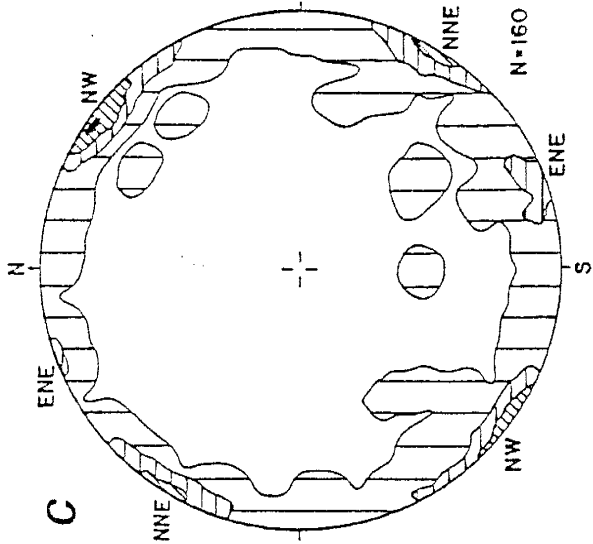
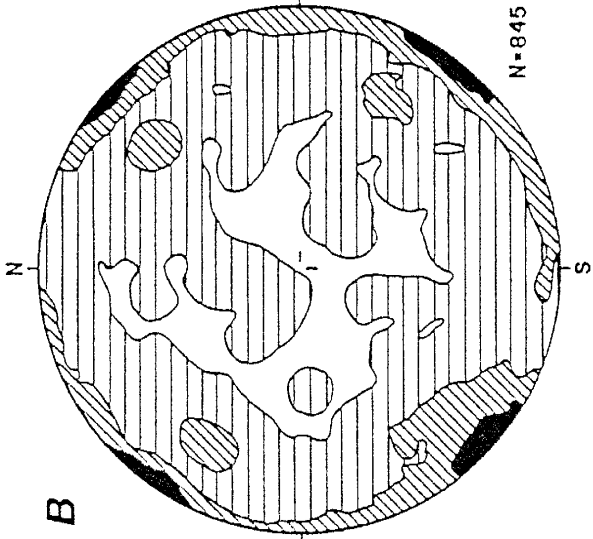
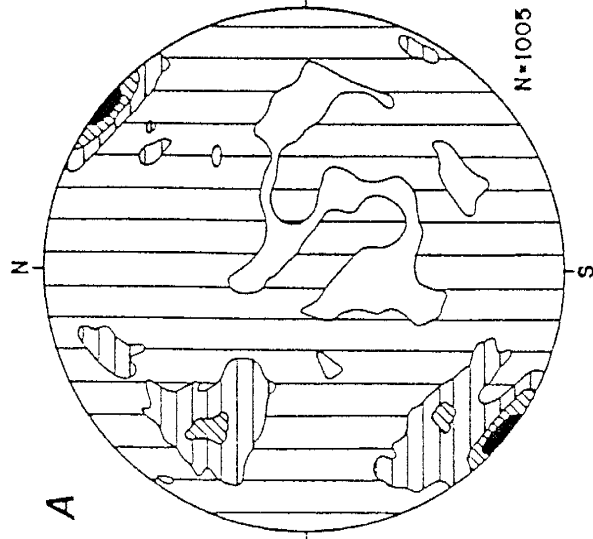
Some faults in the Joyita Hills (Fig. 2.9d, restored) are not well understood, and have been classified as unknown faults. These faults have been observed where the style of faulting could not be determined, due to outcrop over a small area lacking specific marker horizons, or where a small-scale fault could not be traced to marker horizons, and therefore these faults resisted ready classification as either normal, reverse or strike-slip faults. Observed maxima are of comparable orientation to fault orientations previously defined as normal (Fig. 2.6b), strike-slip (Fig. 2.7b) or thrust (Fig. 2.8b). Fault striae (Fig. 2.9e) define displacement as largely dip slip. The similarity between unknown and known fault orientations suggests that they originated as one or more of the known fault types.

Joint orientations

Joint orientations (Fig. 2.10) constitute the remainder of the primary data set (Fig. 2.5). All joints are treated in a manner analogous to faults, and are plotted with respect to their field-recorded orientations (Fig. 2.10a). Restored joint orientations are separated into featureless and mineralized joint sets (Fig. 2.10b,c). As with faults and dikes, maxima formed by restored joint orientations are enhanced as distinct concentrations that display patterns compatible with Andersonian theory for near-surface brittle failure (Fig. 2.3).

Mineralized joints (Fig. 2.10c) are attributed to extension and when restored, plot as vertical planes that form three distinct maxima. Preferred orientations strike to the north-northeast, northwest and east-northeast, and mineralized joints of each preferred orientation have been observed within Tertiary volcanic rocks. Therefore, each has been attributed to mid-Tertiary normal fault systems (compare with mid-Tertiary dikes, Fig. 2.6e).

Figure 2.10. Joint orientations. A) Field-recorded orientations of all joints; B) restored featureless joints; C) restored mineralized joints and veins (same as Fig. 2.6d); D) restored featureless joints inclined $\geq 75^\circ$ to bedding; E) restored featureless joints inclined $< 75^\circ$ and $\geq 45^\circ$ to bedding; F) restored featureless joints inclined $< 45^\circ$ to bedding. All labels as earlier defined, UNK denotes an unknown concentration of featureless joints. Poles to planes (A through F) contoured at specified intervals per 1% area in lower-hemisphere, equal-area projections.



Featureless joints (Fig. 2.10b) occur as smooth, planar fractures that are devoid of mineralization, striae or slickensides, and exhibit no offset parallel to the plane. Therefore, featureless joints offer little in terms of direct tectonic interpretation on the basis of joint character or texture alone. However, on the basis of orientation, featureless joints are logically the result of both extensional and shear origins. Observed maxima plot as orientations that are identical to known shear and extensional orientations.

When restored, most featureless joints plot as vertical planes (normal to bedding) and to a lesser extent as high-angle planes (roughly 60° to bedding). Comparatively few plot as low-angle joints (roughly 30° to bedding). These angles are analogous to angular relationships between bedding and strike-slip, normal and thrust faults, respectively. Accordingly, featureless joints have been further subdivided on the basis of joint inclination with respect to bedding (Figs. 2.10d,e and f; inclination $\geq 75^\circ$; inclination $< 75^\circ$ and $\geq 45^\circ$; inclination $< 45^\circ$). Although an objective subdivision, it is not entirely arbitrary. Orientations of featureless joints cover much of the stereonet and form maxima of relatively low percentage value, which is attributed to the effects of overprinting and mutual interference of multiple joint patterns associated with multiple stress field orientations. As with faults (Figs. 2.6, 2.7 and 2.8), fractures associated with some stress fields are better developed than others (e.g., thrust fault systems are comparatively poorly developed with respect to normal and strike-slip fault systems; normal faults that strike to the east-northeast are less common than those that strike to the north-northeast and northwest). Subdividing featureless joints on the basis of orientation with respect to bedding reduces the total number of joints in each plot, thereby enhancing the preferred orientations of weak fracture systems that would otherwise be masked by those of stronger systems.

Interpretation of featureless joints that are normal to bedding (Fig. 2.10d) is ambiguous. Subdivision of all featureless joints defines two additional joint concentrations (these strike to the north and east-northeast; compare Fig. 2.10b and d). However,

few of these preferred joint orientations can be conclusively argued to have either extensional or shear origins. This is largely due to the complexity of the structural evolution of the Joyita Hills. All observed concentrations (Fig. 2.10d) are parallel to known shear orientations as defined by Laramide strike-slip faults (Fig. 2.7b); yet most of the preferred joint orientations shown in Fig. 2.10(d) also served as tensile orientations during Rio Grande rift extension (Fig. 2.6d,c). Therefore, only featureless joints of these orientations that have been superimposed on post-Laramide strata (Tertiary volcanic sequences) are certainly extensional in origin. Those superimposed on pre-Laramide strata may have originated as either extension joints (during mid-Tertiary extension) or shear joints (during Laramide wrenching), and conceivably may represent both.

Low- to high-angle featureless joints are less enigmatic. Joint orientations that plot at roughly 60° to bedding (Fig. 2.10e) clearly define maxima orientations that parallel known shear orientations of mid-Tertiary normal faults (Fig. 2.6b). Observed concentrations plot as conjugate pairs that respectively strike to the north-northeast, northwest, and less commonly to the east-northeast, mimicking the relative percentages of normal fault populations. No comparably oriented structures that can be classified as extensional (e.g., mineralized joints, veins or dikes) have been observed.

Low-angle joint orientations that plot at roughly 30° to bedding (Fig. 2.10f) form concentrations that parallel known thrust fault orientations (Fig. 2.8d,e and f). Some concentrations form relatively strong maxima, others form poorly defined ones. Conclusive interpretation of both strong and weak concentrations is hindered by the limited number of joints. The limited number of low-angle joints is thought to be the result of poorly developed thrust fault systems within the study area rather than any inherent reason that low-angle joints should be uncommon. Observed maxima form conjugate pairs of low-angle joints that strike north-northeast (in contrast to the singular maximum of north-northeast-striking thrust faults, Fig. 2.8f) and west-northwest. In a

similar fashion, low-angle joints that strike north-northwest plot as a singular (poorly defined) concentration, whereas north-northwest striking thrust faults plot as a conjugate pair. An additional concentration of joint orientations (labeled 'UNK') is of unknown origin, and has not been observed in any of the plots of known faults (Figs. 2.6-2.9) or tensile fractures (Figs. 2.6d,e and 2.10c) and therefore cannot readily be defined. The joints labelled 'UNK' may simply be the result of overlapping concentrations of west-northwest- and north-northeast-striking joints.

Clearly, preferred orientations of featureless joints parallel known fault orientations. Although featureless joints that are normal to bedding (correspondingly vertical when restored) parallel both shear and tensile orientations, the resultant ambiguity in interpretation can be readily attributed to the complexity of the Joyita Hills area and ample evidence of reactivation of Laramide strike-slip fault orientations (and Proterozoic foliations) during Rio Grande rift tectonism. Featureless joints that are normal to bedding may have had either shear or tensile origins, and perhaps more likely, are the result of both shear and tensile stresses generated during multiple orogenic episodes. Although Pollard and Aydin (1988, p. 1186) discount the very concept of shear joints, the correlation between featureless joint orientations and known fault orientations as defined herein cannot be denied. In that featureless joints plot at 60° and 30° to bedding, and parallel known shear orientations as defined by known faults, the shear joint terminology is considered appropriate.

INTERPRETATION

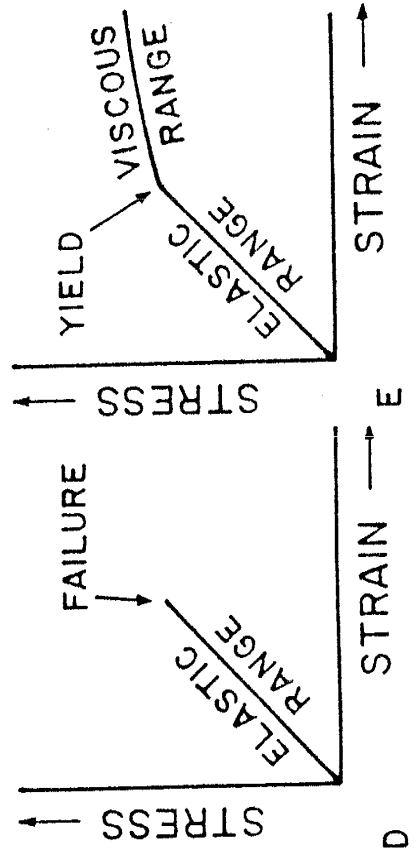
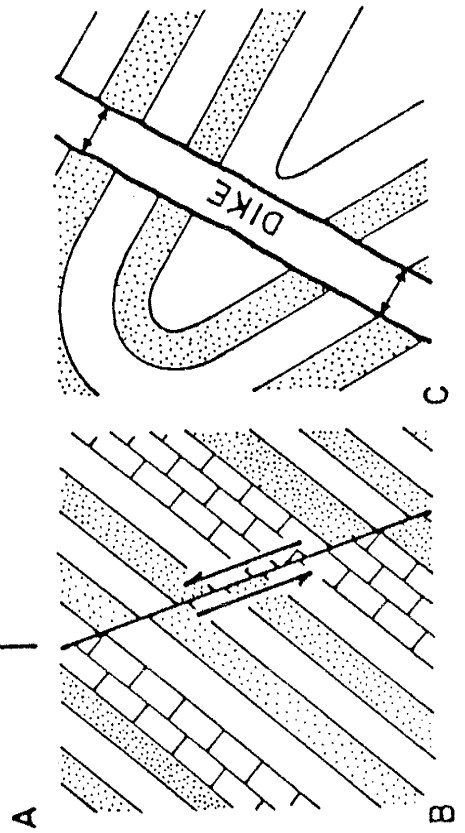
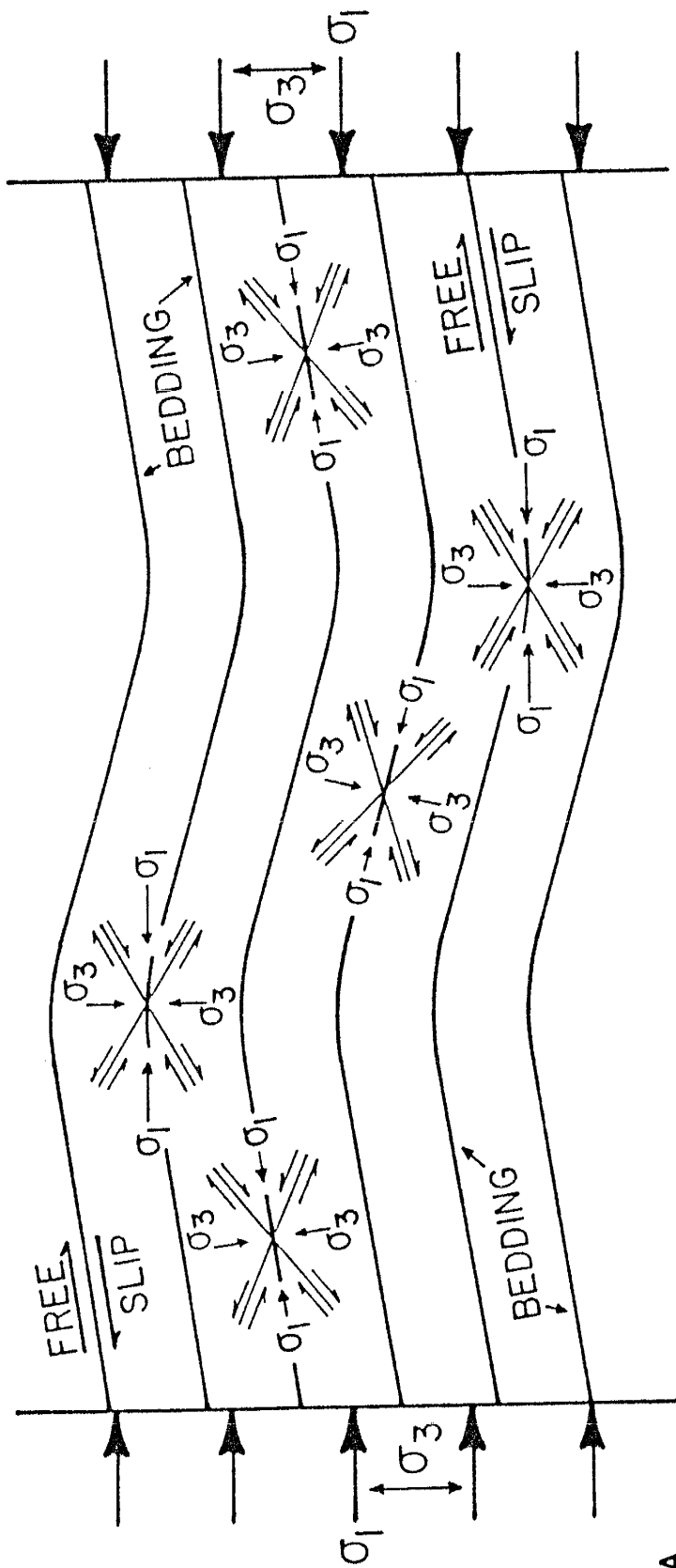
Structural elements associated with brittle deformation in the Joyita Hills (faults and associated striae, joints and dikes), when plotted with respect to bedding (Figs. 2.6, 2.7, 2.8 and 2.10), clearly demonstrate that these structural features maintain preferred angular relationships to bedding. Inferred stress fields are oriented such that one of the principal stress axes was normal to bedding, the remaining two principal stress axes lay within the bedding plane. These relationships can be explained by either of two

means, each of which would produce identical results, yet are inherently different in principle.

One means of explaining the constancy of fracture orientation with respect to bedding is the elastic plate theory and frictionless boundary conditions (e.g., Biot, 1961). If it is assumed that the imposed deformation rates are low, then it is conceivable that folding of sedimentary strata may occur prior to or simultaneously with fracturing. If it is also assumed that bedding–plane slip is essentially frictionless, then a situation occurs that, in many respects, is analogous to Anderson's theories (1951). If bedding plane slip is frictionless, or at least nearly so, the shear stresses generated along bedding planes should be infinitesimally small. Accordingly, the bedding plane effectively serves as a principal plane of stress, and one of the principal stress axes must therefore be perpendicular to bedding, regardless of bedding plane orientation (Fig. 2.11a). The remaining two principal stress axes must lie within the bedding plane. When considered in this manner, conjugate shear orientations would form at equal angles to bedding. The preferred angular relationships between observed fractures and bedding, therefore, may be attributable to elastic plate theory and bedding parallel, frictionless slip.

Application of elastic plate theory and frictionless boundary conditions has been applied to stratified sequences by several researchers, notably Reches (1978; see also Reches and Johnson, 1978) and Jackson and Pollard (1990). The work of these researchers is cited for several reasons: Both evaluate small–scale fault orientations within sedimentary sequences, where reported magnitudes of displacement are of comparable scale to the majority of faults in the Joyita Hills area; both provide stereograms for comparison with analyses and interpretations presented herein; and both give a thorough and reasonable account for their observations and interpretations. In addition, the thickness of the Phanerozoic section within the Joyita Hills area approximates

Figure 2.11. A) Generalized elastic plate theory, where free slip (frictionless) displacement occurs along bedding planes separating sedimentary units of contrasting ductility. If bedding plane slip is essentially frictionless, then one of the principal stress axes (here, σ_3) should be consistently normal to bedding, regardless of bedding orientation; B) hypothetical fault offsetting inclined strata. Fault can alternatively be interpreted as a reverse fault (fault generation post-dates bedding rotation) or as a normal fault (fault generation pre-dates bedding rotation); C) hypothetical dike cross-cutting a fold. The dike clearly post-dates the fold. However, both dike and fold may have been re-oriented subsequent to dike emplacement; D) standard stress/strain diagram applicable to elastic deformation. Failure (fracture generation) occurs at the elastic limit; E) standard stress/strain diagram applicable to viscous deformation.



4 km. A 4 km—thick section was studied by Jackson and Pollard (1990), and a 1—2 km—thick section was studied by Reches (1978).

This author objects to application of elastic plate theory and frictionless boundary conditions to near—surface sedimentary rocks for the following reasons: 1) In terrain where sedimentary strata have been flexed and folded, bedding plane slip may be anticipated. Yet evidence of bedding plane slip is in itself problematic, in that evidence (e.g., brecciation or striae within the bedding plane) necessitates that slip was *frictional*, not frictionless. Although it might be argued that bedding plane slip was "nearly frictionless", this assertion cannot be readily verified. 2) Although the occurrence of bedding plane slip near faults (Jackson and Pollard, 1990, p. 196) is suggestive, it is not conclusive and may simply be coincidental, in that there need not be any temporal correlation between the generation of observed faults and generation of bedding plane slip. In other words, the two types of structures may be temporally sequenced (early fracturing post—dated by flexure of strata) rather than simultaneous (fracturing and folding occurring at the same time). 3) In a similar line of reasoning, if a fault offsets horizontal strata (strata that have undergone no rotation), the observer may conclude that the fault is in its original orientation. However, if a fault cross—cuts inclined strata (Fig. 2.11b), the observer cannot simply draw the same conclusion. Fault generation may have occurred prior to, during or after rotation of bedding. Even where a fault (or dike) offsets an existing fold (Fig. 2.11c), the only relationship that can be concluded is that the cross—cutting structure post—dates the folding. That both fault and fold may have experienced post—formation reorientation cannot be excluded. In short, there is no inherent evidence in any outcrop that allows the observer to conclude that a fault is in its original orientation when observation is made in inclined strata.

An alternative interpretation to elastic plate theory and frictionless boundary conditions, as proposed herein, is that tectonically induced fracturing is superimposed on bedding prior to any significant reorientation of strata. In the foregoing analyses,

brittle structures (faults and associated striae, joints and dikes) have been plotted with respect to bedding by restoring strata to horizontal and rotating fractures by an equivalent amount. The analytical process, therefore, treats fractures as early-formed structures within a deformational event. If fractures have already been superimposed on the sedimentary sequences, then folding should reorient and redistribute both bedding and existing structural elements by equivalent amounts. Resultant, small-scale fracture patterns would look similar to those predicted by elastic plate theory and frictionless boundary conditions, yet would be the result of an inherently different mechanism.

Consideration of standard stress-strain diagrams (Fig. 2.11d,e) indicates that in near-surface deformation, brittle failure occurs at the elastic limit. Therefore, failure may occur in the absence of folding (Fig. 2.11d), or perhaps better put, prior to folding (Fig. 2.11e). If the folds evaluated by Reches (1978) and Jackson and Pollard (1990) are considered as viscous deformation, then one might anticipate that the observed fracturing predated any appreciable folding of strata. Although Biot (1961) indicates that if rates of deformation are low, folding may occur without brittle failure, such need not be the case. If deformation rates are high, and/or if ambient temperatures and pressures are low, then brittle failure would logically be the initial response, rather than folding. Further, in that sedimentary sequences are typically restricted to shallow crustal environments, it may be anticipated that rocks initially respond in an elastic manner, and only begin to fold (viscous response) after ambient temperatures and pressures have been elevated by progressive deformation.

DISCUSSION

What are the implications of early-formed fractures within a tectonic perspective? If tectonically induced fractures (composed of tensile fractures and both shear joints and small faults) form as the initial response, then of necessity, these early-formed structural elements may effectively serve as existing planar weaknesses that are ideally oriented to accommodate imposed strains of increasing magnitude as deformation

develops. Extension fractures would be present to accommodate extension parallel to σ_3 . Shear fractures, originating only as joints and small faults, would already be present to accommodate fault displacements of increasing magnitude. If we assume that these joints and small faults are numerous and widely distributed across the disturbed area, then some of these shear fractures may be utilized to accommodate additional displacements. Some, probably most, will remain unused. Others may develop into mesoscale faults, still fewer may develop into regional faults. However, with increasing displacement, the original angular relationship between the fault plane and bedding may be lost through increasingly developed fault drag and brecciation. In contrast, the multitude of early-formed shear joints and small faults that experience limited displacement serve as comparatively pristine 'markers' that, when combined with tensile fractures, can be utilized to evaluate stress orientations.

The analyses presented herein have demonstrated that tectonically induced fracturing (joints and small-displacement faults) commonly maintain preferred angular relationships with respect to bedding. Others, notably Reches (1976; 1978), Beck and Burford (1985), and Jackson and Pollard (1990) have demonstrated similar relationships. These relationships may be attributed to either elastic plate theory and frictionless boundary conditions or to initial fracturing. Although the analyses and arguments put forth in this paper do not provide a means to distinguish between the two mechanisms, the results of this study indicate that the concept of initial fracturing provides a viable alternative to elastic plate theory combined with frictionless bedding plane slip. The interpretation of initial fracturing is preferred by this author, in that it would seem inherently simpler: When tectonically induced fracturing is considered as the initial response, the orientation of the applied stress field may remain constant for the duration of the tectonic event. Only the strain markers (fracture patterns) need to be rotated, not the stress axes themselves. It is emphasized that the concept of initial fracturing does not preclude the generation of additional faults at later stages within a

deformational event. Rather it suggests that early fractures are ideally oriented to accommodate shear and tensile displacements until either the stress field orientation changes or rotation redistributes early fractures such that they are no longer suitably oriented to accommodate displacement. The structural history of the Joyita Hills was such that early deformational events resulted in only limited rotation of strata. In contrast, Angelier (1989) has recognized both pre- and post-tilt fracture patterns. One should not anticipate a constancy between fracture orientation and bedding in multiply-deformed terrain where early deformational events have resulted in significant re-orientation of strata. In these settings, the relationships between fracture orientation and bedding would be more complex, and beyond the scope of this paper.

Part 3

**NEW FUSULINID DATA AND MULTIPLE EPISODES OF ANCESTRAL ROCKY
MOUNTAIN DEFORMATION IN THE JOYITA HILLS, SOCORRO COUNTY,
NEW MEXICO**

Submitted to New Mexico Geology

April 15, 1992

INTRODUCTION

The Joyita Hills (Los Canoncitos) are located in north-central Socorro County, New Mexico (Fig. 3.1). Previous stratigraphic and paleontologic investigations (Read and Wood, 1947; Kottlowski, 1960; Kottlowski and Stewart, 1970; Stewart, 1970; Siemers, 1978; 1983; Baars, 1982; Altares, 1990) have interpreted the modern-day Joyita Hills area to have been the location of an ancestral Rocky Mountain uplift (the late Paleozoic Joyita uplift). Arkosic sedimentary rocks of the Bursum Formation (Kottlowski and Stewart, 1970; Altares, 1990) represent syntectonic detritus shed from this and other late Paleozoic uplifts (e.g., the Pedernal, Uncompahgre and Zuni uplifts to the east, north and northwest, respectively). On a more regional scale, interpretations of late Paleozoic sedimentation and tectonism have been provided by Armstrong (1962), Armstrong and Mamet (1988), Peterson (1980), Kluth and Coney (1981) and Kluth (1986).

The purpose of this paper is to present new fusulinid data and new structural data relevant to the timing and tectonic development of the Joyita uplift. Earlier biostratigraphic (fusulinid) analyses within the Joyita Hills have been conducted by Kottlowski and Stewart (1970) and Stewart (1970). However, the fusulinids used in their analyses were recovered exclusively from Pennsylvanian strata on the west side of the Proterozoic core, and no fusulinids had been recovered from the overlying syntectonic Bursum Formation. On the basis of both local and regional stratigraphic relationships, Kottlowski and Stewart (1970) inferred that late Paleozoic uplift within the Joyita Hills area was dominantly a Wolfcampian event. Recent mapping of the Joyita Hills by the author has revealed additional exposures of Bursum strata along the east side of the Proterozoic core. Fusulinid-bearing limestone horizons yield *Schwagerina* and *Triticites* fauna (fusulinid identifications courtesy of D.A. Myers, written comm. 1990; 1991). This assemblage establishes the Bursum deposits as early Wolfcampian, and confirms the interpretations of Kottlowski and Stewart (1970).

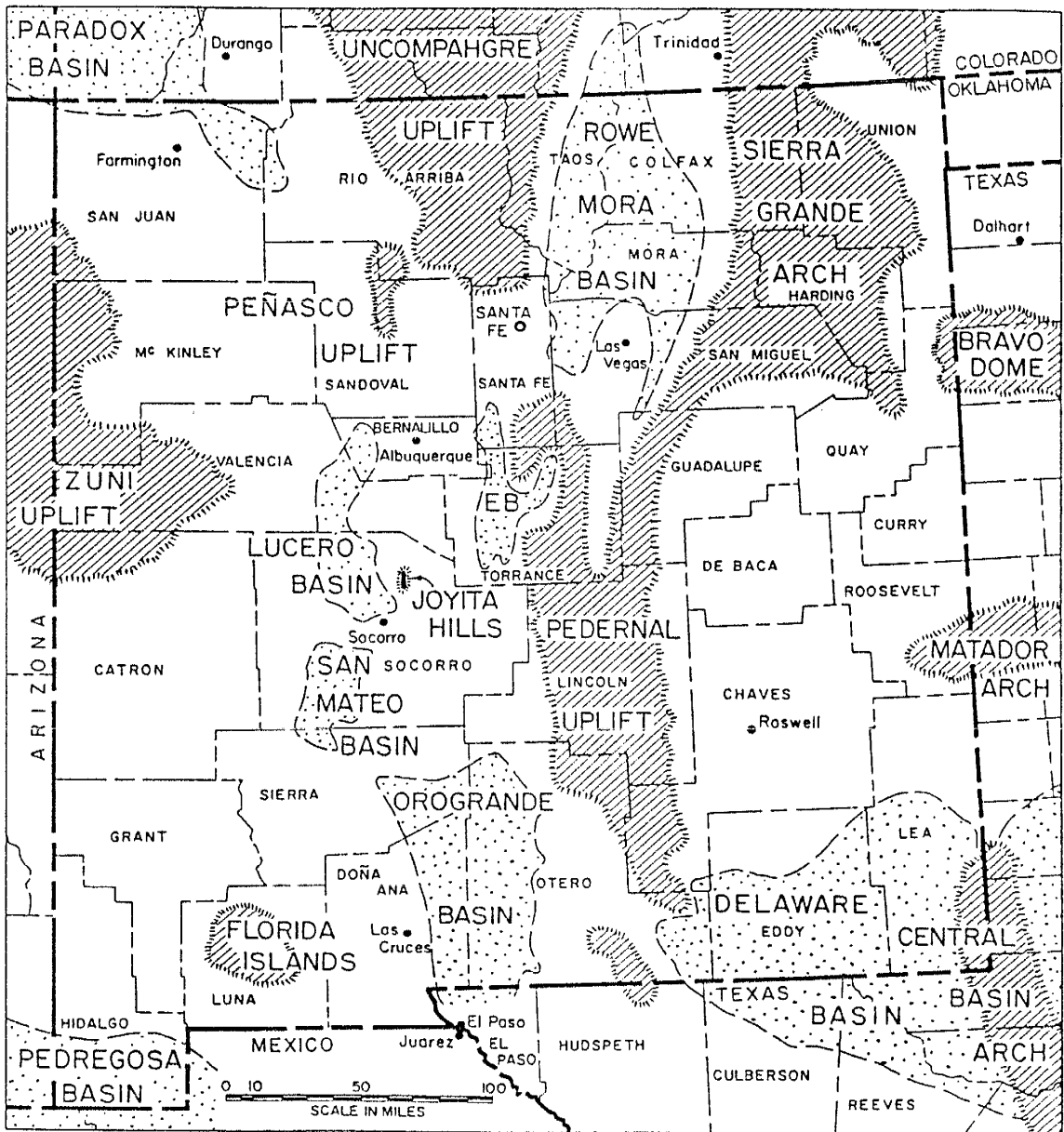


Figure 3.1. Pennsylvanian paleogeographic index map showing the location of major uplifts and depositional basins, and the location of the modern-day Joyita Hills (late Paleozoic Joyita uplift) in north-central Socorro County. From Kottlowski and Stewart (1970).

Structural and tectonic interpretations of Wolfcampian tectonism within central New Mexico have been discussed previously by Beck and Chapin (1991). However, additional structures within the Joyita Hills are indicative of an older deformational episode. Fusulinid analyses (Kottowski and Stewart, 1970; herein) indicate that this early tectonism occurred during the Atokan.

Accordingly, the data presented herein are intended to supplement earlier interpretations of Kottowski and Stewart (1970) and Beck and Chapin (1991).

GENERAL STRATIGRAPHIC RELATIONSHIPS

Pennsylvanian strata within the Joyita Hills range in thickness from 0 to 127 m (Kottowski and Stewart, 1970; 0 to 112 m, Siemers, 1983). Measured sections, petrologic and biostratigraphic analyses of these rocks have been presented in detail by Kottowski and Stewart (1970), Stewart (1970) and Siemers (1978; 1983). That which follows is a general discussion of Pennsylvanian and early Permian stratigraphy (Fig. 3.2) within the Joyita Hills based on the work of Kottowski and Stewart (1970), Siemers (1983) and observations of the author. Permian strata within the Joyita Hills have received much less attention, and a regional analysis of the Permian system by Peterson (1980) has been used to supplement the personal observations and interpretations presented herein.

Pennsylvanian Strata

Proterozoic rocks (augen gneiss) exposed within the core of the Joyita Hills are nonconformably overlain by strata of the Sandia Formation (0 to 49 m, Kottowski and Stewart, 1970; 0 to 48 m, Siemers, 1983). The age of the basal Sandia is uncertain due to an absence of diagnostic fossils. However, the Sandia Formation is thought to be exclusively early Atokan, the underlying Proterozoic rocks having formed a subaerially exposed upland of low topographic relief during Morrowan time. Lenticular, quartzitic sandstones of the basal Sandia filled shallow topographic depressions on this erosional

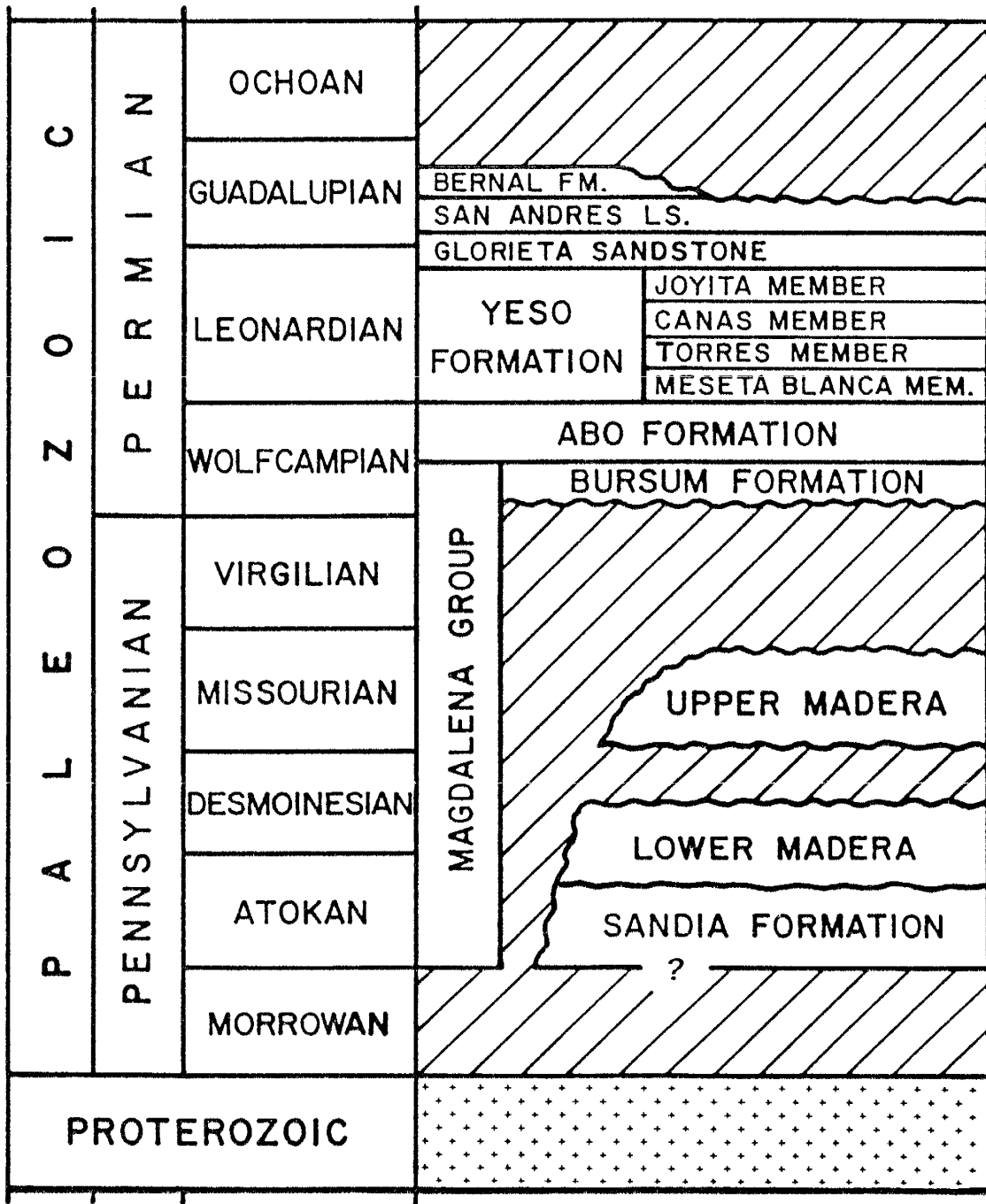


Figure 3.2. Generalized Paleozoic stratigraphic section within the Joyita Hills. Mesozoic and Cenozoic stratigraphic units (not shown) are also exposed within the Joyita Hills and adjacent areas (El Valle de La Joya) to the east and south. Modified from Osburn and Lochman-Balk (1983), Kottlowski and Stewart (1970) and Beck and Chapin (1991).

surface. Overlying strata are dominantly dark gray to black, carbonaceous shales, with lesser, interstratified bone coal, sandstone and limestone horizons. Palaeoenvironments have been interpreted (Kottowski and Stewart, 1970; Siemers, 1983) as shallow, restricted to euxinic lagoon, marsh and intertidal settings (clastics) interrupted by short periods of subaerial exposure and occasional deepening to shallow, less restricted marine shelf settings (carbonates).

The overlying Madera Formation (0 to 78 m, Kottowski and Stewart, 1970; 0 to 64 m, Siemers, 1983) is composed of limestones and subordinate fine-grained clastics. The Madera is broadly subdivided into a lower sequence of massive, cliff-forming limestones and an upper sequence of interbedded limestones and fine-grained clastics. Limestones within the lower sequence span late Atokan to early Desmoinesian time, and consist of grey, cherty mudstones and wackestones, indicative of deposition in normal, open marine, inner to outer shelf settings.

The overlying, interbedded limestone and clastic sequences range in age from early Desmoinesian to Missourian. Interbedded, argillaceous marine limestones and calcareous, fossiliferous shales and micrites are in turn interstratified with red, arkosic shales and mudstones. The clastics represent episodic influx of terrigenous debris shed from Pennsylvanian uplifts. The fine-grained character of the detritus is indicative of distal source areas, which are inferred to have been the Pedernal uplift to the east and the Zuni uplift to the northwest (Fig. 3.1). Both Kottowski and Stewart (1970) and Siemers (1983) indicate that the influx of arkosic debris occurred during Missourian time.

Strata deposited during the foregoing stages of the Pennsylvanian are significantly thinner in the Joyita Hills than those deposited within adjacent basins (typically 610 to 820 m; Kottowski, 1960, fig. 25; Siemers, 1983, fig. 3, tabs. 1 and 2). Therefore, the anomalously thin section can be attributed to tectonic adjustments during sedimentation, rather than uplift and erosion of an initially thick Pennsylvanian section. These adjustments served to elevate the Joyita uplift as a structurally positive block

throughout the Pennsylvanian. Kottowski and Stewart (1970, p. 29) note that late Desmoinesian strata are absent within the Joyita Hills, which has been attributed to middle Desmoinesian uplift and erosion (see also Kluth, 1986, p. 356). Virgilian strata are also absent within the Joyita Hills. On the basis of regional relationships, Kottowski and Stewart (1970) inferred that a thin Virgilian section may have been deposited in the Joyita Hills, but subsequently removed by late Pennsylvanian and early Permian uplift and erosion. In addition to these unconformities, Kottowski and Stewart (1970) report several diastems within the lower Pennsylvanian section of the Joyita Hills. These occur within early and late Atokan strata, along the Atokan/Desmoinesian contact, and within early Desmoinesian strata. The latter two are indicative of localized uplift and erosion, as evidenced by clasts of quartz, feldspar, augen gneiss and reworked limestone.

It is important to note that Kottowski (1960, p. 152) indicates the term "basin" may be misleading, in that depocenters probably were not much deeper than nearby uplifts. Therefore, sedimentation within the basins must have kept pace with subsidence. In contrast to the continuous sedimentation within depocenters, episodes of intermittent subaerial exposure, uplift and erosion recorded in the Joyita Hills section indicate that the Joyita uplift remained as a structurally positive element amid rapidly subsiding basins. The foregoing unconformities, diastems and general thinness of the Pennsylvanian section in the Joyita Hills, relative to the thickness of comparably aged strata within adjacent depositional basins, attest to the persistent, weakly positive nature of the Joyita uplift throughout the Pennsylvanian.

Permian Strata

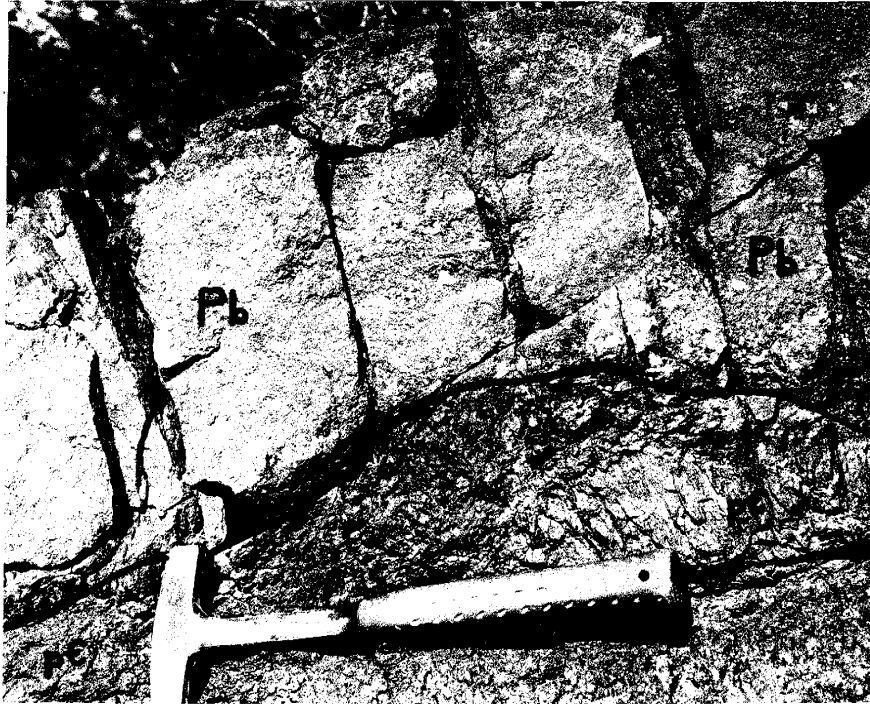
Pennsylvanian strata in the Joyita Hills are unconformably overlain by strata of the syntectonic Bursum Formation. The unconformity is angular, as Bursum strata successively truncate the Missourian, Desmoinesian and Atokan sequences from north to south, until they lie in depositional contact on the Proterozoic augen gneiss within the

southern Joyita Hills (Fig. 3.3a; Kottowski and Stewart, 1970, fig. 2; Beck and Chapin, 1991, fig. 5). Restoration of average bedding orientations within the Sandia, Madera and Bursum formations (using the regional bedding orientation determined from overlying strata exposed within the Joyita Hills) indicates that these strata were gently inclined (5° – 10°) to the east and northeast as a result of late Paleozoic tectonism.

Strata of the Bursum Formation are texturally and compositionally immature, typically 9 m thick, and composed of interstratified, red and less commonly greenish–grey, arkosic shales, mudstones and breccias (Fig. 3.3b), with lesser, discontinuous limestone horizons. The clastics are indicative of proximal deposits shed from a local uplift. Breccias typically contain a sand matrix, with pebble– to cobble– and occasionally boulder–sized clasts of limestone (typically silicified), vein quartz, pink feldspar and augen gneiss derived from the underlying Pennsylvanian and Proterozoic rocks. In the vicinity of Central Canyon (Fig 3.4; "Central Canyon" is an informal name adopted from Kottowski and Stewart, 1970), Bursum sequences stratigraphically overlie the Madera Formation. Both are in fault contact with older Pennsylvanian and Proterozoic rocks (Fig. 3.5). This fault has been interpreted by Beck and Chapin (1991, fig. 6) as an ancestral Rocky Mountain fault. Here, the Bursum strata are anomalously thick and coarse–grained in the hanging wall (west block; downthrown) and were apparently deposited against the exposed fault scarp. In the footwall (east block; upthrown), both Madera and Bursum strata are thinned (the former erosionally, and the latter depositionally and/or erosionally). Both the fault and offset strata are overlain by anomalously thin, unfaulted strata of the Abo Formation. Clearly, the Bursum strata are syntectonic deposits derived from local uplift. On the basis of regional relationships, Kottowski and Stewart (1970; see also Altares, 1990) inferred that the Bursum deposits were early Wolfcampian.

In general, strata of the Wolfcampian Abo Formation conformably overlie, and are intertongued with the Bursum Formation. A potential exception to this generality

Figure 3.3. Selected photographs of lithologies and features within the Bursum and Abo formations. A) Coarse, arkosic Bursum (Pb) in depositional contact with foliated Proterozoic augen gneiss (pC) in the southern Joyita Hills; B) A silicified limestone pebble arkose at the base of the Bursum (interpreted as early Wolfcampian colluvium) lies in depositional contact on erosionally thinned limestones of the Madera Formation in the southern Joyita Hills; C) Limestone pebble conglomerate in the Wolfcampian Abo Formation; and D) Arkosic breccia within the Bursum Formation (east of the Proterozoic core) contains lithic clasts of Proterozoic augen gneiss (pC), vein quartz (Q), silicified limestone (L) and pink feldspar (F).

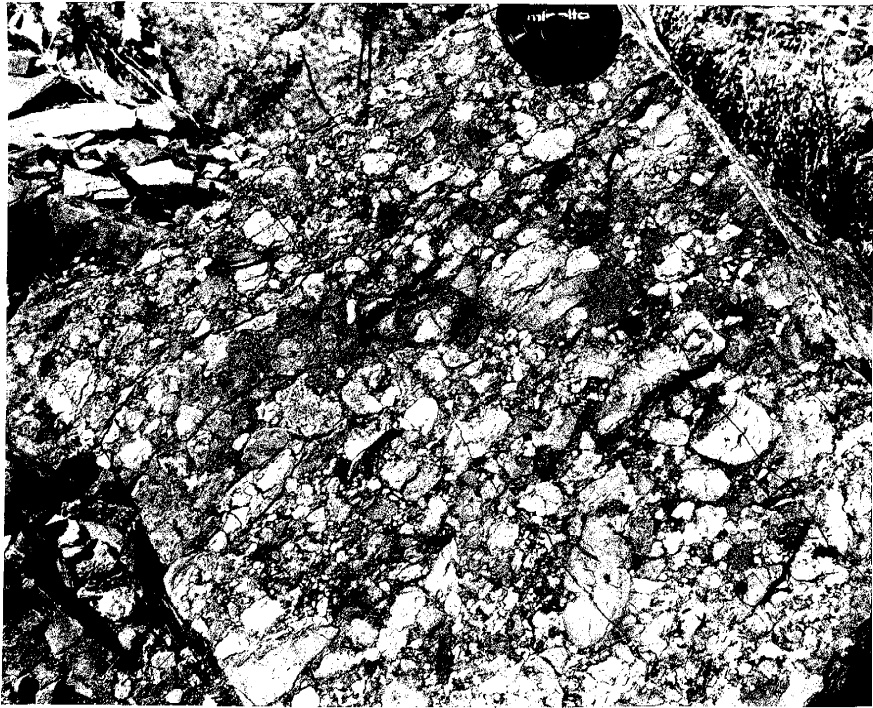


(a)



(b)

Figure 3.3, continued. Selected photographs of lithologies and features within the Bursum and Abo formations. A) Coarse, arkosic Bursum (Pb) in depositional contact with foliated Proterozoic augen gneiss (pC) in the southern Joyita Hills; B) A silicified limestone pebble arkose at the base of the Bursum (interpreted as early Wolfcampian colluvium) lies in depositional contact on erosionally thinned limestones of the Madera Formation in the southern Joyita Hills; C) Limestone pebble conglomerate in the Wolfcampian Abo Formation; and D) Arkosic breccia within the Bursum Formation (east of the Proterozoic core) contains lithic clasts of Proterozoic augen gneiss (pC), vein quartz (Q), silicified limestone (L) and pink feldspar (F).



(c)



(d)

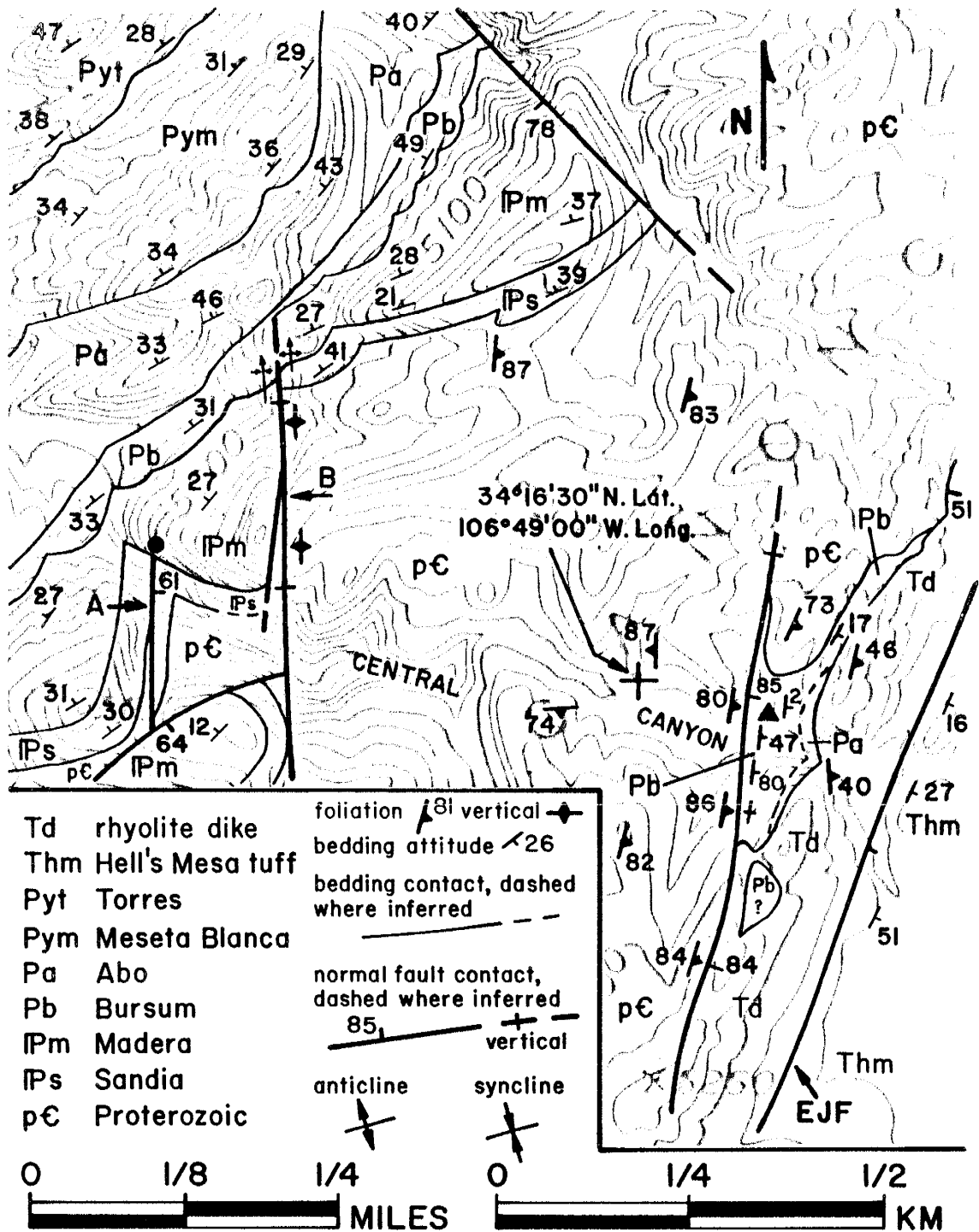
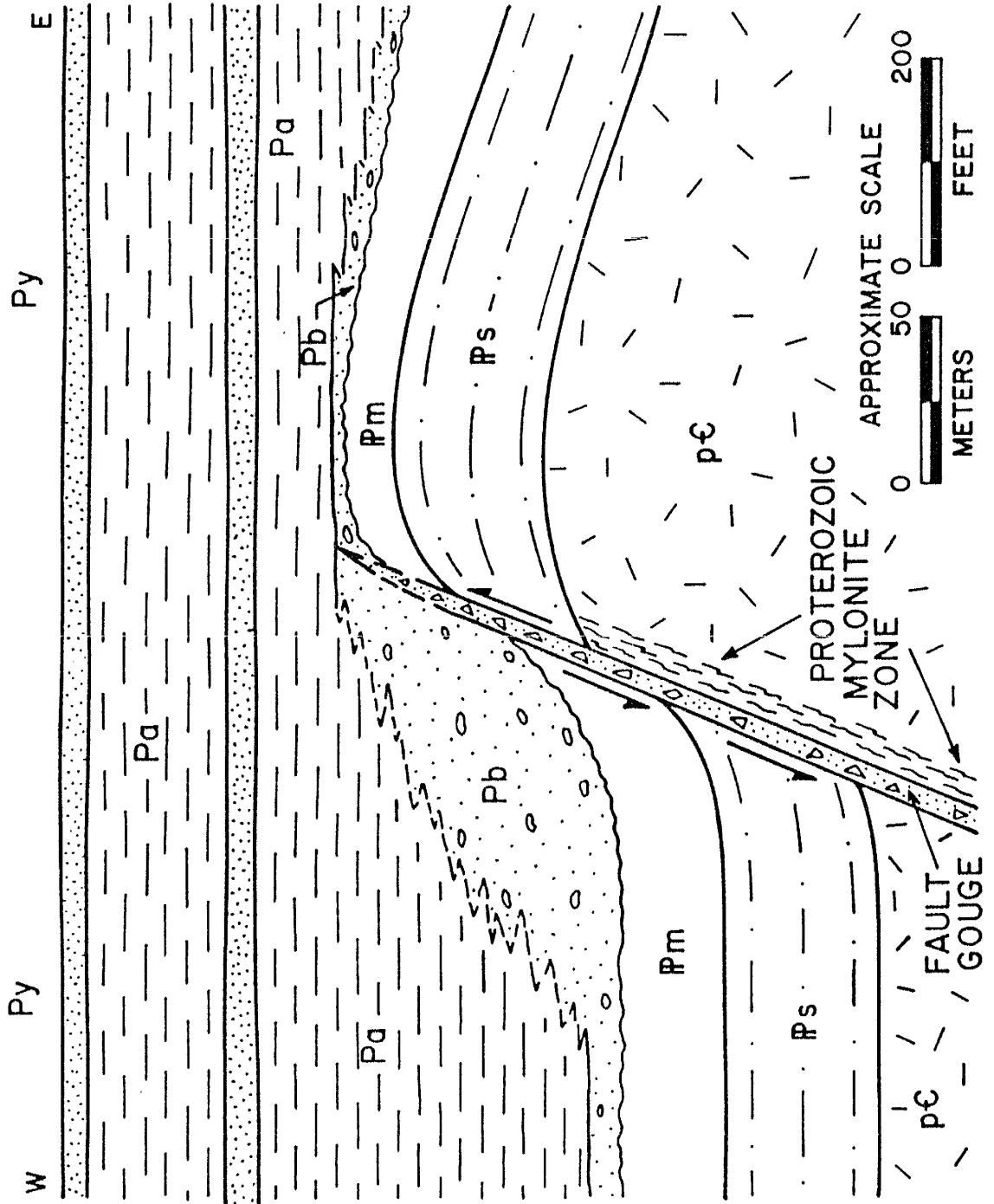


Figure 3.4. Generalized geologic map of the Central Canyon area of the Joyita Hills. With the exception of the East Joyita fault (EIJF), all faults are unnamed. The Atokan and Wolfcampian faults described in text are labelled A and B, respectively. Fusulinid sample localities are marked with ● (Atokan) and ▲ (Wolfcampian). Pb? is interpreted as a Bursum megalith incorporated into the Tertiary dike.

Figure 3.5. Generalized cross section along the early Wolfcampian normal fault (labelled B in Fig. 3.4). Cross section has been restored to its post --ancestral Rocky Mountain orientation by removing 30° of down --to --the --west rotation about a N35°E, horizontal axis. Fault and contacts dashed where obscured; key to formation symbols provided in Figure 3.4. From Beck and Chapin, 1991.



occurs in the southernmost Joyita Hills, where depositionally thinned Abo sequences are separated from underlying Proterozoic rocks by an anomalously thin (1 to 2 m) unit of Bursum-like strata (Fig. 3.3a). This unit of Bursum-like strata may be alternatively interpreted as a thin deposit of the Bursum Formation, or as a Bursum-like lithology at the base of (and within) the Abo Formation. Typically, Abo sequences are red, arkosic mudstones and shales, with lesser channel sandstone horizons. The majority of these sediments were most likely derived from the larger Pedernal, Uncompahgre and Zuni uplifts (to the east, north and northwest, respectively; Fig. 3.1) which eventually covered the comparatively small Joyita uplift. The fine-grained, arkosic sediments of the Abo (typically 110 m thick in the Joyita Hills) are indicative of subaerial sedimentation during the waning stages of ancestral Rocky Mountain tectonism. Occasional limestone pebble conglomerate beds (Fig. 3.3c) have been observed within the lower 75% of the Abo section. These beds are interpreted to indicate that episodic tectonic adjustments occurred during Abo deposition, and/or that local, remnant exposures of limestone uplands persisted well into Wolfcampian time.

Peterson (1980) indicates that the late Paleozoic basins within New Mexico were largely filled with sediment during Wolfcampian time and that most of the late Paleozoic uplifts were completely buried by Leonardian/Guadalupian sedimentation. Within the Joyita Hills and surrounding areas, Leonardian and Guadalupian strata formed extensive, sheet-like layers of compositionally mature, well-sorted clastics and clean carbonates of the Yeso, Glorieta and San Andres formations (Fig. 3.2). These lithologies are indicative of relative tectonic quiescence, and a cessation of ancestral Rocky Mountain tectonism within central New Mexico.

ATOKAN DEFORMATION

Several (6–8) faults of northward strike offset the Sandia Formation and underlying Proterozoic rocks. Most of these faults are poorly exposed and can only be mapped as surface traces. All appear to be of comparable orientation, in that they have a

consistent surface trend and all exhibit a down-to-the-east sense of displacement. Offsets are on the order of a few tens of meters. Cross-sectional exposure of one of these faults (Fig. 3.6) has been observed in Central Canyon (Fig. 3.4). Although partially obscured by colluvium, offset strata of the Sandia are overlain by unfaulted strata of the Madera Formation. Down-to-the-east displacement (as evidenced by fault drag and correlation of a sandstone marker horizon in both eastern and western fault blocks) has been measured at approximately 23 m. Restoration of the fault and contained fault striae (using bedding orientations within the Madera) indicates that the original fault orientation was subvertical, striking N12°E. Restored fault striae indicate subvertical displacement. Strata within both formations are comparably oriented, indicating that the episode of faulting was non-rotational (excluding fault drag). Although Holocene colluvium obscures the basal Madera and the uppermost extent of the fault, it is considered unlikely that approximately 23 m of displacement would die out within the remaining 9 m of covered slope.

Specimens of *Fusulinella famula* Thompson and *F. devexa* Thompson have been recovered from the lower limestones of the Madera Formation in the vicinity of Central Canyon by Kottlowski and Stewart (1970; figs. 4, 5 and 8, section JH 3). Similarly, *Fusulinella* aff. *F. juncea* Thompson has been recovered (Table 3.1) from the lowermost Madera limestones exposed above the aforementioned fault (Fig. 3.6). The *Fusulinella* biozone dates these lower Madera limestone horizons as late Atokan (Kottlowski and Stewart, 1970, p. 22). Offset strata of the underlying Sandia Formation have been established as early Atokan (Kottlowski and Stewart, 1970; Siemers, 1983), and therefore this faulting episode can be constrained as an Atokan event.

WOLFCAMPIAN FUSULINIDS

Recent structural investigations and detailed mapping in the Joyita Hills have found previously unmapped exposures of the Bursum Formation in the vicinity of Central Canyon (Fig. 3.4). These rocks are exposed between the East Joyita fault and an

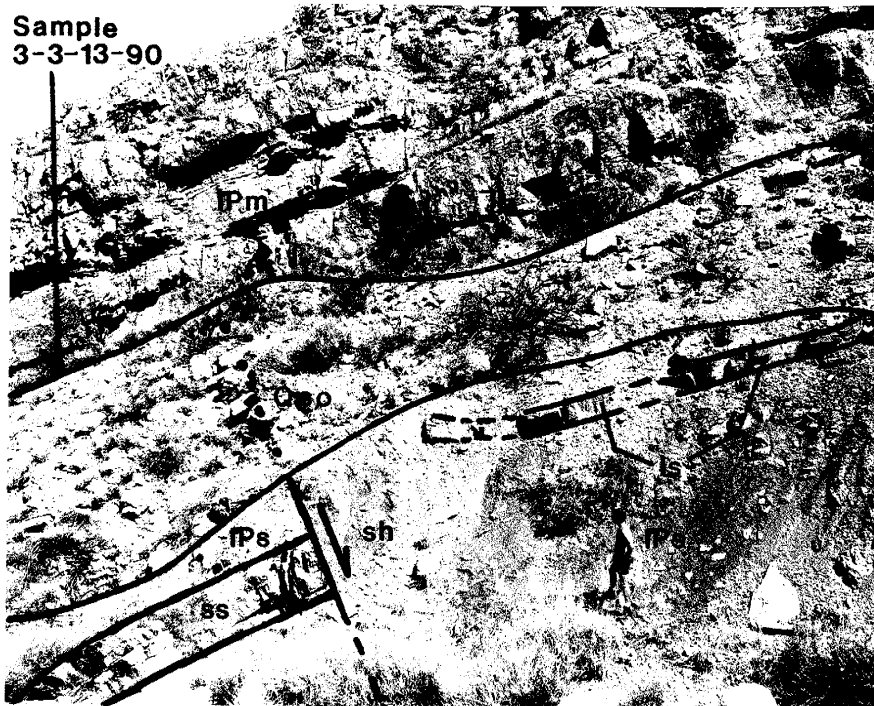


Figure 3.6. Cross-sectional exposure of the Atokan fault (labelled A in Fig. 3.4); view to north. Down-to-the-east displacement approximates 23 m. Fusulinid sample 3-3-13-90 collected from lowermost limestone exposed above colluvium (arrow). Ip = Sandia; Im = Madera; Qco = colluvium; ss = sandstone; ls = limestone; sh = shale. M.D. Boryta for scale.

Table 1. Fusulinid identifications (D. A. Myers, written communication, 1990; 1991). * Read as "sample #3, collected on March 13, 1990."

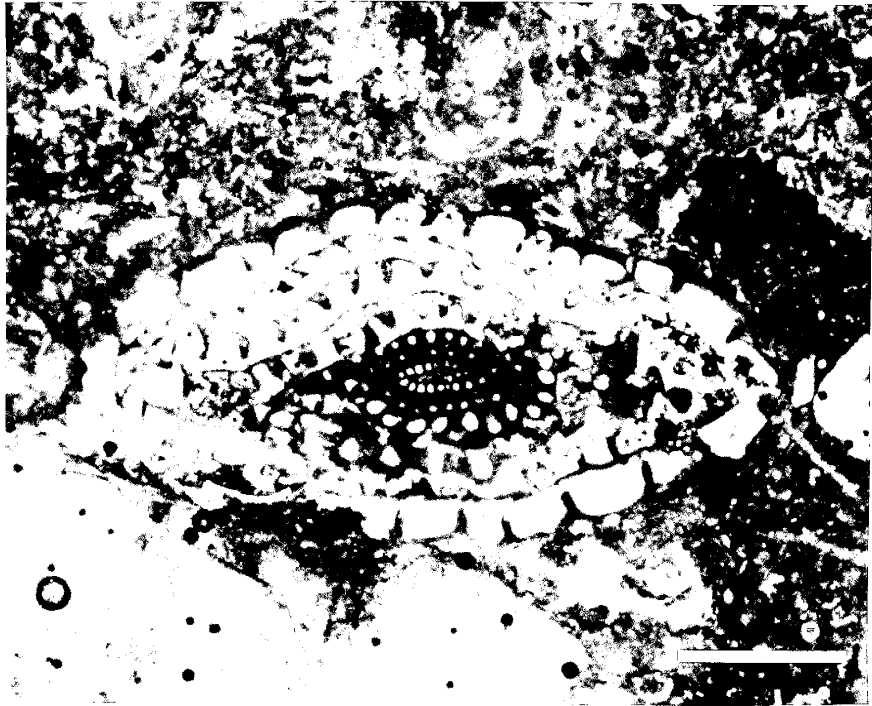
Sample	Identification	Interpretation	Figure
3-3-13-90*	<i>Fusulinella</i> aff. <i>F. juncea</i> Thompson	Atokan	
4-3-13-90	<i>Schwagerina</i> cf. <i>S. pinosensis</i> Thompson <i>Triticites</i> aff. <i>T. creekensis</i> Thompson	Wolfcampian-Bursum Wolfcampian-Bursum	7a
8-10-29-90	<i>Triticites</i> aff. <i>T. creekensis</i> Thompson	Wolfcampian-Bursum	
10-10-29-90	<i>Triticites</i> aff. <i>T. creekensis</i> Thompson	Wolfcampian-Bursum	
11-10-29-90	<i>Triticites</i> aff. <i>T. creekensis</i> Thompson	Wolfcampian-Bursum	7b
12-10-29-90	<i>Triticites</i> aff. <i>T. creekensis</i> Thompson	Wolfcampian-Bursum	

unnamed, north–striking fault of ancestral Rocky Mountain origin. Both faults exhibit a down–to–the–east displacement, which is attributed to Oligocene–Miocene extension (the original, late Paleozoic displacement on the unnamed fault was down–to–the–west; Beck and Chapin, 1991). Relationships are further obscured by an intrusive, mid–Tertiary rhyolite dike (31.3 ± 1.2 Ma, Aldrich et al., 1986, p. 6201, stress indicator #324). Consequently, the base and top of the Bursum are only locally exposed. Where the base of the Bursum is exposed, the Bursum appears to be in depositional contact with Proterozoic rocks. Where the top is exposed, the Bursum strata are overlain by strata of the Abo Formation. However, the combination of known fault and intrusive dike contacts, much vegetation and Holocene colluvium and alluvium prohibits an accurate determination of the true thickness of the Bursum.

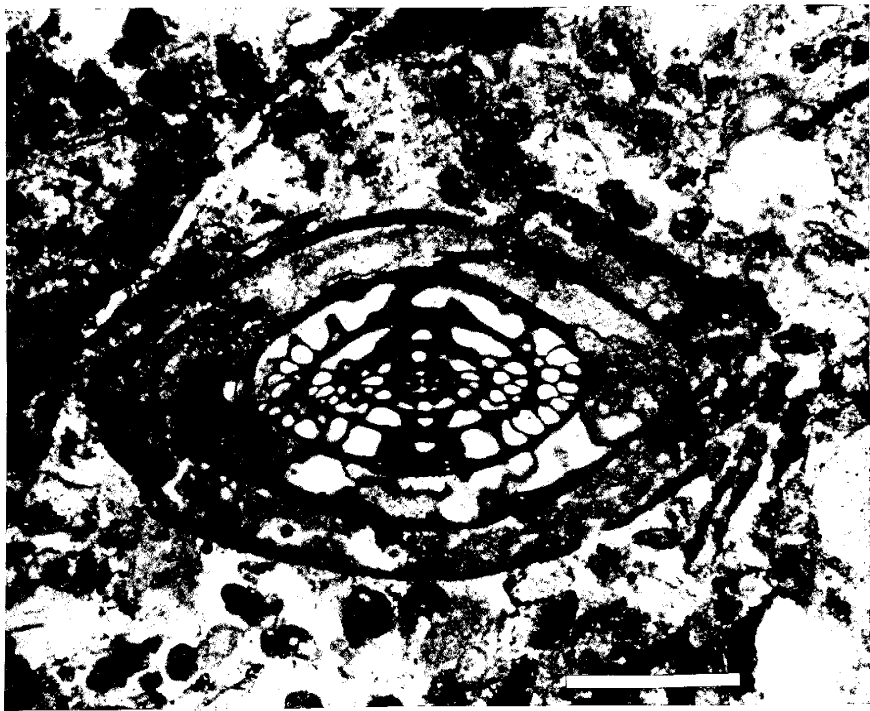
These outcrops of the Bursum Formation are comparable to those on the west side of the Proterozoic core. Reddish–brown and less commonly greenish–grey, coarse–grained sandstones, gravels and breccias predominate. Arkosic mudstones and shales are also present. The sandstones and gravels are poorly to moderately sorted and predominantly composed of subangular quartz and potassium feldspar grains. Breccias (Fig. 3.3d) contain a sand matrix and gravel– to pebble–sized lithic clasts of augen gneiss (similar to the augen gneiss within the Proterozoic core), vein quartz, pink feldspar, and silicified limestone.

Occasional limestone beds are interstratified with the arkosic clastic sequences, and are thought to represent lack of detrital influx due to episodic tectonic quiescence and/or rapid sea level rise due to eustacy. The limestones appear to be discontinuous, lenticular (maximum 1 m thick) horizons that are composed of light to medium grey, calcareous grainstones and packstones, and less commonly, calcareous mudstones. Specimens of the genera *Schwagerina* and *Triticites* have been recovered and identified (Table 1), including *Schwagerina* cf. *S. pinosensis* Thompson (Fig. 3.7a) and *Triticites* aff. *T. creekensis* Thompson (Fig. 3.7b). These fusulinids date the syntectonic Bursum

Figure 3.7. Fusulinids recovered from limestones within the Bursum Formation on the east side of the Proterozoic core of the Joyita Hills (Fig. 3.4). A) *Schwagerina* cf. *S. pinosensis* Thompson; B) *Triticites* aff. *T. creekensis* Thompson. Scale bars equivalent to 1 mm.



(a)



(b)

Formation as early Wolfcampian, and indicate that the dominant phase of tectonism associated with the Joyita uplift was an early Wolfcampian event.

SUMMARY

The new fusulinid data and new structural data presented herein are intended to supplement earlier interpretations of late Paleozoic sedimentation and tectonism (Kottlowski and Stewart, 1970; Beck and Chapin, 1991). Fusulinid analyses of Kottlowski and Stewart (1970) and Stewart (1970) have been presented in more detail. However, they did not recover fusulinids from the syntectonic Bursum Formation. Limestones within Bursum outcrops west of the Proterozoic core, where Kottlowski and Stewart (1970) conducted their analyses, are apparently barren with respect to fusulinid content. Newly recognized outcrops of Bursum strata east of the Proterozoic core, however, do contain fusulinid-bearing limestones. The *Schwagerina* and *Triticites* fauna recovered from these newly sampled outcrops establish the syntectonic Bursum sediments as early Wolfcampian, and confirm the earlier interpretations of Kottlowski and Stewart (1970).

Similarly, the analyses and discussion of Atokan tectonism are hindered by the limited number of faults and poor exposure. Although constrained as an Atokan event, this episode of structural deformation is poorly understood. Restoration indicates down-to-the-east, subvertical displacement occurred along subvertical, northerly striking faults. The limited displacements observed along these faults suggest that this event was comparatively minor.

The structural trends that were to control late Paleozoic uplift and sedimentation began to develop during Chesterian time (late Mississippian; Armstrong, 1962; Armstrong and Mamet, 1988; Kluth, 1986). These trends persisted throughout the Pennsylvanian (Kottlowski, 1960) and into the Permian (Peterson, 1980). The persistent, weakly positive nature of the Joyita uplift (Kottlowski and Stewart, 1970; Siemers, 1983) throughout the Pennsylvanian indicates that tectonic adjustments must have

occurred during Pennsylvanian sedimentation. The unconformities and diastems observed within the Pennsylvanian section of the Joyita Hills (Kottlowski and Stewart, 1970), observed Atokan structures, and inferred middle Desmoinesian uplift and erosion (Kottlowski and Stewart, 1970) are thought to reflect these adjustments. However, they were apparently minor events during the tectonic development of the Joyita uplift, and only precursors to the major orogenic episode during the early Wolfcampian (Kottlowski and Stewart, 1970; Beck and Chapin, 1991).

Part 4

**STRUCTURAL AND TECTONIC EVOLUTION OF THE JOYITA HILLS,
CENTRAL NEW MEXICO: IMPLICATIONS OF BASEMENT CONTROL ON
RIO GRANDE RIFT**

Submitted to the Geological Society of America

August 26, 1992

INTRODUCTION

The Joyita Hills (Los Canoncitos) area is a north–northeast–trending, west–tilted, normal–fault block at the southern end of the Albuquerque Basin (Fig. 4.1). Approximately 4 km of inclined Phanerozoic sedimentary and volcanic strata are well exposed in the Joyita Hills and adjacent areas to the east and south (El Valle de La Joya; Figs. 4.1 and 4.2). Proterozoic basement rocks (augen gneiss) are also exposed in the core of the Joyita Hills. These rock sequences represent much of the known section in central New Mexico, and record the faults, folds and other structures that formed in response to a minimum of three recognized Phanerozoic orogenic events. Previous stratigraphic and biostratigraphic investigations (Read and Wood, 1947; Kottowski, 1960; Kottowski and Stewart, 1970; Baars, 1982; and Siemers, 1978, 1983) have identified the Joyita Hills area as the location of an ancestral Rocky Mountain uplift (the late Paleozoic Joyita uplift). Structural and tectonic interpretations of the Joyita uplift have been previously discussed by Beck and Chapin (1991) and Beck and Johnson (1992). In addition to ancestral Rocky Mountain deformation, partial omission of late Paleozoic and Mesozoic strata west of the East Joyita fault (Figs. 4.1 and 4.2) is indicative of Laramide uplift and erosion, and west–tilted Oligocene volcanic strata attest to deformation associated with Rio Grande rift extension.

Resultant overprinting of diverse structural styles has resulted in a complex array of fault types and orientations. Observed structures include those associated with crustal extension, wrench tectonics, and to a lesser extent, thrust faulting. Fortuitously, the stratigraphic units preserved in the Joyita Hills and El Valle de La Joya (Fig. 4.2) represent pre–, syn–, and post–tectonic sequences that roughly bracket each recognized tectonic episode. For example, middle Permian (Leonardian and Guadalupian) and Mesozoic sedimentary units postdate ancestral Rocky Mountain deformation and predate Laramide tectonism; Oligocene volcanic units postdate Laramide deformation and represent pre– and syntectonic units with respect to Rio Grande rift

Figure 4.1. Generalized geologic map of northeast Socorro County, New Mexico. Data presented herein were collected from Proterozoic and Phanerozoic exposures in the Joyita Hills (JH) and El Valle de La Joya (EVLJ). Regional faults include the East Joyita fault (EJF), Del Curto fault (DCF) and Montosa fault (MF). pC = Proterozoic; P/eP = Pennsylvanian and earliest Permian strata; P = Permian strata; R = Triassic strata; K = Cretaceous strata; Teb = Eocene basin deposits; Tv = latest Eocene - Oligocene volcanics; Ti = Oligocene intrusives (dikes and plugs); Tb = Pliocene basalt flows; QTbf = Quaternary and Tertiary basin fill; Qa = Quaternary alluvium. Modified from Osburn (1984) and Myers *et al.* (1986).

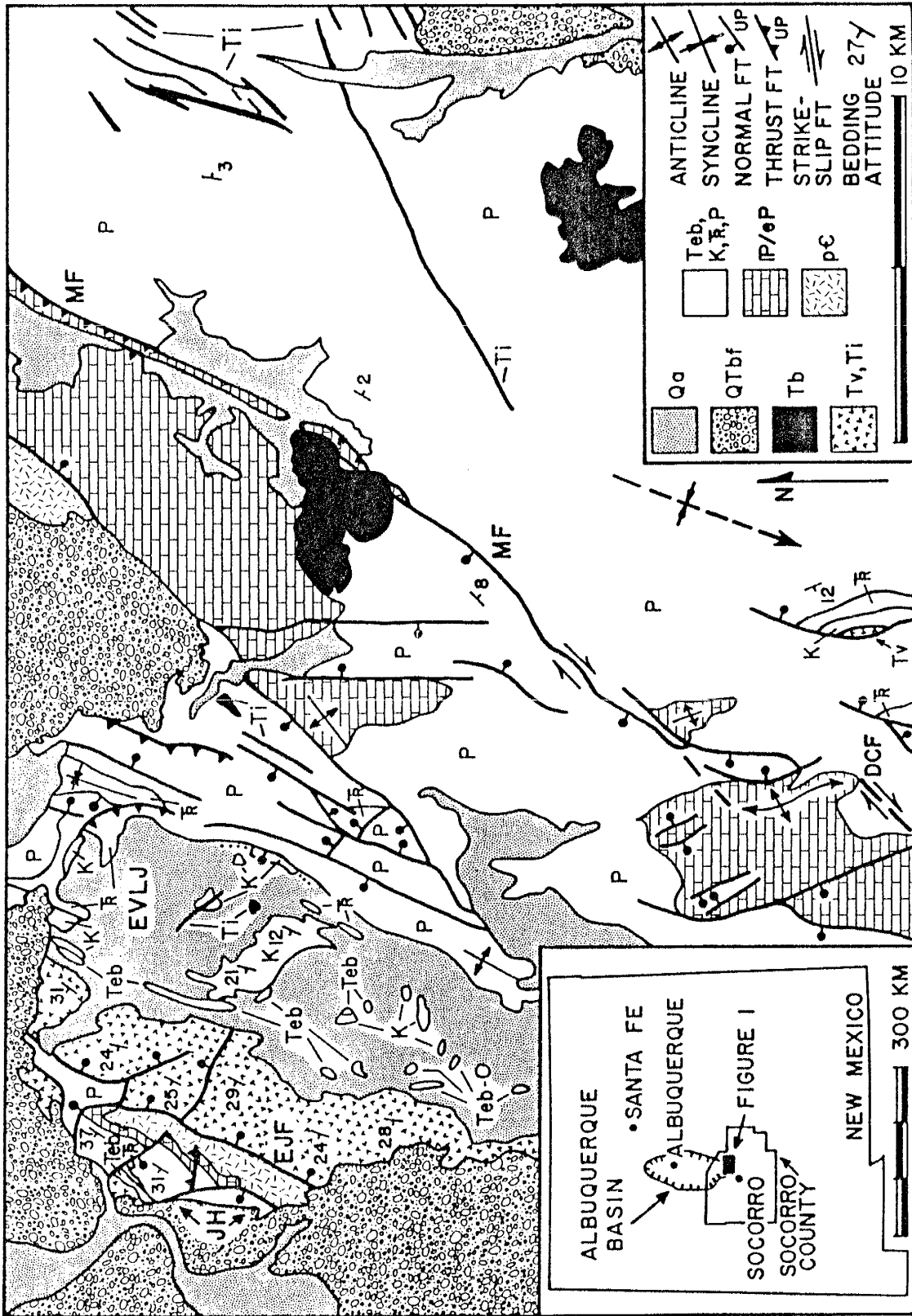
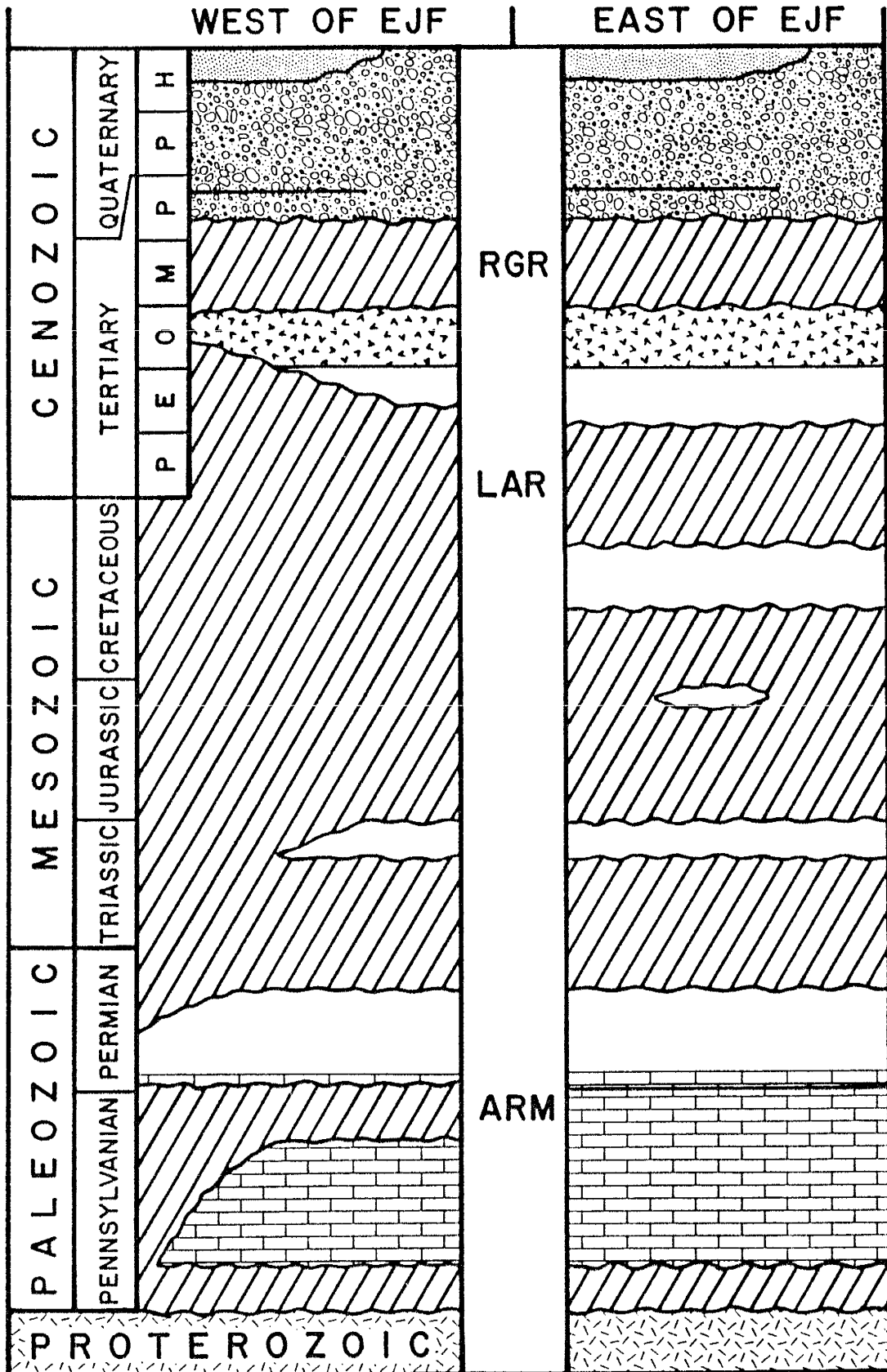


Figure 4.2. Generalized stratigraphy exposed to the west (Joyita Hills) and east (El Valle de La Joya) of the East Joyita fault (EJF). Initially horizontal sedimentary and/or volcanic sequences were deposited prior to and after each recognized tectonic episode, allowing a direct correlation between observed structural styles and specific orogenic events. RGR = Rio Grande rift; LAR = Laramide; ARM = ancestral Rocky Mountain. Continuous deposition of Pennsylvanian and Permian strata to the east of the East Joyita fault (not observed in field area) inferred from Read and Wood (1947), Kottlowski (1960) and Peterson (1980). Continuous deposition during this interval also occurred to the west and south of the Joyita Hills (Kottlowski, 1960). Lithologic patterns correlated with those of Fig. 4.1; diagonal rule indicates absence (either non-deposition or erosion) of stratigraphic record. Modified from Osburn and Lochman-Balk (1983).



extension. These stratigraphic sequences record the differing structures that developed during each successive orogeny, and the stratigraphic interval that a given structural style overprints has been used to correlate structures with specific tectonic events.

The purpose of this paper is to present structural data associated with each of the foregoing deformational episodes and to formulate structural and tectonic interpretations within a temporal perspective. Although both ductile (Proterozoic) and brittle (Phanerozoic) structures are well exposed, emphasis has been placed on structures associated with Phanerozoic deformation. Fault, fault striae, dike and fold axis orientations have been grouped into compatible systems in order to evaluate structural styles, associated kinematics, and where possible, to infer applied stress orientations. Reactivation of existing structures was a fundamental aspect of these deformational episodes. Orientations of Proterozoic foliations and amphibolites have been plotted in order to evaluate the influence of basement structures during Phanerozoic deformation and the extent to which reactivation has occurred.

METHOD OF ANALYSIS

Evaluation of Phanerozoic structures and kinematics has been accomplished largely through fracture analyses. Data collection has been coordinated with detailed mapping (minimum scale of 1:12,000; 1:6,000 where structurally complex), and stratigraphic relationships have been used to supplement structural and kinematic interpretations. Structural attitudes, including bedding, fault, fault striae and dike orientations, were described and recorded in the field. Displacements (net slips) along individual faults range from less than 1 cm to several km (as along the East Joyita fault, which displays approximately 3 km of down-to-the-east displacement; Fig. 4.1). Most faults observed and used in the following analyses, however, exhibit net slips of a few meters to one hundred meters.

Fault and dike orientations have been used to infer applied stress orientations in a manner similar to that proposed by Anderson (1951) for shallow-crustal, brittle

deformation. Anderson (1951) proposed that in near-surface settings, one of the principal stress axes should be vertical, and accordingly, conjugate fault orientations would be equally disposed to horizontal. However, field observation in the Joyita Hills area indicated that what appeared to be conjugate fault orientations were not equally disposed to horizontal, but rather were equally inclined with respect to bedding. For example, faults rather consistently cut across bedding at approximately 30° (thrust faults), 60° (normal faults) or 90° (strike-slip faults), regardless of bedding orientation. Similarly, extensional fractures (mid-Tertiary mafic dikes) were consistently oriented at roughly 90° to bedding. These relationships were interpreted to indicate that these structures were superimposed on bedding prior to appreciable rotation associated with a given tectonic event, and that rotation had removed early formed fractures from their original orientation.

The consistency between fracture orientation and bedding has been demonstrated by plotting structural elements with respect to bedding. This was accomplished by restoring inclined bedding to horizontal, and rotating contained structural elements by a comparable amount. The analytical method, therefore, treats the foregoing structural features as early formed elements within a deformational episode, and produces orientations of faults, fault striae and inferred stress axes that are compatible with observed structures, brittle deformation and Andersonian theory.

The concept of brittle failure prior to rotation of strata (initial fracturing) is not new. Previous investigations (e.g., Melton, 1929; Parker, 1942; Reches, 1976; Beck, 1984; Beck and Burford, 1985) have also treated tectonically induced fractures in this manner. Neither is it the only means by which the consistency between fracture orientation and bedding may be explained. Alternatively, the consistency may be explained using elastic plate theory, in which it is inferred that frictionless bedding-plane slip occurred during deformation. In this latter approach, the bedding plane would be a principal plane of stress, and one of the principal stress axes would be consistently

oriented normal to the bedding plane, regardless of bedding orientation. Analyses which have utilized this latter interpretation have been provided by Reches (1978) and Jackson and Pollard (1990). The analyses that follow take the former approach, and brittle structures are treated as early formed structural elements within a given deformational episode. The reasoning behind this approach, and a more detailed analysis of brittle structures in the Joyita Hills area, has been provided in Part 2.

This analytical technique has been applied to fractures associated with Rio Grande rift and Laramide tectonisms, and applied stress orientations have been inferred for both of these events. In contrast, ancestral Rocky Mountain structures have been overprinted and reactivated by these younger deformational events, which has made application of the foregoing analytical technique to late Paleozoic structures difficult. Fortunately, ancestral Rocky Mountain structures have been determined through field observation and recognition of buried structure. Late Paleozoic structures (faults and fault striac), as well as Proterozoic structures (foliations and amphibolite dikes), have been restored to their approximate original orientations by using regional bedding.

PROTEROZOIC BASEMENT STRUCTURES

Proterozoic rocks (augen gneiss) in the core of the Joyita Hills (Fig. 4.1) host a number of planar structures. These include joints, faults, foliations, and amphibolite, pegmatite and aplite dikes. Previous petrologic, structural and descriptive interpretations of these structures have been provided by Herber (1963a,b).

Foliations are gneissic to mylonitic, strongly lineated, and occur along three common trends. Amphibolite dikes are also foliated and lineated. Where observed, foliations and lineations within the amphibolites parallel those in the surrounding gneiss. The amphibolites, therefore, are interpreted as pre- or synmetamorphic structures. In contrast, pegmatite and aplite dikes are unfoliated structures that both parallel and cross-cut the older foliations.

Restoration of foliations and amphibolites has been accomplished by removing the combined effects of Phanerozoic rotations (29° of down-to-the-west rotation about a N32°E, horizontal axis; Fig. 4.3a). Restored foliations (Fig. 4.3b) are high-angle to vertical structures that strike north, northwest and east-northeast. North and east-northeast-striking foliations are most common. Amphibolites (Fig. 4.3c) are also high-angle structures that parallel the east-northeast-striking foliations. Given the limited rotations associated with ancestral Rocky Mountain and Laramide tectonisms (Fig. 4.3a), the orientations of restored foliations and amphibolites (Fig. 4.3b,c) approximate the attitudes of basement structures in the underlying basement rocks of the Joyita Hills area prior to mid-Tertiary rotation.

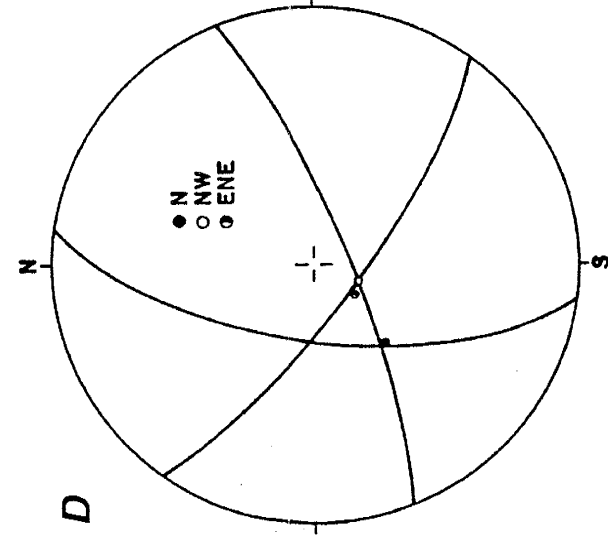
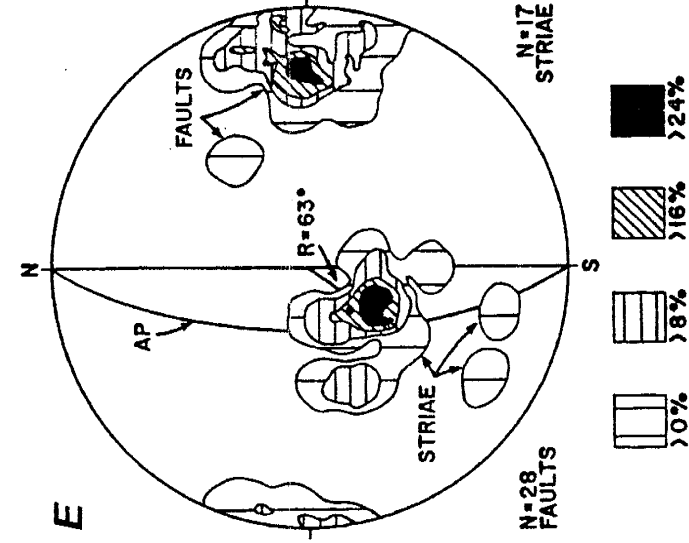
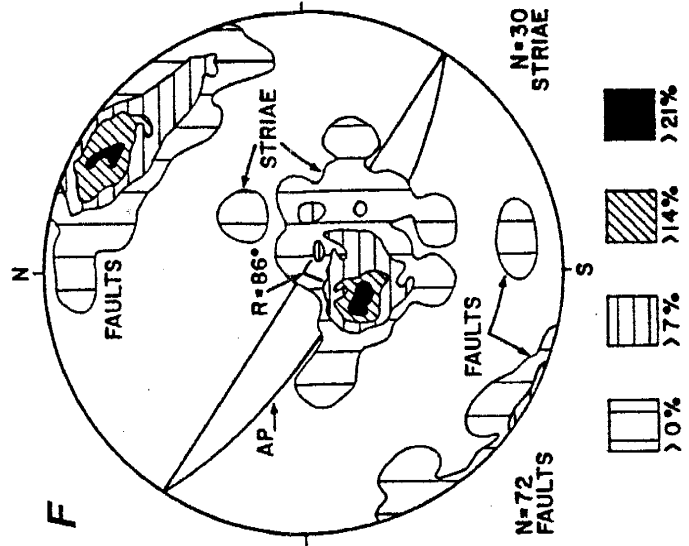
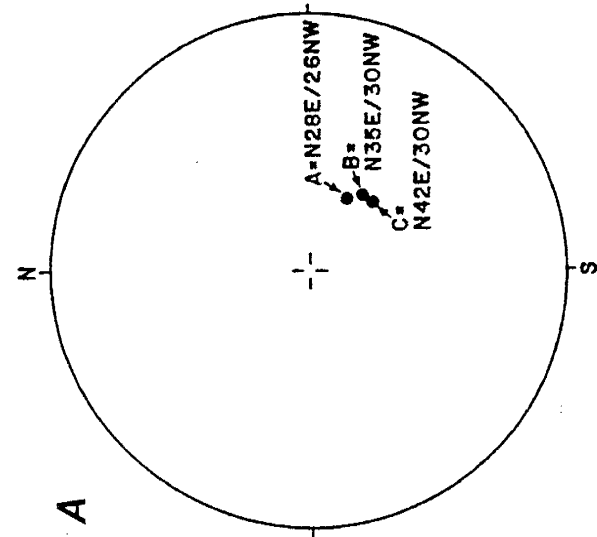
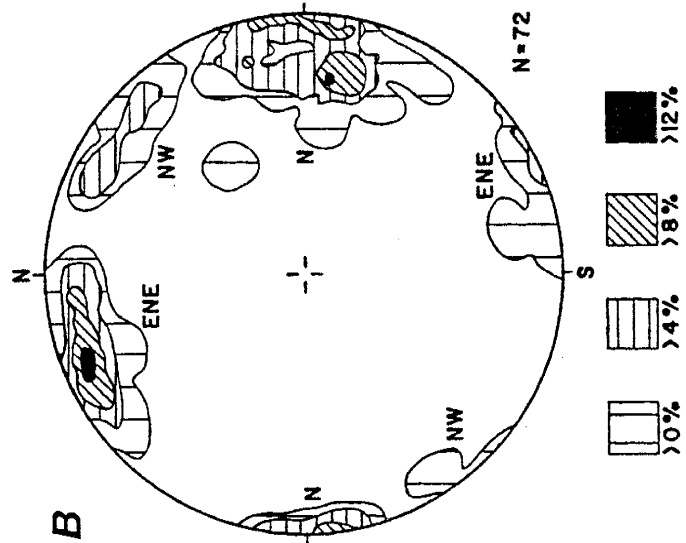
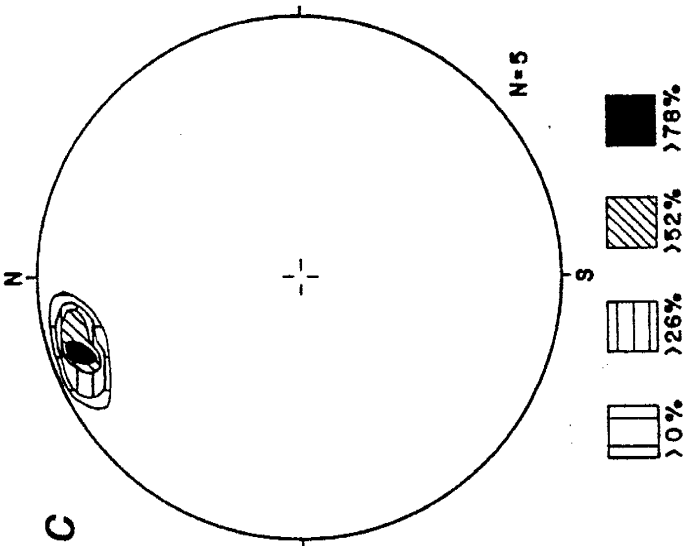
Preferred orientations of observed lineations are subparallel to the approximate lines of intersection formed by foliation planes (Fig. 4.3d). The implications behind this correlation are not understood, because neither preliminary field observation or petrographic inspection supports the interpretation that these lineations are the result of intersecting foliations (intersection lineations). Rather, field observation indicates that these lineations are the result of mineral elongation (stretching lineations). Correspondingly, it is inferred that ductile displacements paralleled lines of intersection during metamorphism. The respective senses of shear have not been determined, which further obscures interpretation. However, the average orientations of foliations and stretching lineations have been presented in the interest of providing available data and for the purpose of identifying potential avenues for continued research in the Joyita Hills.

ANCESTRAL ROCKY MOUNTAIN DEFORMATION

General Stratigraphic Relationships

Regional aspects of late Paleozoic sedimentation and tectonism have been previously discussed by Peterson (1980), Kluth and Coney (1981) and Kluth (1986). In New

Figure 4.3. Lower-hemisphere, equal-area projections of regional bedding, Proterozoic and late Paleozoic structural orientations. A) Regional bedding, where A represents average orientation of Tertiary volcanic rocks (post-Laramide, pre- and syn-Rio Grande rift sequences; refer to Fig. 4.2); B represents average orientation of middle-Permian through Eocene sedimentary rocks (post-ancestral Rocky Mountain, pre- and syn-Laramide sequences); and C represents average orientation of Pennsylvanian and earliest Permian strata (pre- and syn-ancestral Rocky Mountain sequences). B) Restored orientations of Proterozoic foliations, which strike north (N), northwest (NW) and east-northeast (ENE); C) restored Proterozoic amphibolite dikes, which also strike east-northeast; D) synoptic diagram of average (restored) foliation orientations and associated stretching lineations; E, F) restored north-striking and northwest-striking ancestral Rocky Mountain faults and contained striae, respectively. AP denotes average fault plane; R denotes approximate rake of striae. Poles to planes (B, C) and composite poles to planes and lineations (E, F) contoured at specified intervals per 1% area.



Mexico, deformation resulted in basins and uplifts of dominantly north and northwest trend. These trends began to develop as early as latest Mississippian (Chesterian) time (Armstrong, 1962; Armstrong and Mamet, 1988; Kluth, 1986), persisted throughout the Pennsylvanian (Kottowski, 1960), and into the early Permian (Peterson, 1980). On a more local scale, stratigraphic investigations (Read and Wood, 1947; Kottowski, 1960; Kottowski and Stewart, 1970; Baars, 1982; Siemers, 1978, 1983) have identified the Joyita Hills area as the location of an ancestral Rocky Mountain uplift (the Joyita uplift).

Accumulations of Pennsylvanian sediments in depositional basins to the west, south and east of the Joyita Hills attain thicknesses of up to 820 m (Fig. 4.4; Read and Wood, 1947; Kottowski, 1960; Baars, 1982; Siemers, 1983). These strata are typically shallow water (continental shelf) carbonates and subordinate clastics (Kottowski, 1960). These sequences represent nearly continuous sedimentation that spanned Atokan through Virgilian time (Kottowski, 1960; Siemers, 1983), and therefore subsidence must have kept pace with sedimentation. In contrast, Pennsylvanian sequences in the Joyita Hills are anomalously thin (0–127 m, Kottowski and Stewart, 1970; 0–112 m, Siemers, 1983). These sequences also consist of shallow water (restricted lagoon, intertidal, and inner to outer shelf) carbonates and subordinate clastics that were deposited during Atokan through Missourian time. Kottowski and Stewart (1970) inferred that Virgilian strata were also deposited in the Joyita Hills, but subsequently were removed by late Pennsylvanian or early Permian uplift and erosion. Several stratigraphic discontinuities have been observed in this section (Kottowski and Stewart, 1970). Diastems occur in early and late Atokan sequences, along the Atokan/Desmoinesian boundary, and in early Desmoinesian strata. The latter two are indicative of localized uplift and erosion, as evidenced by clasts of augen gneiss, feldspar, quartz and reworked limestone. A disconformity occurs between early Desmoinesian and Missourian strata, which has also been attributed to uplift and erosion during middle Desmoinesian time

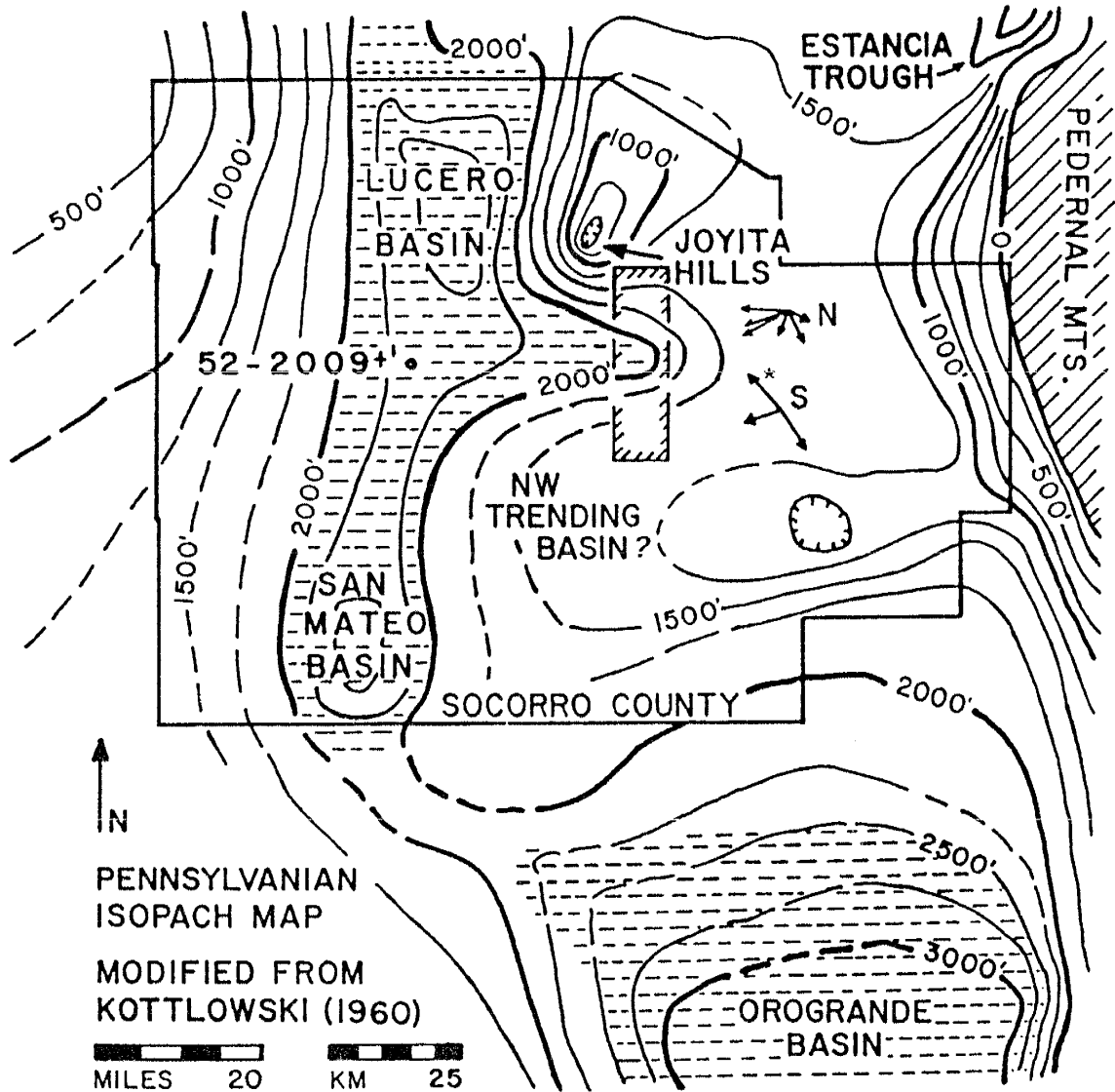


Figure 4.4. Modified Pennsylvania isopach map superimposed with early Wolfcampian paleocurrent data (Altares, 1990). Hachured box outlines location of Altares' (1990) field area. Paleocurrent directions (vector means) labelled N and S are from the northern and southern parts of Altares' field area; length of each vector is proportional to vector strength. Drill-core data (Krewedl, 1974; C.E. Chapin, unpublished core log; control point 52, Kottowski, 1960) documents stratigraphic thickness to be in excess of 2000 ft (610 m), and redefines the Lucero and San Mateo basins as one continuous, north-trending basin. Contour interval = 250 ft.

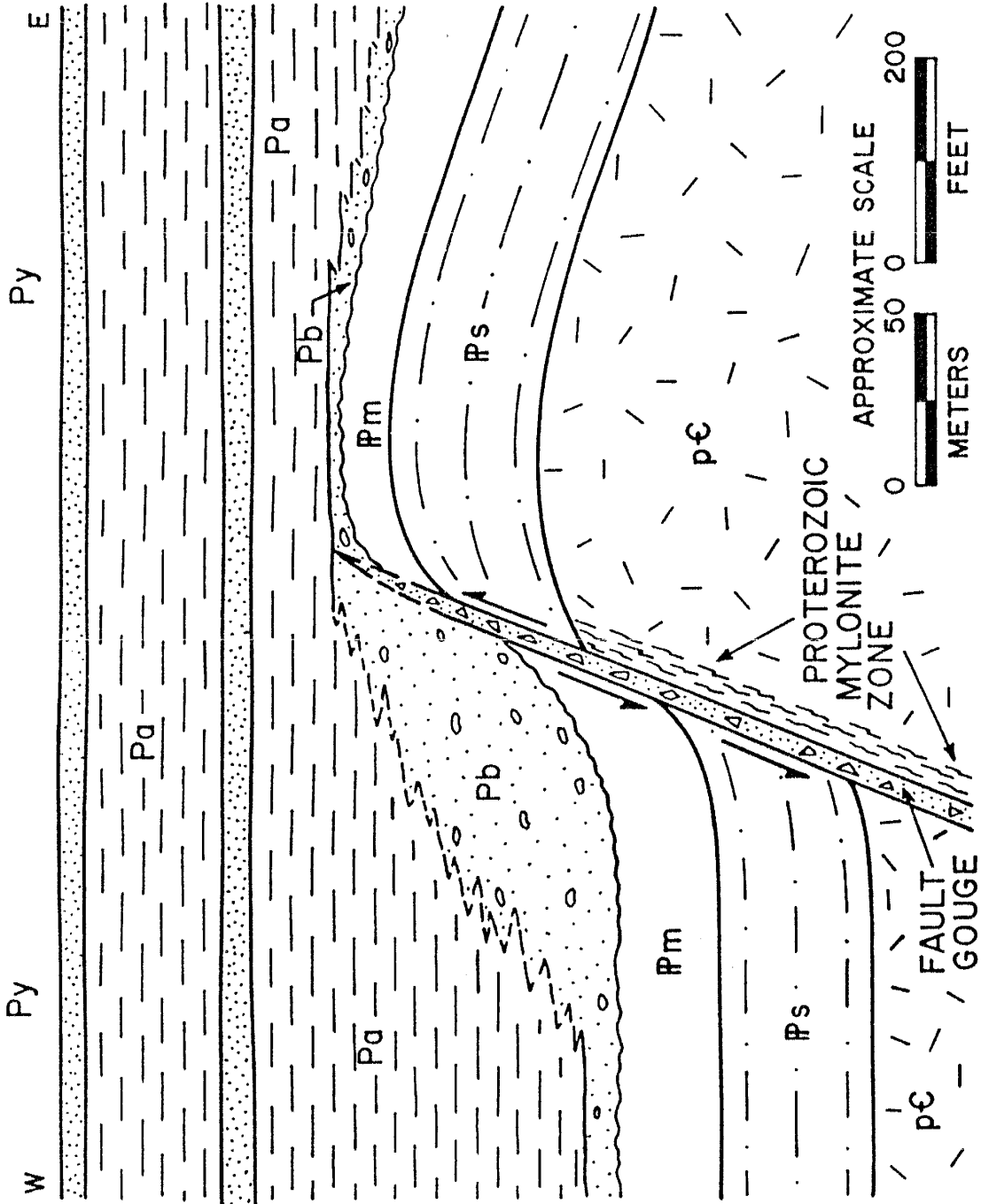
(Kottowski and Stewart, 1970; see also Kluth, 1986). In addition, an early (Atokan) episode of faulting has been observed in the Joyita Hills (Beck and Johnson, 1992). Down-to-the-east displacements along subvertical, north-striking faults offset early Atokan strata (Sandia Formation), but are overlain by unfaulted, late Atokan strata (basal Madera Formation).

Accordingly, the anomalously thin Pennsylvanian section in the Joyita Hills can be attributed to tectonic adjustments during sedimentation, rather than uplift and erosion of an initially thick Pennsylvanian section. The foregoing stratigraphic discontinuities and evidence of Atokan deformation are thought to reflect these adjustments, which served to elevate the Joyita uplift as a structurally positive block amid subsiding basins throughout the Pennsylvanian.

Ancestral Rocky Mountain Structures

Ancestral Rocky Mountain tectonism in the Joyita Hills reached its culmination during early Wolfcampian (earliest Permian) time (Kottowski and Stewart, 1970; Beck and Johnson, 1992). Deformation in the Joyita Hills occurred along two fault sets: North-striking, west-dipping to subvertical normal faults and northwest-striking, southwest-dipping normal faults (Beck and Chapin, 1991). North-striking faults have been found within or along the fault-bounded margins of Proterozoic through early Wolfcampian rocks, and typically occur as wide (3 – 7 m) gouge zones that are conspicuously marked by south-plunging fault striae and mullion structures. Most faults of this orientation have been reactivated and display a down-to-the-east sense of displacement. These reactivated faults are found in proximity to the East Joyita fault (which exhibits approximately 3 km of mid-Tertiary, down-to-the-east displacement), and reactivation is thought to have occurred as a result of mid-Tertiary extension (discussed below). Other faults of this orientation display a down-to-the-west displacement, and do not appear to have been reactivated. One of these faults (the fault is unnamed; Fig. 4.5) is comparatively well exposed. Along this fault, Proterozoic

Figure 4.5. Generalized cross section normal to one of the north-striking, ancestral Rocky Mountain normal faults that has not been reactivated. Cross section has been restored to its post-ancestral Rocky Mountain orientation by removing 29° of down-to-the-west rotation about a $N32^\circ E$, horizontal axis; Fig. 4.3a). Py = Yeso; Pa = Abo; Pb = Bursum; Pm = Madera; Ps = Sandia; pC = Proterozoic basement. Fault and contacts dashed where obscured. The location of this fault has been provided by Beck and Chapin (1991) and Beck and Johnson (1992).



through early Wolfcampian rocks display a stratigraphic offset of approximately 100 m. Syntectonic strata (Bursum Formation) are anomalously thick and coarse grained in the hanging wall (west block, downthrown) and apparently were deposited along the exposed fault scarp. In the footwall (east block, upthrown), syntectonic clastics overlies erosionally thinned Pennsylvanian (Madera Formation) limestones. Both the fault and offset strata are overlain by depositionally thinned, unfaulted mid-Wolfcampian strata (Abo Formation), and the fault is therefore interpreted as a buried ancestral Rocky Mountain fault that has not been reactivated.

Northwest-striking faults are more problematic, in that all faults of this orientation appear to have been reactivated during mid-Tertiary extension (discussed below). However, subtle differences in fault character and orientation indicate that these faults were also active during late Paleozoic tectonism. Similar to the north-striking faults, northwest-striking normal faults superimposed on early-Wolfcampian (Bursum Formation) and older rocks also occur as wide (3 – 7 m) gouge zones, are marked by well-developed fault striae and mullion structures, and dip consistently to the southwest. In contrast, northwest-striking normal faults superimposed on mid-Wolfcampian (Abo Formation) and younger strata occur as discrete fault planes that exhibit limited brecciation, poorly developed fault striations, and occur as conjugate fault orientations. These changes in fault character occur at the boundary between early- and mid-Wolfcampian strata. Although interpretive, it is thought that the disparity in observed strain over such a short stratigraphic interval cannot readily be attributed to a single deformational episode. Rather, it is thought that the greater strain observed in early-Wolfcampian and older rocks is attributable to structural deformation during two different orogenic episodes.

Restoration of both fault sets has been accomplished by using regional bedding (removing 29° of down-to-the-west rotation about a N32°E, horizontal axis; Fig. 4.3a). Restoration defines the fault sets as north-striking, west-dipping to subvertical

normal faults (Fig. 4.3c) and northwest–striking, southwest–dipping normal faults (Fig. 4.3f). Restored fault striae define fault displacements as normal, left–oblique slip along north–striking faults (striae rake approximately 63° southward), and as dip slip along northwest–striking normal faults.

Comparison of ancestral Rocky Mountain fault orientations (Figs. 4.3e,f) with those of north– and northwest–striking Proterozoic foliations (Fig. 4.3c) indicates that orientations are similar. Reactivation of north–striking foliations has been verified in the field along the foregoing north–striking ancestral Rocky Mountain fault (Fig. 4.5). Reactivation of northwest–striking foliations is also thought to have occurred, given the comparable orientations, although this correlation has not been verified by field observation. Moreover, late Paleozoic fault striae orientations are similar to Proterozoic stretching lineations (Fig. 4.3d), indicating that late Paleozoic faults not only reactivated existing planar weakness in the Proterozoic basement, but also utilized comparable slip vectors. The reasons for this latter similarity are not clear, and may simply be coincidental.

Interpretation of Ancestral Rocky Mountain Deformation

Modified Pennsylvanian isopach maps (Fig. 4.4) support the foregoing fault orientations and define the Joyita uplift as a north–trending structural element. The uplift was bordered to the west and southwest by depositional basins (the Lucero and San Mateo basins). Modifications to the isopach map (originally drawn by Kottlowski, 1960) consist of redefining contour patterns between the Lucero and San Mateo basins. These changes are the result of more recent drill–core data from a mineral exploration hole on the west flank of the Magdalena Mountains (Krewedl, 1974; C.E. Chapin, unpublished core log) which encountered 2009^{+} ft (612^{+} m) of Pennsylvanian strata. This drill–core data indicates that the San Mateo and Lucero basins were one continuous, north–trending basin. Both the Joyita uplift and modified San Mateo/Lucero basin probably extended northward as continuous structures to the Sierra Nacimiento area

and the adjacent Cabezón sag (to the west of Sierra Nacimiento [the Penasco uplift of Kottowski, 1960, fig. 30]; see also Baars, 1982; Read and Wood, 1947).

Although they do not bear directly on Pennsylvanian rocks, paleocurrent data from early Wolfcampian strata (Altares, 1990) have also been superimposed on the Pennsylvanian isopach map (Fig. 4.4). Altares' (1990) field area spans the north–south dimension of a poorly delineated prong extending from the San Mateo/Lucero basin. Northwest–trending isopachs along the northern margin of the prong are reasonably well defined by control points (Kottowski, 1960) and are compatible with the northwest–striking normal faults observed in the Joyita Hills (Fig. 4.3f). In contrast, isopach trends along the southern margin of the prong, as well as between the San Mateo/Lucero and Orogrande basins in general, are poorly constrained due to a paucity of control points (Kottowski, 1960). Altares' (1990) paleocurrent data to both north and south of the prong indicate general paleoflow directions to the south and southwest, indicating that the depositional axis of the prong lay further to the southwest than originally drawn by Kottowski (1960). Although the northwest–trending paleocurrent vector (marked with an asterisk in Figure 4.4) may not appear compatible with this interpretation, it should be noted that this vector occurs near the top of the Bursum section (Altares, 1990). The northwesterly directed flow indicated by this paleocurrent vector may be indicative of changing tectonic and/or paleoflow patterns during the latter stages of Bursum deposition. All other paleocurrent vectors occur comparatively lower in the Bursum section, and are compatible with the foregoing interpretation.

The limited amount of data between the San Mateo/Lucero and Orogrande basins, in terms of both paleocurrent vectors and control points for delineating isopach trends, makes interpretation difficult. However, the combination of the southeast–trending isopachs at the southern end of the Joyita Hills (Fig. 4.4), northwest–striking normal faults in the Joyita Hills (Fig. 4.3f), paleoflow directions to the south and southwest, and northwest–trending isopachs between the southern end of the San Mateo/Lucero

basin and the northern end of the Orogrande basin indicate that the two basins were connected by a northwest-trending basin (Figs. 4.4 and 4.6) during late Paleozoic deformation.

North-striking faults in the Joyita Hills are comparable, in terms of both orientation and sense of offset, to other late Paleozoic structures in the Sierra Nacimiento area to the north (Baars, 1982), and in the Sacramento Mountains to the south (Pray, 1961). Similarly, the timing of deformation in these three areas was approximately synchronous. The dominant phase of uplift in the Joyita Hills was early Wolfcampian (Kottowski and Stewart, 1970; Beck and Johnson, 1992). Several episodes of late Paleozoic deformation in the Sierra Nacimiento area were reported by Baars (1982), the youngest in post-Madera, pre-Abo time (compare with Fig. 4.5). Pray (1961) also concluded that the dominant phase of deformation in the Sacramento Mountains occurred during late Pennsylvanian to early Wolfcampian time. The compatibility of observed structural styles and comparable timing of deformation in the three areas indicate that a large part of the crust in New Mexico was subjected to the same style of deformation during ancestral Rocky Mountain tectonism.

Integration of the foregoing fault orientations, associated kinematics and the spatial distribution and orientation of known and inferred basins suggests that late Paleozoic deformation in central New Mexico was the result of sinistral wrench faulting (Fig. 4.6). The north-trending San Mateo/Lucero and Orogrande basins are arranged in a left-stepping, en echelon pattern and represent the principal zones of sinistral shear. The two basins were probably connected by a northwest-trending basin (Figs. 4.4 and 4.6) which is interpreted as either a rhomb-graben or a releasing bend (Ramsay and Huber, 1987, figs. 23.37 and 23.38) between the two shear zones. The former alternative is presented in Figure 4.6. Bounding structures between basins and adjacent uplifts were high-angle to vertical normal faults (Fig. 4.3e,f). The predominance of normal displacement along both fault sets indicates that the inferred wrench fault system must

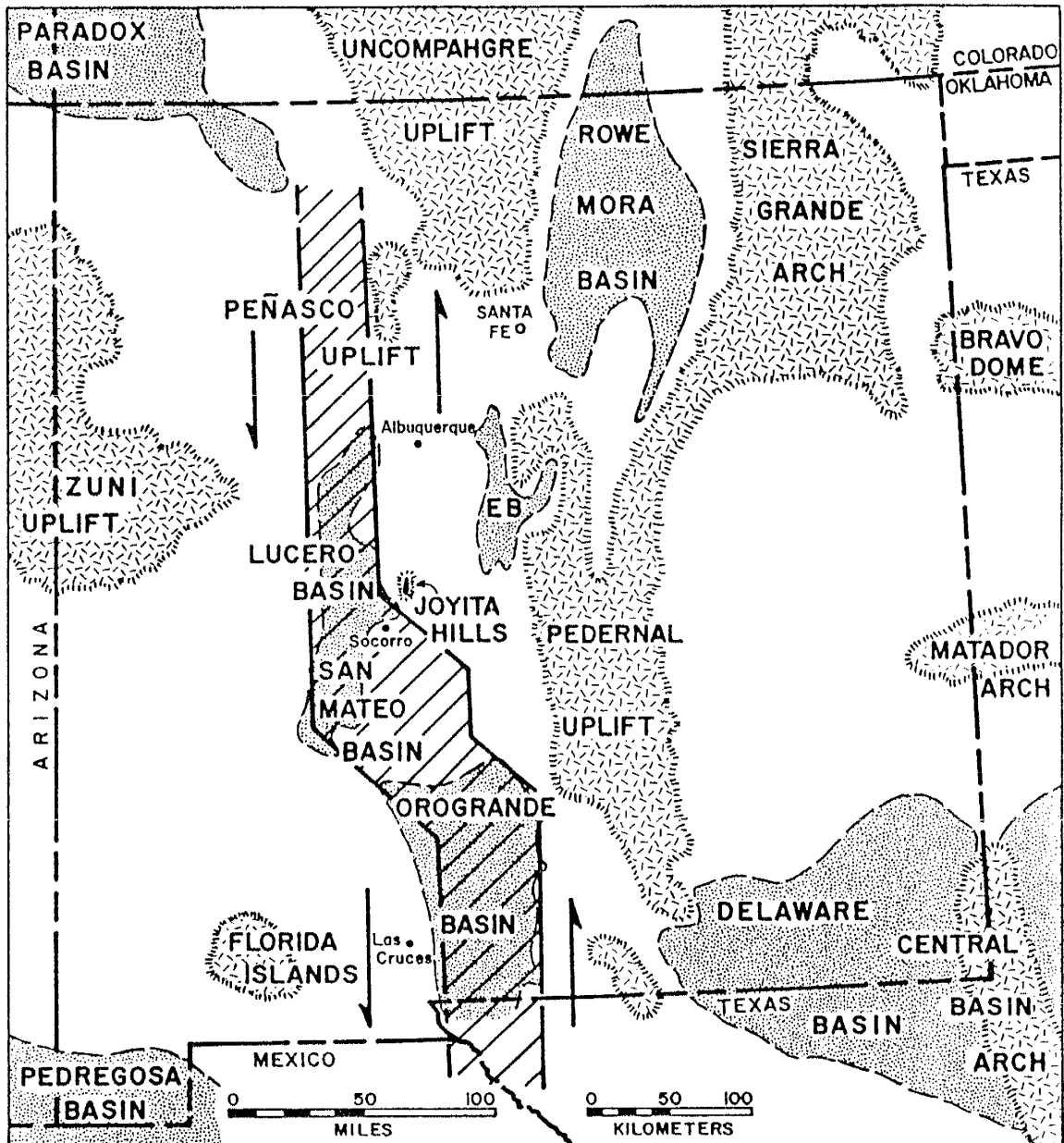


Figure 4.6. Inferred divergent, sinistral wrench fault system superimposed on Pennsylvanian paleogeographic map. The north-trending San Mateo/Lucero and Orogrande basins developed within principal zones of sinistral shear. The inferred northwest-trending basin is envisioned as a rhomb-graben between two left-stepping, sinistral shear zones. Paleogeographic base map from Kottlowski and Stewart (1970). Note that the Sierra Nacimiento area (used in text) is coincident with the Peñasco uplift of Kottlowski and Stewart (1970).

have been largely divergent, with sinistral offset along north–striking faults being a lesser component of deformation. The impetus for sinistral displacement is not clear, but most likely was the result of continental suturing between North America and South America–Africa (Kluth, 1986). Resultant, northerly directed compression along the Marathon–Ouachita belt of west Texas, Oklahoma and Arkansas (to the east and southeast of New Mexico) reactivated existing basement flaws (Proterozoic foliations; Fig. 4.3b) of both north and northwest trend, and resulted in a north–trending, divergent, sinistral wrench fault system in central and southern New Mexico during the late Paleozoic.

LARAMIDE DEFORMATION

General Stratigraphic Relationships

Late Paleozoic (middle Permian) and Mesozoic sedimentary rocks represent post–ancestral Rocky Mountain, pre–Laramide strata (Fig. 4.2). Middle to late Wolfcampian rocks of the Abo Formation are composed of red, arkosic mudstones, shales and lesser channel sandstone beds. These strata represent subaerial sedimentation during the waning stages of late Paleozoic tectonism (Beck and Johnson, 1992). Overlying Leonardian and Guadalupian strata of the Yeso, Glorieta and San Andres formations formed extensive, sheet–like deposits of clean carbonates and mature clastics that eventually buried the late Paleozoic uplifts (Peterson, 1980), and signalled an end to ancestral Rocky Mountain tectonism in central New Mexico.

Triassic strata consist of texturally and compositionally immature conglomerates, sandstones (micaceous litharenites and graywackes) and mudstones of the Moenkopi and San Pedro Arroyo Formations (Lucas, 1991). Jurassic strata have been observed only locally. Mature sediments (claystones, siltstones and micrites) of the Brushy Basin Member of the Morrison Formation (Hayden *et al.*, 1990) occur as erosional remnants between Triassic and Cretaceous strata along the eastern margin of El Valle de La Joya. Cretaceous strata (1300 ft⁺; 396 m⁺) are composed of interstratified, well–sorted

sandstones, siltstones, shales and thin coal beds of the Dakota Sandstone, Mancos Shale, Tres Hermanos Formation, Gallup Sandstone, and Crevasse Canyon Formation (Baker, 1981).

Where observed, strata deposited during each of the foregoing periods exhibit disconformable contact relationships, and with the exception of Triassic strata, all sequences are composed of well-sorted clastics and clean carbonates indicative of relative tectonic stability. Although Smith (1983) has inferred a post-middle Permian, pre-late Triassic deformational event in the Socorro Region, no field evidence has been recognized to support this interpretation in the Joyita Hills. Rather, the typically mature sediments and disconformable contact relationships between the stratigraphic sequences indicate that the interval between ancestral Rocky Mountain and Laramide tectonisms was one of relative tectonic quiescence in the Joyita Hills area.

In contrast, syntectonic strata of the Eocene Baca Formation are indicative of tectonic instability and late Laramide uplift and erosion (Cather, 1980; Cather and Johnson, 1986). These sequences consist of compositionally and texturally immature conglomerates, sandstones (lithic arkoses, feldspathic litharenites and sublitharenites) and mudstones that unconformably overlie Cretaceous, Triassic and Permian rocks. More specifically, fundamentally different stratigraphic columns in the western and eastern portions of the study area attest to proximal uplift (Figs. 4.1 and 4.2). To the east (El Valle de La Joya), Baca sediments overlie Cretaceous rocks through disconformable to mildly angular contact relationships. To the west (Joyita Hills), however, Cretaceous strata are absent, and conglomerates of the Baca Formation overlie erosionally thinned Triassic and Permian (Leonardian and Guadalupian) rocks along an angular unconformity. The north-northeast- to northeast-striking East Joyita fault appears to be the boundary between these two distinct stratigraphic columns, and the partial omission of strata is indicative of Laramide uplift and erosion west of the East Joyita fault.

Laramide Structures

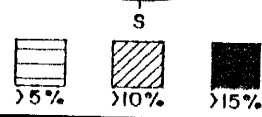
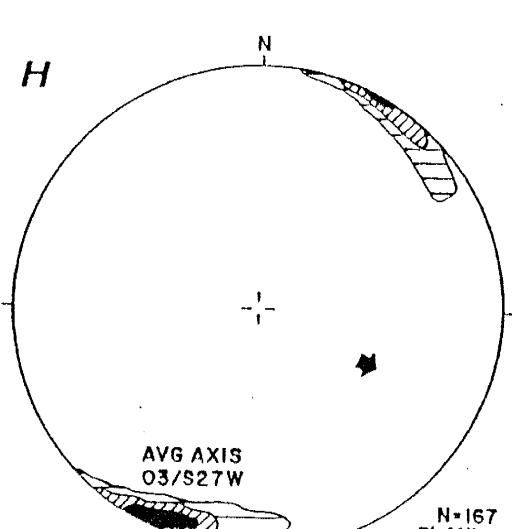
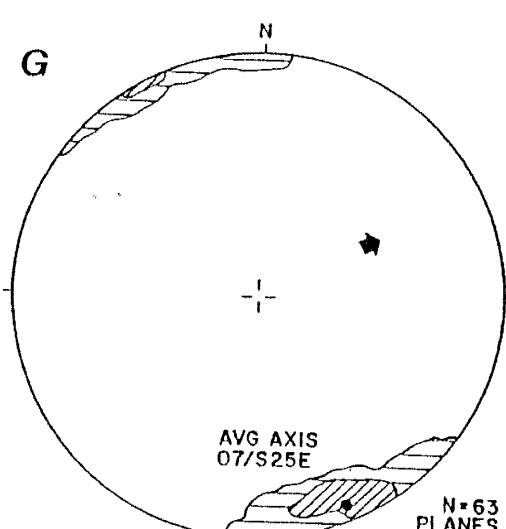
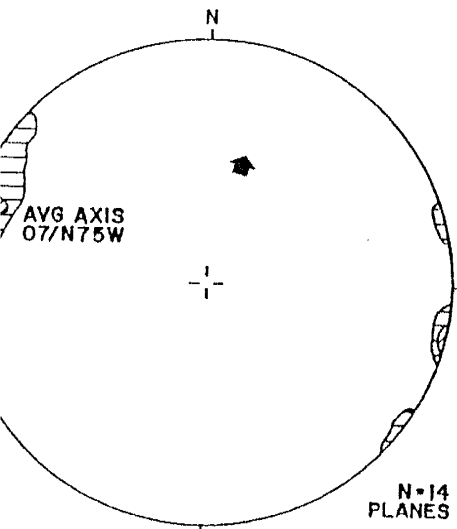
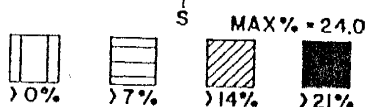
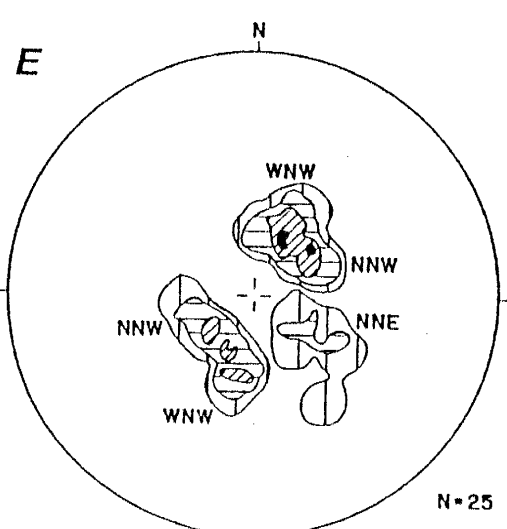
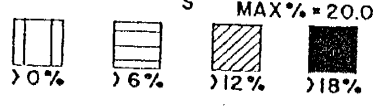
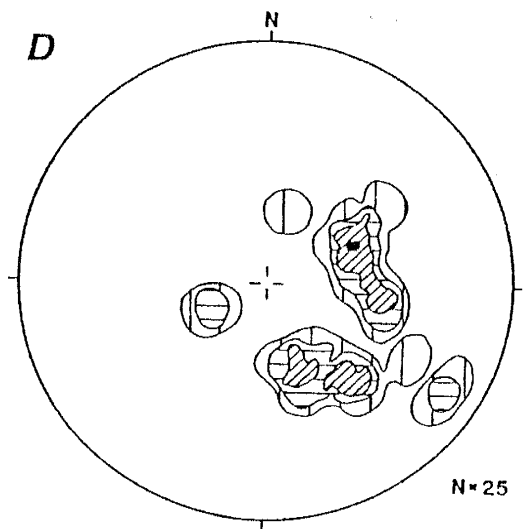
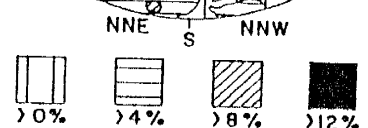
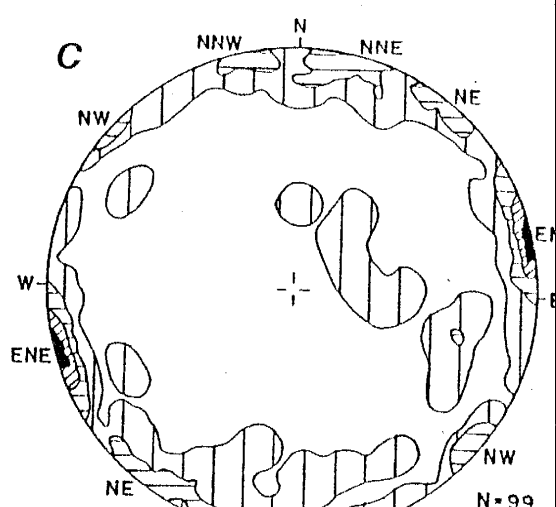
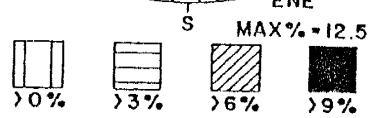
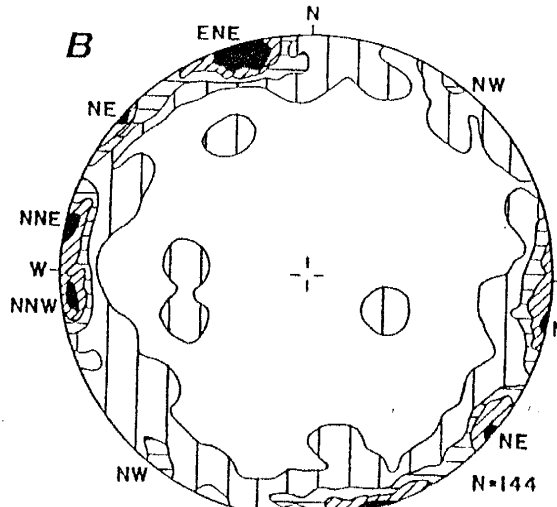
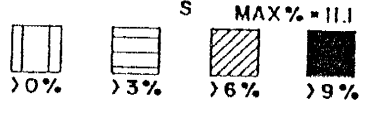
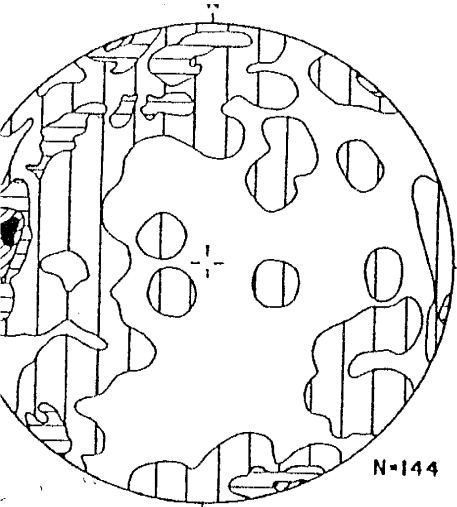
Laramide deformation in the Joyita Hills area resulted in both wrench faulting and subordinate thrust faulting (Part 2). Strike-slip faults have been observed predominantly in Proterozoic through Cretaceous rocks, and only a limited number (<2%) of strike-slip faults have been observed in post-Laramide strata (Tertiary volcanic rocks). Thrust faults and associated folds have been found exclusively in Cretaceous and older strata, and no folds (other than fault drag) have been observed in Tertiary volcanic rocks. Accordingly, both strike-slip faults and thrust faults are attributed to Laramide deformation.

Field observations indicate that strike-slip faults most commonly occurred as high-angle to vertical structures (Fig. 4.7a) marked by low-rake (typically 0° to 30°) fault striae. Observation also indicated that these strike-slip faults were consistently oriented at roughly 90° to bedding, regardless of present bedding orientation. The constancy between fault orientation and bedding has been demonstrated by plotting the strike-slip faults with respect to bedding (herein referred to as "restored" orientations). This was accomplished by restoring inclined bedding to horizontal (using the specific bedding orientation at the locality where the faults were observed) and rotating (restoring) the faults by a comparable amount. The analyses, therefore, treat the strike-slip faults as early formed structural elements that predate appreciable rotation of strata.

Comparison of Figures 4.7a and b indicates that when restored (Fig. 4.7b), strike-slip faults plot as subvertical to vertical planes in accordance with Andersonian theory for strike-slip deformation. Restored strike-slip faults form five concentrations (preferred orientations or maxima) that are both enhanced as distinct concentrations and increased in maxima percent value. These preferred orientations strike north-northwest, north-northeast, northeast, east-northeast, and less commonly northwest. Comparably restored fault striae (Fig. 4.7c) plot as horizontal to subhorizontal

Figure 4.7. Lower-hemisphere, equal-area projections of Laramide strike-slip fault, thrust fault and fold axis orientations.

A) Field-recorded strike-slip fault orientations; B) restored strike-slip faults; preferred orientations strike north-northwest (NNW), north-northeast (NNE), northeast (NE), east-northeast (ENE) and northwest (NW); C) restored fault striae; preferred orientations correspond to each observed concentration of restored strike-slip faults in B; D) field-recorded thrust fault orientations; E) restored thrust faults; preferred orientations strike to west-northwest (WNW), north-northwest (NNW) and north-northeast (NNE; singular maxima); F, G and H) restored fold axes trend WNW, SSE (NNW) and SSW (NNE), respectively. Black arrows denote observed vergence direction. Poles to planes (A, B, D and E), lineations (C) and contoured beta diagrams (F, G and H) contoured at specified intervals per 1% area.



lineations that correspond to each observed concentration of strike-slip fault orientations (Fig. 4.7b). Interpretation of fault steps (Durney and Ramsay, 1973) on the fault surface indicate dextral displacements on faults that strike north-northwest, north-northeast and northeast, and sinistral displacements on east-northeast-striking faults. The sense of displacement on northwest-striking faults has not been determined.

In addition to strike-slip faults, Laramide deformation resulted in reverse faulting and associated folding of strata. Observed reverse faults occurred as moderate- to high-angle structures of diverse strike (Fig. 4.7d). However, observation also indicated that these reverse faults were consistently oriented at 25° – 30° to bedding. Accordingly, reverse faults have been evaluated in a manner similar to that used for strike-slip faults. Comparison of field-recorded (Fig. 4.7d) and restored (Fig. 4.7c) reverse faults indicates that when restored, reverse faults plot as shallow-dipping structures, or true thrust faults in accordance with Andersonian theory. When restored, observed maxima are enhanced as distinct concentrations and/or increased in maxima percent value, and form three distinct fault systems. Two of these systems are represented by diametrically opposed concentrations that define conjugate thrust fault orientations. These partially overlapping concentrations strike west-northwest and north-northwest. The third fault system, striking north-northeast, consists of a singular fault set.

Folds are relatively uncommon in the Joyita Hills area. Where observed, folds occur as broad, open structures or asymmetric anticlinal/synclinal pairs or fold trains that occupy a small percentage of the field area. Folds have been restored by using the regional bedding orientation determined from Tertiary volcanic strata (26° of down-to-the-west rotation about a horizontal, $N28^{\circ}E$ trending axis of rotation to compensate for rotation associated with Rio Grande rift deformation; Fig. 4.3a). When restored, Laramide fold axes plot as subhorizontal fold axes that trend west-northwest,

north–northwest and north–northeast (Figs. 4.7f,g,h) and correspond to the strike direction of each inferred thrust fault system (Fig. 4.7c).

Interpretation of Laramide Deformation

Strike–slip faulting was the dominant style of Laramide deformation in the Joyita Hills area. Although thrust faults and folds are present, thrust faults are comparatively less numerous and folds are either poorly developed or of limited extent. In some cases, however, the orientations of fold and thrust fault systems can be directly related to strike–slip fault systems.

Preferred orientations of restored strike–slip faults are interpreted as respective parts of two separate dextral wrench fault systems. Dextral faults that strike north–northeast and north–northwest, and sinistral faults that strike east–northeast are interpreted as respective elements of a north–trending, dextral wrench fault system. Respectively, these faults are interpreted as synthetic, secondary synthetic and antithetic shears (or, using Riedel shear terminology, R, P and R' shears; Christie–Blick and Biddle, 1985, fig. 5). Here, allowance is made for the differences between pure shear (Andersonian) and simple shear (wrench) models (e.g., Sylvester, 1988, p. 1673). Inferred regional average stress axes were oriented such that σ_1 was horizontal, trending northeast; σ_2 was vertical; and σ_3 was horizontal, trending northwest. As defined, the inferred dextral wrench fault system is compatible with interpretations of Chapin and Cather (1981) and Chapin (1983) for Laramide deformation in New Mexico.

The second wrench fault system is based on the combination of dextral, northeast–striking faults and the north–northwest–trending fold and thrust fault system. Dextral displacement has been documented along the Montosa and Del Curto fault zones (to the east and southeast of the study area, Fig. 4.1; Brown, 1987; Hayden, 1991). Spatial relationships between these two fault zones and a north–northwest–trending anticlinal flexure (Fig. 4.1) may be interpreted as a convergent overstep structure associated with dextral wrenching along the left–stepping, northeast–striking faults.

This interpretation is also compatible with late Laramide dextral wrench fault interpretations of Chapin and Cather (1981) and Chapin (1983). The dextral, northeast-striking faults and north-northwest-trending folds observed in the Joyita Hills and El Valle de La Joya are thought to represent similar (but smaller scale) structures as those observed along the Montosa and Del Curto fault systems.

Comparison of restored strike-slip fault orientations (Fig. 4.7b) with Proterozoic foliations and amphibolite dikes (Fig. 4.3b,c) indicates that orientations are similar, and fault striae indicative of strike-slip displacements have occasionally been observed along foliation planes. Accordingly, it is inferred that the orientations of Laramide strike-slip faults were controlled by reactivation of existing planar weaknesses in the basement rocks of the Joyita Hills area. These consist of north-northwest- and north-northeast-striking dextral faults (collectively influenced by the generally north-striking foliations) and the sinistral east-northeast-striking faults (controlled by both foliations and amphibolite dikes). Reactivation of northwest-striking foliations during Laramide tectonism is also inferred. However, strike-slip faults of this orientation are comparatively uncommon, and their tectonic significance is not fully understood at this time.

Observed thrust faults (Fig. 4.7e) are interpreted to be the result of three separate fault systems. These systems strike west-northwest, north-northwest and north-northeast. Each inferred fault system corresponds to the restored orientations of Laramide fold axes (Fig. 4.7f,g,h), and the combination of fault sets and fold axes is thought to represent realistic orientations of applied stress fields during Laramide deformation. The inferred stress fields were oriented such that in each system, σ_1 was horizontal and normal to fault strike and fold axis trend; σ_2 was horizontal and parallel to fault strike and fold axis trend; and σ_3 was vertical.

Laramide uplift to the west of the East Joyita fault is due, at least in part, to deformation associated with the west-northwest fold and thrust fault system. Uplift along a

west–northwest–striking thrust fault (Fig. 4.8) resulted in erosional stripping of Cretaceous and older rocks. Restoration of bedding orientations (using the average orientation of Oligocene volcanic rocks, Fig. 4.3a) indicates that Paleozoic and remnant Triassic strata in proximity to the fault were inclined an average of 8° – 10° to the north–northeast. These strata were bevelled and partially buried by syntectonic deposits of the Eocene Baca Formation, which overlie and progressively truncate older sequences from north–northeast to south–southwest. This uplift (Fig. 4.8) has been observed only to the west of the East Joyita fault, and only a few small–displacement (< 1 m) thrust faults of comparable orientation have been observed in El Valle de La Joya. The East Joyita fault appears to bound the uplift to the east, and although prominently marked by dip–slip fault striae (the East Joyita fault was also active during Rio Grande rift tectonism, discussed below), overprinted fault striae indicative of strike–slip displacement have been observed along various segments of this fault. The East Joyita fault is subparallel to the dextral Montosa fault, and it is inferred that dextral displacement also occurred along the East Joyita fault. It is thought that the observed west–northwest–striking thrust fault (Fig. 4.8) originated as a result of compression associated with dextral displacement along the East Joyita fault (Fig. 4.9).

However, this deformation need not be the only cause of Laramide uplift to the west of the East Joyita fault. Folds associated with the north–northeast fold and thrust fault system have been observed in proximity to the East Joyita fault and in El Valle de La Joya. Folds of this orientation become more pronounced to the east and northeast of the study area (Fig. 4.1). Myers *et al.* (1986) mapped comparably oriented structures between El Valle de La Joya and the Montosa fault, and documented an early (Laramide?) episode of up–to–the–west reverse faulting along the Montosa fault zone (interpreted as transpressional, dextral reverse slip by Hayden, 1991). The East Joyita fault is a north–northeast– to northeast–striking structure, and conceivably, the up–to–the–west displacement may be the result of compressional deformation associated

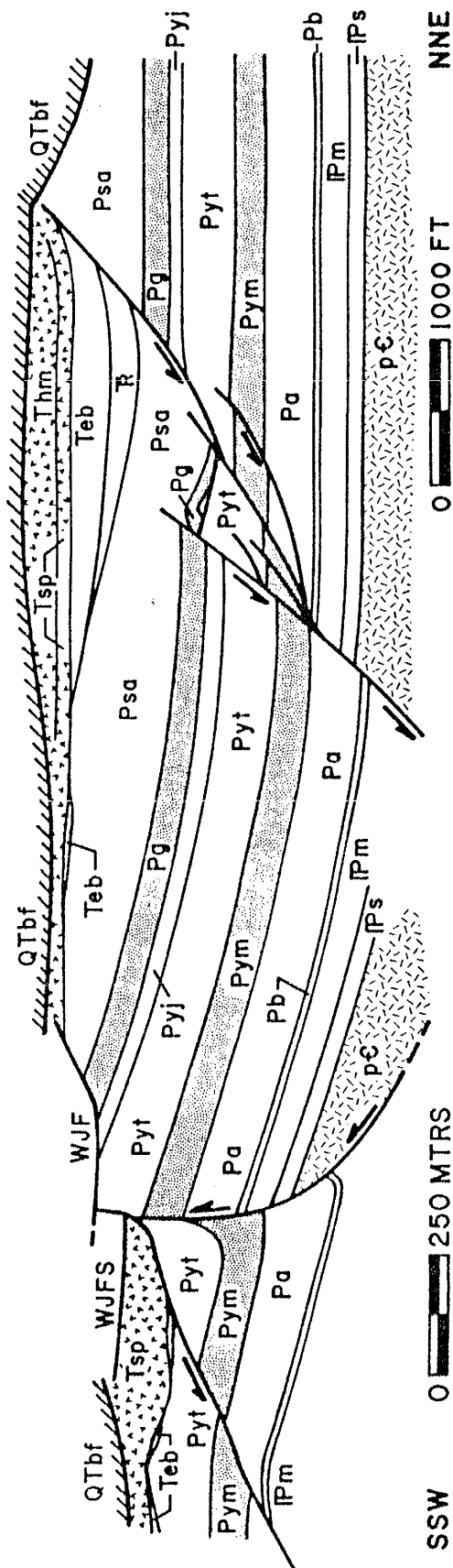
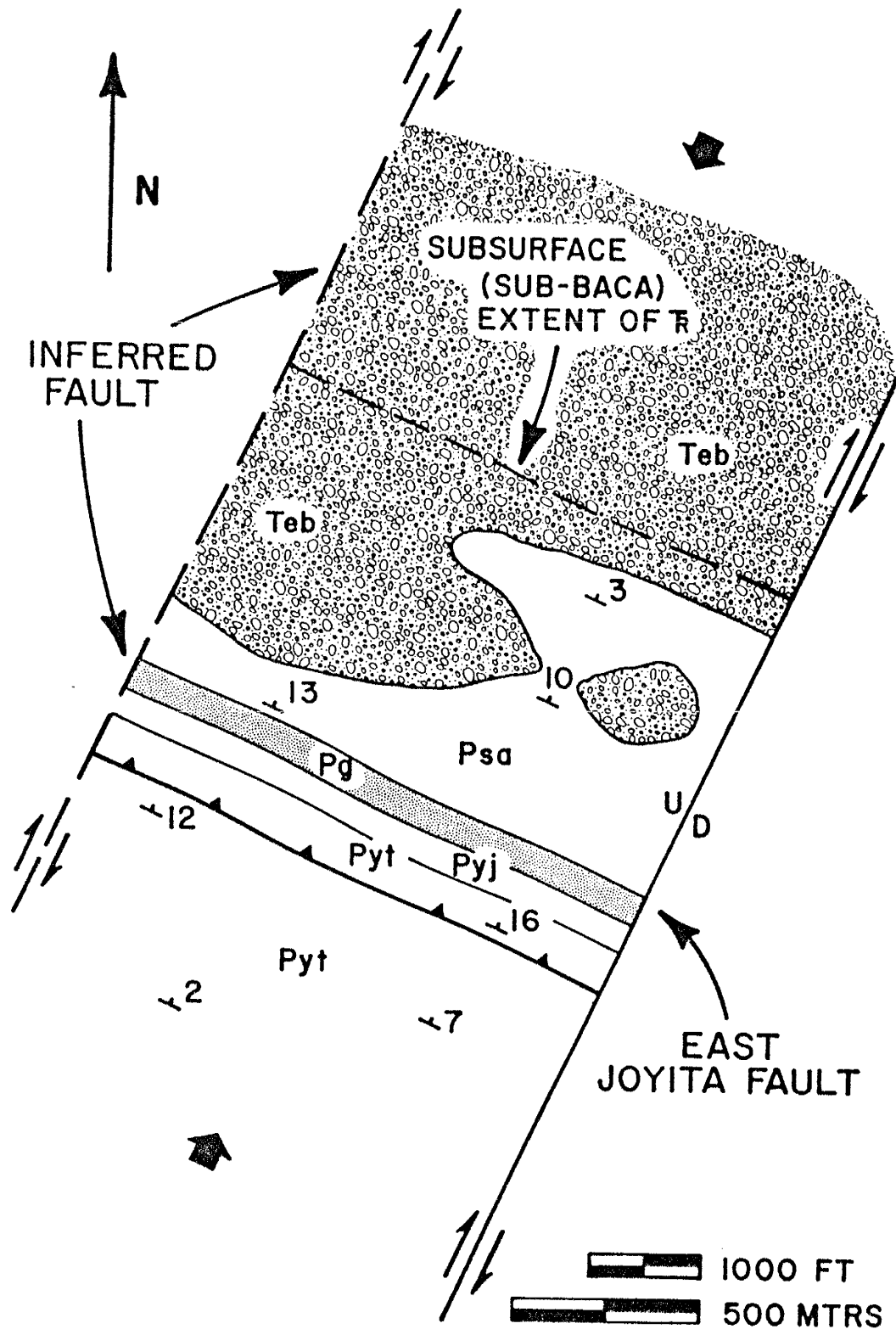


Figure 4.8. Generalized structural profile of Laramide uplift west of the East Joyita fault (compare with Figs. 4.2 and 4.7e,f). Profile oriented N25°E, 60°SE to compensate for down-to-the-west rotation associated with mid-Tertiary extension. Normal faults are of mid-Tertiary (Rio Grande rift) origin, thrust fault is of Laramide origin. Northeastward tilting, absence of Cretaceous strata and southwestward truncation of Triassic (R) and middle Permian rocks by the overlying, syntectonic Baca Formation (Teb) attest to Laramide uplift and erosion prior to deposition of mid-Tertiary volcanic sequences (Tsp = Spears Formation; Thm = Hells Mesa Tuff). Uppermost extent of section obscured by down-to-the-west displacement along the West Joyita fault (WJF), a subparallel fault splay (WJFS) and basin-fill sediments (QTbf). pC = Proterozoic basement; Ps = Sandia; Pm = Madera; Pb = Bursum; Pa = Abo; Pym, Pyt and Pyj = Meseta Blanca, Torres and Joyita Members of the Yeso Formation; Pg = Glorieta; Psa = San Andres.

Figure 4.9. Plan view of structural relationships west of the East Joyita fault after Laramide uplift and prior to deposition of the Spears Formation (compare with Fig. 4.8). West–northwest–striking bedding and thrust fault are interpreted to be the result of compression directed from north–northeast to south–southwest as a result of dextral displacement along the East Joyita fault. Both the existence and the location of the dextral fault to the west–northwest of the East Joyita fault are inferred. Formation symbols keyed to those of Fig. 4.8.



with the north–northeast–striking fold and thrust fault system. Here, analogy is made between observed displacements in the Joyita Hills area and seemingly similar deformational styles along the Montosa fault zone (Myers *et al.*, 1986; Hayden, 1991). Conceivably, Laramide uplift of the Joyita Hills block may be the result of both west–northwest and north–northeast fold and thrust fault systems.

RIO GRANDE RIFT DEFORMATION

General Stratigraphic Relationships

Syntectonic strata of the Baca Formation are positionally overlain by approximately 2 km of Tertiary volcanic sequences. The volcanic section of the Joyita Hills has previously been mapped, measured and described by Spradlin (1976). However, the stratigraphic nomenclature has been largely redefined (Osburn and Chapin, 1983). Interbedded volcanoclastics, lava flows and ash–flow tuffs of the Spears Formation (latest Eocene–early Oligocene; Cather, 1986) form the basal unit of the volcanic section. The Spears Formation is overlain by a series of interstratified, Oligocene rhyolitic ash–flow tuffs (Hells Mesa Tuff, Tuff of South Crosby Peak, and La Jencia, Vicks Peak, Lemitar and South Canyon tuffs) and basaltic andesite flows (collectively, the La Jara Peak Basaltic Andesite). Detailed descriptions, paleomagnetic analyses and time–stratigraphic ($^{40}\text{Ar}/^{39}\text{Ar}$) assignments of these volcanic rocks have been provided by Spradlin (1976), Osburn and Chapin (1983), McIntosh (1983) and McIntosh *et al.*, (1992).

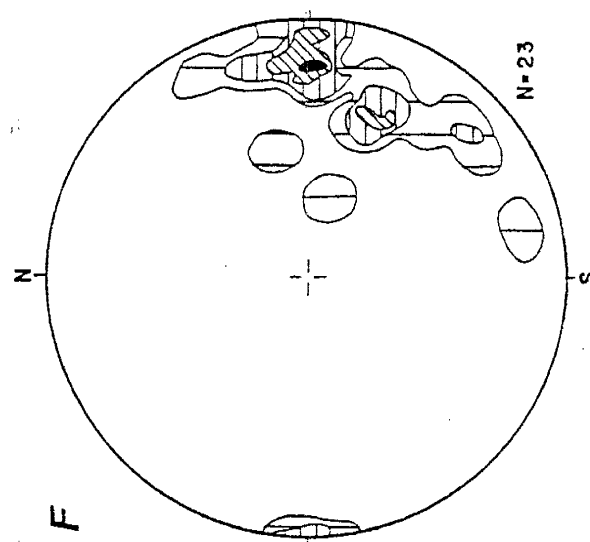
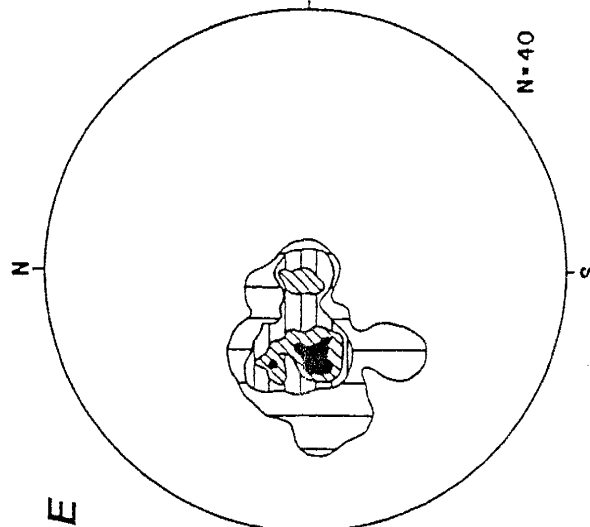
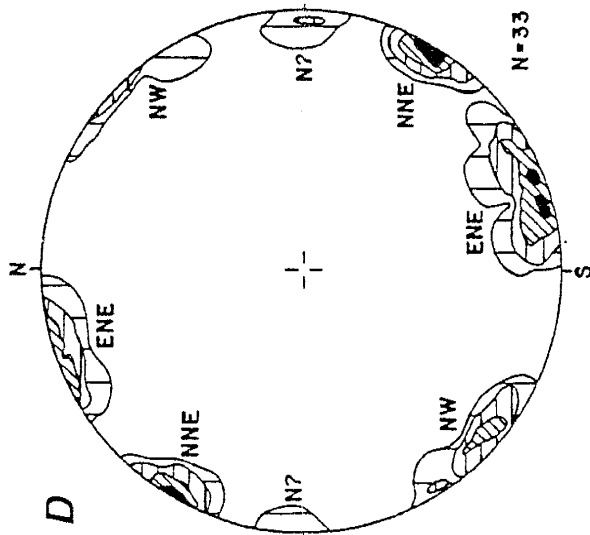
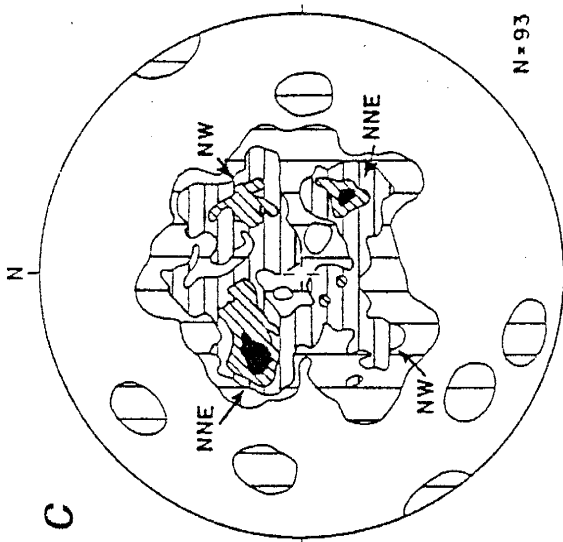
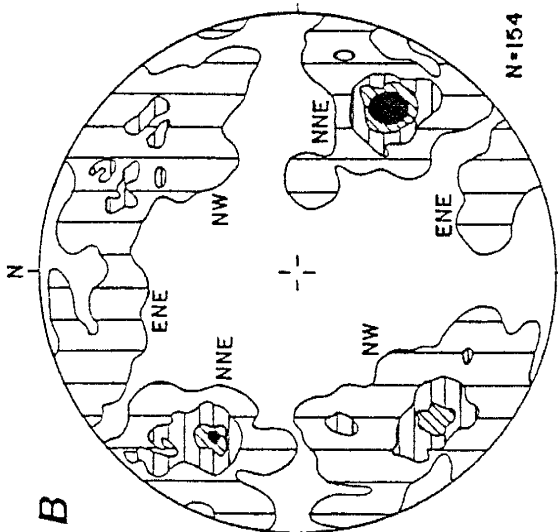
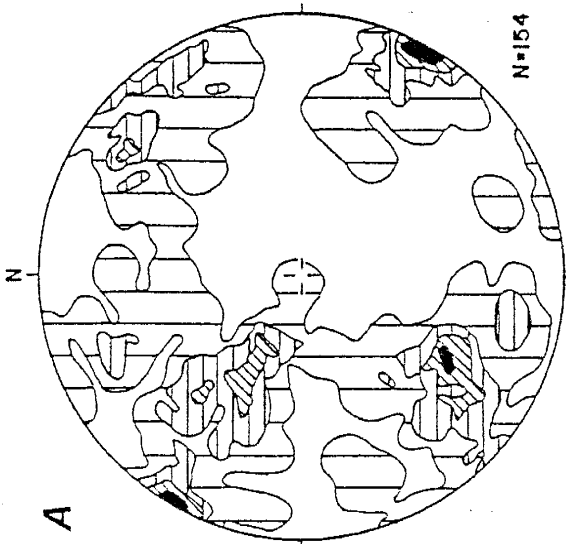
Stratigraphic differences in the volcanic section also occur to the west and east of the East Joyita fault. To the east, thick accumulations of the Spears Formation overlie the Baca Formation. Cather (1986) reported 740 to 1480 m (2428 to 4856 ft), with abrupt thickening of the Spears Formation across an inferred northwest–striking reverse fault. Spradlin (1976, plate 2) reported approximately 884 m (2900 ft). In contrast, accumulations of the Spears are comparatively thin to the west of the East Joyita fault, and rest in depositional contact on rocks of Eocene or middle Permian age.

Relationships between the Spears and underlying Eocene and/or Permian strata and overlying Hells Mesa Tuff are commonly obscured by mid-Tertiary normal faults, making an accurate determination of the thickness of the Spears Formation difficult. However, two exposures have been observed in which it is thought that reliable thickness determinations can be made. These yield stratigraphic thicknesses of 38 m (125 ft) and approximately 125 m (410 ft) for the Spears (to the north and south of the thrust fault depicted in Fig. 4.8, respectively; the latter aided by a marker horizon in proximity to the West Joyita fault). The anomalously thin Spears section west of the East Joyita fault is thought to reflect the persistence of the uplifted Joyita fault block (Laramide deformation) as a topographic high through most of Spears time (latest Eocene-early Oligocene). However, it is also possible that additional, down-to-the-east displacements along the East Joyita fault occurred during Spears deposition. If so, indicators of these additional displacements have gone unrecognized. In contrast, overlying Oligocene ash-flow tuffs and basaltic andesites apparently blanketed terrane to both east and west of the East Joyita fault.

Rio Grande Rift Structures

Mid-Tertiary extension in the Joyita Hills area resulted in both high- and low-angle normal faults. These faults offset Tertiary volcanic and older rocks, and exhibit a variety of orientations. Field observations indicate that most of these faults were consistently oriented at roughly 60° to bedding, regardless of present bedding orientation. Accordingly, normal faults have been evaluated in a manner identical to that used for strike-slip and thrust faults of Laramide origin, i.e., normal faults were evaluated as both pre- and post-rotational structures. Comparison of field-recorded (Fig. 4.10a) and restored (Fig. 4.10b) normal fault orientations indicates that when restored, most normal faults plot as diametrically opposed (conjugate) orientations that are both enhanced as distinct concentrations and/or increased in maxima percent value. These faults define three distinct fault systems that respectively strike north-northeast,

Figure 4.10. Lower-hemisphere, equal-area projections of Rio Grande rift normal fault, dike and detachment fault orientations. A) Field—recorded normal fault orientations; B) restored normal faults; conjugate pairs strike north—northeast (NNE), north-west (NW) and less commonly east—northeast (ENE); C) restored normal fault striae (labelled with respect to the fault system, rather than trend of striae); D) restored mid-Tertiary mafic dikes; E) field—recorded detachment faults; F) field—recorded detachment fault striae. Poles to planes (A, B, D and E) and lineations (C and F) contoured at specified intervals per 1% area.



northwest, and less commonly, east–northeast. Restored fault striae (Fig. 4.10c) indicate that fault displacements were predominantly dip slip.

Other structures of mid–Tertiary origin include mafic (basaltic andesite) dikes. Restoration of these extensional structures (Fig. 4.10d) indicates that when restored, mid–Tertiary dikes plot as subvertical structures that preferentially strike north–northeast, northwest, and east–northeast, bisecting the acute angle formed by each inferred fault pair.

An additional set of normal faults have also been observed in the Joyita Hills. In contrast to the foregoing faults, these faults occurred as shallow (0° to 30°), east–dipping planes of north and north–northeast strike (Fig. 4.10e), and typically showed no consistent orientation with respect to bedding. Geologic mapping and field observations indicate that these low–angle normal faults are commonly associated with allochthonous terrane. Allochthonous blocks composed of Oligocene volcanic and older rocks form the upper plates of these faults. Additionally, these relatively flat faults display differences in fault character that have not been observed on the originally high–angle faults. Some of the shallow–dipping faults exhibit microbrecciated fault surfaces (1–2 in; 2–5 cm) and locally, as along the southernmost exposure of the East Joyita fault, are overlain by 0–100 ft (0–30 m) of tectonic melange.

Interpretation of Rio Grande Rift Deformation

Comparative analysis of mid–Tertiary normal fault orientations as both post–tilt (Fig. 4.10a) and pre–tilt (Fig. 4.10b) structures indicates that most faults were originally pre–tilt, high–angle (60° – 65°) normal faults that experienced dip–slip displacements. Preferred orientations of mid–Tertiary mafic dikes respectively bisect the acute angle formed by each inferred fault system. The combination of restored shear and extensional orientations yields three distinct fracture systems compatible with Andersonian (1951) theory for shallow crustal deformation. These fracture systems are therefore interpreted as early formed structural elements during Rio Grande rift

tectonism. Inferred stress axes were oriented such that in each system, σ_1 was vertical; σ_2 was horizontal and parallel to strike of dikes and faults; and σ_3 was horizontal and normal to strike of dikes and faults. Each stress field orientation and resultant fracture pattern can be correlated to reactivation of existing structures (discussed below). Therefore, these three apparently distinct stress field orientations may be indicative of one overall stress field where $\sigma_1 > \sigma_2 \sim \sigma_3$. In this interpretation, small changes in relative magnitudes of σ_2 and σ_3 would allow significant changes in the direction of extension, with fracture patterns preferentially aligned parallel to existing structural grains.

Mid-Tertiary normal fault and dike orientations (Fig. 4.10b,d) are similar to the orientations of Proterozoic foliations and amphibolite dikes (Fig. 4.3b,c). It is interpreted that northwest- and east-northeast-striking normal fault and dike systems were controlled by, and represent reactivation of, northwest- and east-northeast-striking planar anisotropies in the Proterozoic basement. Here, extensional orientations are subparallel to, and conjugate shears symmetrically disposed about, the preferred orientations of Proterozoic structures. To date, no comparable correlation can be made for the north-northeast-striking normal fault and dike system. Rather, it is inferred that this normal fault and dike system represents reactivation of the north-northeast-striking thrust fault and fold system of Laramide origin. Tertiary volcanic rocks strike north-northeast and are inclined 25° – 30° to the west-northwest. Accordingly, the shallow-dipping thrust faults of north-northeast strike may have influenced or enhanced rotation about a north-northeast-trending, horizontal axis during Rio Grande rifting.

Reactivation of the East Joyita fault also occurred during Rio Grande rift deformation. Down-to-the-west rotation (25° – 30° , Fig. 4.3a) reoriented the initially subvertical East Joyita fault to a steeply east-dipping orientation. Renewed down-to-the-east displacements then juxtaposed Oligocene ash-flow units against the Proterozoic core of the Joyita Hills (Fig. 4.1). Combined Rio Grande rift and Laramide

down-to-the-east offsets approximate 3 km of stratigraphic throw. The modern-day East Joyita fault exhibits a very complex geometry. Although a generally north-northeast-striking structure, the fault is actually composed of a series of right-stepping, north-striking, steeply (55° – 85°) east-dipping planes. Field observations indicate that these fault segments are reactivated ancestral Rocky Mountain faults and Proterozoic foliation planes. In addition, a mid-Tertiary rhyolite dike (31.3 ± 1.2 Ma, Aldrich *et al.*, 1986, their stress indicator #324) was injected along both the East Joyita fault and the foregoing, late Paleozoic faults and Proterozoic foliation planes. Elsewhere, as in the southernmost exposure of the Proterozoic core, the East Joyita fault displays fairly shallow (30°) east-dipping fault surfaces. Fault striae observed on both shallow and steeply dipping fault segments indicate that mid-Tertiary displacements along the East Joyita fault were predominantly dip slip.

Other normal faults were not originally high-angle (Fig. 4.10c). These faults typically occur as shallow (0° – 30°), east-dipping faults. Consideration of these faults as pre-tilt structures indicates that they could not have been steeper than 25° – 55° . In contrast to originally high-angle normal faults, low-angle faults are associated with and underlie allochthonous terrane. These low-angle normal faults are interpreted as extensional detachment faults, and are thought to represent the near surface segments of the detachment faults detected in seismic sections across the Albuquerque Basin (e.g., Cape *et al.*, 1983; De Voogd *et al.*, 1988; Russell and Snelson, 1990). Field observation indicates that originally high-angle normal faults are abruptly truncated by the detachment faults. The detachment faults are therefore interpreted as comparatively young structures that cut the older, originally high-angle faults in a manner analogous to excising detachment faults (Lister and Davis, 1989). It is inferred that normal displacement along the detachment faults accommodated rotation and developed contemporaneously with rotation. Rotation of bedding and originally high-angle faults resulted in domino-style faulting in extensionally detached terrane (see also

Chamberlin, 1983). Observations of westward tilting of the Phanerozoic section (Fig. 4.3a), when combined with the orientation of faults and fault striae (Fig. 4.10e,f), indicate a hanging wall displacement direction to the east and east-southeast.

Unfaulted, subhorizontal basin-fill deposits of the Sierra Ladrones Formation of the Santa Fe Group (Fig. 4.2; approximately 5 Ma, Osburn and Chapin, 1983) overlie allochthonous terrane, detachment faults and rotated and eroded volcanic strata as young as the South Canyon Tuff (27.4 Ma, McIntosh *et al.*, 1992). Therefore, mid-Tertiary deformation in the Joyita Hills can be broadly constrained as an Oligocene-Miocene event.

SUMMARY

Structures associated with three Phanerozoic orogenic events have been recorded and preserved in the sedimentary and volcanic strata of the Joyita Hills area. Reactivation of existing structures, most notably the foliations and amphibolite dikes in the Proterozoic basement, was the rule rather than the exception. Resultantly, fault and dike orientations preferentially developed along north, northwest and east-northeast trends.

Ancestral Rocky Mountain deformation is thought to be the result of sinistral displacements along a north-striking wrench fault system (Fig. 4.6). Late Paleozoic fault orientations represent reactivation of Proterozoic foliations of both north and northwest strike. Northward thrusting in the Marathon-Ouachita orogenic belt (Kluth, 1986) resulted in sinistral displacements along north-striking zones of weakness, resulting in basins and uplifts of dominantly north and subordinate northwest trend. The north-trending Joyita uplift and adjacent San Mateo/Lucero basin probably extended northward through the Albuquerque Basin to the Sierra Nacimiento area, as earlier proposed by Baars (1982) and Read and Wood (1947).

The main obstacle to conclusively demonstrating a late Paleozoic sinistral wrench fault system is the result of overprinting by younger deformation. North-striking

dextral wrench faulting of Laramide origin has been documented in New Mexico by Chapin and Cather (1981) and Chapin (1983), along the Nacimiento fault by Baltz (1967), and within the Joyita Hills area (Fig. 4.7b). Laramide dextral wrenching reactivated Proterozoic basement structures of north and east–northeast strike, the former in a dextral (synthetic) sense, the latter in a sinistral (antithetic) sense. Northwest–striking foliations were also reactivated in a strike–slip sense at this time, although the causal mechanisms for faults of this orientation have not been recognized.

Additional Laramide structures include northeast–striking dextral faults, thrust faults and folds. Both northeast–striking dextral faults and north–northwest oriented thrusts and folds are interpreted to be related to dextral wrench faulting along the Montosa and Del Curto fault zones (Fig. 1; Brown, 1987; Hayden, 1991).

Laramide uplift in the Joyita Hills area occurred to the west of the East Joyita fault. Uplift resulted in partial stripping of Mesozoic and middle Permian strata prior to deposition of the syntectonic Eocene Baca sediments (Fig. 4.8). The East Joyita fault during Laramide time was a north–northeast–striking, subvertical fault, and was subparallel to the dextral Montosa fault system. It is inferred that the East Joyita fault originated during Laramide deformation as a dextral strike–slip fault. Remnant strike–slip fault striae support this interpretation, although younger, normal displacements have overprinted and removed all but a few strike–slip fault striae.

Anomalously thin (125 to 410 ft; 38 to 125 m) strata of the Spears Formation occur to the west of the East Joyita fault, indicating that Laramide uplift persisted as a topographic high through much of Spears time (latest Eocene–early Oligocene). The East Joyita fault was reactivated as a down–to–the–east normal fault during Rio Grande rift tectonism. Although a generally north–northeast–striking structure, down–to–the–east displacement reactivated numerous north–striking ancestral Rocky Mountain fault planes and Proterozoic foliation planes. Combined Laramide and

mid-Tertiary, down-to-the-east displacements along the East Joyita fault approximate 3 km of stratigraphic throw.

Deformation associated with Rio Grande rifting resulted in both high-angle normal faults and low-angle, extensional detachment faults. Originally high-angle faults developed along three directions, two of which represent reactivation of Proterozoic structures of northwest and east-northeast strike. The third normal fault system is thought to have reactivated the north-northeast-striking fold and thrust fault system of Laramide origin. Extensional detachment faults occur as low-angle structures (Fig. 4.10e) that are commonly associated with microbrecciated fault surfaces, tectonic melange and allochthonous terrane. These structures are interpreted as the shallow crustal analogs to the deeper detachment faults in the Albuquerque Basin detected by seismic investigations (e.g., Russell and Snelson, 1990; De Voogd *et al.*, 1988). An extensional model compatible with Lister and Davis (1989) is favored, in which comparatively younger, excising detachment faults cut older, originally high-angle normal faults. Associated rotation of both bedding and high-angle normal faults resulted in domino-style faulting within allochthonous terrane. Both high- and low-angle normal faults offset Oligocene and older rocks, but are overlain by unfaulted strata of the Sierra Ladrones Formation of the Santa Fe Group. Therefore, mid-Tertiary extensional deformation in the Joyita Hills area can be constrained as an Oligocene-Miocene event.

SUMMARY

Specific structures associated with ancestral Rocky Mountain, Laramide and Rio Grande rift tectonisms have been identified and documented. The analytical technique utilized herein has demonstrated that tectonically induced fractures most commonly maintain consistent angular relationships with respect to bedding. These relationships have been interpreted to indicate that tectonically induced fracturing was superimposed on bedding prior to appreciable rotation of bedding from horizontal, and these relationships have been used to evaluate applied stress orientations. The analytical technique has been used to evaluate structures associated with Laramide and Rio Grande rift orogenies, and stress orientations have been inferred for both of these events. The technique has not been applied to ancestral Rocky Mountain deformation, because late Paleozoic structures have been overprinted by younger structures of comparable orientation and/or structural style. Rather, ancestral Rocky Mountain structures have been identified through field observation and recognition of specific late Paleozoic structures.

Ancestral Rocky Mountain deformation in the Joyita Hills area was the result of north-trending, sinistral wrench faulting during early Wolfcampian time. The compatibility of structures observed in the Joyita Hills with previously documented structures in the Sierra Nacimiento area and the Sacramento Mountains indicates that much of central and southern New Mexico was deformed in a similar structural style during the late Paleozoic.

Laramide deformation in the Joyita Hills area resulted predominantly in wrench faulting, with a lesser component of thrust faulting. North-striking synthetic faults and east-northeast-striking antithetic faults are interpreted as respective parts of a north-trending, dextral wrench fault system. Other dextral wrench faults strike to the northeast, and parallel the dextral Montosa and Del Curto fault zones. Laramide fold

axes trend to the north–northeast, west–northwest and north–northwest, and are interpreted to have been related to Laramide wrench fault systems.

Deformation associated with the Rio Grande rift resulted in both high–angle and low–angle normal faults. Low–angle normal faults postdate the high–angle faults, and are interpreted as extensional detachment faults. Detachment faults are thought to have accommodated rotation and to have developed penecontemporaneously with rotation, resulting in domino–style faulting within extensionally detached terrane. Westward tilting of the Phanerozoic section, when combined with the orientation of detachment faults and associated striae, indicate a hanging wall displacement direction to the east and east–southeast. This deformational event can be constrained as an Oligocene–Miocene event.

Reactivation of Proterozoic foliation and amphibolite dike orientations was a common occurrence during each Phanerozoic orogeny. Once formed, basement fabrics served as existing planar weaknesses that were intermittently rejuvenated during the geologic history of the Joyita Hills area. Reactivation of north–striking foliations has been verified in the field along a buried ancestral Rocky Mountain fault. Comparison of Laramide and Rio Grande rift fault and dike orientations with Proterozoic foliation and amphibolite dikes indicates that reactivation also occurred during these younger deformational events. Laramide deformation reactivated Proterozoic structures in a strike–slip sense, and Rio Grande rifting reactivated Proterozoic structures in an extensional sense.

REFERENCES

- Aldrich, M.J., Jr., Chapin, C.E., and Laughlin, A.W., 1986, Stress history and tectonic development of the Rio Grande rift, New Mexico: *Journal of Geophysical Research*, v. 91, no. B6, p. 6199–6211.
- Altares, T., III, 1990, Stratigraphic description and paleoenvironments of the Bursum Formation, Socorro County, New Mexico [M.S. thesis]: Socorro, New Mexico Institute of Mining and Technology, 189 p.
- Anderson, E.M., 1951, The dynamics of faulting and dyke formation with applications to Britain: Edinburgh, Oliver and Boyd, 206 p.
- Angelier, J., 1989, From orientation to magnitudes in palcostress determinations using fault slip data: *Journal of Structural Geology*, v. 11, p. 37–50.
- Armstrong, A.K., 1962, Stratigraphy and paleontology of the Mississippian System in southwestern New Mexico and adjacent southeastern Arizona: *New Mexico Bureau of Mines and Mineral Resources, Memoir 8*, 99 p.
- Armstrong, A.K., and Mamet, B.L., 1988, Mississippian (lower Carboniferous) biostratigraphy, facies, and microfossils, Pedregosa basin, southeastern Arizona and southwestern New Mexico: *U.S. Geological Survey, Bulletin 1826*, 40 p.
- Baars, D.L., 1982, Paleozoic history of the Albuquerque trough: Implications of basement control on Rio Grande rift: *New Mexico Geological Society, Guidebook 33*, p. 153–157.
- Baker, B.W., 1981, Geology and depositional environments of upper Cretaceous rocks, Sevilleta Grant, Socorro County, New Mexico [M.S. thesis]: Socorro, New Mexico Institute of Mining and Technology, 159 p.

- Baltz, E.H., 1967, Stratigraphy and regional tectonic implications of part of upper Cretaceous and Tertiary rocks, east-central San Juan Basin, New Mexico: U.S. Geological Survey, Professional Paper 552, 101 p.
- Beasley, A.J., 1981, A computer program for printing geometrically accurate structural fabric diagrams: *Computers and Geosciences*, v. 7, p. 215–227.
- Beck, W.C., 1984, Joint analyses of the Casper Mountain/Emigrant Gap Anticline juncture, Natrona County, Wyoming [M.S. thesis]: Akron, University of Akron, 101 p.
- Beck, W.C., *in review*, Polydeformation in the Joyita Hills, central New Mexico, U.S.A.: Structural analysis through consideration of initial fracturing: Submitted to the *Journal of Structural Geology*, spring 1992.
- Beck, W.C., and Burford, A.E., 1985, Stress analysis of the Casper Mountain – Emigrant Gap Anticline juncture, Natrona County, Wyoming: Wyoming Geological Association, Guidebook 36, p. 59–65.
- Beck, W.C., and Chapin, C.E., 1991, Structural data from the Joyita uplift: Implications for ancestral Rocky Mountain deformation within central and southern New Mexico: *New Mexico Geological Society, Guidebook 42*, p. 183–190.
- Beck, W.C., and Johnson, D.B., 1992, New fusulinid data and multiple episodes of ancestral Rocky Mountain deformation in the Joyita Hills, Socorro County, New Mexico: *New Mexico Geology*, v. 14, no. 3, p. 53–59.
- Biot, M.A., 1961, Theory of folding of stratified viscoelastic media and its implications in tectonics and orogenesis: *Geological Society of America Bulletin*, v. 72, p. 1595–1620.

- Brown, K.B., 1987, Geology of the southern Canoncito de la Uva area, Socorro County, New Mexico [M.S. thesis]: Socorro, New Mexico Institute of Mining and Technology, 89 p.
- Cape, C.D., McGeary, S., and Thompson, G.A., 1983, Cenozoic normal faulting and the shallow structure of the Rio Grande rift near Socorro, New Mexico: *Geological Society of America Bulletin*, v. 94, p. 3–14.
- Cather, S.M., 1980, Petrology, diagenesis, and genetic stratigraphy of the Eocene Baca Formation, Alamo Navajo Reservation and vicinity, Socorro County, New Mexico [M.S. thesis]: Austin, University of Texas, 244 p.
- Cather, S.M., 1986, Volcano–sedimentary evolution and tectonic implications of the Datil Group (latest Eocene, early Oligocene), west–central New Mexico [Ph.D. dissertation]: Austin, University of Texas, 484 p.
- Cather, S.M., and Johnson, B.D., 1986, Eocene depositional systems and tectonic framework of west–central New Mexico and eastern Arizona; *in* Peterson, J.A., ed., *Paleotectonics and sedimentation*: American Association of Petroleum Geologists, Memoir 41, p. 623–652.
- Chamberlin, R.M., 1983, Cenozoic domino–style crustal extension in the Lemitar Mountains, New Mexico: A summary: *New Mexico Geological Society, Guidebook 34*, p. 111–118.
- Chapin, C.E., 1983, An overview of Laramide wrench faulting in the southern Rocky Mountains with emphasis on petroleum exploration; *in* Lowell, J.D., ed., *Rocky Mountain foreland basins and uplifts*: Rocky Mountain Association of Geologists, p. 169–179.
- Chapin, C.E., and Cather, S.M., 1981, Eocene tectonics and sedimentation in the Colorado Plateau–Rocky Mountain area; *in* Dickinson, W.R., and

- Payne, M.D., eds., Relations of tectonics to ore deposits in the southern Cordillera: Arizona Geological Society Digest, v. 14, p. 173–198.
- Christie–Blick, N., and Biddle, K.T., 1985, Deformation and basin formation along strike–slip faults; *in* Biddle, K.T., and Christie–Blick, N., eds., Strike–slip deformation, basin formation, and sedimentation: Society of Economic Paleontologists and Mineralogists, p. 1–34.
- Davis, G.H., 1984, Structural geology of rocks and regions: New York, John Wiley & Sons, 492 p.
- De Voogd, B., Serpa, L., and Brown, L., 1988, Crustal extension and magmatic processes: COCORP profiles from Death Valley and the Rio Grande rift: Geological Society of America Bulletin, v. 100, p. 1550–1567.
- Durney, D.W., and Ramsay, J.G., 1973, Incremental strains measured by syntectonic crystal growths; *in* De Jong, K.A., and Scholten, R., eds., Gravity and tectonics: New York, John Wiley & Sons, p. 67–96.
- Hayden, S.N., 1991, Dextral oblique–slip deformation along the Montosa fault zone at Abo Pass, Valencia and Socorro Counties, New Mexico (abs.): New Mexico Geology, v. 13, no. 3, p. 64.
- Hayden, S.N., Lucas, S.G., Hunt, A.P., and Beck, W.C., 1990, Triassic–Jurassic stratigraphy, Palo Duro Canyon, Sevilleta Grant, Socorro County, New Mexico (abs.): New Mexico Geology, v. 12, no. 3, p. 65.
- Herber, L.J., 1963a, Structural petrology and economic features of the Precambrian rocks of La Joyita Hills [M.S. thesis]: Socorro, New Mexico Institute of Mining and Technology, 36 p.
- Herber, L.J., 1963b, Precambrian rocks of La Joyita Hills: New Mexico Geological Society, Guidebook 14, p. 180–184.

- Hobbs, B.E., Means, W.D., and Williams, P.F., 1976, An outline of structural geology: New York, John Wiley & Sons, 571 p.
- Jackson, M.D., and Pollard, D.D., 1990, Flexure and faulting of sedimentary host rocks during growth of igneous domes, Henry Mountains, Utah: *Journal of Structural Geology*, v. 12, p. 185–206.
- Kluth, C.F., 1986, Plate tectonics of the ancestral Rocky Mountains; *in* Peterson, J.A., ed., *Paleotectonics and sedimentation: American Association of Petroleum Geologists, Memoir 41*, p. 353–369.
- Kluth, C.F., and Coney, P.J., 1981, Plate tectonics of the ancestral Rocky Mountains: *Geology*, v. 9, p. 10–15.
- Kottlowski, F.E., 1960, Summary of Pennsylvanian sections in southwestern New Mexico and southeastern Arizona: *New Mexico Bureau of Mines and Mineral Resources, Bulletin 66*, 187 p.
- Kottlowski, F.E., and Stewart, W.J., 1970, The Wolfcampian Joyita uplift in central New Mexico: *New Mexico Bureau of Mines and Mineral Resources, Memoir 23, Part I*, p. 1–31.
- Krewedl, D.A., 1974, *Geology of the central Magdalena Mountains, Socorro County, New Mexico [Ph.D. dissertation]: Tucson, University of Arizona*, 128 p.
- Lister, G.S., and Davis, G.A., 1989, The origin of metamorphic core complexes and detachment faults formed during Tertiary continental extension in the northern Colorado River region, U.S.A.: *Journal of Structural Geology*, v. 11, no. 1/2, p. 65–94.
- Lucas, S.G., 1991, Triassic stratigraphy, palontology and correlation, south–central New Mexico: *New Mexico Geological Society, Guidebook 42*, p. 243–259.

- McIntosh, W.C., 1983, Preliminary results from a paleo- and rock-magnetic study of Oligocene ash-flow tuffs in Socorro County, New Mexico: New Mexico Geological Society, Guidebook 34, p. 205-210.
- McIntosh, W.C., Chapin, C.E., Ratte', J.C., and Sutter, J.F., 1992, Time-stratigraphic framework for the Eocene-Oligocene Mogollon-Datil volcanic field, southwest New Mexico: Geological Society of America Bulletin, v. 104, p. 851-871.
- Melton, F.A., 1929, A reconnaissance of the joint-systems in the Ouachita Mountains and central Plains of Oklahoma: Journal of Geology, v. 37, p. 729-746.
- Myers, D.A., Sharps, J.A., and McKay, E.J., 1986, Geologic map of the Becker SW and Cerro Montoso quadrangles, Socorro County, New Mexico: U.S. Geological Survey, Map I-1567.
- Osburn, G.R., 1984, Socorro County geologic map: New Mexico Bureau of Mines and Mineral Resources, Open-file Report 238.
- Osburn, G.R., and Chapin, C.E., 1983, Nomenclature for Cenozoic rocks of northeast Mogollon-Datil volcanic field, New Mexico: New Mexico Bureau of Mines and Mineral Resources, Stratigraphic Chart 1.
- Osburn, G.R., and Lochman-Balk, C., 1983, Stratigraphic nomenclature chart; New Mexico Geological Society, Guidebook 34, p. 98.
- Otte, C., Jr., 1959, Late Pennsylvanian and early Permian stratigraphy of the northern Sacramento Mountains, Otero County, New Mexico: New Mexico Bureau of Mines and Mineral Resources, Bulletin 50, 111 p.
- Parker, J.M., III, 1942, Regional systematic jointing in slightly deformed sedimentary rocks: Bulletin of the Geological Society of America, v. 53, p. 381-408.

- Perry, W.J., Jr., 1981, FABSTAT: A card-imaged FORTRAN program to be used for axially distributed planar-structural data: U. S. Geological Survey, Open-file Report 81-158, 29 p.
- Peterson, J.A., 1980, Permian paleogeography and sedimentary provinces, west-central United States; *in* Fouch, T.D., and Magathan, E.R., eds., Paleozoic paleogeography of west-central United States: Society of Economic Paleontologists and Mineralogists, Rocky Mountain Section, Symposium 1, p. 271-292.
- Philips, F.C., 1971, The use of stereographic projection in structural geology: London, Edward Arnold, 90 p.
- Pollard, D.D., and Aydin, A., 1988, Progress in understanding jointing over the past century: Geological Society of America Bulletin, v. 100, p. 1181-1204.
- Pray, L.C., 1961, Geology of the Sacramento Mountains escarpment, Otero County, New Mexico: New Mexico Bureau of Mines and Mineral Resources, Bulletin 35, 144 p.
- Price, N.J., 1966, Fault and joint development in brittle and semi-brittle rock: New York, Pergammon Press, 176 p.
- Price, N.J., and Cosgrove, J.W., 1990, Analysis of geological structures: New York, Cambridge University Press, 502 p.
- Priest, S.D., 1985, Hemispherical projection methods in rock mechanics: London, Allen & Unwin, 124 p.
- Ramsay, J.G., and Huber, M.I., 1983, The techniques of modern structural geology, volume 1: Strain analysis: London, Academic Press, 307 p.
- Ramsay, J.G., and Huber, M.I., 1987, The techniques of modern structural geology, volume 2: Folds and fractures: London, Academic Press, 391 p.

- Read, C.B., and Wood, G.H., 1947, Distribution and correlation of Pennsylvanian rocks in late Paleozoic sedimentary basins of northern New Mexico: *Journal of Geology*, v. 55, p. 220–236.
- Reches, Z., 1976, Analysis of joints in two monoclines in Israel: *Geological Society of America Bulletin*, v. 87, p. 1654–1662.
- Reches, Z., 1978, Development of monoclines: Part I. Structure of the Palisades Creek branch of the East Kaibab monocline, Grand Canyon, Arizona; *in* Matthews, V., III, ed., Laramide folding associated with basement block faulting in the western United States: *Geological Society of America, Memoir 151*, p. 235–271.
- Reches, Z., and Johnson, A.M., 1978, Development of monoclines: Part II. Theoretical analysis of monoclines; *in* Matthews, V., III, ed., Laramide folding associated with basement block faulting in the western United States: *Geological Society of America, Memoir 151*, p. 273–311.
- Roswell Geological Society, 1956, West–east correlation section, San Andres Mountains to New Mexico – Texas line, southeastern New Mexico: Roswell, Stratigraphic Research Committee, Roswell Geological Society.
- Russell, L.R., and Snelson, S., 1990, Structural style and tectonic evolution of the Albuquerque Basin segment of the Rio Grande rift; *in* Pinet, B., and Bois, C., eds., *The potential of deep seismic profiling for hydrocarbon exploration*: Paris, Editions Technip, p. 175–207.
- Siemers, W.T., 1978, The stratigraphy, petrology, and paleoenvironments of Pennsylvanian rocks in west–central New Mexico [Ph.D. dissertation]: Socorro, New Mexico Institute of Mining and Technology, 275 p.

- Siemers, W.T., 1983, The Pennsylvanian system, Socorro region, New Mexico: Stratigraphy, petrology, depositional environments: New Mexico Geological Society, Guidebook 34, p. 147–155.
- Smith, C.T., 1983, Structural problems along the east side of the Socorro Constriction, Rio Grande rift: New Mexico Geological Society, Guidebook 34, p. 103–109.
- Spradlin, E.J., 1976, Stratigraphy of Tertiary volcanic rocks, Joyita Hills area, Socorro County, New Mexico [M.S. thesis]: Albuquerque, University of New Mexico, 73 p.
- Stewart, W.J., 1970, Fusulinids of the Joyita Hills, Socorro County, central New Mexico: New Mexico Bureau of Mines and Mineral Resources, Memoir 23, Part II, p. 32–82.
- Sykes, L.R., 1978, Intraplate seismicity, reactivation of preexisting zones of weakness, alkaline magmatism, and other tectonism postdating continental fragmentation: *Reviews of Geophysics and Space Physics*, v. 16, p. 621–688.
- Sylvester, A.G., 1988, Strike–slip faults: *Geological Society of America Bulletin*, v. 100, p. 1666–1703.
- Watson, J.V., F.R.S., Reading, H.G., Watterson, J., and White, S.H., 1986, Major crustal lineaments and their influence on the geological history of the continental lithosphere: *Philosophical Transactions of the Royal Society of London*, v. A317, p. 1–290.
- Watterson, J., 1975, Mechanism for the persistence of tectonic lineaments: *Nature*, v. 253, p. 520–522.

APPENDIX A

PROGRAM ROTATE

```

c*****
c
c   This program is a modification of Wm. J. Perry, Jr.'s FABSTAT
c   fortran program (U.S. Geological Survey, OFR 81-158). Principal
c   modifications to the program include the following: 1) acceptance
c   of both linear or planar data as input, using either quadrant or
c   azimuth notation; 2) output in any of eight modes, see below; and 3)
c   omission of statistical calculations performed in the original
c   program, in that they are not applicable to the task at hand.
c   Perry's (1981) program still forms the core of this modified
c   program, and much of the original program, including some of the
c   comments, remain unchanged.
c

```

```

c*****
c
c           Program - - - fabstat.fortran - - - August, 1980
c           modified 5-19-83 by D.A. Cullen and W.C. Beck
c           modified 5-20-89 by W.C. Beck and M.W. Knoper
c           modified 4-26-90 by W.C. Beck
c

```

EXPLANATION OF TERMINOLOGY

```

c Main arrays and matrices:
c

```

```

c   alpha(n) - strike (bearing) of planes (lines). see input
c   options 1 and 2 below.
c   beta (n) - dip (plunge) of planes (lines). see input options
c   1 and 2 below.
c
c   c(i,60) - direction cosine matrix of poles to planes (or
c   lineations) designated by alpha and beta. convention: "i"
c   varies from 1 to 3. 1 - north (x axis); 2 - east (y axis);
c   3 - down (z axis).
c
c   cm(70,i) - direction cosine matrix of mean poles (or
c   lineations), "i" as above. matrix used in mid-program to
c   store all data to be rotated to bedding flat.
c

```

```

c Rotation matrix:
c

```

```

c   a(i,j) - derived from "al", the strike of bedding, and "be",
c   the dip of bedding. by matrix multiplication (a(i,j)x
c   cm(70,j)), the coordinate axes are changed such that the
c   data are rotated to horizontal bedding.
c

```

```

c*****
c
c           INPUT AND OUTPUT FORMATS
c

```

```

c   Data input and output formats have been modified from the
c   original program to accommodate input formats used in the "rose" and
c   "equal-area" programs developed by Tang Ning-hua at the University
c   of Akron (1981, unpublished), and the 'Schmidt' program developed by
c   A.J. Beasley (Computers & Geosciences, vol. 7, 1981).
c

```

c As many as 9 planar or linear orientations can be linked to an
 c individual bedding orientation. Bedding is rotated to horizontal
 c (about a rotation axis parallel to strike) and structural elements
 c are re-oriented by an equivalent amount. An individual bedding
 c orientation and its contained structural elements are herein defined
 c as a 'data set'. Any number of data sets may be rotated in the same
 c run, provided that sets are formatted to a sequential input file.

c Data set-up is as follows. All data is to be left-justified,
 c beginning in column 1.

c
 c Line 1: Defines the following options:

- c 1: FOROPT=format option, where either a '1' (azimuth notation)
 c or a '2' (quadrant notation) is typed into column 1.
 c 2: INPOPT=input option, where either a '1' (planar data) or a
 c '2' (linear data) is typed into column 3.
 c 3: OUTOPT= output option, where an integer (1 through 8) is
 c typed into column 5, where:
 c 1 - defines azimuth notation, planar data
 c 2 - defines azimuth notation, linear data (or pole to plane
 c 3 - defines quadrant notation, planar data
 c 4 - defines quadrant notation, linear data (or pole to plane
 c 5 - defines dip direction and dip, planar data-schmidt format
 c 6 - defines bearing and plunge, linear data-schmidt format
 c (or pole to plane)
 c 7 - defines bedding only, equal-area program format
 c 8 - defines bedding only, schmidt program format
 c 4: ROTOPT= rotation option, where either a '0' (no rotation) or
 c a '1' (rotation) is typed into column 7.

c Note that regardless of input formats, output may be obtained in
 c any desired format. Data that is to be used in the 'rose' or
 c 'equal-area' programs must select output options 3 or 4.
 c Data that is to be used in the schmidt program must select
 c output options 5 or 6. Note that planar data that is output
 c to linear format (outopt = 2, 4 or 6) is equivalent to pole
 c to plane.

c Line 1 also defines the TITLE for a particular run, is printed
 c once at the head of output, and is equivalent to TITLE in the
 c equal-area and schmidt programs. The title begins in column
 c 7, and may be up to 40 columns in length, consisting of any
 c combination of symbols, characters or numbers. If desired,
 c the title may be left blank.

c Line 2: Is the beginning of the first data set. An integer
 c representing the number (0 to 9) of structural orientations
 c (lines or planes) to be linked to and rotated with the
 c corresponding bedding plane is typed into columns 1 and 2. The
 c number of data is referred to as NUMDAT in the program.

c Line 3: Defines the orientation of bedding, indicates whether
 c bedding is upright or overturned, and assigns a name (SETNAM) to
 c that particular data set. If desired, setnam may be omitted from
 c output by 'commenting-out' write statement (6,1730), or left
 c blank.

c The orientation of bedding must be entered as a planar
c orientation and begins in column 1. Bedding format varies with
c the value of foropt: each is illustrated below.

c Bedding must be defined as either upright or overturned by
c typing a '1' (upright) or a '0' (zero, overturned) into the
c second column following the bedding orientation.

c A name (setnam) for the individual data set begins in the
c fifth column after the bedding orientation, and may be up to 40
c columns in length, and may contain any combination of characters,
c numbers or symbols. If desired, setnam may be left blank.

c Lines 4 through numdat+3: Define the orientation of data (planes or
c lines) to be rotated with bedding to horizontal bedding. Data
c formats are dependent upon the values of foropt and inpopt; each
c is illustrated below. Data begins in column 1. A 'LABEL' may be
c assigned to each data line, and the label begins in the third
c column following the data. The label may be up to 40 columns in
c length, and may contain any combination of characters, numbers or
c symbols. Label may also be left blank.

c Line numdat+4: Contains a single digit integer, typed into column
c 1. If there are more data sets to be rotated, enter the value of
c 'numdat' for the next data set, signifying the beginning of the
c data set. If the last data set in this run has just been read, a
c '-1' (minus one) is typed into this line to signify the end of
c data.

c*****

c CONVENTIONS

c The following conventions are required in order for this
c program to function properly.

c Azimuth notation (foropt=1):

c Planar data (inpopt=1): Data entered as strike (0 to 360) and
c dip, using the convention that dip is 90 degrees clockwise
c from strike, e.g., N61E/50SE=061/50; N61E/50NW=241/50.

c Linear data (inpopt=2): Data entered as plunge and bearing,
c e.g., 25/N10W=25/350; 73/S23E=73/157.

c Quadrant notation (foropt=2):

c Planar data (inpopt=1): Data entered as strike (0 to 90) and
c dip, e.g., 355/14=N05W/14NE; 210/63=N30E/63SE. Strike must be
c entered with respect to the northern hemisphere.

c Linear data (inpopt=2): Data entered as plunge and bearing,
c e.g., 48/240=48/S60W; 05/005=05/N05E.

c Schmidt notation (outopt=5 or 6; meaning output is given in suitable
c format for entry into the schmidt program.

c Planar data (outopt=5): Output is given in azimuth notation,
c ten pairs (azimuth of dip direction and dip value) per data
c line, using a (20i4) free format.

c Linear data (outopt=6): Output is given in azimuth notation, ten
 c pairs (azimuth of bearing and plunge value) per data line,
 c using a (20i4) free format.

c Bedding: Is always entered in planar format.
 c Overturned bedding: Enter the field-recorded orientation.
 c Program will restore bedding to horizontal by rotating beds
 c through vertical, i.e., bedding restored to its younging-
 c upward orientation.

c Vertical bedding: Dip direction must be entered as the younging
 c direction of the beds to assure that bedding is restored to
 c its younging-upward orientation, e.g., N45W/90NE will be
 c rotated down to the southwest.

c Note: The final data line requires a '-1' (minus one) in columns 1
 c and 2 to signify the end of data.

c *****

SAMPLE DATA SETS AND INPUT FORMATS

c Line 1 options: 1 1 1 1 Title (azimuth, planar input+output, rotate)
 c Line 2 numdat: 5
 c Line 3 bedding: 045/45 1 Setnam:(optional) Azimuth, planar input
 c Data n=1 number 320/16 Label...(optional) to 40 characters
 c n=2 of data 015/53 Label...
 c n=3 lines 214/30 Label...
 c n=4 equals 235/61 Label...
 c n=5 numdat 135/14 Label...
 c Line numdat+4 -1

c options: 1 2 4 0 (output to quadrant, linear format, no rotation)
 c numdat: 2
 c bedding: 285/37 1 Azimuth format, linear input
 c data: 12/012 Label...
 c data: 18/318 Label...
 c numdat: 3
 c bedding: 212/67 0 Bedding is overturned
 c data: 06/350 Label...
 c data: 36/026 Label...
 c data: 62/317 Label...
 c end: -1

c 2 1 3 0 (output to quadrant format, planar data, no rotation)
 c 2
 c N75W/37NE 1 Quadrant format, planar input
 c N78W/78SW Label...
 c N48E/72SE Label...
 c -1

c 2 2 1 1 (output to azimuth format, planar data, rotated)
 c 3
 c N75W/37NE 1 Quadrant format, linear input
 c 12/N12E Label...
 c 18/N42W Label...

```

c 49/N45W Label...
c 5
c N32E/67NW 0 Bedding is overturned
c 06/N10W Label...
c 36/N26E Label...
c 62/N43W Label...
c 02/N80W Label...
c 11/N79E Label...
c -1
c
c*****
c
c
c          DIMENSIONS AND INTERNAL DEFINITIONS
c
c          dimension a(3,3),label(70,40)
c          dimension u(3),q(3),prod(3),final(9),init(9),title(40),setnam(40)
c          dimension xz(2000),yb(2000)
c          common /one/cm(70,3)
c          common /two/alpha(70),beta(70)
c          common /three/c(3,60)
c          integer b,final,foreopt,inpopt,outopt,rotopt,overt,z,xz,yb
c          character*1 stdr1(60),stdr2(60),hs,hw
c          character*2 ddr(60),hne,hsw,hnw
c          double precision rad
c          rad=0.017453293d0
c          data hs/'S'/,hw/'W'/,hne/'NE'/,hsw/'SW'/,hnw/'NW'/
c*****
c
c          READING OF DATA AND INITIAL SORTING OPERATIONS
c
c*
c*          read options and title
c*
c*          read (5,1000) foreopt,inpopt,outopt,rotopt,(title(j),j=1,40)
c*          1000 format(i1,1x,i1,1x,i1,1x,i1,1x,40a1)
c*          write(6,1010) foreopt,inpopt,outopt,rotopt
c*          1010 format(10x,' format option',1x,i1,/,10x,' input option',1x,i1,/,
c*             110x,' output option',1x,i1,/,10x,' rotation option',1x,i1)
c*          write (6,1020) (title(j),j=1,40)
c*          1020 format (40a1)
c*
c*          read number of data
c*
c*          1030 continue
c*          read (5,1040) numdat
c*          1040 format (i2)
c*          if (numdat.lt.0) go to 2140
c*          if (foreopt.eq.2) go to 1060
c*
c*          read bedding, azimuth notation
c*
c*          read (5,1050) malpha,nbeta,overt,(setnam(j),j=1,40)
c*          1050 format (i3,1x,i2,1x,i1,2x,40a1)
c*          go to 1090
c*          1060 continue
c*

```

```

c*   read bedding, quadrant notation
c*
      read (5,1070) stdr1(1),malpha,stdr2(1),
      2nbeta,ddr(1),overt,(setnam(j),j=1,40)
      1070 format (a1,i2,a1,1x,i2,a2,1x,i1,2x,40a1)
c     write(6,1080) numdat,stdr1(1),malpha,stdr2(1),nbeta,ddr(1)
      1080 format(' ',//,10x,' number of data = ',i2,/,
      210x,' bedding plane = ',a1,i2,a1, '//',i2,a2)
c*
c*   define variables for outopt 7 and 8
c*
      istr=malpha
      idip=nbeta
      1090 if(overt.ne.0) go to 1110
c     write(6,1100)
      1100 format(20x,' bedding is overturned')
      1110 alpha(1)=float(malpha)
      beta(1)=float(nbeta)
      if (numdat.eq.0.and.outopt.ge.7) go to 1760
      if (numdat.eq.0) go to 1030
      num=1
c "num"=number of sets considered from one locality, herein set at 1
      n=0
      bed=alpha(1)+beta(1)
      if (bed.gt.0.) n=1
      i=1
      init(i)=n+1
      l=init(i)
c "init(i)" is the first element of set "i".
      n=n+numdat
c "numdat" is the number of data in set "i".
      final(i)=n
c "final(i)" is the last element of set (i)
      do 1200 k=2,n
      if (foropt.eq.2) go to 1150
      if (inpopt.eq.2) go to 1130
c*
c*   read planar data, azimuth notation
c*
      read (5,1120) malpha,nbeta,(label(k,m),m=1,40)
      1120 format (i3,1x,i2,2x,40a1)
      go to 1190
c*
c*   read linear data, azimuth notation
c*
      1130 read (5,1140) nbeta,malpha,(label(k,m),m=1,40)
      1140 format (i2,1x,i3,2x,40a1)
      go to 1190
      1150 if (inpopt.eq.2) go to 1170
c*
c*   read planar data, quadrant notation
c*
      read (5,1160) stdr1(k),malpha,stdr2(k),nbeta,ddr(k),
      2(label(k,m),m=1,40)
      1160 format(a1,i2,a1,1x,i2,a2,2x,40a1)
      go to 1190

```

```

c*
c*   read linear data, quadrant notation
c*
1170 read (5,1180) nbeta, stdr1(k), malpha, stdr2(k), (label(k,m), m=1, 40)
1180 format (i2, 1x, a1, i2, a1, 2x, 40a1)
1190 alpha(k)=float(malpha)
      beta(k)=float(nbeta)
1200 continue
      last=final(num)
      if (foropt.eq.1) go to 1400
      do 1270 k=1, num
      if (stdr1(k).eq.hs) go to 1210
      go to 1230
1210 write (6,1220)
1220 format (10x, 'wrong input format, strike of bedding')
      go to 2020
1230 continue
c*
c*   convert bedding in quadrant notation to azimuth
c*
      if (ddr(k).eq.hne) go to 1240
      if (ddr(k).eq.hnw) go to 1250
      if (ddr(k).eq.hsw) go to 1260
      go to 1270
1240 alpha(k)=360-alpha(k)
      go to 1270
1250 alpha(k)=180+alpha(k)
      go to 1270
1260 alpha(k)=180-alpha(k)
1270 continue
c   write (6,1280) alpha(1), beta(1), overt
1280 format ('bedding defined as', 1x, 'alpha(1)=' , f8.4,
21x, 'beta(1)=' , f8.4, 1x, 'overt=' , i1)
      if (inpopt.eq.2) go to 1360
c*
c*   convert planar data in quadrant notation to azimuth
c*
      do 1350 k=2, last
      if (stdr1(k).eq.hs) go to 1290
      go to 1310
1290 write(6,1300)
1300 format(10x, ' wrong input format, strike of data')
      go to 2020
1310 continue
      if (ddr(k).eq.hne) go to 1320
      if (ddr(k).eq.hnw) go to 1330
      if (ddr(k).eq.hsw) go to 1340
      go to 1350
1320 alpha(k)=360-alpha(k)
      go to 1350
1330 alpha(k)=180+alpha(k)
      go to 1350
1340 alpha(k)=180-alpha(k)
1350 continue
      go to 1410
c*

```



```

c*   convert linear data in quadrant notation to azimuth
c*
1360 do 1400 k=2,last
      if (stdr1(k).eq.hs) go to 1380
      if (stdr2(k).eq.hw) go to 1370
      go to 1400
1370 alpha(k)=360-alpha(k)
      go to 1400
1380 if (stdr2(k).eq.hw) go to 1390
      alpha(k)=180-alpha(k)
      go to 1400
1390 alpha(k)=180+alpha(k)
1400 continue
1410 if (bed.eq.0.) go to 1450
      al=alpha(1)
      be=beta(1)
c*
c*   convert for overturned bedding
c*
      if (overt.ne.0) go to 1420
      al=al+180.
      be=180.-be
1420 do 1430 i=2,last
      n=i-1
      alpha(n)=alpha(i)
      beta(n)=beta(i)
1430 continue
      do 1440 in=1,num
      init(in)=init(in)-1
      final(in)=final(in)-1
1440 continue
      last=last-1
1450 continue
      last=final(num)
c
c*****
c
c   INITIAL WRITE STATEMENTS, COMPUTATION OF POLES TO PLANES AND
c   COMPUTATION OF DIRECTION COSINES OF POLES TO PLANES:
c
      j=init(i)
      k=final(i)
      if (inopt.eq.2) go to 1490
c*
c*   convert planar data to pole to plane
c*
      do 1480 n=1,last
      alpha(n)=alpha(n)-90
      if(alpha(n).lt.0.) alpha(n)=360.+alpha(n)
      if(beta(n))1460,1470,1470
1460 beta(n)=- (90.+beta(n))
      go to 1480
1470 beta(n)=90.-beta(n)
1480 continue
1490 continue
      do 1550 i=1,num

```

```

        j=init(i)
        k=final(i)
        if (inopt.eq.2) go to 1520
c       write (6,1500)
1500 format ('poles to input planes, plunge and bearing')
c       write(6,1510) (1,beta(1),alpha(1),l=j,k)
1510 format(10x,'l=',i1,10x,f6.2,5x,f6.2)
        go to 1550
1520 continue
c       write (6,1530)
1530 format ('input lineations, plunge and bearing')
c       write (6,1540) (1,beta(1),alpha(1),l=j,k)
1540 format(7x,'l=',i1,8x,f6.2,6x,f6.2)
1550 continue
c*
c*   convert to radians
c*
        do 1560 n=1,last
        alpha(n)=alpha(n)*rad
        beta(n)=beta(n)*rad
1560 continue
c*
c*   convert to direction cosines
c*
        do 1570 i=1,last
        c(1,i)=cos(alpha(i))*cos(beta(i))
        c(2,i)=sin(alpha(i))*cos(beta(i))
        c(3,i)=sin(beta(i))
1570 continue
c
c*****
c
c   DETERMINATION OF MEAN AND ANGLES OF ERROR FOR EACH NON-TRIVIAL
c   SET:
c
        no=0
        do 1620 i=1,num
        j=init(i)
        k=final(i)
        n=k-j+i
c       if(j.eq.k) go to 1620
        no=no+1
        call mean(j,k,no,xm)
c "xm" is the radius of confidence calculated by subroutine mean for
c the set.
c "no" is the subscript value of the 'no'th calculated mean vector.
c "j,k" are respectively the initial and final subscript values of the
c set.
        if(xm.eq.0.) go to 1620
c       write(6,1580) rdconf,rad,xm
1580 format(2x,f10.2,2x,f10.2,2x,f10.2)
        if(xm.gt.1.0) xm=1.0
        if(xm.lt.-1.0) xm=-1.0
c       write(6,1590) acos(xm)
1590 format(2x,f10.2)
        rdconf=acos(xm)/rad

```

```

      call angle(no)
c      write(6,1600) i,alpha(no),beta(no),xm,rdconf
1600 format(' ',4hset ,i1,2x,' mean pole and its radius of
1confidence',/,10x,' azimuth',1x,f6.2,2x,' dip in azimuth
2direction',1x,f5.2,/,10x,' radius of confidence',f8.4,/,10x,
3' angle of error',f6.2,1x,' degrees',/,10x,' the probability is
45% that the angle of error',/,10x,' will exceed this value (i.e.,
595% confidence level).')
      str=alpha(no)+90
      if(str.gt.360.) str=str-360.
      dip=90-beta(no)
c      write(6,1610) i,str,dip
1610 format(' ',7x,' mean plane, set no.',i1,/,10x,' strike:',f6.1,1x,
2'dip:',f6.1,4x,/,7x,' dip direction is 90 degrees clockwise from
3strike',/)
1620 continue
c
c*****
c
c      DETERMINATION OF THE ROTATION MATRIX:
c
c      if(be.eq.0.0) go to 1030
c*
c*      if data is not to be rotated, redefine bedding dip as horizontal
c*      prior to calculations to bypass rotation
c*
c*      if (rotopt.eq.0) be=0.0
c*
c*      convert bedding to radians
c*
c*      al=al*rad
c*      be=be*rad
c "u" is axis of rotation and strike of bedding
      u(1)=cos(al)
      u(2)=sin(al)
      u(3)=cos(be)
      u11=u(1)**2
      u22=u(2)**2
c "q" is a unit vector perpendicular to "u", the axis of rotation,
c which determines the angle of rotation. if below the horizon to the
c west by angle "be", the coordinate system is rotated counterclockwise
c from north by "be" degrees. if below the horizon to the east by angle
c "be" the coordinate system is rotated clockwise "be" degrees.
      q(1)=-sin(be)*u(2)
      q(2)=sin(be)*u(1)
      q(3)=cos(be)
      a(1,1)=u11+q(3)*u22
      a(2,2)=u22+q(3)*u11
      a(1,2)=u(1)*u(2)*(1-q(3))
      a(2,1)=a(1,2)
      do 1630 i=1,3
      a(i,3)=q(i)
1630 continue
      a(3,1)=-a(1,3)
      a(3,2)=-a(2,3)
c a(i,j) is the rotation matrix

```

```

        do 1660 i=1,3
          r=0.0
          do 1640 j=1,3
            r=r+a(i,j)**2
1640      continue
          r=sqrt(r)
          do 1650 j=1,3
            a(i,j)=a(i,j)/r
1650      continue
1660      continue
c
c*****
c
c          ROTATION OF DATA TO BEDDING FLAT
c
        do 1680 i=1,last
          n=no+i
          do 1670 j=1,3
            cm(n,j)=c(j,i)
1670      continue
1680      continue
          last=last+no
          do 1720 i=1,last
            do 1700 j=1,3
              sum=0.0
              do 1690 l=1,3
                sum=sum+a(j,l)*cm(i,l)
1690          continue
              prod(j)=sum
1700          continue
              do 1710 l=1,3
                cm(i,l)=prod(l)
1710          continue
              call unvec(i)
              call angle(i)
1720          continue
c*
c*      convert radians to angles
c*
          alr=al/rad
          ber=be/rad
c
c*****
c
c          FINAL SORTING AND FINAL WRITE STATEMENTS
c
        it=0
        do 1760 i=1,num
          j=init(i)+no
          k=final(i)+no
          n=k-j+1
          it=it+1
c      write(6,1730) (setnam(n),n=1,40)
1730 format(' ',/,11x,40a1,/)
          if (inopt.eq.2) go to 1740
          str=alpha(it)+90

```

```

        if(str.gt.360.) str=str-360.
        dip= 90-beta(it)
1740 continue
c      write(6,1750) i,str,dip
1750 format(' ',7x,' mean plane, set no.',i1/,10x,' strike:',f6.1,lx,
        2'dip:',f6.1,4x/,7x,' dip direction is 90 degrees clockwise from
        3strike',/)
1760 continue
c*
c*      routing given value of outopt
c*
c*      go to (1770,1800,1830,1930,2030,2050,2070,2090) outopt
c*
c*      outopt=1, azimuth notation, planar data
c*
1770 continue
        do 1790 l=j,k
        z=ifix(alpha(l)+90)
        if (z.gt.360) z=z-360
        b=ifix(90-beta(l))
        write (6,1780) z,b,(label(l,m),m=1,40)
1780 format (i3,'/',i2,2x,40a1)
1790 continue
        go to 1030
1800 continue
c*
c*      outopt=2, azimuth notation, linear data (or pole to plane)
c*
c*
        do 1820 l=j,k
        z=ifix(alpha(l))
        b=ifix(beta(l))
        write (6,1810) b,z,(label(l,m),m=1,40)
1810 format (i2,'/',i3,2x,40a1)
1820 continue
        go to 1030
1830 continue
c*
c*      outopt=3, quadrant notation, planar data (for equal-area program)
c*
c*
        do 1920 l=j,k
        kk=kk+1
        z=ifix(alpha(l))
        b=ifix(90-beta(l))
        if(z.ge.0.and.z.lt.90) go to 1840
        if(z.ge.90.and.z.lt.180) go to 1860
        if(z.ge.180.and.z.lt.270) go to 1880
        if(z.ge.270.and.z.lt.360) go to 1900
1840 z=90-z
        write(6,1850)z,b,(label(l,m),m=1,40)
1850 format('N',i2,'W/',i2,'SW',2x,40a1)
        go to 1920
1860 z=z-90
        write(6,1870)z,b,(label(l,m),m=1,40)
1870 format('N',i2,'E/',i2,'NW',2x,40a1)
        go to 1920
1880 z=270-z

```

```

        write(6,1890)z,b,(label(1,m),m=1,40)
1890 format('N',i2,'W/',i2,'NE',2x,40a1)
        go to 1920
1900 z=z-270
        write(6,1910)z,b,(label(1,m),m=1,40)
1910 format('N',i2,'E/',i2,'SE',2x,40a1)
1920 continue
        go to 1030
1930 continue
c*
c*   outopt=4, quadrant notation, linear data (or pole to plane (for
c*   equal-area program))
c*
        do 2020 l=j,k
        kk=kk+1
        z=ifix(alpha(1))
        b=ifix(beta(1))
        if (z.ge.0.and.z.le.90) go to 1940
        if (z.gt.90.and.z.le.180) go to 1960
        if (z.gt.180.and.z.le.270) go to 1980
        if (z.gt.270.and.z.le.360) go to 2000
1940 write (6,1950) b,z,(label(1,m),m=1,40)
1950 format (i2,'/N',i2,'E',2x,40a1)
        go to 2020
1960 z=180-z
        write (6,1970) b,z,(label(1,m),m=1,40)
1970 format (i2,'/S',i2,'E',2x,40a1)
        go to 2020
1980 z=z-180
        write (6,1990) b,z,(label(1,m),m=1,40)
1990 format (i2,'/S',i2,'W',2x,40a1)
        go to 2020
2000 z=360-z
        write (6,2010) b,z,(label(1,m),m=1,40)
2010 format (i2,'/N',i2,'W',2x,40a1)
2020 continue
        go to 1030
2030 continue
c*
c*   outopt=5, azimuth notation, planar data, dip direction and dip
c*   (for schmidt program)
c*
        do 2040 l=j,k
        kk=kk+1
        z=ifix(alpha(1) + 180)
        if (z.ge.360) z=z-360
        b=ifix (90-beta(1))
        xz(kk)=z
        yb(kk)=b
        ll=kk
2040 continue
        go to 1030
2050 continue
c*
c*   outopt=6, azimuth notation, linear data (or pole to plane), trend
c*   and plunge, (for schmidt program)

```

```

c*
do 2060 l=j,k
kk=kk+1
z=ifix(alpha(l))
b=ifix(beta(l))
xz(kk)=z
yb(kk)=b
ll=kk
2060 continue
go to 1030
2070 continue
c*
c* outopt=7, bedding only, quadrant format (equal-area program)
c*
kk=kk+1
write (6,2080) stdr1(1),istr,stdr2(1),
2idip,ddr(1),overt,(setnam(j),j=1,40)
2080 format(a1,i2,a1,'/',i2,a2,1x,i1,2x,40a1)
go to 1030
2090 continue
c*
c* outopt=8, bedding only, azimuth format (schmidt program)
c*
kk=kk+1
if (ddr(1).eq.hne) go to 2100
if (ddr(1).eq.hnw) go to 2110
if (ddr(1).eq.hsw) go to 2120
go to 2130
2100 istr=360-istr
go to 2130
2110 istr=180+istr
go to 2130
2120 istr=180-istr
2130 continue
istr=istr+90
if (istr.gt.360) istr=istr-360
z = istr
b = idip
xz(kk)=istr
yb(kk)=idip
ll=kk
go to 1030
2140 continue
c*
c* print counter for equal-area program
c*
if (outopt.eq.3) write (6,2150) kk
if (outopt.eq.4) write (6,2150) kk
if (outopt.eq.7) write (6,2150) kk
2150 format ('number of data=',i5)
if(outopt.le.4.or.outopt.eq.7) go to 2170
c*
c* print output matrix for schmidt program
c*
write (6,2160) (xz(kk),yb(kk),kk=1,ll)
2160 format(20i4)

```

```

2170 continue
      end
c
c*****
c
c          SUBROUTINE MEAN
c
c this subroutine calculates the mean and radius of confidence of sets
c of unit vectors in array "c(i,60)".
c
      subroutine mean(j,k,no,xm)
c "j" and "k" define the range of "c" to be considered.
      common /one/cm(70,3)
      common /three/c(3,60)
      double precision r,cs(3)
      x=k-j+1
      do 30 l=1,3
      r=0.0
      do 20 i=j,k
      r=r+c(l,i)
20 continue
      cm(no,l)=r
      cs(l)=r**2
30 continue
      r=((cs(1)+cs(2)+cs(3))**.5)
c "r" is now the length of the vector sum
      do 50 l=1,3
      cm(no,l)=cm(no,l)/r
50 continue
c "cm" is now the vector mean (the mean pole)
      ex=x-2
      if(r.gt.ex) go to 60
c      write(6,400) j,k
400 format (1h0,10x,'set of data including planes no.',1x,i2,1x,
2'through no.',1x,i2,1x,'cannot be treated accurately by this
3program',/,10x,'as r is less than or equal to the number of
4planes minus two (n-2).',/,10x,'a valid measure of dispersion
5 is not computed.',/)
      xm=0
      go to 70
60 g=1./(x-1.)
      qa=0.05
      xm=1.-((x-r)*((1./qa)**g-1.))/r
70 return
      end
c
c*****
c
c          SUBROUTINE ANGLE
c
c this subroutine converts the direction cosine array to azimuth and
c plunge.
c
c
      subroutine angle(i)
      common /one/cm(70,3)

```



```

common /two/alpha(70),beta(70)
double precision rad
rad=0.017453293d0
abort=cm(i,1)+cm(i,2)+cm(i,3)
if(abort.eq.0.0) go to 20
if(cm(i,3)) 4,8,8
4 cm(i,1)=-cm(i,1)
  cm(i,2)=-cm(i,2)
  cm(i,3)=-cm(i,3)
8 if(cm(i,3).eq.1.) go to 18
  cm(i,1)=cm(i,1)/sqrt(cm(i,1)**2+cm(i,2)**2)
  alpha(i)=acos(cm(i,1))/rad
  b=cm(i,3)/((1.-cm(i,3)**2)**.5)
  beta(i)=atan(b)/rad
  if(cm(i,1)) 10,14,14
10 if(cm(i,2)) 12,16,16
12 alpha(i)=360.-abs(alpha(i))
  go to 20
14 if(cm(i,2).gt.0) go to 20
  alpha(i)=360.-alpha(i)
  go to 20
16 if(alpha(i).gt.90) go to 20
  alpha(i)=180.-abs(alpha(i))
  go to 20
18 alpha(i)=0
  beta(i)=90
20 return
end

c
c*****
c
c
c          SUBROUTINE UNVEC
c
c this subroutine verifies that unit vector array "cm(n,i)" is
c unitized.
c
c  subroutine unvec(j)
c  common /one/cm(70,3)
c  r=0.0
c  do 10 i=1,3
c  r=r+cm(j,i)**2
10 continue
  if(r.eq.0.) go to 20
  r=sqrt(r)
  do 15 i=1,3
  cm(j,i)=cm(j,i)/r
15 continue
20 return
end

```

PROGRAM CONVRT

```

c*****
c
c   This program is used to convert a continuous data file in
c   quadrant notation into suitable azimuth format for entry into the
c   SCHMDT program.  Assumedly, the input file is typed by the user or
c   created as output by program ROTATE (outopt = 3,4 or 7).  Only minor
c   modifications to the output file created by program ROTATE are re-
c   quired to make it suitable as input into this program.  Input formats
c   are specified below, where:  NPLOT is the number of datasets to be
c   converted; INDEX is a numerical value defining type of data to be
c   converted (1 = planar data; 2 = linear data; 0 = end of data); NOBSNM
c   is the number of individual orientations to be converted in a given
c   data set.
c
c*****
c   Program - - - convrt.f - - - Version of October, 1990 - - W.C. Beck
c
c*****
c   SAMPLE DATA SETS AND INPUT FORMATS
c
c
c   005                               nplot
c   1                                 index
c   00012                             nobsnm
c   planar data, set #1  title
c   N45W/45SW   (GOES TO...)         225  45
c   N20W/40SW                                     250  40
c   N45W/20SW                                     225  20
c   N10W/70SW                                     260  70
c   N60E/45SE                                     150  45
c   N30E/61NW                                     300  61
c   N45W/58NE                                     45  58
c   N10W/25NE                                     80  25
c   N20E/64NW                                     290  64
c   N50E/90NW                                     320  90
c   N16E/16SE                                     106  16
c   N37E/00SE                                     127  00
c   2                                           index
c   00005                                       nobsnm
c   linear data, set #2   title
c   12/N50E                               50  12
c   87/S21E                               159  87
c   49/S62W                               242  49
c   62/N75W                               285  62
c   77/N90E                               90  77
c   2                                           index
c   00004                                       nobsnm
c   linear data, set #3   title
c   55/N46W                               314  55
c   61/S20W                               200  61
c   89/S72E                               108  89
c   67/N05E                               5   67
c   1                                           index

```

```

c 00004 nobsnm
c planar data, set #4 title
c N45E/45SE 135 45
c N45W/45SW 225 45
c N45E/45NW 315 45
c N45W/45NE 45 45
c 1 index
c 00006 nobsnm
c planar data, set #5 title
c N10E/90SE 100 90
c N89E/52NW 359 52
c N10W/52SW 260 52
c N90W/62NE 0 62
c N00W/00SW 270 0
c N14W/85SW 256 85
c 0 to end program index
c
c*****
c
c DIMENSIONS AND INTERNAL DEFINITIONS
c
c dimension title(40), xz(2000), yb(2000)
c integer b, z, xz, yb
c character*1 stdr1, stdr2, hs, hw
c character*2 ddr, hne, hsw, hnw
c data hs, hw, hne, hsw, hnw/'S', 'W', 'NE', 'SW', 'NW'/
c
c*****
c
c*
c* begin program
c*
c* read (5,1000) nplot
c* 1000 format (i3)
c* do 1200 i=1,nplot
c* read (5,1010) index
c* 1010 format (i1)
c* if (index.eq.0) go to 1210
c* read (5,1020) nobsnm
c* 1020 format (i5)
c* read (5,1030) (title(j), j=1,40)
c* 1030 format (40a1)
c* kk=0
c* do 1160 k=1,nobsnm
c* if (index.eq.2) go to 1090
c*
c* read planar data
c*
c* read (5,1040) stdr1,malphi, stdr2,nbeta, ddr
c* 1040 format (a1,i2,a1,lx,i2,a2)
c* alpha=float(malphi)
c* beta=float(nbeta)
c* if (ddr.eq.hne) go to 1050
c* if (ddr.eq.hnw) go to 1060
c* if (ddr.eq.hsw) go to 1070
c* go to 1080

```

```

1050 alpha=360.-alpha
      go to 1080
1060 alpha=180.+alpha
      go to 1080
1070 alpha=180.-alpha
1080 continue
      alpha=alpha-90.
      if (alpha.lt.0.0) alpha= 360.+alpha
      beta=90.-beta
      go to 1140
1090 continue
c*
c*   read linear data
c*
      read (5,1100) nbeta,stdr1,malpha,stdr2
1100 format (i2,1x,a1,i2,a1)
      beta=float(nbeta)
      alpha=float(malpha)
      if (stdr1.eq.hs) go to 1120
      if (stdr2.eq.hw) go to 1110
      go to 1140
1110 alpha=360.-alpha
      go to 1140
1120 if (stdr2.eq.hw) go to 1130
      alpha=180.-alpha
      go to 1140
1130 alpha=180.+alpha
1140 continue
c*
c*   all data now converted to line, azimuth format
c*
      if (index.eq.2) go to 1150
c*
c*   set up array, planar data
c*
      kk=kk+1
      z=ifix(alpha+180.)
      if (z.ge.360) z=z-360
      b=ifix(90.-beta)
      xz(kk)=z
      yb(kk)=b
      ll=kk
      go to 1160
1150 continue
c*
c*   set up array, linear data
c*
      kk=kk+1
      zz=ifix(alpha)
      bb=ifix(beta)
      xz(kk)=zz
      yb(kk)=bb
      ll=kk
1160 continue
c*
c*   print title

```

```

c*
      write (6,1170) (title(j), j=1,40)
1170 format (40a1)
c*
c*   print output array
c*
      write (6,1180) (xz(kk),yb(kk), kk=1,nobsnm)
1180 format (20i4)
c*
c*   print number of data
c*
      write (6,1190) l1
1190 format ('number of data= ',i5)
1200 continue
1210 continue
      end

c
c
c* ***Planar data may be subdivided into multiple arrays
c* ***according to dip value by substituting the following
c* ***after line 1140.
c*
c*
c*   all data now converted to line, azimuth format
c*
c   if (index.eq.2) go to 1150
c*
c*   set up array, planar data
c*
c   z=ifix(alpha+180.)
c   if (z.ge.360) z=z-360
c   b=ifix(90.-beta)
c   if (b.ge.45.and.b.lt.75) go to 1145
c   if (b.lt.45) go to 1148
c   kk=kk+1
c   xz(kk)=z
c   yb(kk)=b
c   ll=kk
c   go to 1160
c 1145 continue
c   km=km+1
c   xm(km)=z
c   ym(km)=b
c   lm=km
c   go to 1160
c 1148 continue
c   kn=kn+1
c   xn(kn)=z
c   yn(kn)=b
c   ln=kn
c   go to 1160
c 1150 continue
c 1160 continue
c*
c*   print title
c*

```

```
c      write (6,1170) (title(j), j=1,40)
c 1170 format (40a1)
c*
c*      print output array
c*
c      write (6,1180) (xz(kk),yb(kk), kk=1,11)
c 1180 format (20i4)
c*
c*      print number of data
c*
c      write (6,1190) l1
c 1190 format ('number of data= ',i5)
c      write (6,1181) (xm(km),ym(km), km=1,lm)
c 1181 format (20i4)
c      write (6,1182) lm
c 1182 format ('number of data= ', i5)
c      write (6,1183) (xn(kn),yn(kn), kn=1,ln)
c 1183 format (20i4)
c      write (6,1184) ln
c 1184 format ('number of data= ', i5)
c 1200 continue
c 1210 continue
c      end
```

PROGRAM SCHMDT

```

C*****
C
C   A FORTRAN IV (ICL 1901A) program for printing an equal-area
C   density diagram of structural orientation data.
C
C   Program by A.J. BEASLEY, GEOLOGY DEPT., UNIVERSITY OF ZIMBABWE,
C   P.O. BOX MP167, MOUNT PLEASANT, SALISBURY, ZIMBABWE.
C
C   Three types of structural data can be processed:
C
C   Mode 1:  Vectors or lineations, the data must be supplied as
C   azimuth measured clockwise from north, and dip or plunge.
C
C   Mode 2:  Poles to planes; data must be supplied as azimuth of the
C   dip direction (i.e., perpendicular to strike, and in the down-dip
C   direction) and dip angle.
C
C   Mode 3:  Beta intersections of planes; data as for mode 2.
C
C   Any number of sets of data may be processed in a computer run.
C
C   For each set of data the following cards are required:
C   Card 1:  format (I1, 19a4, a3); mode and title:
C           column 1:  mode as above (single digit)
C           columns 2 - 80:  title
C   Card 2 et seq.:  format 20i4); orientations of data; each card
C   bears 10 pairs of positive integer values of azimuth and dip.
C   After the last pair of data, the final card must contain a
C   negative dummy azimuth, with the remaining fields containing
C   dummy values, zero for example.  When there are an exact multiple
C   of ten data, a dummy set-terminator card must be added, complying
C   with the above requirements; i.e., a negative digit followed by
C   19 other dummy digits.
C
C   After the last set of data, a batch terminator card is required;
C   this contains a zero in column 1.
C
C*****
      common
      1      /blk1/rad,dx,dy,prcnt,kontrs,kmid,kmax,lmid,lmax,num
      3      /blk3/title(20)
      5      /blk5/a1(3896),b1(3896),c1(3896)
      8      /blk8/kount(3896)
C
C   * calculate parameters required during program
      call params
C
C   * calculate parameters of node at center of projection-circle, in
C   case it is not scanned during program; center node must be
C   numbered because it is addressed specifically in subroutine
C   'print'.
      call dcnode (kmid,lmid)
C
C   * read operating mode, and title
      10 read (5,1001) mode,title

```

```

      if (mode .eq. 0) stop
c
      * print title and headings for data
      write (6,1002) title
c
c      * initialize 'kount' array to zero
      do 20 n = 1,num
20 kount(n) = 0
c
c      * initialize number of data (np) to zero
      np = 0
c
c      * read and write a line of data
30 call card (mode,ndata)
      if (ndata .eq. 0) go to 60
c
c      * process data from card
      do 60 i = 1,ndata
c
c      * increment number of data
      np = np + 1
c
c      * calculate direction cosines of vector, and coordinates of
c      nearest node to its projection onto the projection plane.
      call dcvect (i, a, b, c, k, l)
c
c      * if beta diagram required, store direction cosines, otherwise
c      plot vector
      go to (40, 40, 50) mode
40 call count (a, b, c, k, l)
      go to 60
50 a1(np) = a
      b1(np) = b
      c1(np) = c
60 continue
c
c      * if card contains ten pairs of data, read another card
      if (ndata .eq. 10) go to 30
70 continue
c
c      * if beta diagram required, calculate intersections of planes,
c      and plot vectors of intersections.
      if (mode .eq. 3) call beta(np,nbeta)
c
c      * print diagram
      call print (mode, np, nbeta)
      go to 10
1001 format (i1, 19a4, a3)
1002 format (1h1,10x,19a4,a3,/,1h0,11x,10(6haz dip,5x))
      end
c
c*****
c
c      block data
c
c      definitions of constants

```



```

c
c   rad.....radius of plotted diagram (mm)
c   dx.....grid interval along x-axis; all printing positions
c           of line-printer (mm)
c   dy.....grid interval along y-axis; every line (mm)
c   prcnt.....area of scanning circle; as percentage of equal-area
c           plot
c   kontr.....number of contour intervals on an equal-area plot
c*****
c
c   common
c   1      /blk1/rad, dx, dy, prcnt, kontr, kmid, kmax, lmid, lmax, num
c   data rad/ 100. /
c   data dx,dy/ 2.54000,3.17500 /
c   data prcnt/1./
c   data kontr/4/
c   end
c
c*****
c
c   subroutine params
c
c   calculates various parameters dependent upon the radius of the
c   primitive circle, the line and character spacings of the line-
c   printer and the size of the scanning cone.
c*****
c   common
c   1      /blk1/rad, dx, dy, prcnt, kontr, kmid, kmax, lmid, lmax, num
c   2      /blk2/cscrit, check, krange, lrange
c   6      /blk6/node(77,61)
c
c   * determine number of columns and rows within projection circle,
c   and array indices of center column and row.
c   kmid = (int(rad*2./dx)-1)/2+1
c   kmax = kmid*2-1
c   lmid = (int(rad*2./dy)-1)/2+1
c   lmax = lmid*2-1
c   num = 0
c
c   * initialize array 'node'; outside projection circle = -1;
c   inside = 0
c   do 60 l = 1, lmax
c   y = dy * (lmid - l)
c   x = sqrt (rad*rad - y*y)
c   kmin = kmid - int(x/dx)
c   if (kmin-1) 40, 40, 10
c 10 do 20 k = 1, kmin-1
c 20 node(k, l) = -1
c   do 30 k = kmax-kmin+2, kmax
c 30 node(k, l) = -1
c 40 continue
c   do 50 k = kmin, kmax-kmin+1
c 50 node(k, l) = 0
c 60 continue
c
c
c

```

```

c      * calculate the cosine of the angle subtended by the scanning-
c      circle at the center of the hemisphere
c      cscrit = 1.-prcnt/100
c
c      * calculate the critical z-axis direction cosine for which the
c      scanning-circle overlaps the perimeter of the projection-
c      circle; it equals sin(angle of scanning-cone).
c      check = sqrt(1. - cscrit*cscrit)
c
c      * calculate range of lines and columns to be scanned
c      rsmall = rad*check
c      krange = rsmall/dx
c      lrange = rsmall/dy
c      return
c      end
c
c*****
c
c      subroutine dcnode (k,l)
c
c      numbers a node within the projection circle, initializes the
c      count-value at that node, and calculates the direction cosines of
c      the vector through the node.
c
c      explanation of subroutine arguments
c
c      k,l.....column and row numbers of a node
c*****
c
c      common
c      1      /blk1/rad,dx,dy,prcnt,kontrs,kmid,kmax,lmid,lmax,num
c      6      /blk6/node(77,61)
c      7      /blk7/a(3896),b(3896),c(3896)
c      8      /blk8/kount(3896)
c
c      num = num + 1
c      node(k,l) = num
c      kount(num) = 0
c      x = dx * (k-kmid)
c      y = dy * (lmid-l)
c      rsq = x*x + y*y
c      r = sqrt(rsq)
c      costh = 1. - rsq/(rad*rad)
c      sinth = sqrt(1. - costh*costh)
c      if (r .eq. 0) go to 10
c      f1 = sinth/r
c      a(num) = x*f1
c      b(num) = y*f1
c      go to 20
c 10 a(num) = 0
c      b(num) = 0
c 20 c(num) = costh
c      return
c      end
c
c*****
c

```

```

subroutine card (mode,ndata)
c
c reads a data card, determines the number of data pairs, and, for
c planar data, converts to pole azimuth and plunge.
c
c explanation of subroutine arguments
c
c mode.....flag controlling type of diagram produced; 1 = vectors
c or lineations; 2 = poles to planes; 3 = beta-intersec-
c tions of planes; 0 = end of batch.
c
c ndata....number of data pairs on a card.
c*****
c
c common
c 3 /blk3/title(20)
c 4 /blk4/iphi(10),itheta(10)
c read (5,1001) (iphi(i),itheta(i), i = 1,10)
c
c * determine number of data pairs on card (ndata); -ve iphi
c terminates
c ndata = 0
c do 10 i = 1,10
c if (iphi(i)) 20, 10, 10
10 ndata = i
20 continue
c if (ndata) 40, 40, 30
30 write (6,1002) (iphi(i),itheta(i), i = 1, ndata)
c
c * for planar data, convert azimuth and dip to pole vector
c directions
c if (mode .eq. 1) return
c do 40 n = 1,ndata
c iphi(n) = iphi(n) + 180
c itheta(n) = 90 - itheta(n)
40 continue
c return
1001 format (20i4)
1002 format (11x,10(i3,i4,4x))
c end
c
c*****
c
c subroutine dcvect (i, a, b, c, k, l)
c
c calculates the direction cosines of a data-vector, and determines
c the nearest node to its projection onto the projection-plane.
c
c explanation of subroutine arguments
c
c i.....array index of azimuth iphi(-) and dip itheta(-) of data
c vector.
c a,b,c..direction cosines of vector whose azimuth and dip are
c iphi(i) and itheta(i).
c k,l....column and row number of the node nearest to the
c projection of the data vector.

```

```

C*****
C
      common
      1      /blk1/rad,dx,dy,prcnt,kontrs,kmid,kmax,lmid,lmax,num
      4      /blk4/phi(10),itheta(10)
      data fpi/0.017453292 /
C      ( fpi = pi/180 )
C
      gamma = fpi*(90-itheta(i))
      c = cos(gamma)
      r = rad*sqrt(1.-c)
      phi = fpi*(90-phi(i))
      singm = sin(gamma)
      csphi = cos(phi)
      snphi = sin(phi)
      a = csphi*singm
      b = snphi*singm
      k = nint(r*csphi/dx) + kmid
      l = lmid - nint(r*snphi/dy)
      return
      end
C
C*****
C
      subroutine count (aa, bb, cc, kk, ll)
C
C      scans the nodes in the vicinity of a data-vector projection and
C      increments 'kount' for nodes within the scanning-cone.
C
C      explanation of subroutine arguments
C
C      aa, bb, cc..direction cosines of the vector.
C      kk, ll.....column and row numbers of the node nearest to the
C      projection of the vector.
C*****
C
      common
      1      /blk1/rad,dx,dy,prcnt,kontrs,kmid,kmax,lmid,lmax,num
      2      /blk2/cscrit,check,krange,lrangle
      6      /blk6/node(77,61)
      7      /blk7/a(3896),b(3896),c(3896)
      8      /blk8/kount(3896)
C
C      * 'iflag' records whether inverse vector has been considered
      iflag = 1
      10 continue
C
C      * determine scanning limits within lines and columns
      ll = max0(ll-lrange,1)
      l2 = min0(ll+lrangle,lmax)
      k1 = max0(kk-krange,1)
      k2 = min0(kk+krange,kmax)
C
C      * commence scan
      do 50 l = ll,l2
      do 50 k = k1,k2

```

```

      n = node(k,1)
c
c      * if node = -1, it is outside primitive circle; skip.
c      if zero, direction cosines have not been calculated yet; do so.
      if (n) 50, 20, 30
20 call dcnode (k,1)
      n = num
c
c      * calculate cosine of angle between data vector and vector
c      through node
30 cosan = abs(aa*a(n) + bb*b(n) + cc*c(n))
c
c      * if data vector within critical angle of node vector, increment
c      'kount' for the node.
      if (cosan - cscrit) 50, 50, 40
40 kount(n) = kount(n) + 1
50 continue
c
c      * check whether scanning-cone overlaps perimeter of projection-
c      circle; if so, repeat above routine for inverse vector.
      go to (60,80) iflag
60 if (cc-check) 70, 70, 80
70 aa = -aa
      bb = -bb
      cc = -cc
      kk = kmax + 1 - kk
      ll = lmax + 1 - ll
      iflag = 2
      go to 10
80 return
      end
c
c*****
c
      subroutine beta (np,nbeta)
c
c      calculates the direction cosines of the intersections of all
c      pairs of planes, and calls 'count' to plot them.
c
c      !!!!!!!!!!!!!to run beta plots on tech computer!!!!!!!!!!!!!!
c      calculations require a significant run time: can send output to
c      file using: "schmdt.out < datafile > outputfile" - - - then
c      view/print output file. for some as of yet unknown reason, beta
c      plots do not function well when there is an even multiple of ten
c      data, yet other values of ndata work.
c
c      explanation of subroutine arguments
c
c      np.....number of data vectors
c      nbeta...number of beta intersections
c*****
c
      common
1      /blk1/rad, dx, dy, prcnt, kontrs, kmid, kmax, lmid, lmax, num
5      /blk5/a1(3896), b1(3896), c1(3896)
c

```

```

c      * initialize the number of beta intersections to zero
      nbeta = 0
c
c      * commence processing of data, in pairs
      do 70 i = 1, np-1
      do 70 j = i+1, np
c
c      * skip parallel planes
      10 if (a1(i)-a1(j)) 40, 20, 40
      20 if (b1(i)-b1(j)) 40, 30, 40
      30 if (c1(i)-c1(j)) 40, 70, 40
c
c      * increment number of beta intersections
      40 nbeta = nbeta + 1
c
c      * calculate direction cosines of beta vector
      a = b1(i)*c1(j)-b1(j)*c1(i)
      b = c1(i)*a1(j)-c1(j)*a1(i)
      c = a1(i)*b1(j)-a1(j)*b1(i)
      fabc = 1./sqrt(a*a+b*b+c*c)
      a = a * fabc
      b = b * fabc
      c = c * fabc
c
c      * if c is negative, reverse vector
      if (c) 50, 60, 60
      50 a = -a
      b = -b
      c = -c
c
c      * calculate grid coordinates of beta-projection on projection
c      plane
      60 fc = rad/sqrt(1.+c)
      k = nint(a*fc/dx+kmid)
      l = nint(lmid-b*fc/dy)
c
c      * plot beta vector
      call count (a, b, c, k, l)
      70 continue
      return
      end
c
c*****
c
c      subroutine print (mode, np, nbeta)
c
c      prints the completed fabric diagram
c
c      explanation of subroutine arguments
c
c      mode.....see subroutine 'card'
c      np,beta....see subroutine 'beta'
c*****
c
c      dimension isym(10), north(5), line(78)
c      common

```

```

1      /blk1/rad,dx,dy,prcnt,kontrs,kmid,kmax,lmid,lmax,num
3      /blk3/title(20)
6      /blk6/node(77,61)
8      /blk8/kount(3896)
      data isym/lha,lhb,lhc,lhd,lhe,lhf,lhg,lhh,lhi,lhj/
      data iblank, idot, istar, iplus/lh , lh., lh*, lh+/
      data north/lhn,lho,lhr,lht,lhh/
c
c      * find maximum value of 'kount' (ktmax)
      ktmax = 0
      do 10 n = 1,num
10     ktmax = max0(ktmax,kount(n))
c
c      * calculate maximum value of 'kount' as a percentage of the total
c      number of data or beta vectors.
      go to (20, 20, 30) mode
20     nv = np
      go to 40
30     nv = nbeta
40     pc = 100./float(nv)
      pcmax = float(ktmax)*pc
c
c      * calculate integral scaling factor such that maximum percentage
c      is less than 'kontrs'.
      iscale = pcmax/kontrs+1
c
c      * calculate scaling factor to be applied to all 'kount' values.
      factor = pc/float(iscale)
c
c      * initialize 'maxs', the number of grid points at which
c      'kount'='ktmax'
      maxs = 0
c
c      * substitute printing symbols in 'kount'
      do 90 n = 1,num
      if (kount(n)) 50, 50, 60
c
c      * 'kount' is zero, insert dot
50     kount(n) = idot
      go to 90
60     if (ktmax-kount(n)) 70, 70, 80
c
c      8 'kount' equals maximum; insert '*' and increment 'maxs'
70     kount(n) = istar
      maxs = maxs + 1
      go to 90
80     kount1 = float(kount(n))*factor+1
c
c      * insert appropriate symbol
      kount(n) = isym(kount1)
90     continue
c
c      * store symbol at center in 'imid', and substitute '+' at center
      imid = kount(1)
      kount(1) = iplus
c

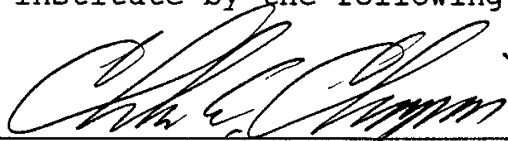
```

```

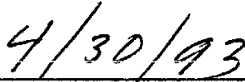
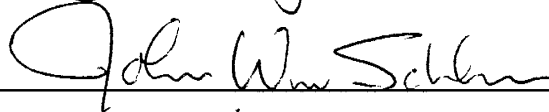
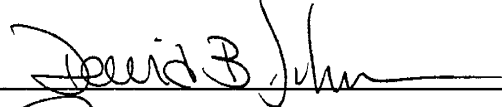
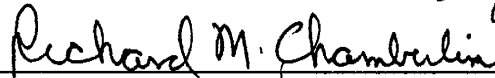
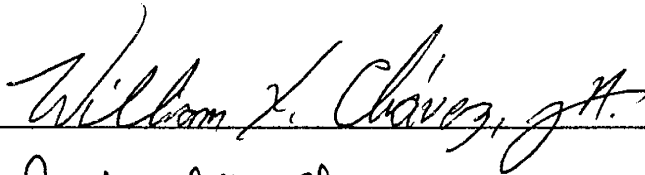
c      * print diagram
      go to (100, 110, 120) mode
100 write (6,1008)
      go to 130
110 write (6,1009)
      go to 130
120 write (6,1010)
130 continue
      write (6,1001) title, (iblack, k = 1, kmid - 2), north
      do 180 l = 1, lmax
      do 170 k = 1, kmax
      n = node(k,l)
      if (n) 140, 150, 160
c
c      * node = -1, so it is outside plotting circle, insert blank
140 line(k) = iblack
      go to 170
c
c      * node is zero, so has not yet been scanned; therefore 'kount'
c      must be zero
150 line(k) = idot
      go to 170
160 line(k) = kount(n)
170 continue
c
c      * print line
      write (6,1002) (line(k), k = 1, kmax)
180 continue
      write (6,1006) imid
      write (6,1012) prcnt
      write (6,1004) (isym(i), I = 1, kontrs)
      write (6,1003) (i, i = iscale, iscale*kontr, iscale)
      write (6,1007) np
      if (mode .eq. 3) write (6,1011) nbeta
      write (6,1005) maxs, pmax
      return
1001 format (1h0, 22x, 19a4, a3, //, 21x, 44a1)
1002 format (22x, 78a1)
1003 format (23x, 11hPERCENT 0, 10i4)
1004 format (1h0, 22x, 9hSYMBOL , 10(2x, a2) )
1005 format (1h0, 22x, 10hMAXIMUM AT, i4, 19h POINTS MARKED '**:',
1      f5.1, 2h %)
1006 format (1h+, 22x, 9hCENTER: , a1)
1007 format (1h0, 22x, 12hNO. OF DATA:, i4)
1008 format (22x, 'EQUAL AREA PROJECTION OF LINEATIONS')
1009 format (22x, 'EQUAL AREA PROJECTION OF PLANES')
1010 format (22x, 'EQUAL AREA PROJECTION OF BETA INTERSECTIONS')
1011 format (1h+, 48x, 26hNO. OF BETA INTERSECTIONS:, i4)
1012 format (1h0, 22x, 24hPERCENTAGE OF VECTORS IN, f4.1,
1      22h PERCENT SCANNING AREA)
1013 format (1h )
      end

```


This dissertation is accepted on behalf of the faculty
of the Institute by the following committee:



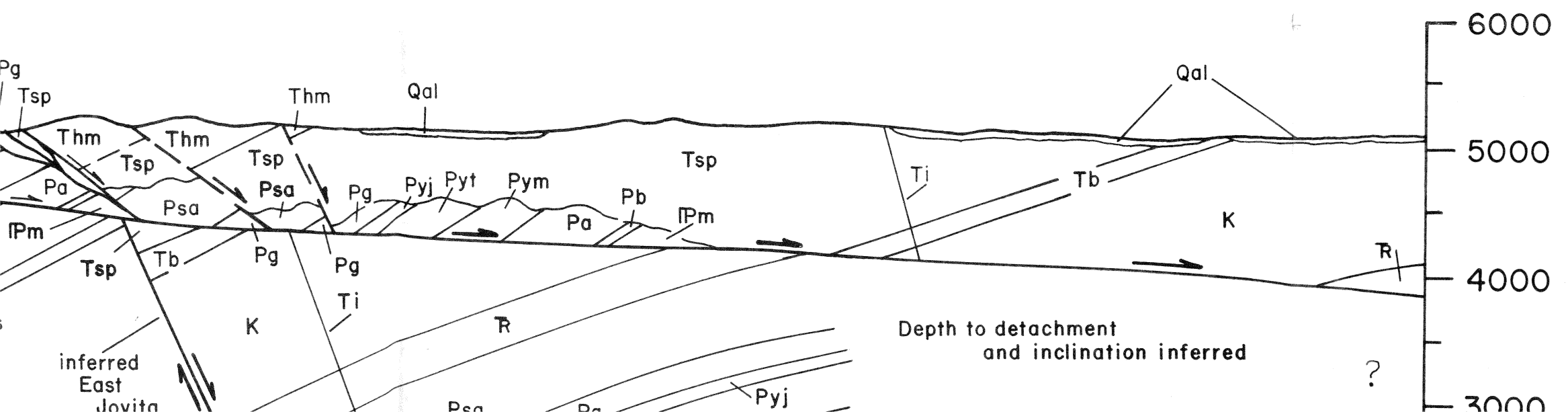
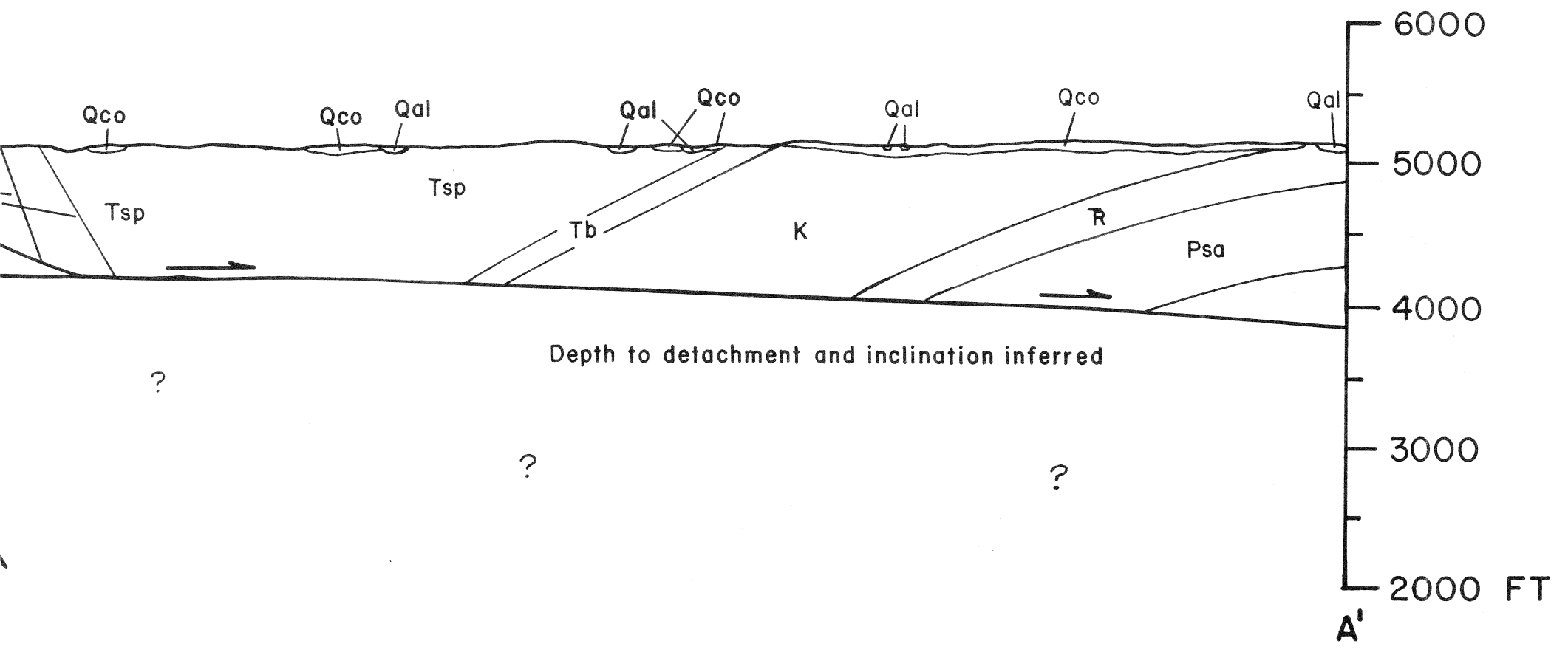
Adviser

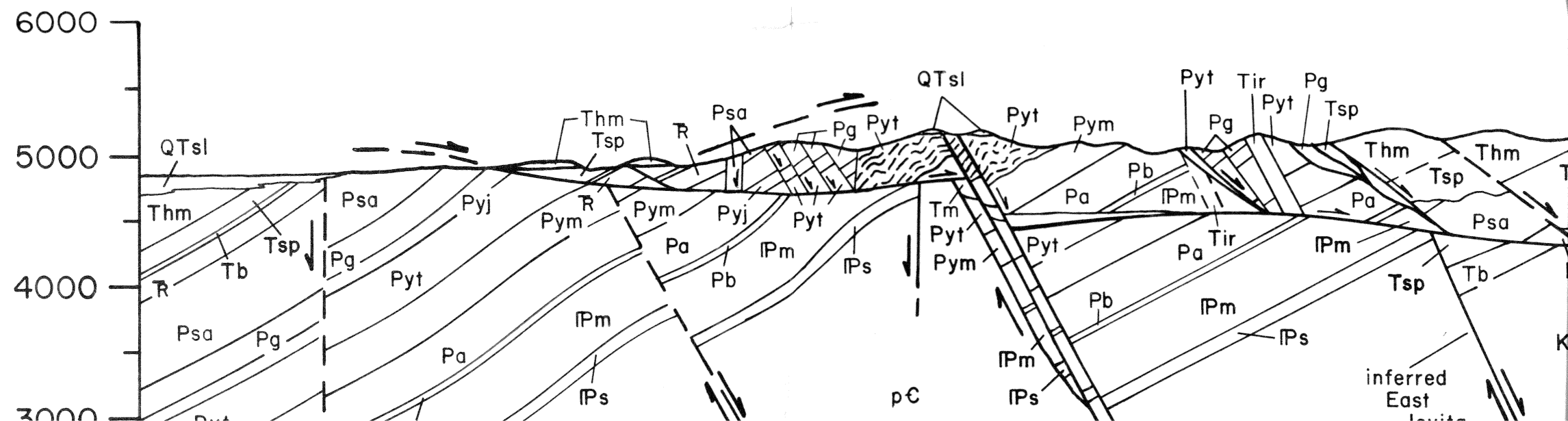
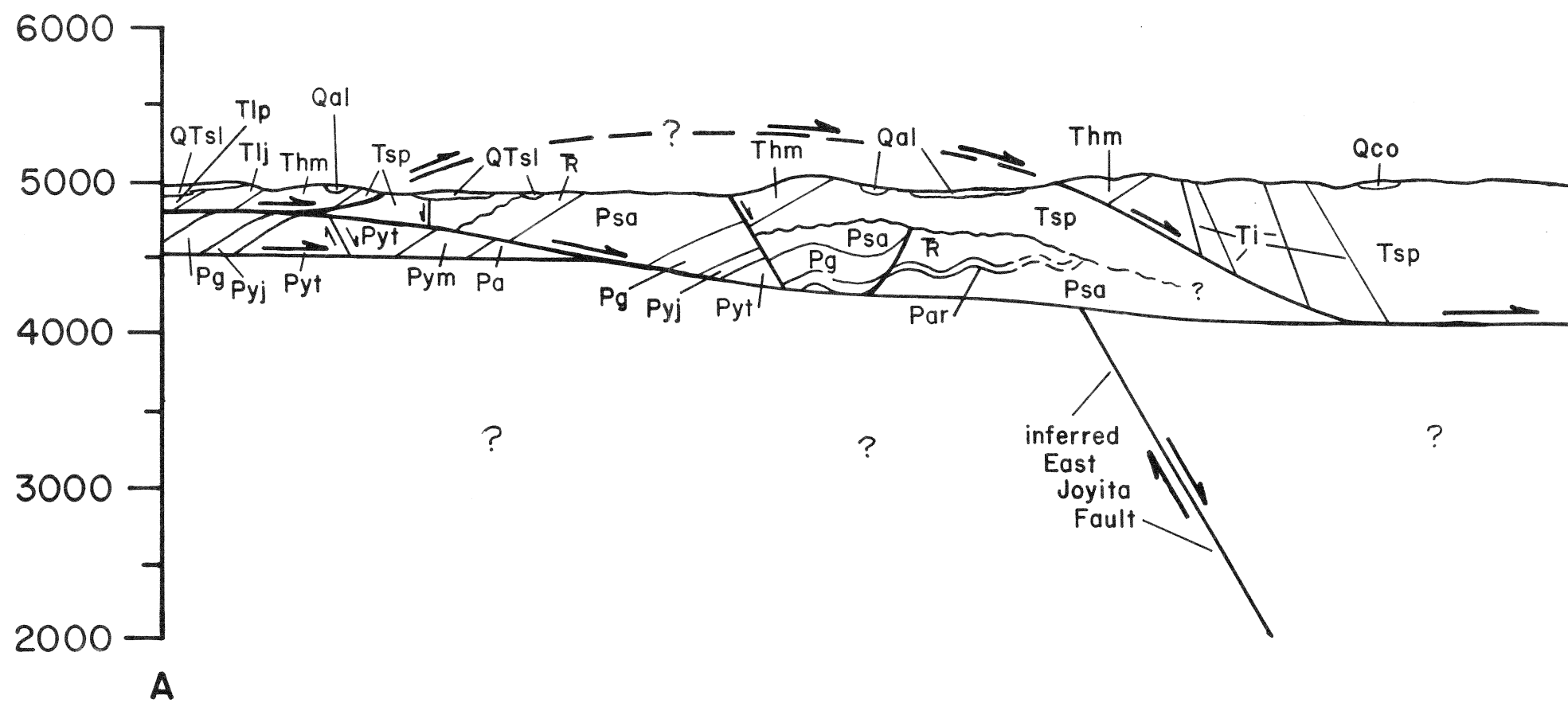


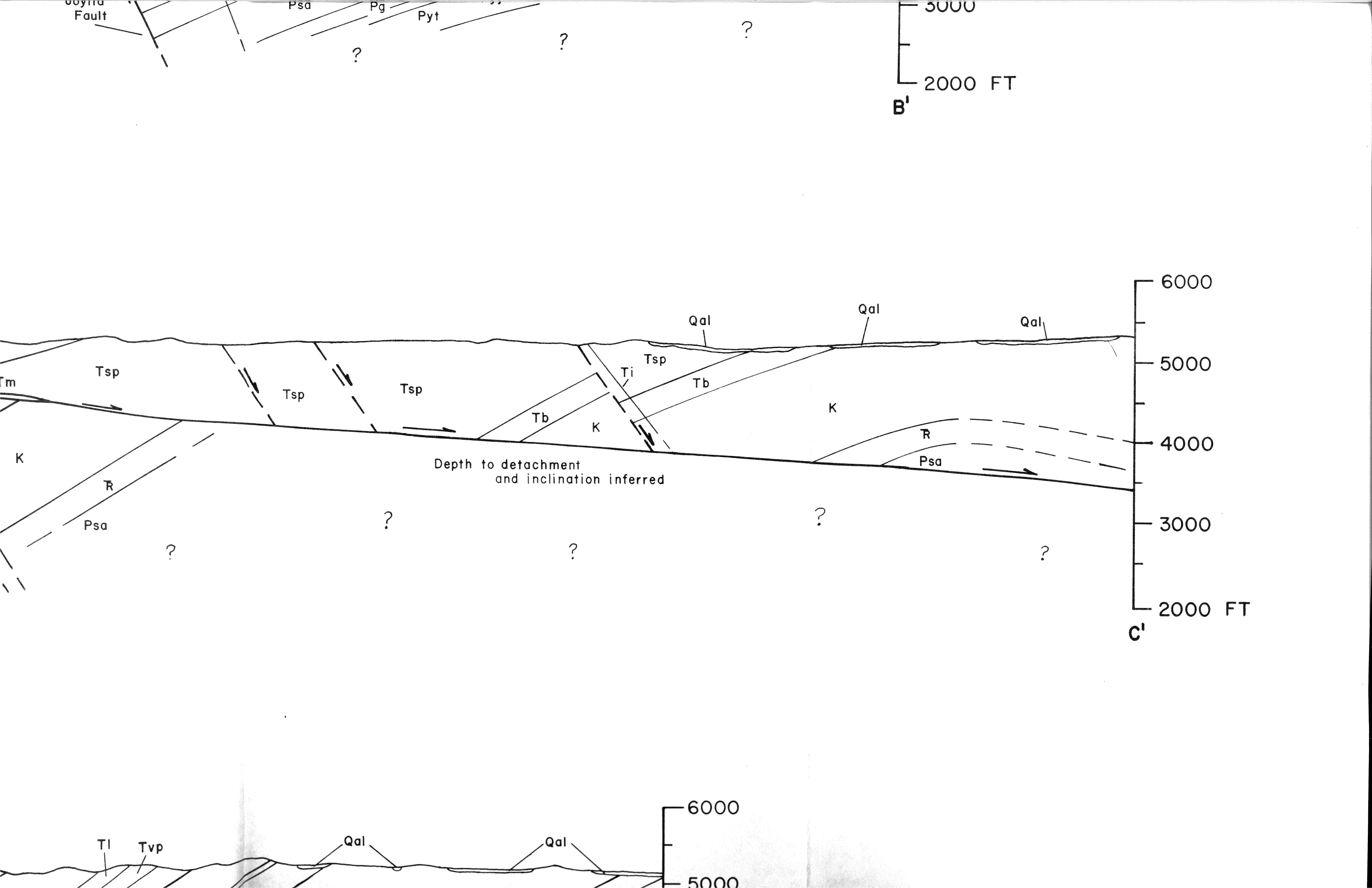
Date

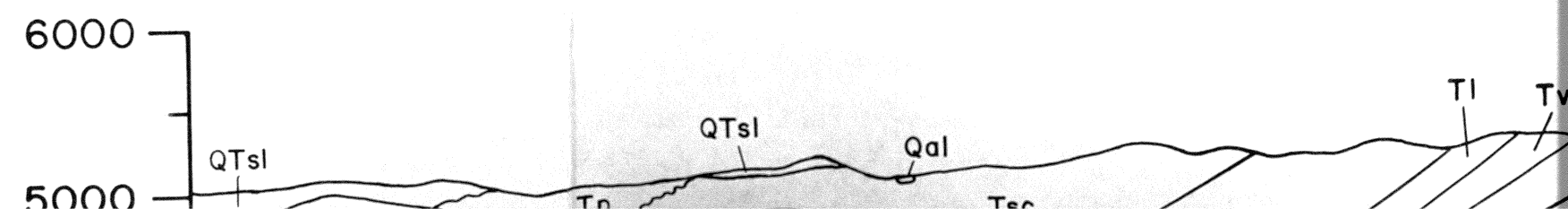
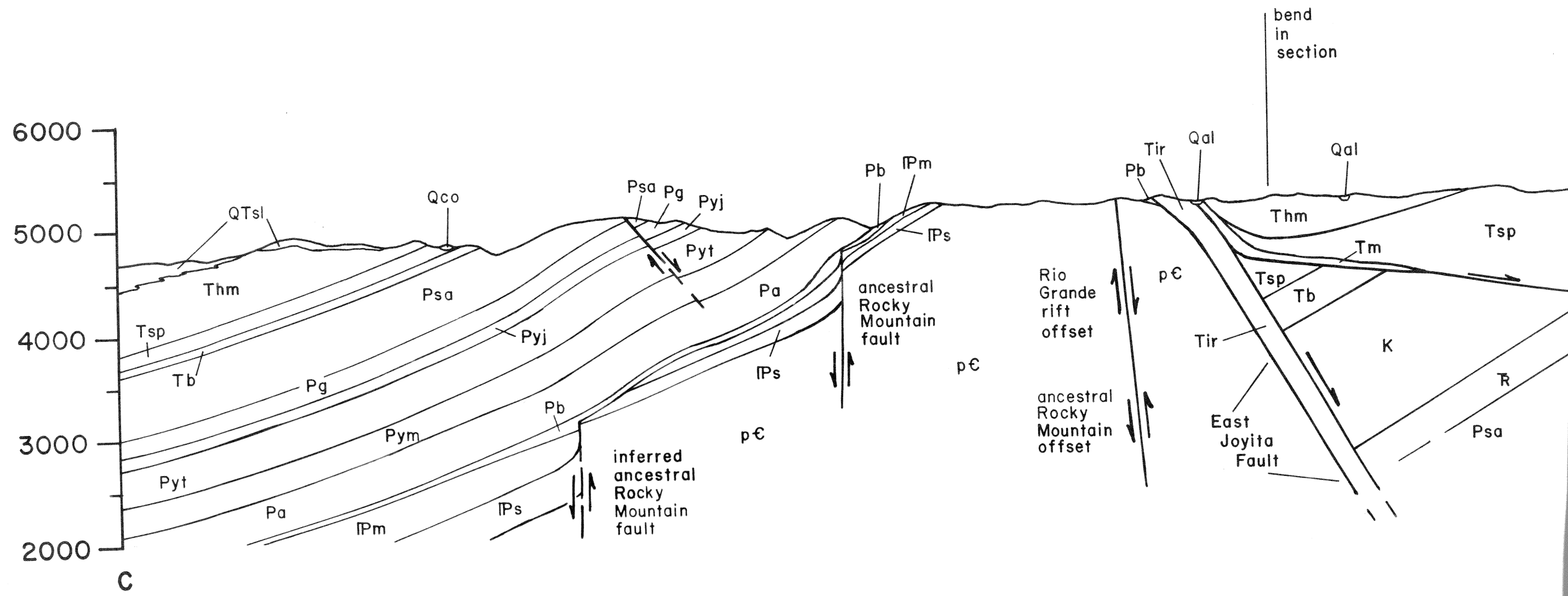
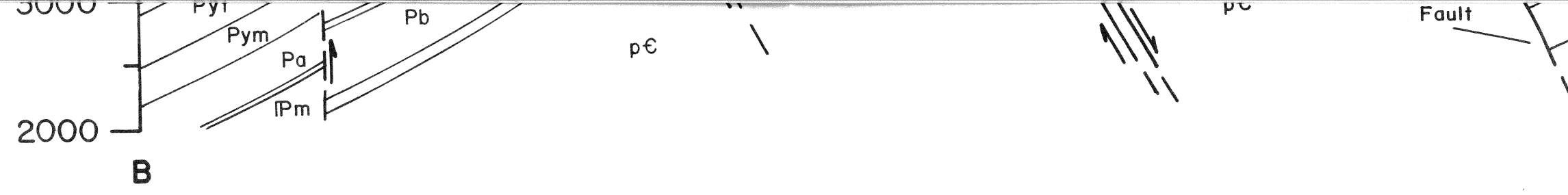
PLATE 2

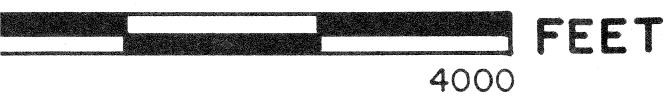
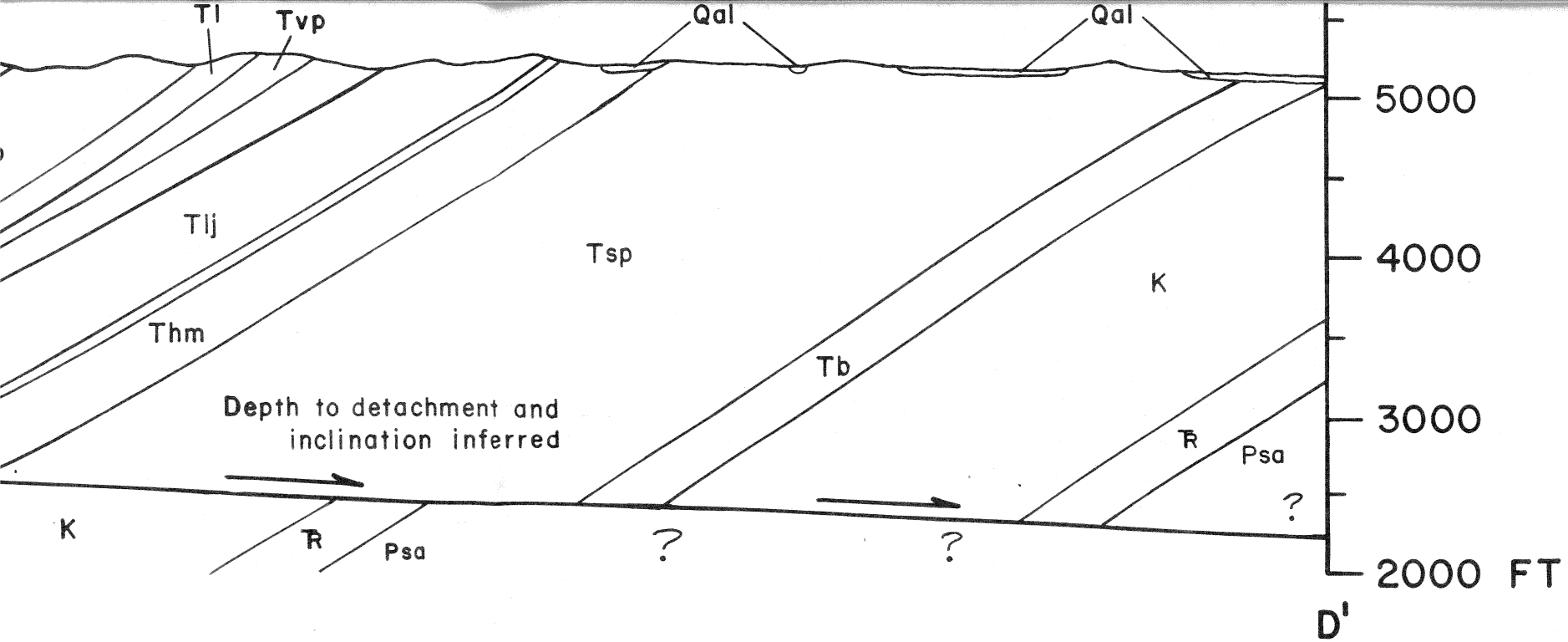
PLATE 2





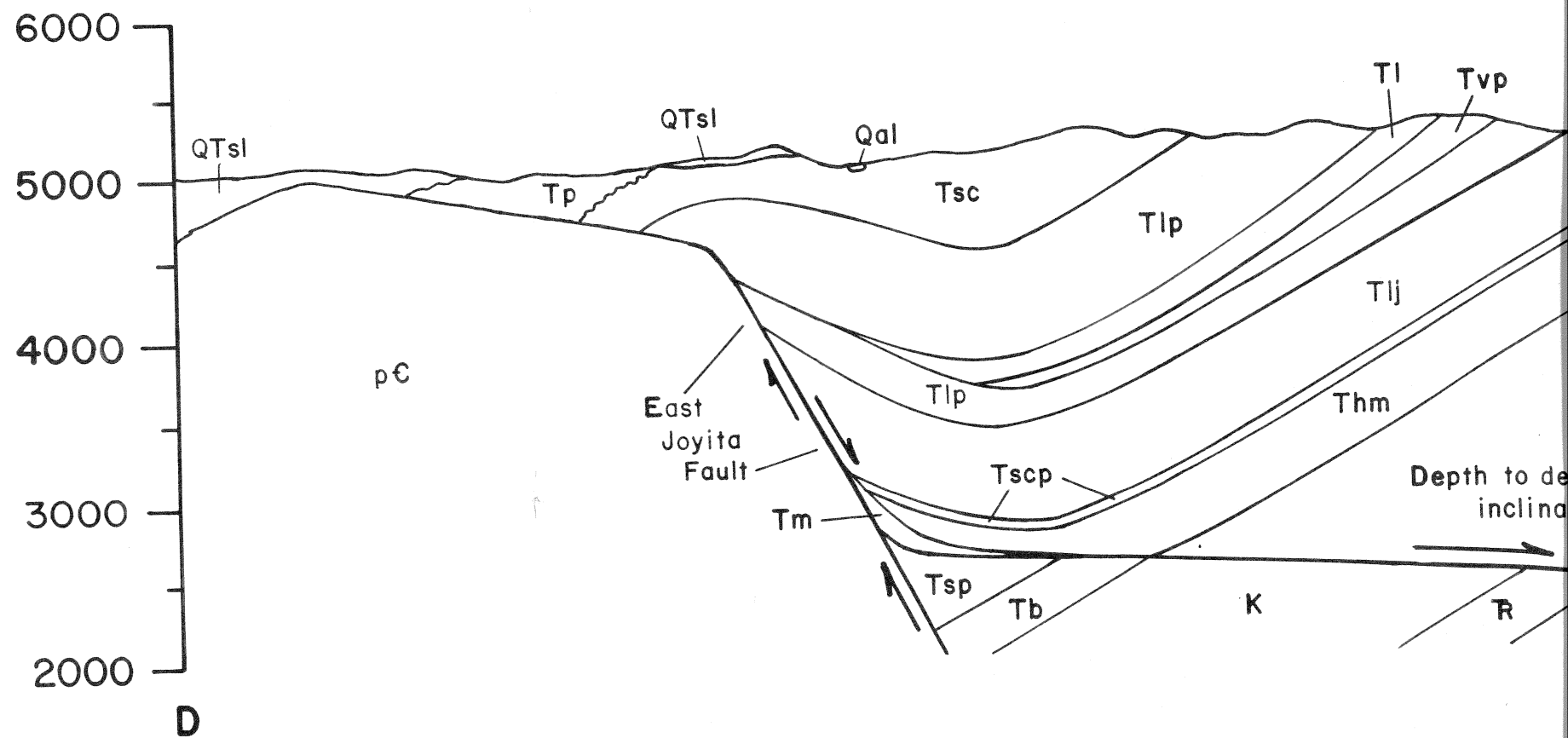






THE JOYITA HILLS AREA, COUNTY, NEW MEXICO

C. BECK, 1993



HORIZONTAL AND VERTICAL SCALES:



CROSS SECTIONS OF THE J SOCORRO COUNTY, N

WILLIAM C. BECK

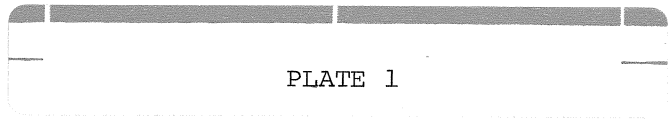


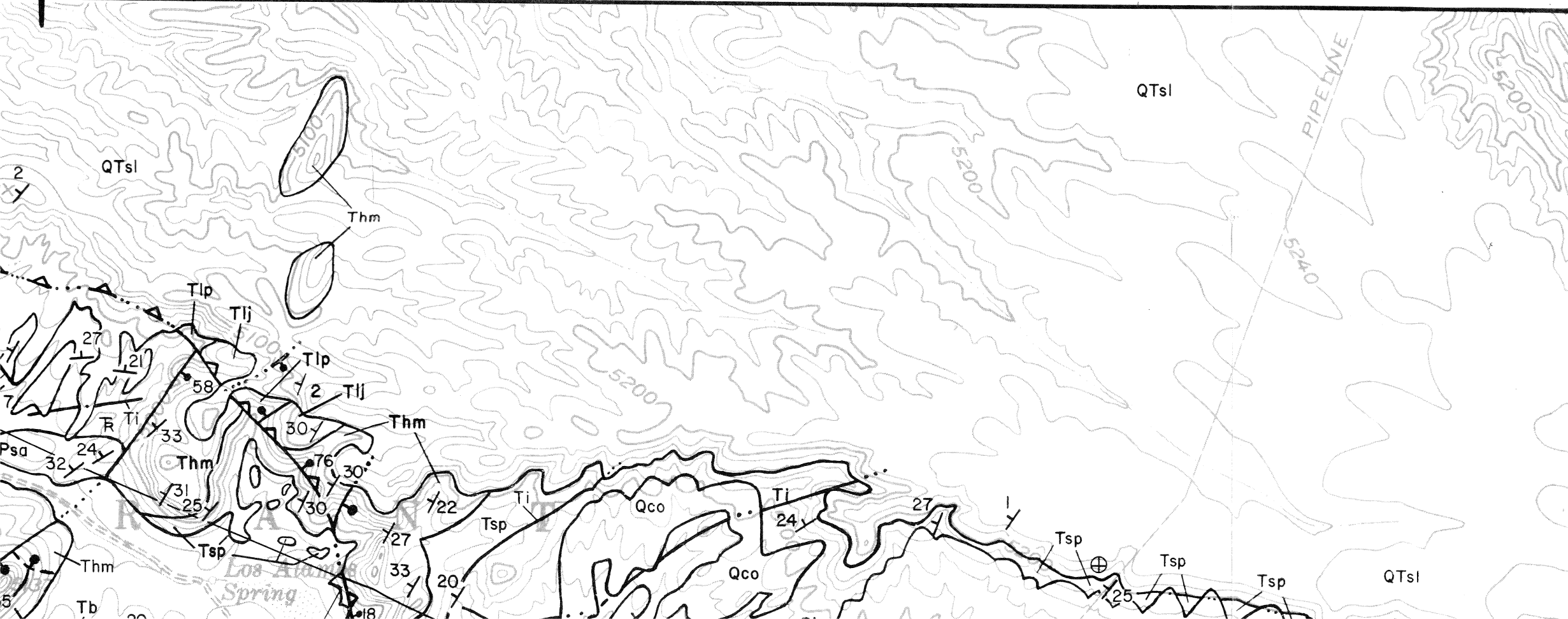
PLATE 1

TA HILLS AREA, MEXICO

993

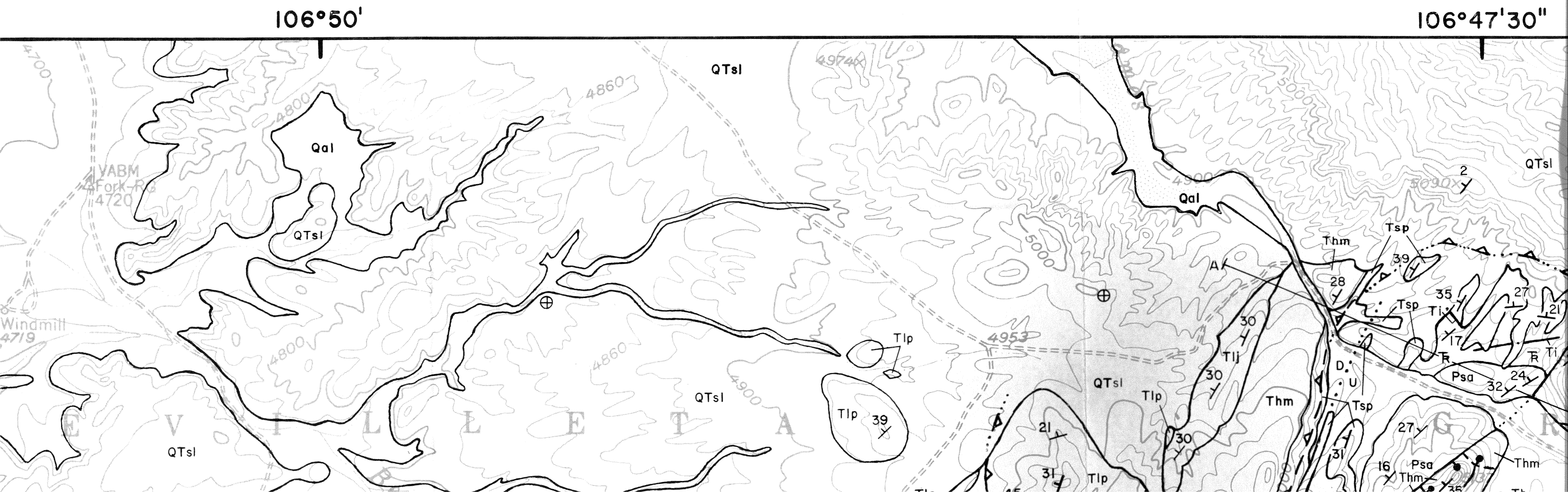
106°47'30"

106°45'

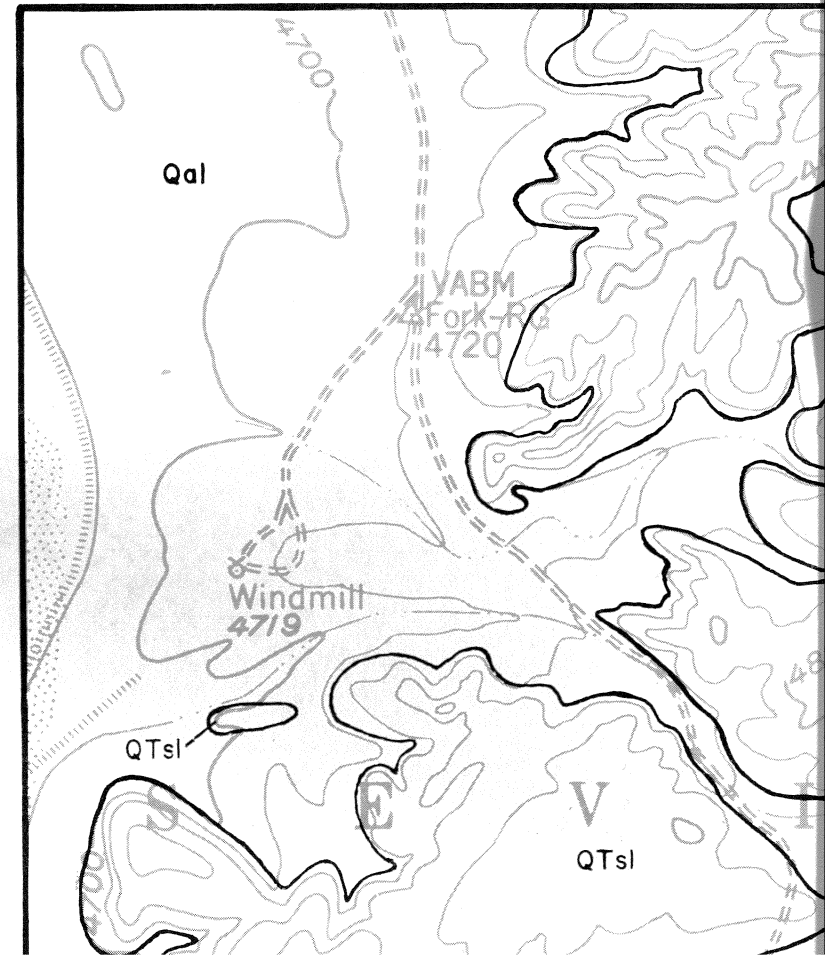
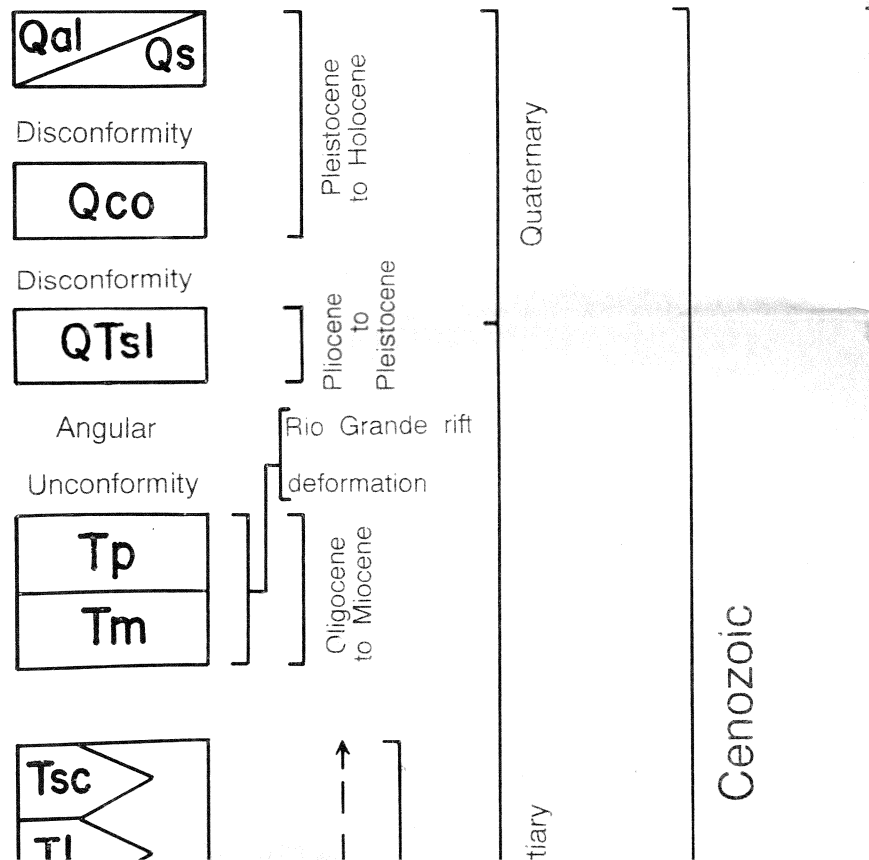


GEOLOGIC MAP OF THE JOYITA HILLS SOCORRO COUNTY, NEW MEXICO

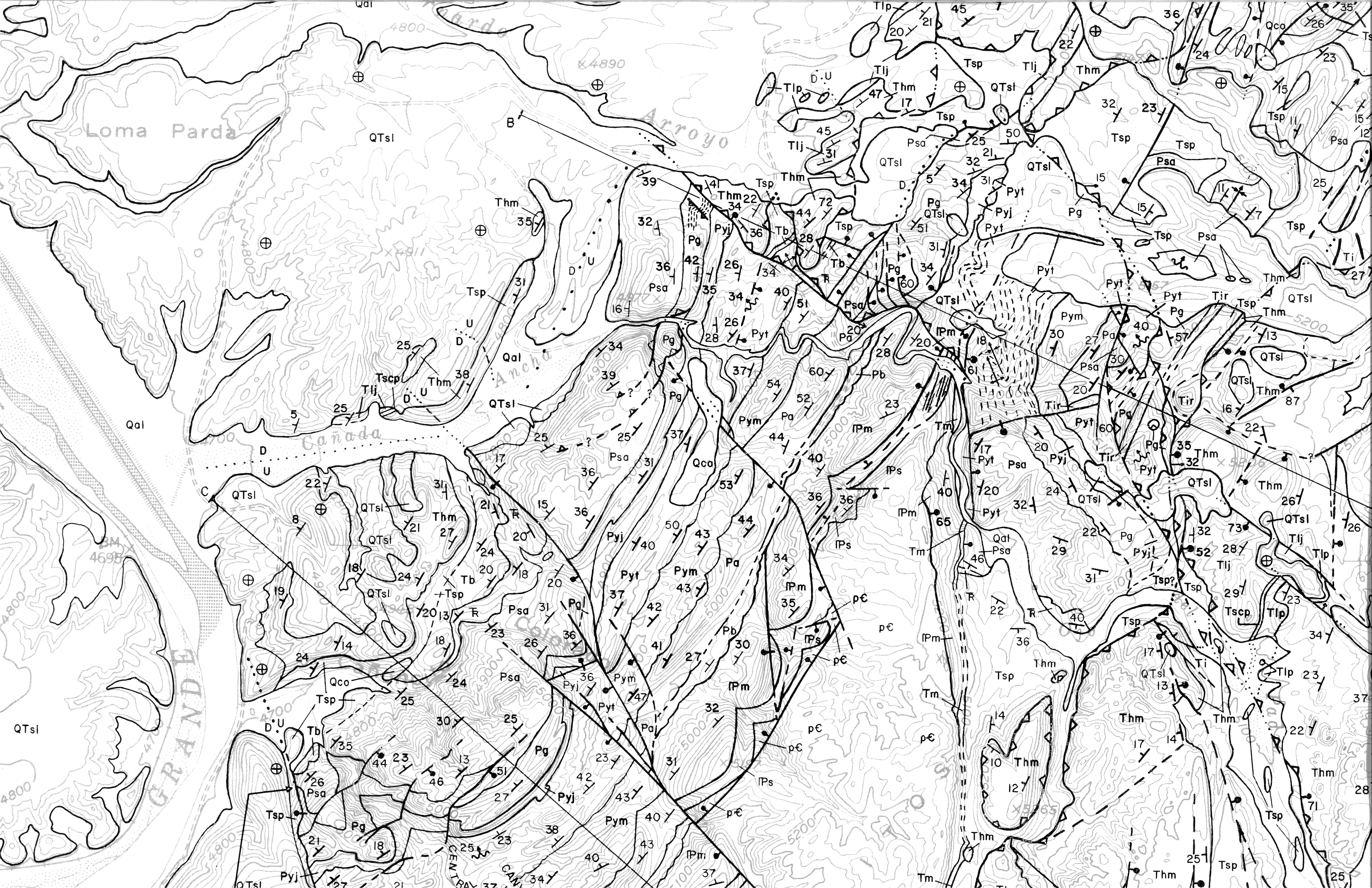
WILLIAM C. BECK, 1993

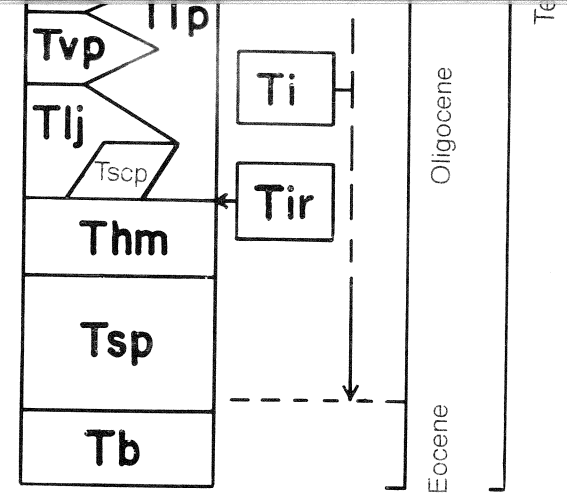


MAP UNITS



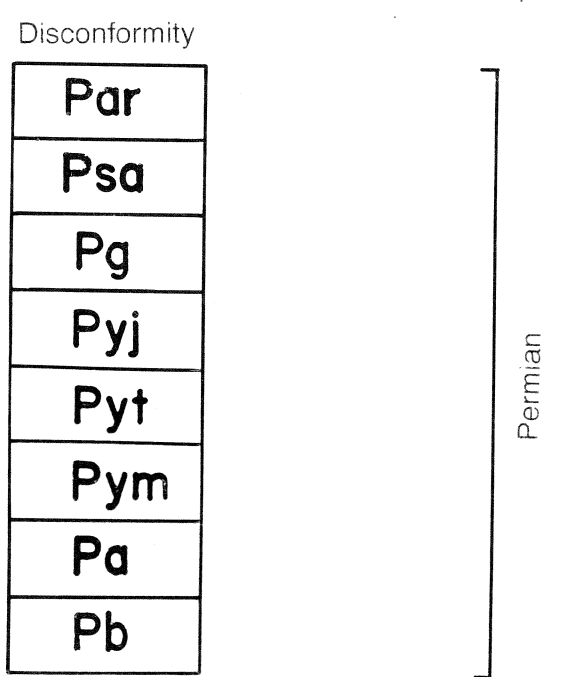
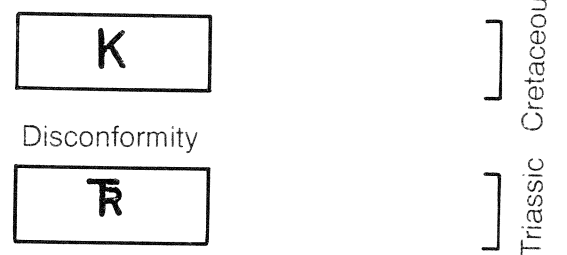






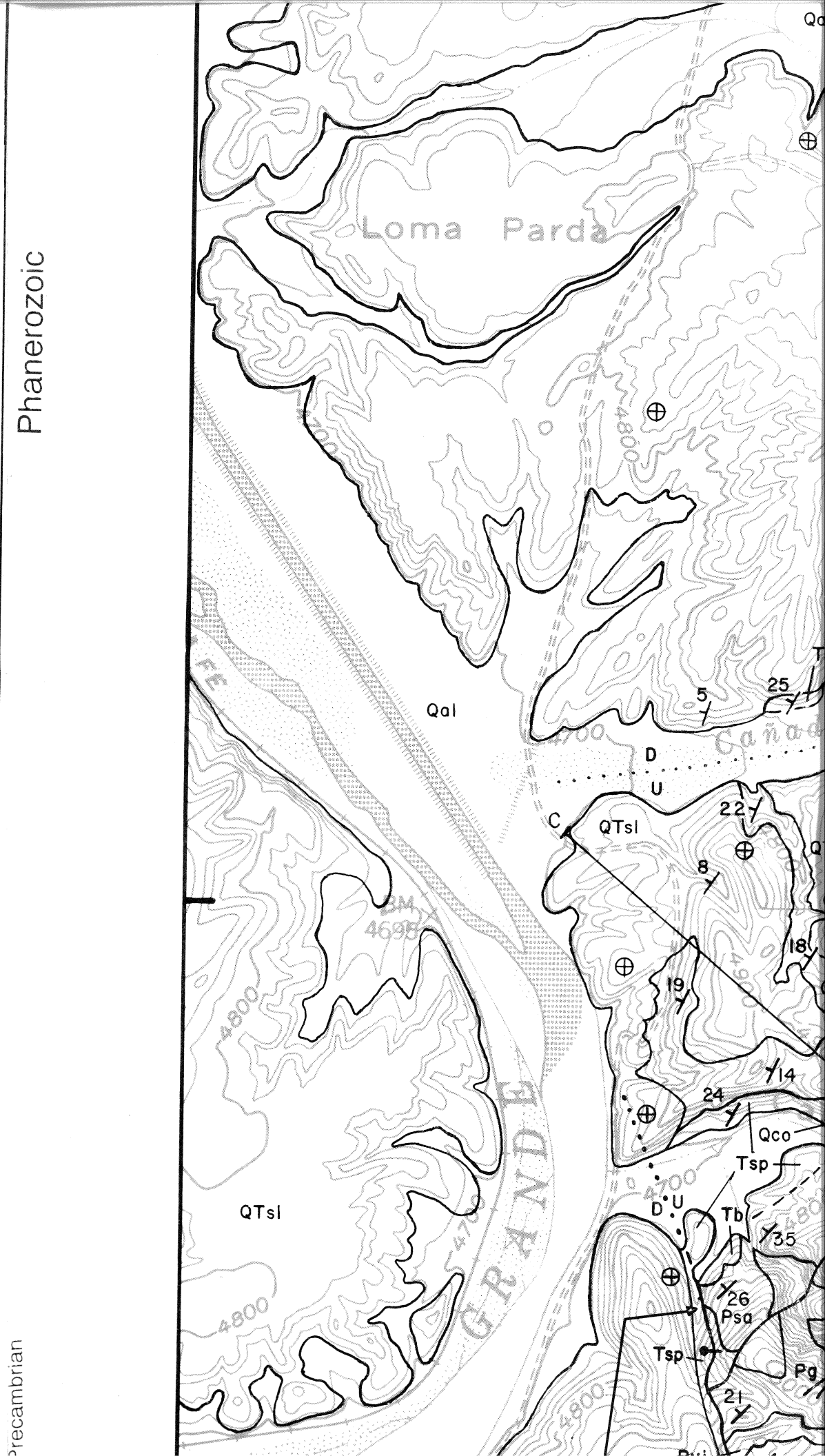
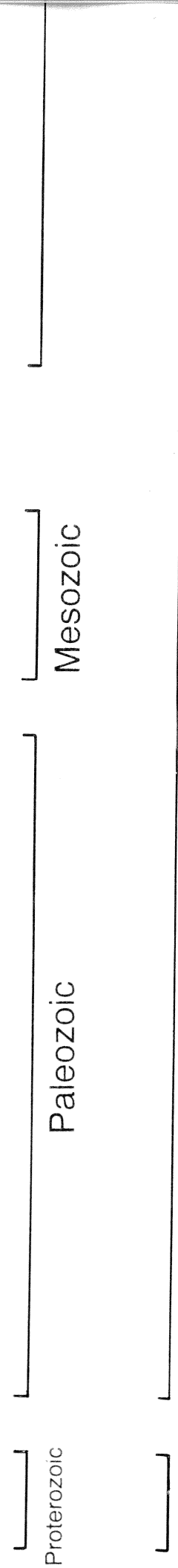
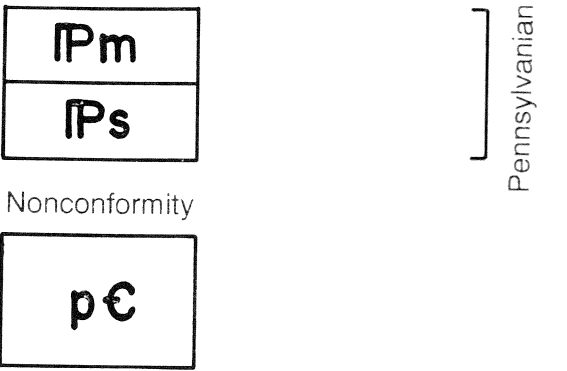
Disconformity to Angular Unconformity

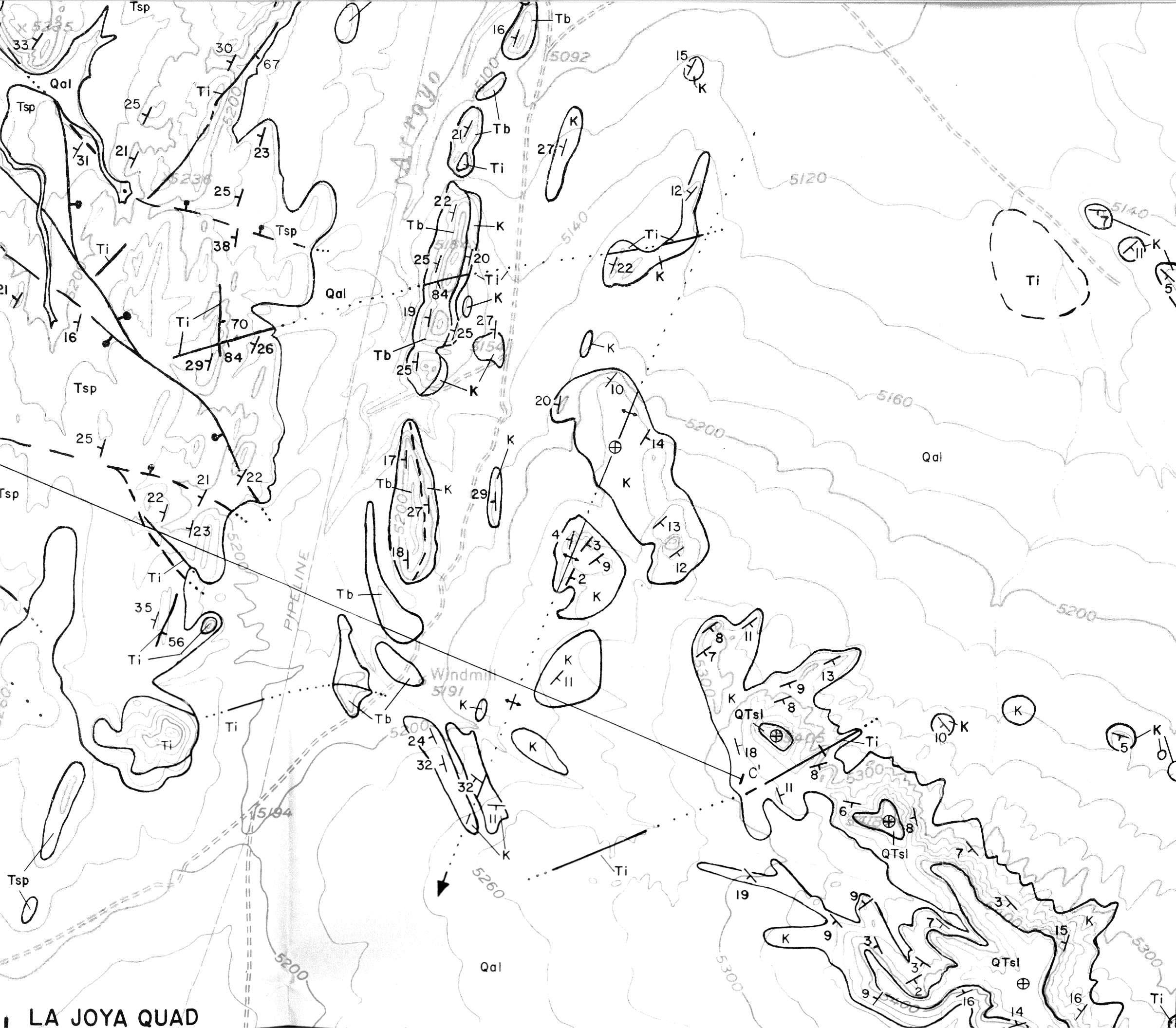
Laramide deformation



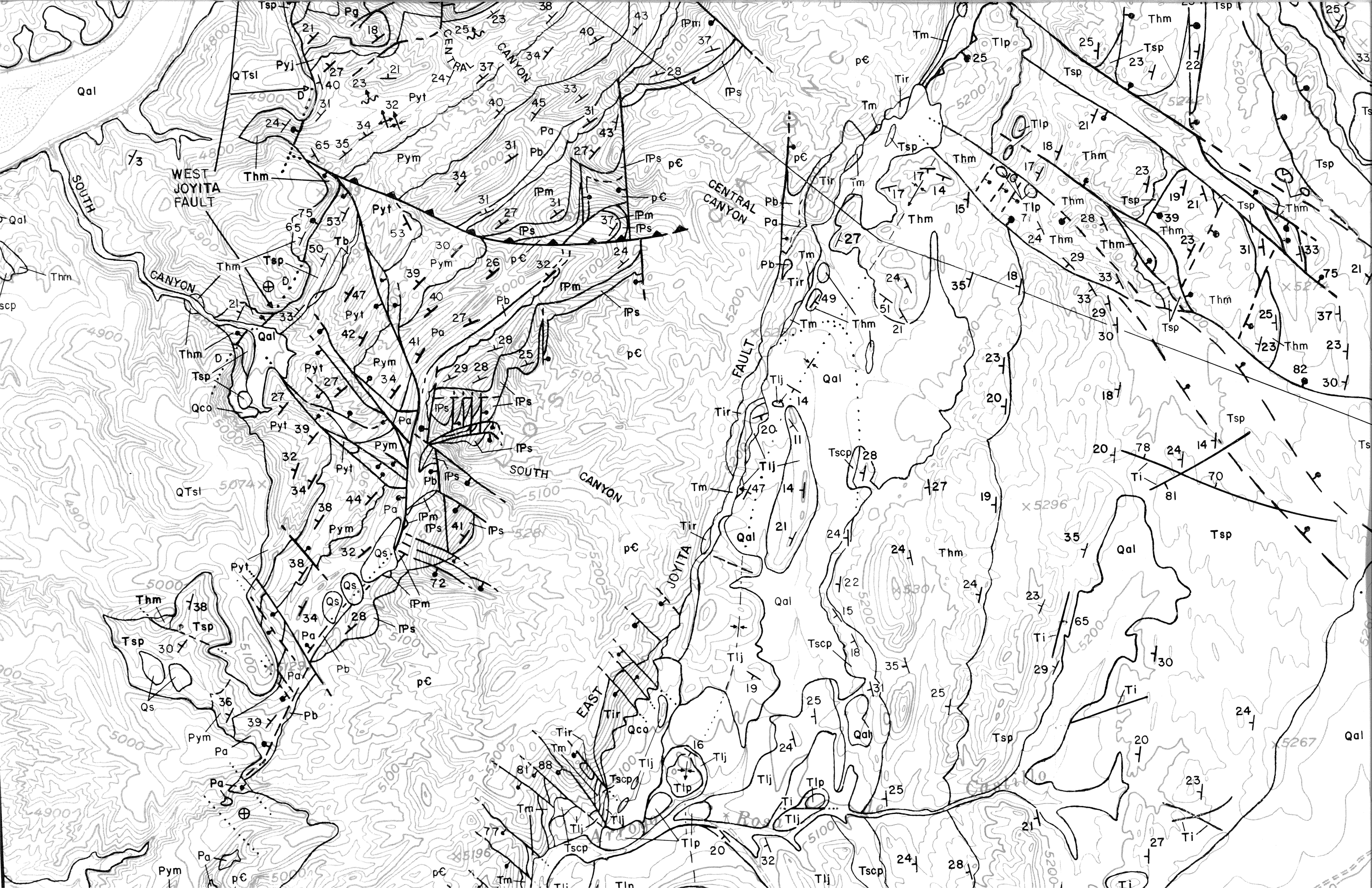
Angular Unconformity

Ancestral Rocky Mountain deformation





LA JOYA QUAD



Nonconformity

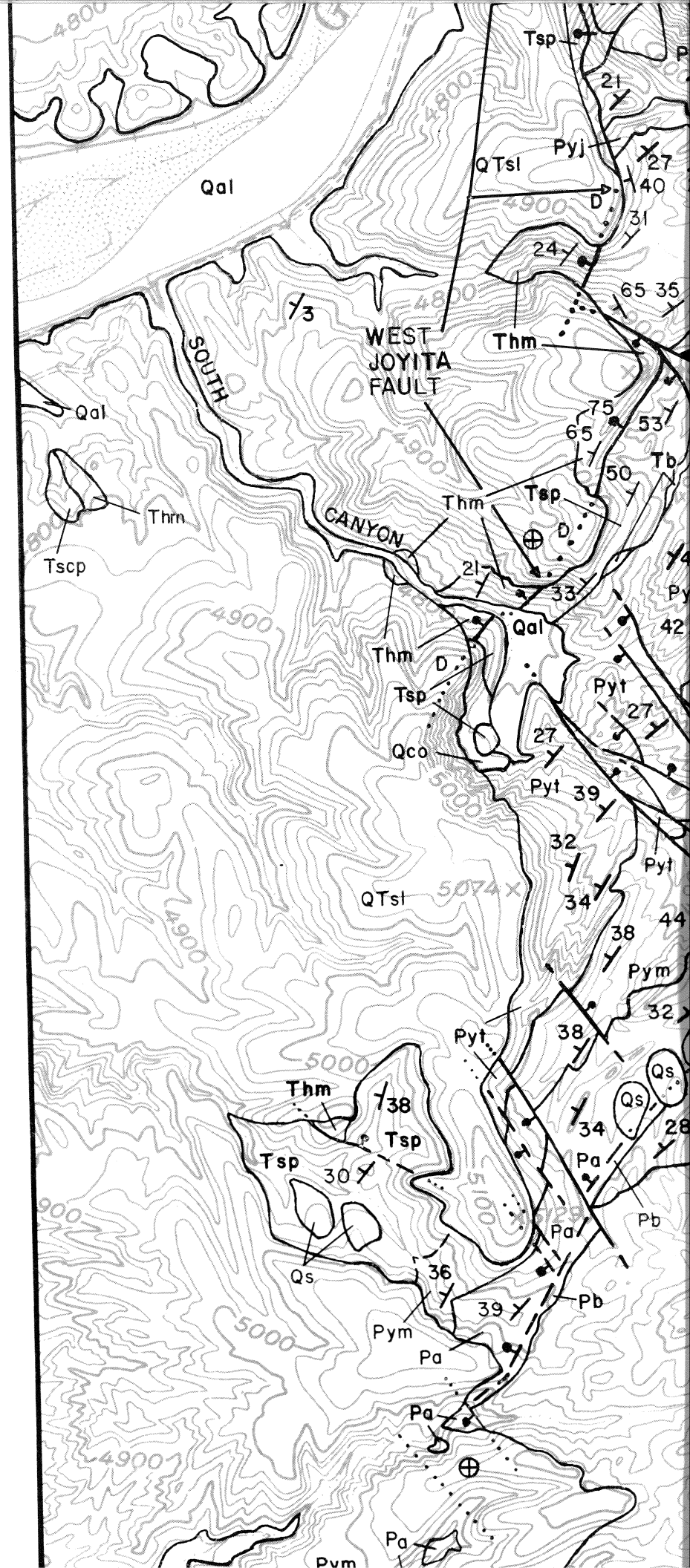
p€

Pen

Proterozoic

Precambrian

Qal / Qs	alluvium and eolian sand	
Qco	colluvium	
QTsl	Sierra Ladrones Fm	} Santa Fe Group
Tp	Popotosa Fm	
Tm	Tectonic melange	
Tsc	South Canyon Tuff	
Tlp	La Jara Peak Basaltic Andesite	
Tl	Lemitar Tuff	
Tlp	La Jara Peak Basaltic Andesite	
Tvp	Vicks Peak Tuff	
Tlp	La Jara Peak Basaltic Andesite	
Tlj	La Jencia Tuff	
Tscp	Tuff of South Crosby Peak	
Tlp	La Jara Peak Basaltic Andesite	
Thm	Hells Mesa Tuff	Tir intrusive
		Ti mafic dikes and intrusives

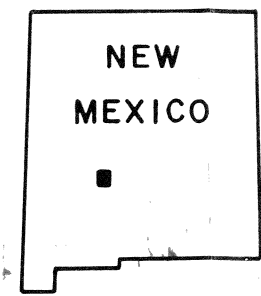
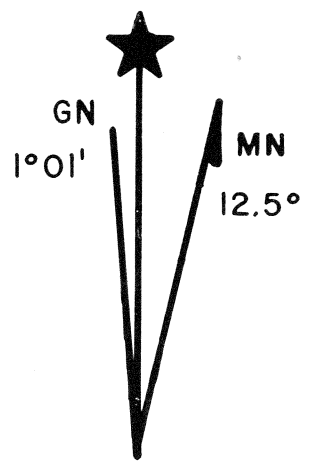


LA JOYA QUAD
MESA DEL YESO QUAD

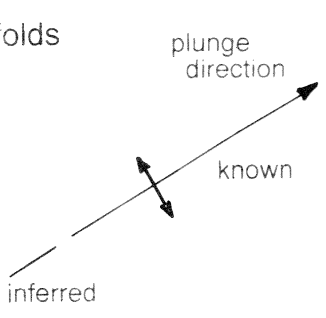
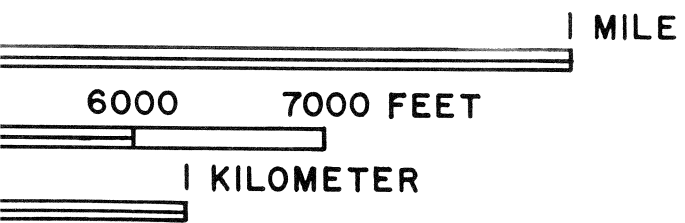
34°15'

106°45'

7'30"



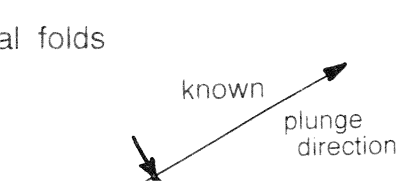
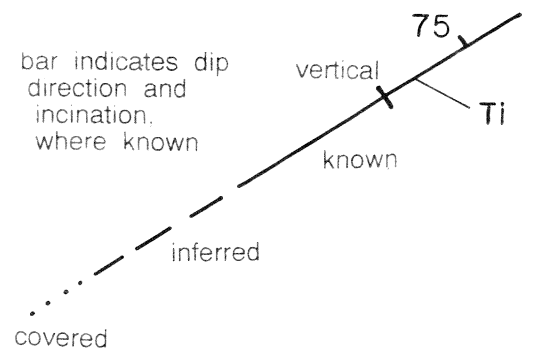
MAP LOCATION



Small-scale folds

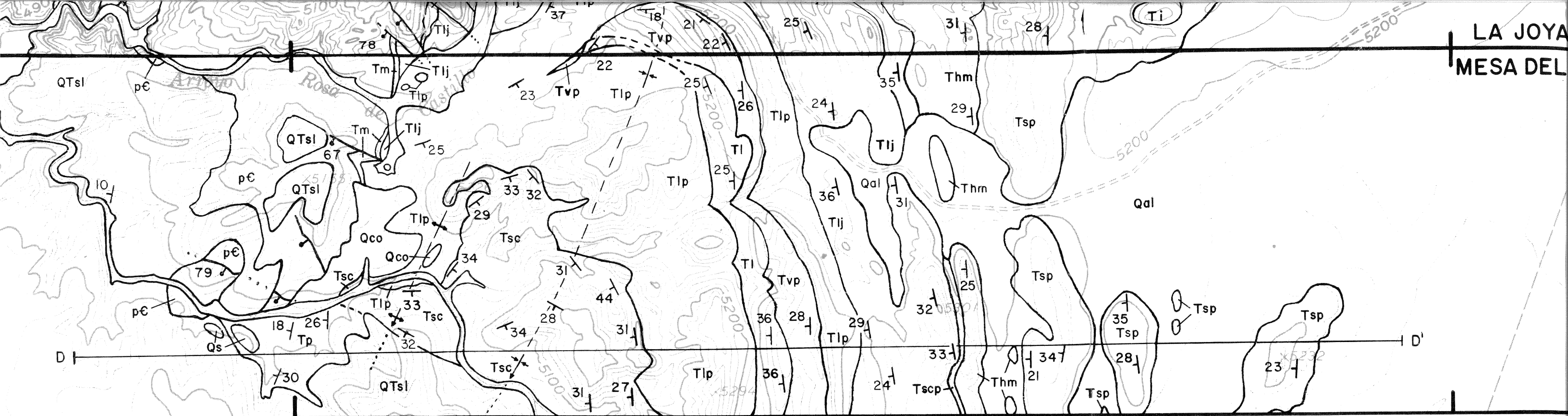


Mafic dikes



Medium-scale folds

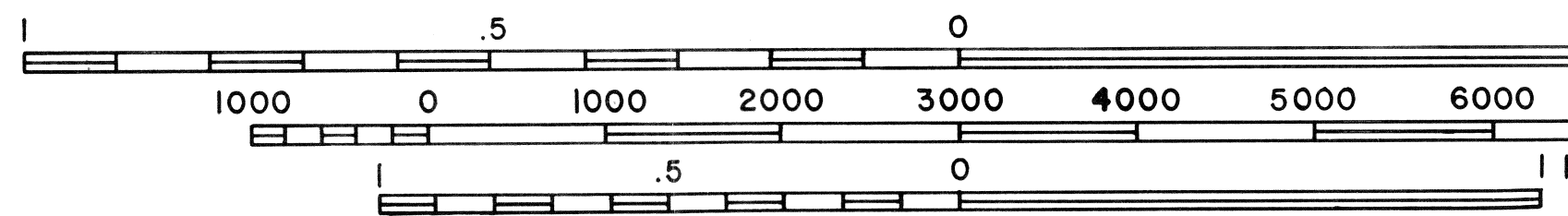
surface trace of marker beds



106°50'

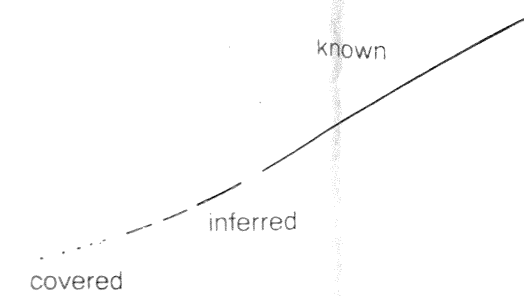
106°47'30"

SCALE 1:12000

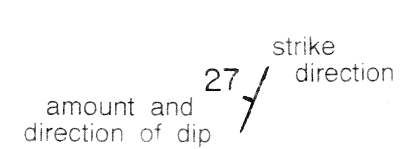


CONTOUR INTERVAL 20 FEET

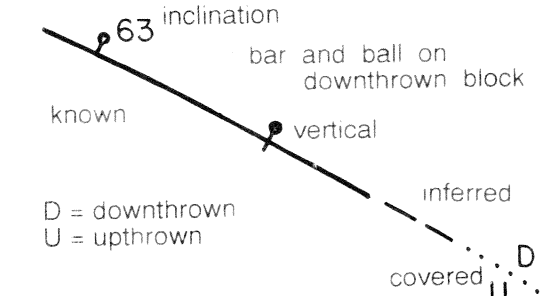
Bedding contact



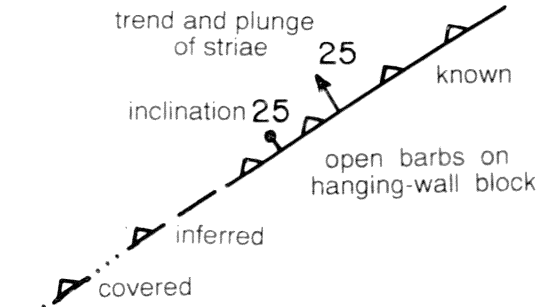
Bedding attitude



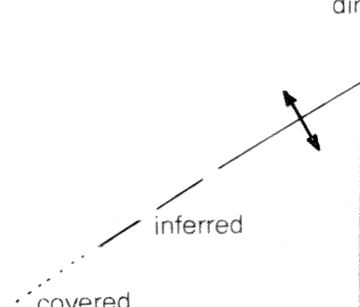
Normal faults



Extensional detachment faults



Anticlinal folds



Thrust faults



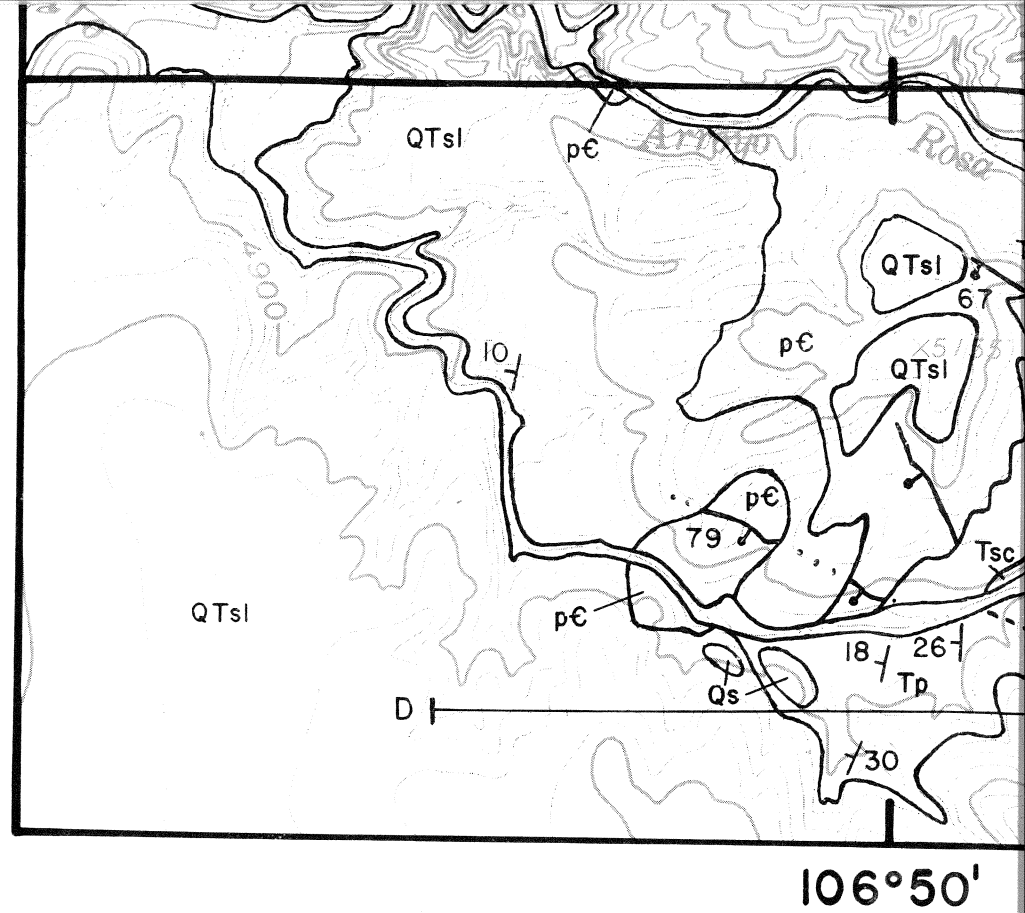
Strike-slip faults



Synclinal folds

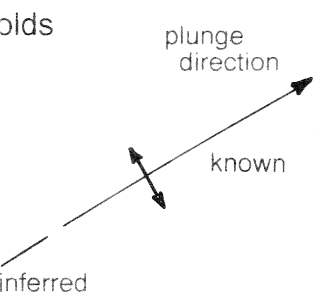
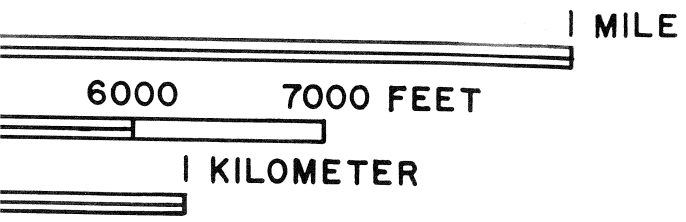


K	Cretaceous (undifferentiated)	
T	Triassic (undifferentiated)	
Par	Artesia Fm	
Psa	San Andres Fm	
Pg	Glorieta Fm	
Pyj	Joyita Member	} Yeso Fm
Pyt	Torres Member	
Pym	Meseta Blanca Member	
Pa	Abo Fm	
Pb	Bursum Fm	} Magdalena Group
IPm	Madera Fm	
IPs	Sandia Fm	
pC	Proterozoic	



Bedding c

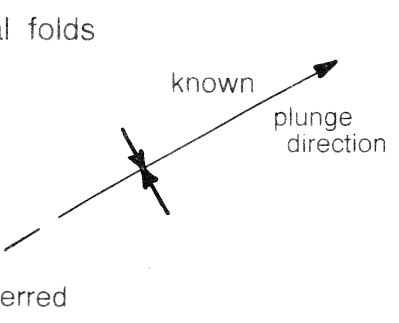
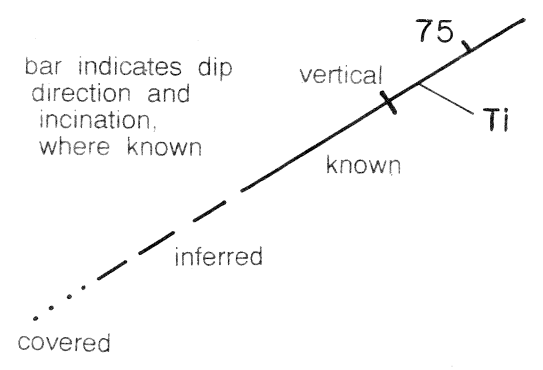
covered



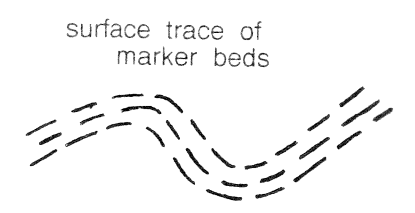
Small-scale folds

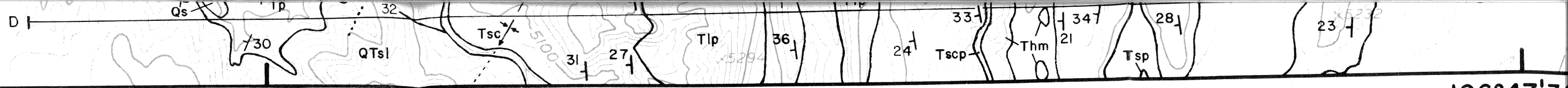


Mafic dikes



Medium-scale folds

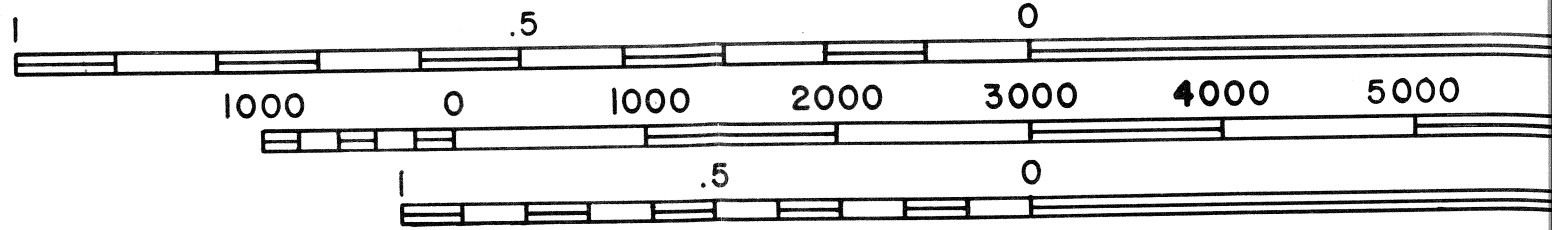




106°50'

106°47'30"

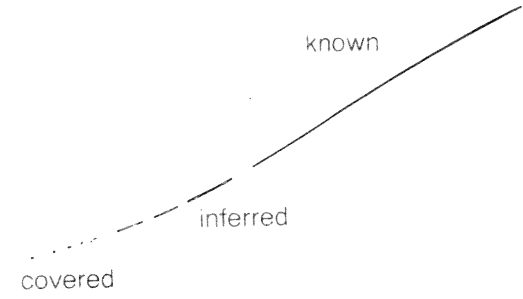
SCALE 1:12000



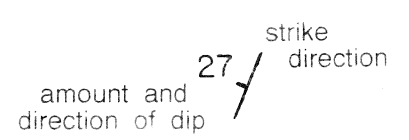
CONTOUR INTERVAL 20 FEET

MAP SYMBOLS

Bedding contact



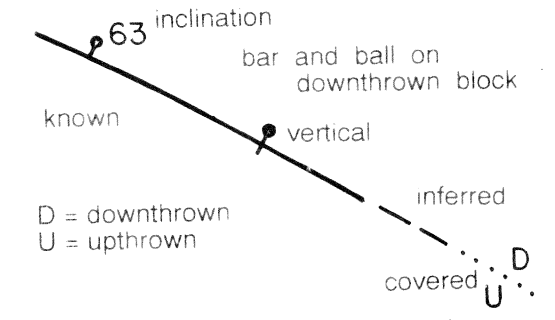
Bedding attitude



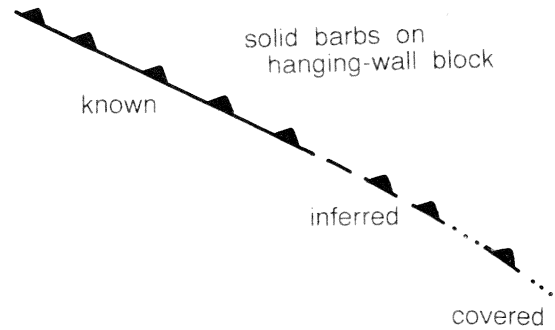
Horizontal bedding



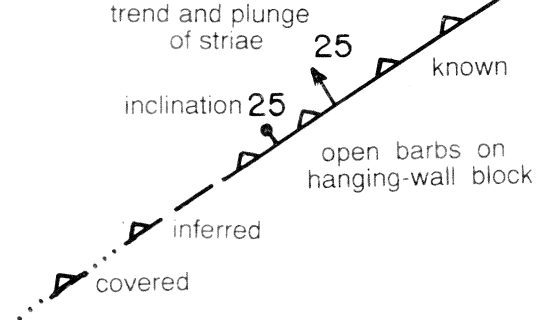
Normal faults



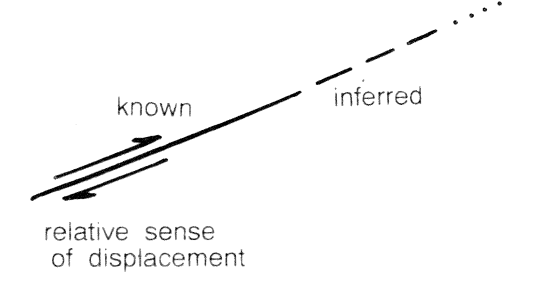
Thrust faults



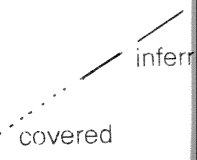
Extensional detachment faults



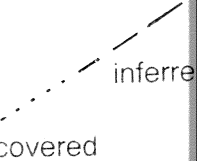
Strike-slip faults



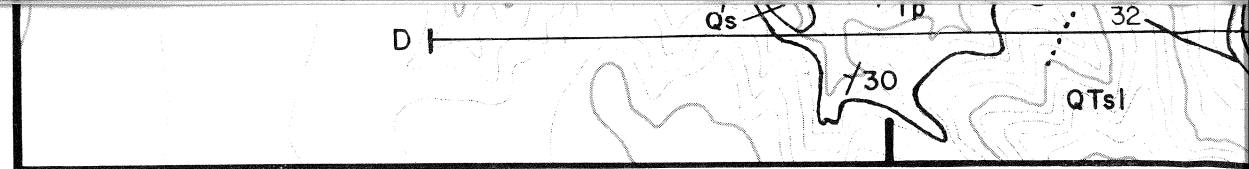
Anticlinal folds



Synclinal folds



- Pyr Torres Member } Teso Fm
- Pym Meseta Blanca Member }
- Pa Abo Fm
- Pb Bursum Fm } Magdalena Group
- Pm Madera Fm }
- Ps Sandia Fm }
- pC Proterozoic



106°50'

Bedding contact

